

# Annual Report 2013

Laboratory of Radiochemistry and Environmental Chemistry

### Cover

The accelerator mass spectrometer MICADAS (MIni CARbon DAting System) was developed by ETH Zurich for radiocarbon ( $^{14}\text{C}$ ) dating with wide-spread applications in geosciences and archeology. In order to strengthen palaeoclimate research at the University of Bern, a new MICADAS was set up in our laboratory, jointly funded by the Swiss National Science Foundation, the Swiss Federal Office of Public Health, and the University of Bern (contributing parties: the University Board of Directors, the Department of Chemistry and Biochemistry, and the Oeschger Centre for Climate Change Research). The pictures show from the top in clockwise direction the MICADAS system, the automated graphitization equipment for production of solid measurement targets, the gas inlet system for direct introduction of gaseous  $\text{CO}_2$  samples, and the determination of calendar ages from  $^{14}\text{C}$  measurement results using the IntCal calibration curve. (Photos: A. Boutellier)

PAUL SCHERRER INSTITUT



$u^b$

LABOR FÜR RADIO- UND UMWELTCHEMIE  
DER UNIVERSITÄT BERN UND  
DES PAUL SCHERRER INSTITUTS

b  
UNIVERSITÄT  
BERN

# Annual Report 2013

Laboratory of Radiochemistry and Environmental Chemistry

**Editors**

A. Türler, M. Schwikowski, A. Blattmann

**Paul Scherrer Institut**

Labor für Radio- und Umweltchemie  
5232 Villigen PSI  
Switzerland  
Durchwahl +41 56 310 24 04  
Sekretariat +41 56 310 24 01  
Fax +41 56 310 44 35

**Universität Bern**

Departement für Chemie und Biochemie  
Labor für Radio- und Umweltchemie  
Freiestrasse 3, 3012 Bern, Switzerland  
Durchwahl +41 31 631 42 64  
Sekretariat +41 31 631 42 42  
Fax +41 31 631 42 20

**Reports are available from**

Angela Blattmann  
angela.blattmann@psi.ch  
Paul Scherrer Institut  
5232 Villigen PSI  
Switzerland



See also our web-page

<http://www.psi.ch/lch/>



## TABLE OF CONTENTS

Editorial.....	1
<b>Heavy Elements</b>	
DECOMPOSITION STUDIES ON THE STABILITY OF TUNGSTEN- AND MOLYBDENUM CARBONYL COMPLEXES PERFORMED AT RIKEN (JAPAN) .....	3
I. Usoltsev for the Carbonyl collaboration	
SYNTHESIS AND CHEMICAL INVESTIGATION OF Sg (CO) <sub>6</sub> .....	4
J. Even, A. Yakushev, Ch.E. Düllmann, H. Haba, M. Asai, T.K. Sato, H. Brand, A. Di Nitto, R. Eichler, F. Fangli, W. Hartmann, M. Huang, E. Jäger, D. Kaji, J. Kanaya, Y. Kaneya, J. Khuyagbaatar, B. Kindler, J.V. Kratz, J. Krier, Y. Kudou, N. Kurz, B. Lommel, S. Miyashita, K. Morimoto, K. Morita, M. Murakami, Y. Nagame, H. Nitsche, K. Ooe, M. Schädel, J. Steiner, T. Sumita, M. Takeyama, K. Tanaka, A. Toyoshima, K. Tsukada, A. Türler, I. Usoltsev, Y. Wakabayashi, Y. Wang, N. Wiehl, S. Yamaki, Q. Zhi	
FORMATION OF STABLE DINITROGEN CARBONYL COMPLEXES PRODUCED IN HOT-ATOM CHEMISTRY .....	5
I. Usoltsev, R. Eichler, A. Türler, Y. Wang	
CONFIRMATION OF Cn CHEMISTRY & HINTS TO THE MISSING Fl.....	6
R. Eichler for the flerovium collaboration	
TOWARDS SELENIDES OF THE SUPERHEAVY ELEMENTS Cn AND Fl .....	7
N. M. Chiera, R. Eichler, A. Türler	
EFFECT OF SURFACE STRUCTURING ON THE MOLECULAR FLOW .....	8
P. Steinegger, R. Eichler, A. Türler	
<b>Surface Chemistry</b>	
HUMIDITY DEPENDENCE OF N <sub>2</sub> O <sub>5</sub> UPTAKE TO CITRIC ACID AEROSOL.....	9
G. Gržinić, T. Berkemeier, T. Bartels-Rausch, A. Türler, M. Ammann	
ORGANIC NITRATE FORMATION DURING GROWTH OF $\alpha$ -PINENE SECONDARY ORGANIC AEROSOL.....	10
T. Berkemeier, M. Shiraiwa, G. Gržinić, M. Ammann	
HONO RELEASE FROM PHOTOLYSIS OF NITROPHENOLS.....	11
E. De Laurentiis, D. Vione, T. Bartels-Rausch, S. Steimer, M. Ammann	
UPTAKE OF HO <sub>2</sub> RADICALS TO SECONDARY ORGANIC AEROSOLS.....	12
P.S.J. Matthews, M. Krapf, J. Slovic, J. Dommen, L.K. Whalley, T. Ingham, M.T. Baeza-Romero, D.E. Heard, M. Ammann	
RADICAL PRODUCTION FROM THE PHOTOSENSITIZATION OF IMIDAZOLES .....	13
L. Gonzalez, S. Steimer, S. Coburn, K. Coue, T. Bartels-Rausch, M. Ammann, R. Volkamer	
UPTAKE OF OZONE TO SHIKIMIC ACID FILMS AT DIFFERENT HUMIDITIES .....	14
S. Steimer, A. Huisman, U. Krieger, C. Marcolli, T. Peter, M. Ammann	
PROCESSING OF SHIKIMIC ACID PARTICLES OBSERVED VIA MICROSPECTROSCOPY: FINAL RESULTS .....	15
S. Steimer, A. Huisman, U. Krieger, C. Marcolli, T. Peter, E. Coz, G. Gržinić, M. Lampimäki, M. Ammann	

FLOW TUBE EXPERIMENTS OF OZONE UPTAKE TO MIXED SODIUM BROMIDE/CITRIC ACID SOLUTIONS.....	16
M.T. Lee, A. Türler, T. Bartels-Rausch, M. Ammann	
THE AIR-AQUEOUS INTERFACIAL COMPOSITION OF MIXED SODIUM BROMIDE / CITRIC ACID SOLUTIONS.....	17
M.T. Lee, S. Kato, M. A. Brown, J. A. van Bokhoven, A. Kleibert, M. Lampimäki, A. Türler, M. Ammann	
QUANTITATIVE DEPTH PROFILE OF A CERIA NANOCUBE CATALYST UNDER REACTIVE GAS ATMOSPHERES .....	18
S. Kato, C. Proff, T. Bartels-Rausch, M. Lampimäki, T. Huthwelker, M. Birrer, M.T. Lee, C. Paun, M. Ammann, J. A. van Bokhoven	
IN SITU XPS ANALYSIS CHAMBER FOR GAS-SOLID REACTIONS.....	19
S. Kato, T. Bartels-Rausch, C. Proff, M. Birrer, M. Lampimäki, A. Kleibert, J. A. van Bokhoven, M. Ammann	
IMPLEMENTING AUGER ELECTRON YIELD X-RAY ABSORPTION SPECTROSCOPY AT AMBIENT PRESSURE .....	20
T. Bartels-Rausch, X. Wang, J. Krempasky, M. Muntwiler, T. Huthwelker, S. Kato, M. A. Brown, J.A. van Bokhoven, M. Ammann	

## Analytical Chemistry

LATE HOLOCENE TEMPERATURE RECONSTRUCTION FOR SIBERIA.....	21
P.-A. Herren, A. Eichler, S. Brütsch, T. Papina, M. Schwikowski	
RADIATION DRIVEN MELTING AT A MONGOLIAN GLACIER.....	22
P.-A. Herren, A. Eichler, S. Brütsch, T. Papina, M. Schwikowski	
MAJOR ION CONCENTRATIONS IN THE LOMONOSOVFONNA ICE CORE.....	23
I. Wendl, S. Brütsch, A. Eichler, E. Isaksson, T. Martma, M. Schwikowski	
BLACK CARBON RECORD FROM THE LOMONOSOVFONNA ICE CORE .....	24
I. Wendl, M. Gysel, I. Budde, D. Osmont, E. Isaksson, M. Schwikowski	
RADIOCARBON ( <sup>14</sup> C) OF ORGANIC CARBON AND ELEMENTAL CARBON RECORDED IN AN ALPINE ICE/FIRN CORE OVER 1940-2002.....	25
F. Cao, Y.L. Zhang, S. Szidat, L. Wacker, M. Schwikowski	
EVIDENCE OF ENHANCED ANTIMONY POLLUTION SINCE THE EARLY SPANISH CONQUEST IN BOLIVIA ARCHIVED IN AN ILLIMANI ICE CORE .....	26
G. Gramlich, L. Tobler, A. Eichler, T. Kellerhals, M. Schwikowski	
300 YEARS OF MERCURY EMISSIONS RECORDED IN A BELUKHA ICE CORE .....	27
S. Eyrikh, A. Eichler, L. Tobler, T. Papina, M. Schwikowski	
ALTITUDE EFFECT OF DEUTERIUM EXCESS IN THE ALPINE REGION.....	28
I. Mariani, A. Eichler, T.M. Jenk, M. Schwikowski	
POLYCHLORINATED BIPHENYLS DEPOSITION HISTORY FROM THE ALPS .....	29
P.A. Pavlova, P. Schmid, C. Bogdal, M. Schwikowski	
RELEASE OF ENVIRONMENTAL POLLUTANTS BY GLACIER MELTING .....	30
P.A. Pavlova, P. Schmid, C. Bogdal, M. Jäggi, F. Anselmetti, M. Schwikowski	
TEMPERATE ICE: DATING CHALLENGES FOR THE SILVRETTA ICE CORE.....	31
T.M. Jenk, P.A. Pavlova, E. Vogel, J. Eikenberg, M. Schwikowski	
MEASUREMENT OF WATER STABLE ISOTOPES FROM THE GRENZGLETSCHER ICE CORE WITH A NEW LASER TECHNIQUE.....	32
I. Mariani, S. Brütsch, A. Eichler, M. Schwikowski	

AIR POLLUTANTS IN SNOW FROM TWO CHILEAN GLACIERS .....	33
T.M. Jenk, A. Rivera, J. Schindler, M. Schwikowski	
AN EXTRACTION SYSTEM FOR RADIOCARBON MICROANALYSES OF DISSOLVED ORGANIC CARBON (DOC).....	34
J. Schindler, S. Szidat, M. Schwikowski	
DEVELOPMENT AND FIRST APPLICATION OF A NEW METHOD FOR THE QUANTIFICATION OF GLYOXAL AND METHYLGLYOXAL IN SNOW AND ICE BY STIR BAR SORPTIVE EXTRACTION AND LIQUID DESORPTION-HPLC-ESI-MS.....	35
C. Müller-Tautges, A. Eichler, M. Schwikowski, T. Hoffmann	
STUDYING <sup>10</sup> Be VARIATIONS IN THE FIRST NON-POLAR ICE CORE - TSAMBAGARAV, MONGOLIA.....	36
F. Inceoglu, M. Faurshou Knudsen, C. Karoff, J. Olsen, P.-A. Herren, M. Schwikowski	
RECENT ACCUMULATION RATES ON FINDELENGLETSCHER DERIVED FROM AIRBORNE GPR AND FIRN CORES.....	37
L. Sold, A. Eichler, M. Hoelzle, M. Huss, M. Schwikowski	
TRITIUM FALLOUT FROM FUKUSHIMA ACCIDENT IN SWITZERLAND?.....	38
A. Eichler, J. Eikenberg, M. Rüthi, L. Sold, M. Hoelzle, M. Schwikowski	

## Radwaste Analytics

RADIOACTIVE ION BEAMS FROM ACCELERATOR WASTE A TOOL TO INVESTIGATE EXPLOSIVE STARS .....	39
R. Dressler, V. Margerin, A. StJ. Murphy, D. Schumann, C. Seiffert, T. Stora, T. Stowasser	
DETERMINATION OF THE <sup>14</sup> C CONTENT IN ACTIVATED STEEL COMPONENTS FROM A NUCLEAR POWER PLANT.....	40
D. Schumann, T. Stowasser, I. Günther-Leopold, H.P. Linder, E. Wieland, B. Volmert	
DETERMINATION OF <sup>36</sup> Cl IN REACTOR GRAPHITE .....	41
T. Stowasser, D. Schumann, H.-F. Beer, E. Hartmann, H. Kramer, C. Vockenhuber	
THERMOCHROMATOGRAPHY STUDY OF ELEMENTAL POLONIUM .....	42
E. A. Maugeri, J. Neuhausen, R. Eichler, D. Piguet, A. Vögele, D. Schumann, T. Melo Mendonça, T. Stora	
ADSORPTION OF VOLATILE POLONIUM SPECIES ON GOLD IN VARIOUS GAS ATMOSPHERES .....	43
E. A. Maugeri, J. Neuhausen, R. Eichler, D. Piguet, A. Vögele, D. Schumann	
SOLUTION ENTHALPY AND LOCAL INTERACTION OF Po AND Te WITH SOLID LEAD-BISMUTH EUTECTIC, A COMPUTATIONAL STUDY.....	44
K. Rijpstra, A. Van Yperen-De Deyne, J. Neuhausen, V. Van Speybroeck, S. Cottenier	
DETERMINATION OF THE DIFFUSION COEFFICIENT OF POLONIUM IN LEAD, BISMUTH AND THEIR EUTECTIC.....	45
S. Heinitz, J. Neuhausen, D. Schumann	
γ-SPECTROMETRY RESULTS FROM THE ANALYSIS OF THE ABSORBER FOILS IN THE EXPANSION TANK OF THE MEGAPIE TARGET .....	46
B. Hammer, A. Türler, D. Schumann, J. Neuhausen, H.P. Linder, V. Boutellier, M. Wohlmuther	
RADIOCHEMICAL DETERMINATION OF <sup>129</sup> I AND <sup>208-210</sup> Po IN THE ABSORBER FOILS OF THE MEGAPIE EXPANSION TANK .....	47
B. Hammer, A. Türler, D. Schumann, J. Neuhausen, H.P. Linder, V. Boutellier, M. Wohlmuther, C. Vockenhuber	
ANALYTICS OF α-EMITTERS <sup>146</sup> Sm, <sup>148</sup> Gd AND <sup>150</sup> Gd FROM PROTON IRRADIATED LEAD .....	48
T. Lorenz, D. Schumann, Y. Dai, A. Türler	

## Radionuclide Development

<sup>44</sup> Sc PRODUCTION DEVELOPMENT BY CYCLOTRON IRRADIATION OF <sup>44</sup> Ca FOR RADIOPHARMACEUTICAL APPLICATION .....	49
M. Bunka, A. Türler, C. Müller, J. Reber, R. Schibli, K. Domnanich, N. van der Meulen	
PRODUCTION AND EVALUATION OF THE THERAPEUTIC RADIONUCLIDE <sup>161</sup> Tb - AN ALTERNATIVE TO <sup>177</sup> Lu? .....	50
H. Dorrer, C. Müller, S. Haller, J. Reber, R. Schibli, A. Türler, N. van der Meulen	
CROSS SECTIONS OF PROTON-INDUCED REACTIONS ON <sup>152</sup> Gd AND <sup>155</sup> Gd WITH EMPHASIS ON THE PRODUCTION OF SELECTED Tb RADIONUCLIDES.....	51
G.F. Steyn, C. Vermeulen, F. Szelecsényi, Z. Kovács, A. Hohn, N. van der Meulen, R. Schibli, T.N. van der Walt	

## Environmental Radionuclides Universität Bern

TOWARDS CONTINUOUS-FLOW AEROSOL SOURCE APPORTIONMENT BY <sup>14</sup> C ACCELERATOR MASS SPECTROMETRY HYPHENATION .....	52
K. Agrios, G. Salazar, S. Szidat	
COUPLING OF AN ELEMENTAL ANALYZER WITH AMS OR FAST <sup>14</sup> C ANALYSIS OF AEROSOL SAMPLES .....	53
G. Salazar, Y.L. Zhang, S. Szidat	
<sup>14</sup> C ANALYSIS AND SAMPLE PREPARATION AT THE NEW BERN LABORATORY FOR THE ANALYSIS OF RADIOCARBON WITH AMS (LARA).....	54
S. Szidat, G. Salazar, E. Vogel, M. Battaglia, L. Wacker, H.-A. Synal, A. Türler	
<sup>14</sup> C-BASED SOURCE APPORTIONMENT OF ELEMENTAL CARBON AND ORGANIC CARBON AT A BACKGROUND SITE ON HAINAN ISLAND, SOUTH CHINA .....	55
Y.L. Zhang, J. Li, G. Zhang, P. Zotter, A.S.H. Prévôt, S. Szidat	
<sup>14</sup> C-BASED SOURCE APPORTIONMENT OF CARBONACEOUS AEROSOLS FROM WINTER SMOG EPISODES IN SWITZERLAND FROM 2008-2012 .....	56
P. Zotter, V.G. Ciobanu, Y.L. Zhang, S. Szidat, I. El-Haddad, U. Baltensperger, A.S.H. Prévôt	

List of publications.....	57
Reports and technical notes.....	63
Contributions to conferences, workshops and seminars .....	64
Public relations and outreach activities .....	76
Lectures and courses.....	78
Members of scientific committees, external activities .....	80
Doctoral/Master thesis .....	81
Awards .....	84
Summer Students.....	85
Visiting guests .....	86
Organigram .....	89
Author index .....	90
Affiliation index.....	92

## EDITORIAL

While the Paul Scherrer Institute celebrated its 25<sup>th</sup> anniversary with a lavish party, the Laboratory of Radiochemistry and Environmental Chemistry (LCH) also had reason to celebrate, as LCH's first Annual Report dates back to May 1988, the founding year of PSI.

I am also pleased to announce that LCH established a new record with more than 40 original research papers being published in 2013. This accomplishment did not go unnoticed during our most important event in 2013, the audit of LCH by an external group of renowned scientists. Thanks to the enthusiasm of our PhD students and the guidance of the group leaders, the staff scientists and technical and administrative personnel, LCH received excellent reviews. We can certainly be proud of the outcome and this should strengthen our position within the BIO department and PSI as a whole.

Without being able to do justice to all the achievements of 2013, I still would like to highlight some special events. Here, the inauguration ceremony of the new MICADAS <sup>14</sup>C accelerator mass spectrometer in Bern comes to mind, in which Joel Mesot (director of PSI), Martin Täuber (rector of UNIBE), Werner Zeller from the BAG and Martin Grosjean (director of the Oeschger center) participated, among others. This event gave LCH a lot of positive visibility and I would like to thank Sönke Szidat for making MICADAS a success, as well as Margit Schwikowski, who was instrumental in securing the necessary funds by providing one of the strong science cases for such an investment, the <sup>14</sup>C dating of glacier ice. This year's title page photograph, therefore, shows the new instrument and its associated equipment.

Our PhD students were, once again, very successful: two of the three prizes of the Bern graduate student symposium were awarded to PhD students of LCH, namely, Patrick Steinegger and Johannes Schindler. Patrick also won the best PhD presentation award at the APSORC international conference in Japan and Maruta Bunka won a poster prize at the GDCh Wissenschaftsforum Chemie in Darmstadt, Germany. In addition, a number of PhD students graduated in 2013. Congratulations, especially, go to Pierre-

Alain Herren from Margit Schwikowski's group, who graduated *summa cum laude*.

I would like to take the opportunity to introduce new personnel of our laboratory. I am happy to announce that Nicholas van der Meulen is the new group leader of Radionuclide Development, the joint group between LCH and the Center for Radiopharmaceutical Sciences at PSI (CRS). Things have progressed enormously since he arrived and, thanks to his enthusiasm, even the PSI directorate has gained a new perspective on these activities. In Bern, Oliver Leib joined our unit as a technician and he assisted Josue Moreno in outstanding work to ensure that the GMP (Good Manufacturing Practice) certificate for the radiopharmaceutical laboratory at the Insel Hospital, issued by Swissmedic, was acquired. This laboratory is now allowed to produce radiopharmaceuticals for patients, with the first patient dose already scheduled.

This year's social event took us to the open-air museum, Ballenberg, near Brienz, where we marvelled at the wonderful old houses of rural Switzerland and the technologies in use more than one hundred years ago. After a ride in a historic steam boat across Lake Brienz, we concluded the day with a dinner at Lake Thun. The more adventurous among us continued to spend the night in a cabin in the Simmental, followed by a rather strenuous hike the next day over the Kaiseregg to Schwarzsee. Fortunately, the weather on both days was perfect and swimming in the lake a special treat.

We concluded the successful 2013 with a traditional "fondue", lots of laughter and bowling in Baden.



Andreas Türler



## DECOMPOSITION STUDIES ON THE STABILITY OF TUNGSTEN- AND MOLYBDENUM CARBONYL COMPLEXES PERFORMED AT RIKEN (JAPAN)

*I. Usoltsev (Univ. Bern & PSI) for the Carbonyl collaboration*

The Sg carbonyl complex,  $\text{Sg}(\text{CO})_6$ , was estimated to be slightly more stable than the complex of its lighter homologue –  $\text{W}(\text{CO})_6$  [1]. In this work we aimed at designing an experiment to verify this prediction. Carbonyl complexes of W and Mo, as lighter homologues of Sg, were chosen for our model experiments. The gas-jet system as well as the detection system used in our work is described in detail elsewhere [2]. Two alpha-active isotopes  $^{163}\text{W}$  and  $^{164}\text{W}$  were produced in the fusion-evaporation reactions  $^{144}\text{Sm}(^{24}\text{Mg},\text{xn})^{163-164}\text{W}$ . Therefore, a  $^{144}\text{Sm}$  target was bombarded with a  $0.66 \mu\text{A}_{\text{part}}$   $^{24}\text{Mg}$  beam provided by the RIKEN Linear Accelerator (RILAC) at a centre-of-target energy of 136 MeV. By changing the target material to  $^{\text{nat}}\text{Zn}$  and adjusting the  $^{24}\text{Mg}$  beam energy to 85 MeV,  $^{87-88}\text{Mo}$  isotopes were produced. The Gas-filled Recoil Ion Separator (GARIS) allowed for an effective separation of the desired evaporation residues from the beam and from multinucleon transfer products. The separated nuclides were thermalized in a recoil transfer chamber flushed by a gas mixture of CO and He, held at 700 mbar. The formed carbonyl products were transported to the decomposition setup through a 8 m long PFA Teflon capillary. The decomposition setup consisted of a decomposition column (Fig. 1) lined by a silver foil and a bypass column of the same size made of PFA. Due to the high inertness towards carbonyl complexes the PFA bypass was implemented to quantify the actual production yield of the carbonyl complexes (100% relative yield). The carbonyls, transported through this bypass or the decomposition column were deposited at the low-temperature end of the COMPACT detector [3] according to their adsorption enthalpy and thus provided quantitative information about the production and the decomposition rates.



**Fig. 1:** Decomposition column. The fused silica 1 m long isothermal decomposition column lined (i.d. 4 mm) with a  $25 \mu\text{m}$  silver foil and heated within a steel cladding tube by means of a resistance furnace.

The decomposition curves in Fig. 2 reflect the change in the activity transported to the COMPACT detector with the changing temperature of the decomposition column. The relative yield, plotted on the y-axis, represents the ratio of the detected activity between the silver column and the PFA bypass. Not all curves recover to the 100% value, as expected from previous experiments with a  $^{252}\text{Cf}$  SF-source [4]. In case of  $\text{Mo}(\text{CO})_6$  (red curve), this effect is especially pronounced – only 40 % of the formed carbonyl complexes were passing the decomposition column at  $250^\circ\text{C}$ . The plateau value does not remain constant at

lower temperatures, but instead, as in case of  $\text{Mo}(\text{CO})_6$ , decreases to zero at  $80^\circ\text{C}$ . This observation can be explained by the formation of an active carbon layer on the silver surface at elevated temperatures. The carbon seems to originate from organic impurities on the silver foil, which decompose at elevated temperatures. Therefore, the observed pattern is a result of two processes: decomposition at elevated temperatures and adsorption on an active carbon surface at lower temperatures.

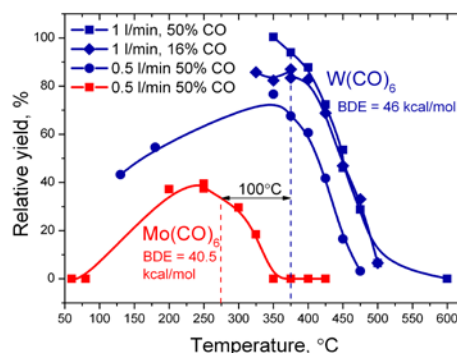


**Fig. 2:**  $^{87}\text{Mo}(\text{CO})_6$  and  $^{163-164}\text{W}(\text{CO})_6$  decomposition curves at different experimental conditions.

The shape of a decomposition curve reflects the kinetics of the decomposition process and is strongly dependent on the applied experimental conditions. The starting temperature of the decomposition on the other hand is defined by the bond dissociation energy (BDE) and is independent on the parameters of the system. Thus the applied approach shall allow for accessing the thermodynamics and the kinetics of the decomposition process. The difference of 5.5 kcal/mol between the BDEs of Mo-CO and W-CO [1] and, therefore, the higher stability of  $\text{W}(\text{CO})_6$ , allows for an experimental distinction between these two complexes. Decomposition of the transported carbonyl complexes starts at  $375^\circ\text{C}$  (see Fig. 2) regardless of the applied conditions, which is  $100^\circ\text{C}$  higher than the corresponding temperature for  $\text{Mo}(\text{CO})_6$ . Fig. 2 suggests that  $50^\circ\text{C}$  temperature interval between the start of decomposition of two given species would correspond to around 3 kcal/mol difference in BDE. Thus, we conclude that if the true BDE value of Sg-CO is around 50 kcal/mol or more, we will be able to experimentally distinguish it from  $\text{W}(\text{CO})_6$  (46 kcal/mol) using the designed setup. The carbon deposition issue can be easily solved by a suitable pre-treatment of the silver foils.

### REFERENCES

- [1] C. S. Nash and B. E. Bursten, *J. Am. Chem. Soc.* 121, 10830-10831 (1999).
- [2] J. Even et al., *Science*, in preparation (2014).
- [3] J. Dvorak et al., *GSI Sci. Rep.*, p. 183 (2004).
- [4] I. Usoltsev et al., *Ann. Rep., Lab. of Radio- & Environ. Chem., Univ. Bern & PSI*, p. 7 (2012).



# FORMATION OF STABLE DINITROGEN CARBONYL COMPLEXES PRODUCED IN HOT-ATOM CHEMISTRY

I. Usoltsev, R. Eichler, A. Türler (Univ. Bern & PSI), Y. Wang (IMP)

Dinitrogen containing carbonyl complexes of transition-metals –  $\text{Me}(\text{CO})_x(\text{N}_2)_y$  – are known for many years [1]. On average the  $\text{Me-N}_2$  bond is two times less stable than  $\text{Me-CO}$  bond; for that reason such complexes have not been isolated as pure substances at ambient conditions. In our work, we have indications for the formation of unexpectedly stable molybdenum dinitrogen carbonyl complexes, which were observed while examining the stability of  $\text{Mo}(\text{CO})_6$  on a silver surface. Here we will focus on the experimental conditions under which formation of  $\text{N}_2$ -containing complexes might take place. The ‘Ms. Piggy’  $^{252}\text{Cf}$  spontaneous fission (SF) source installed at the University of Bern allows for the production of different transition-metal fission products with a wide variety of half-lives. Volatile transition-metal carbonyl complexes were formed *in situ* by thermalizing recoiling fission fragments in a stopping chamber kept at 1.2 bar pressure and flushed at a flow rate of 1 l/min with a gas mixture containing carbon monoxide [2]. The setup used for the decomposition studies is presented in Fig. 1 and a more detailed description of the silver decomposition column is given in [3]. A charcoal trap was used for the quantitative adsorption of the transition-metal carbonyl complexes and was monitored by gamma-ray spectrometry. Decomposition curves were obtained by gradually increasing/decreasing the temperature of the decomposition column and analyzing the corresponding gamma-ray spectra of the trap.

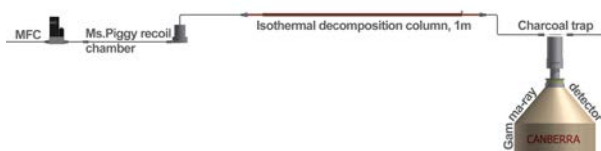


**Fig. 1:** Principal scheme of the setup used for the decomposition studies.

PFA Teflon<sup>®</sup> was found to be inert towards metal carbonyl complexes even at elevated temperatures and, for that reason, was chosen as a reference column material. Fig. 2 illustrates how the decomposition pattern of  $^{104}\text{Mo}$  volatile complexes is dependent on the concentration of CO in a  $\text{CO}/\text{N}_2$  mixture. Relative to a PFA Teflon<sup>®</sup> column of the same size and held at room temperature, the relative production yield of molybdenum carbonyl remains constant in a wide range of CO concentration – from 100% until 2.5%. However, as the carbon monoxide content decreases (0.5% and 0.1%), the observed relationship is changing dramatically – even at ambient temperature the relative yield is not recovering to the 100% value. This indicates that below 2.5% CO content only certain fraction of the transported  $^{104}\text{Mo}$  isotope corresponds to the  $\text{Mo}(\text{CO})_6$  complex, whereas another fraction must have different composition and, therefore, a different decomposition behavior on the silver surface leading to complete decomposition already at room temperature.

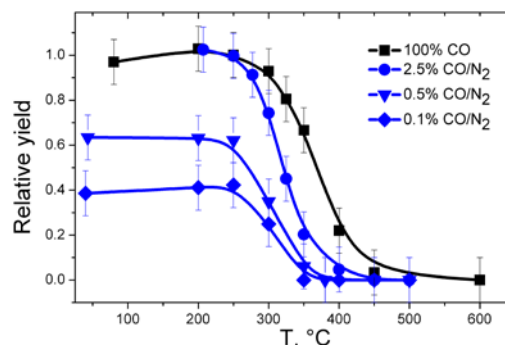


**Fig. 2:**  $^{104}\text{Mo}(\text{CO})_6$  decomposition curves at different CO contents in nitrogen carrier gas at otherwise the same experimental conditions.

The observed behavior at low CO concentration is specific for  $\text{N}_2$  as main carrier gas. Other gases such as Ar, He, or  $\text{CO}_2$  exhibit the ‘expected’ pattern, namely recovering to 100% relative yield at temperatures below 200°C. Therefore, we assume that the less stable compound produced below 2.5% CO content in nitrogen is a dinitrogen carbonyl complex. Carrier free amounts of the produced complex preclude determination of its exact composition. Therefore, we designate it as  $\text{Mo}(\text{CO})_{6-x}(\text{N}_2)_x$ . Fig. 2 indicates that by lowering the CO content from 0.5% to 0.1%, the equilibrium between molybdenum hexacarbonyl and  $\text{Mo}(\text{CO})_{6-x}(\text{N}_2)_x$  will be shifted towards the dinitrogen complex from 40% to 60%, respectively, i.e. 40% relative yield for  $\text{Mo}(\text{CO})_6$  corresponds to 60%  $\text{Mo}(\text{CO})_{6-x}(\text{N}_2)_x$ . The described approach was also applied for investigating the formation of the dinitrogen complex in the three-component gas mixture –  $\text{CO}/\text{Ar}/\text{N}_2$  (see Fig. 3). The dependence of the formation of the complex on the nitrogen partial pressure in the carrier gas mixture is clearly expressed.

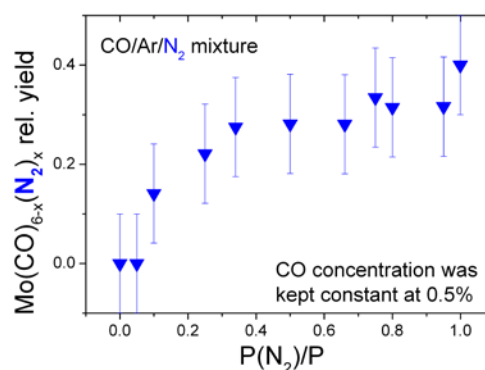


**Fig. 3:** Influence of the  $\text{N}_2$  concentration in a  $\text{CO}/\text{Ar}/\text{N}_2$  mixture on the formation of  $\text{Mo}(\text{CO})_{6-x}(\text{N}_2)_x$ .

## REFERENCES

- [1] D. Cedeno and E. Weitz, J. Phys. Chem. A 2001, 105, 3773-3787.
- [2] I. Usoltsev et al., Ann. Rep. Lab. of Radio- & Environ. Chem., Univ. Bern & PSI, p. 7 (2012).
- [3] I. Usoltsev et al., this report, p. 3.

# CONFIRMATION OF Cn CHEMISTRY & HINTS TO THE MISSING FI

R. Eichler (Univ. Bern & PSI) for the flerovium collaboration

In spring 2013 a new campaign to confirm previously observed chemical properties of superheavy elements (SHE) copernicium and flerovium has been performed. The experimental setup has been described in [1-3]. The only changes applied were: 1) the use of a new recoil chamber providing a stopping range of 6 cm from target to beam stop; 2) the use of a hot aerosol filter detached from the recoil chamber to avoid additional heating of the stopping gas; 3) the use of the PSI pure-COLD digital pile-up rejection electronics. During the experiment, two Pu-oxide targets prepared on 2  $\mu\text{m}$  Ti backings by molecular plaiting were irradiated: Experiment A:  $2.6 \cdot 10^{18}$   $^{48}\text{Ca} \rightarrow$  Target 1: 1.6  $\text{mg}/\text{cm}^2$  of  $^{244}\text{Pu}$ .  $^{242}\text{Pu} \sim 2:1$ ; Experiment B:  $1.5 \cdot 10^{18}$   $^{48}\text{Ca} \rightarrow$  Target 2: 1.8  $\text{mg}/\text{cm}^2$  of  $^{244}\text{Pu}$ .  $^{242}\text{Pu} \sim 20:1$ . In the course of Experiment A five decay chains (Fig. 1, chains 1-3, 9, and 10) have been observed and related to  $^{283}\text{Cn}$  and  $^{285}\text{Cn}$ . In the course of Experiment B as expected from the target composition (mainly  $^{244}\text{Pu}$ ) only decay chains related to  $^{285}\text{Cn}$  (Fig. 1, chains 4-8) were observed. The estimated number of random events indistinguishable from real events ( $N_R$ ) is indicated. This number changes dependent on the position of the observation in the detector due to an uneven distribution of  $^{212}\text{Po}$  emerging from the transport of volatile  $\text{PoH}_2$  [4] and from in-flight decay and deposition of  $^{220}\text{Rn}$  along the detector [1-3] and interfering mainly with the identification of  $^{285}\text{Cn}$ .

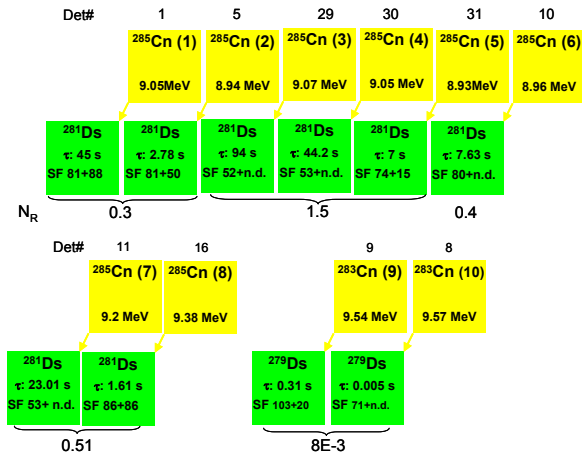


**Fig. 1:** Decay chains related to  $^{283}\text{Cn}$  and  $^{289}\text{Cn}$  observed in the experiments.

The observed thermochromatographic deposition pattern for the Cn atoms is shown in Fig. 2. The previously published adsorption data for copernicium on gold surfaces [1,2] are fully confirmed indicating the high quality of operation of the gas phase chemical experiment. The non-observation of flerovium in both experiments appears problematic. Assuming 10 pb production cross section for  $^{289}\text{Fl}$  [5,6], 8 pb for  $^{288}\text{Fl}$  [5,6], and 5 pb for  $^{287}\text{Fl}$  [6,7] in the corresponding nuclear fusion reactions, we deduce from simple yield estimations (Tab. 1) that the overall yield for Cn has

large uncertainties between 13 and 50% (Tab. 1). However, these estimations assume intact targets and stable production yields throughout the experiment, which are most likely not justified, because a severe damage of the Ti target backing was observed after the experiment. This backing is a crucial prerequisite to the successful stopping of recoiling SHE atoms in the small volume of the recoil chamber. Therefore, one explanation of this uncertainty might be related to non-stopping and implantation of evaporation residues in the recoil chamber despite its larger depth. The prediction of this stopping range is difficult because of the beam plasma induced by the intense heavy ion beam permanently passing through the chamber. Thus, the non-observation of flerovium might also be related to the shorter half-lives of the FI isotopes, which would be decisive for a possible efficient release after implantation into the beam dump.

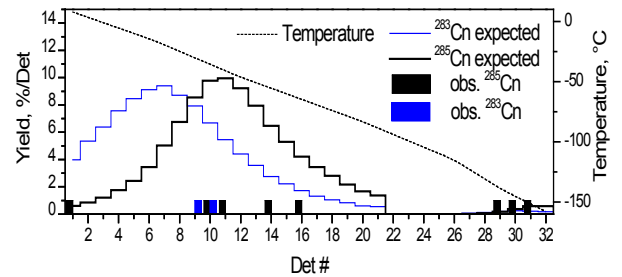


**Fig. 2:** The measured thermochromatographic distributions of  $^{283}\text{Cn}$  (blue bars) and  $^{285}\text{Cn}$  (black bars). Expected deposition patterns deduced using Monte-Carlo simulations applying the published adsorption properties of Cn are shown as stepped lines for both isotopes, respectively.

**Tab. 1:** Expected and observed number of Cn and FI atom.

SHE	Chem. yield %	N expected	N obs.	Yield (0 random) %	N expected at 13 % yield	N expected at 50 % yield
$^{289}\text{Fl}$	22	21	0	0	2.7	10.8
$^{285}\text{Cn}$	41	39	5(8)	13(20)	5.0	20
$^{288}\text{Fl}$	5	4	0	0	0.5	2.2
$^{287}\text{Fl}$	2	0.3	0	0	0.05	0.2
$^{283}\text{Cn}$	30	4	2(2)	50(50)	0.5	2.0

## REFERENCES

- [1] R. Eichler et al., Nature **447**, 72 (2007).
- [2] R. Eichler et al., Angew. Chem. Int. Ed. **47**, 3262 (2008).
- [3] R. Eichler et al., Radiochim. Acta **98**, 133 (2010).
- [4] R. Eichler, J. Phys.: Conf. Ser. **420** (1), 012003 (2013).
- [5] C. Düllmann et al., Phys. Rev. Lett. **104**, 252701 (2010).
- [6] Yu.Ts. Oganessian, J. Phys. G: Nucl. Part. Phys. **34**, R165 (2007).
- [7] P. A. Ellison et al., Phys. Rev. Lett. **105**, 182701 (2010).

## TOWARDS SELENIDES OF THE SUPERHEAVY ELEMENTS Cn AND Fl

N. M. Chiera, R. Eichler, A. Türler (Univ. Bern & PSI)

The aim of this work is to study the chemical behavior of the superheavy elements copernicium ( $Z=112$ ) and flerovium ( $Z=114$ ). Since these superheavy elements are characterized by short half-lives and low production rates, their chemical behavior has to be explored on a single atomic scale. For this purpose gas chromatography on gold surfaces was used, allowing for efficient studies of the interaction of volatile gas-phase species with stationary surfaces [1,2,3]. An experimentally exceptionally favorable case for comparative studies of Cn and Fl is the possibility of a simultaneous production of both elements in  $^{48}\text{Ca}$  induced nuclear fusion reactions with  $^{242}\text{Pu}$  and  $^{244}\text{Pu}$  [4]. Sulphur was chosen as stationary chromatography material for such comparative studies. In fact, extrapolative predictions, in which thermochemical state functions are correlated mutually, showed that both Cn and Fl may form stable sulfides and the stability trends of sulfides are predicted to be opposite in group 12 and 14 [5]. In preparation of chemical investigations of these superheavy elements, isothermal model experiments with Hg and sulfur surfaces were conducted. Although the formation of  $\text{HgS(s)}$  is thermodynamically favored ( $\Delta H_{\text{ads}}^{\text{Hg}}(\text{S}) < -75 \text{ kJ/mol}$ ), it was difficult to obtain reproducible results due to the slow interaction kinetics between the sulfur  $\text{S}_8$  rings (dominant sulfur allotrope at room temperature), and Hg. Recent studies reported amorphous nano-selenium as an efficient mercury sorbent, due to the high affinity of Se towards Hg and the high surface-to-mass ratios of the nanoparticles [6]. Hence, extrapolative predictions for the group 12 and 14 selenide formation were made. Fig. 1 shows the correlation of the standard formation enthalpies,  $\Delta H_f^{298}(\text{M})$ , of the monoatomic gaseous elements, with the standard formation enthalpies of their selenides in the solid state,  $\Delta H_f^{298}(\text{MSe})$  [7,8].

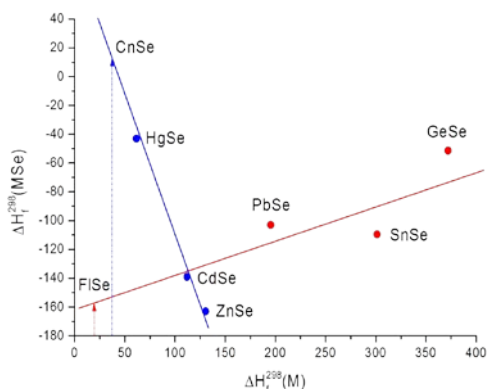


**Fig. 1:** Correlation of the formation enthalpy of selenides in group 12 (in blue) and 14 (in red) with the formation enthalpies of the mono-atomic gaseous state of the elements to depict the stability trends within the corresponding groups.

Again, stability trends in group 12 and 14 are predicted to be opposite: the formation of  $\text{FlSe}$  is expected to be favored or at least similar to the homologue selenides, while the interaction between Cn and selenium is expected to be a weak physisorption. First model experiments on the interaction of elemental Hg with red amorphous selenium surfaces, obtained through supercooling of high temperature Se vapors on quartz tubes, were performed (Fig. 2).

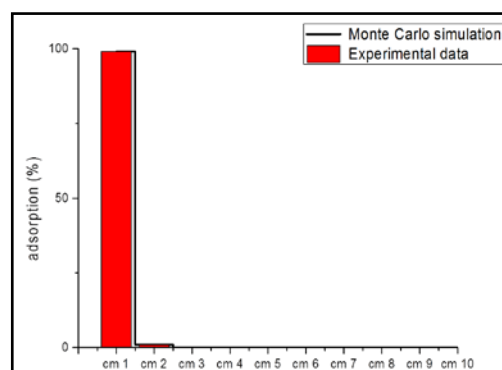


**Fig. 2:**  $^{197}\text{Hg}$  experimental deposition ( $T = 25 \text{ }^\circ\text{C}$ , 20 ml/min He gas flow) on a 10 cm selenium column. The Monte-Carlo simulations of a diffusion controlled deposition are in good agreement with the experimental data, assuming as upper interaction limit  $\Delta H_{\text{ads}}^{\text{Hg}}(\text{Se}) < -85 \text{ kJ/mol}$  for a 95% selenium surface coverage. The deposition of  $^{197}\text{Hg}$  was determined by  $\gamma$ -ray spectrometry using a HPGe-detector positioned behind a lead collimator (window size  $1.0 \times 1.0 \text{ cm}^2$ , lead thickness 1 cm).

Further experiments will be conducted in order to characterize the Se surface and its stability, as well as the Hg deposition with both off-line and on-line methods at various experimental conditions. A further step towards a future experiment with SHE will be the coverage of silicon PIN diodes with a stable homogeneous Se layer of some hundred nanometers in thickness.

## REFERENCES

- [1] M. Schädel in “The chemistry of Superheavy Elements” 2-d ed., Springer (2013).
- [2] R. Eichler et al., *Nature* **447**, 72 (2007).
- [3] R. Eichler et al., *Radiochim. Acta* **98**, 133 (2010).
- [4] Yu.Ts. Oganessian, *J. Phys. G: Nucl. Part. Phys.* **34**, R165 (2007).
- [5] N. Chiera, *Ann. Rep. Lab. of Radio- & Environ. Chem., Univ. Bern & PSI*, p. 9 (2012).
- [6] N. Ralston, *Nature Nanotech.* **9**, 527 (2008).
- [7] L. Von Szentpály, *J. Phys. Chem. A* **112**, 12695 (2008).
- [8] <http://www.hbcnetbase.com/>

# EFFECT OF SURFACE STRUCTURING ON THE MOLECULAR FLOW

*P. Steinegger, R. Eichler, A. Türlér (Univ. Bern & PSI), R. Dressler (PSI)*

## INTRODUCTION

Molecular flow dominates in evacuated systems if the mean free path of atoms and molecules is considerably larger compared to the setup dimensions. In contrast to continuum flow, where driving forces in the form of a pressure difference can be established, it seems to be very difficult to influence the transport character of a species in the molecular flow regime. Here we present results from finite element computational fluid dynamics calculations using the COMSOL Multiphysics rarefied flow package [1]. The influence of column surface onto the molecular flow was investigated for different macroscopically stepped surfaces (see Fig. 1). The columns are characterized by means of their length  $L$  to radius  $R$  ratio  $L/R$  as well as by the angles  $\theta_1$  and  $\theta_2$  of the step structure.

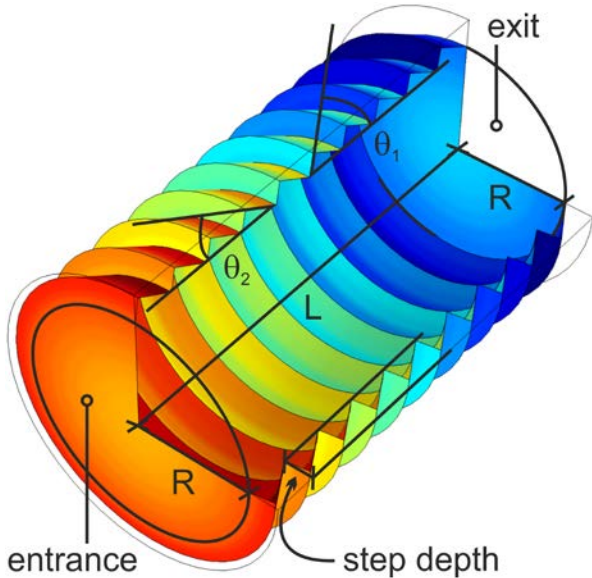


**Fig. 1:** Example of a column geometry with  $\theta_1 = 80^\circ$  and  $\theta_2 = 30^\circ$ ; the column entrance is shown in orange and the column exit is displayed in blue.

## MODEL & CALCULATION SPECIFICS

The molecular flow modelling was done by using the angular coefficient method, assuming completely diffuse scattering at all surfaces in the geometry (Knudsen's cosine law [2]). The ratio between outgoing and incident flux, results in the conductance of the corresponding column. The conductance was calculated for columns with various combinations of  $\theta_1$  and  $\theta_2$  (see Fig. 1), whereas the two angles were both ranged from  $5^\circ$  to  $80^\circ$  in steps of  $5^\circ$ . The various angle combinations result in different lengths  $L$ , while the column radius  $R$  was kept constant (10 mm). However, for angle combinations, where the values for  $\theta_1$  and

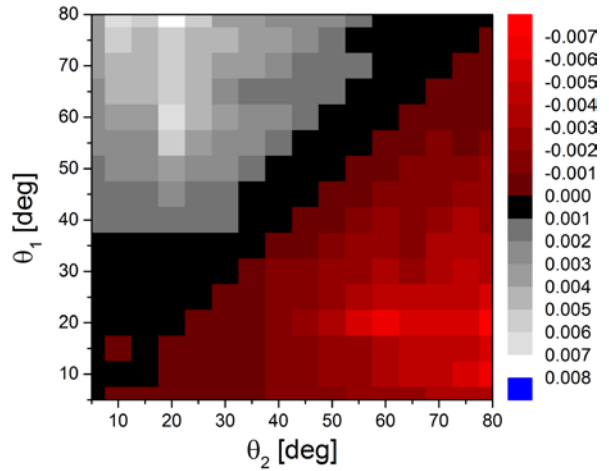


**Fig. 2:** The differences of the conductance of columns with all possible transposed angle combinations.

$\theta_2$  are transposed, the same length  $L$  and, therefore, the same  $L/R$  ratio is obtained. The only difference then is simply the opposite step symmetry. Taking the difference between the two conductance values for a certain angle combination, allows for the determination of the more favourable step geometry. In Fig. 2, the differences between the conductance values of all angle combinations are shown (symmetric appearance with a mirror axis from bottom left to top right). The number of surface steps ( $n = 10$ ) as well as the step depth (3 mm) remained unchanged during all calculations.

## CONCLUSIONS

As seen in Fig. 2, there is an obvious effect on the conductance in dependence of the step geometry. Comparing the extreme case with a shallow angle in combination with a sharp one, it is evident that in case of the steep step side facing the exit ( $\theta_1 > \theta_2$ ), the conductance is slightly larger compared to the opposite case ( $\theta_1 < \theta_2$ ). However, the absolute effect on the conductance is rather small for the investigated cases. Further, more sophisticated calculations are planned, additionally taking into account finite life times of the species under observation.

## REFERENCES

- [1] COMSOL Multiphysics® version 4.3b <http://www.comsol.com> (2013).
- [2] M. Knudsen, *Annalen der Physik.*, **28** (1909), pp. 75 - 130.

# HUMIDITY DEPENDENCE OF N<sub>2</sub>O<sub>5</sub> UPTAKE TO CITRIC ACID AEROSOL

G. Gržinić (Univ. Bern & PSI), T. Berkemeier (MPIC), T. Bartels-Rausch (PSI), A. Türler (Univ. Bern & PSI), M. Ammann (PSI)

## INTRODUCTION

Heterogeneous hydrolysis of N<sub>2</sub>O<sub>5</sub> on aqueous aerosol particles influences the night time tropospheric chemistry of nitrogen oxides [1]. We therefore studied the dependence of N<sub>2</sub>O<sub>5</sub> uptake to citric acid aerosol particles upon humidity and thus their water content. Citric acid is used as a proxy for highly oxidized and highly functionalized organic aerosol constituents. In this system water not only participates in the chemical reaction (cf. Fig. 1), but also influences the physico-chemical properties of the organic matrix such as the viscosity. We thus attempt to parameterize the humidity-dependence using several sources of viscosity data

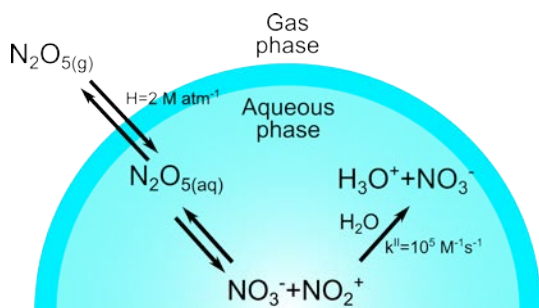


Fig. 1: Mechanism of N<sub>2</sub>O<sub>5</sub> uptake to aerosol particles

## EXPERIMENTAL

In our experiments we used the short-lived radioactive tracer <sup>13</sup>N produced at PSI's PROTRAC facility [2]. <sup>13</sup>NO from PROTRAC is mixed with non-labeled NO and O<sub>3</sub> in a gas flow reactor where N<sub>2</sub>O<sub>5</sub> is synthesized under dry conditions. The N<sub>2</sub>O<sub>5</sub> flow is fed into an aerosol flow tube and mixed with a humidified aerosol prepared by ultrasonic nebulization of a citric acid solution. The length of the aerosol flow tube can be adjusted via movable inlets. A Scanning Mobility Particle Sizer (SMPS) system is placed behind the aerosol flow tube to characterize the aerosol. The remaining gas flow is then directed into a parallel plate diffusion denuder system, where the gaseous species can be selectively separated. The aerosol particles are trapped at the end of the denuder system with a particle filter. Scintillation counters placed on the denuder plates and the particle filter are used to monitor the radioactivity of the trapped <sup>13</sup>N labeled species.

## RESULTS

Fig. 2 shows the measured uptake coefficients for citric acid together with literature values for some other polycarboxylic acids [3]. A parameterization of the humidity dependence of N<sub>2</sub>O<sub>5</sub> uptake to citric acid has been attempted using the resistor model formulation presented in Eq. 1 [3].

$$\gamma = \left\{ \frac{1}{\alpha_b} + \frac{c}{4HRT(D_l k^{II} [H_2O])^{0.5}} \left[ \coth\left(\frac{r}{l}\right) - \left(\frac{l}{r}\right) \right] \right\}^{-1}$$

Eq. 1: Parameterization of the uptake coefficient of N<sub>2</sub>O<sub>5</sub> on aqueous aerosol particles.

In Eq. 1,  $\alpha_b$  denotes the bulk accommodation coefficient,  $H$  the Henry's Law constant,  $R$  the gas constant,  $T$  the temperature,  $D_l$  the liquid phase diffusion coefficient,  $k^{II}$  the apparent liquid phase rate constant between N<sub>2</sub>O<sub>5</sub> and water,  $r$  the particle radius and  $l$  the reacto-diffusive length. The major source of uncertainty appears to be  $D_l$ . We have estimated its value from previously published data of viscosity of citric acid [4]. New measurements (J. Reid, personal communication) and an estimate based on comparison to sucrose substantially differ from the older data. The variability in the uptake data does not allow constraining this further.

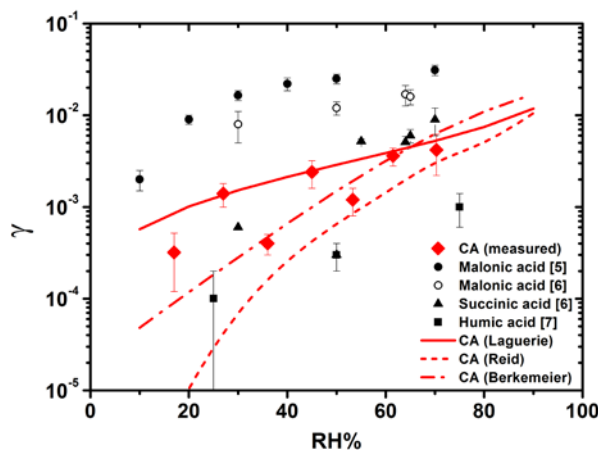


Fig. 2: Comparison of uptake coefficients for citric acid (CA, red symbols) with those for other polycarboxylic acids (black symbols) and with the parameterization for the dependence of uptake to citric acid on humidity (lines).

## ACKNOWLEDGEMENT

This work has been supported by the Swiss National Science Foundation (grant no. 130175).

## REFERENCES

- [1] Chang, W. L., et al., *Aerosol Sci. Technol.*, **45**, 665 (2011).
- [2] Ammann, M., *Radiochim. Acta*, **89**, 831 (2001).
- [3] Ammann, M., et al., *Atmos. Chem. Phys.*, **13**, 8045–8228 (2013).
- [4] Laguerie, C., et al., *J. Chem. Eng. Data*, **21** (1), 85–87 (1976).

# ORGANIC NITRATE FORMATION DURING GROWTH OF $\alpha$ -PINENE SECONDARY ORGANIC AEROSOL

T. Berkemeier, M. Shiraiwa (MPIC), G. Gržinić, M. Ammann (PSI)

## INTRODUCTION

Secondary organic aerosol (SOA) particles are formed by oxidation of volatile organic precursors by atmospheric oxidants such as ozone,  $\text{NO}_3$  and OH radicals. Nitrogen oxides ( $\text{NO}$ ,  $\text{NO}_2 \equiv \text{NO}_x$ ) have been shown to affect the underlying chemistry by formation of organic nitrates [1,2] (cf. Fig. 1) and thus alter the total mass yield. However, the formation and partitioning of nitrogen containing compounds into SOA particles is still poorly understood. Our collaboration unites a suitable experimental method available at PSI and new advances in the numerical description of growing particulates to unravel the kinetics of the process. The numerical simulations will be based on the Master Chemical Mechanism (MCM) [3] used with the kinetic flux model KM-GAP [4] that accounts for mass transport from the gas phase to the particle bulk and chemical reaction along the way.

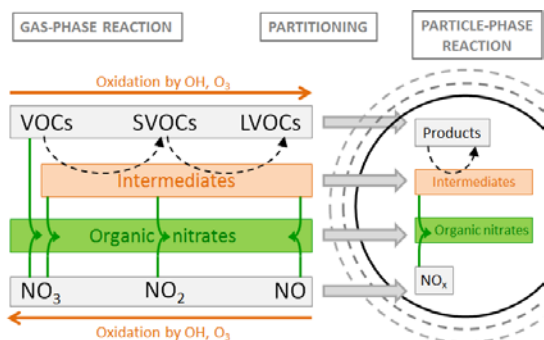


**Fig. 1:** Schematic representation of SOA formation, involving oxidation of volatile organic compounds (VOCs) to semi and low volatility organic compounds (SVOCs and LVOCs), which partition into the particle phase (grey arrows). Intermediates may react with nitrogen oxides to form organic nitrates in both, gas and particle phase (green arrows).

## EXPERIMENTAL

We used the short-lived radioactive tracer  $^{13}\text{N}$  [5] to quantify the amount of organic nitrates produced and retained in SOA particles. SOA particles are produced from ozonolysis of  $\alpha$ -pinene in presence of  $^{13}\text{NO}$  in an aerosol flow tube system. The length of the aerosol flow tube can be adjusted via movable inlets. A Scanning Mobility Particle Sizer (SMPS) system is placed behind the aerosol flow tube to determine the size distribution. The remaining gas flow is then directed into a detection system that separates gas and particle phase species and detects the trapped labelled nitrogen compounds via scintillation counters.

## RESULTS

SOA formation measurements have been conducted

under varying conditions with respect to relative humidity ( $< 5 - 80\%$  RH) and  $\text{NO}_x$  levels (0-100 ppb) as a function of residence time in the flow tube. While high  $\text{NO}_x$  levels decreased the total SOA mass, a direct effect of RH was not observed. Figure 2 shows the evolution of total SOA mass and the  $^{13}\text{N}$  signal detected at the particle filter for a typical experiment.

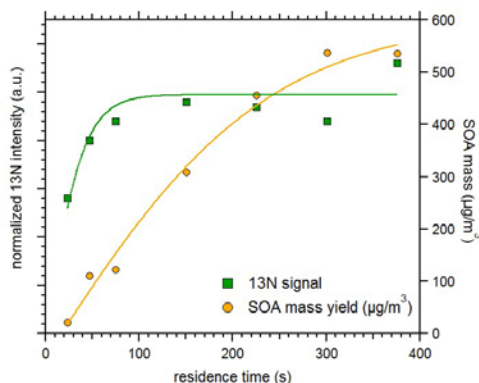


**Fig. 2:** SOA mass (orange circles) and normalized  $^{13}\text{N}$  signal (green squares) in the particle phase as function of residence time in the flow tube reactor. The solid lines are to guide the eye.

Both quantities tend to reach a plateau. However, the  $^{13}\text{N}$  signal in the particle phase is consistently seen to reach its plateau well before the total SOA production has leveled off, indicating rapid formation of organic nitrates only in the early stages of the process. Possible explanations include depletion of nitrogen oxides (removal by oxidation to organic nitrates or  $\text{NO}_3$ ) or a higher tendency of first and second generation intermediates to form organic nitrates. We plan to further investigate this issue using the KM-GAP model coupled with MCM.

## ACKNOWLEDGEMENT

We thank M. Birrer and A. Arangio for their help in experiments and U. Pöschl for support. This work is supported by Max Planck Society. M. A. appreciated support by the Swiss National Science foundation (grant 130175).

## REFERENCES

- [1] Ziemann, P.J., and Atkinson, R., *Chem. Soc. Rev.*, 41, 6582–6605 (2012).
- [2] Renbaum, L. H., and Smith, G. D., *Phys. Chem. Chem. Phys.*, 11, 8040–8047 (2009).
- [3] Shiraiwa *et al.*, *Atmos. Chem. Phys.*, 12, 2777–2794 (2012).
- [4] Saunders *et al.*, *Atmos. Chem. Phys.*, 3, 161–180 (2003).
- [5] Ammann, M., *Radiochim. Acta*, 89, 831 (2001).

## HONO RELEASE FROM PHOTOLYSIS OF NITROPHENOLS

*E. De Laurentiis, D. Vione (Univ. Torino), T. Bartels-Rausch, S. Steimer, M. Ammann (PSI)*

### INTRODUCTION

Aromatic organic compounds are omnipresent in the environment and significantly participate in the photochemistry in aerosols and in the aquatic environment. Nitrophenols have been of particular interest, ever since their phototoxic properties have been related to the forest decline [1].

This integrated research project aims at the complete description of the photochemical products, rates, and transition states of nitro phenols in solutions. Here we report first results on detailed kinetic experiments on the nitrite yields from the photolysis of 4-nitrophenol.

Nitrophenols have been detected in aerosols and in surface waters with concentrations of up to 100 micrograms per liter. Their sources include emissions from the combustion of coal and wood and from industrial processes, as well as the in-situ formation in the atmosphere. Nitrite is a major chromophore in surface waters influencing the fate of other toxins in open waters. It is further of concern, because it can be released to the atmosphere in its protonated form (HONO). In the gas phase, HONO is a source of hydroxyl radicals which contribute to the oxidative capacity of the atmosphere.

Until now, yields and mechanisms of the photochemistry of nitro phenols are not entirely clear.

### EXPERIMENTAL

Central to the set-up is a coated wall flow tube at atmospheric pressure that allows precise determination of the kinetic rates of photolytic experiments (Fig. 1).



**Fig. 1:** Photolysis reactor. The reactive solution covers the inner wall of a temperature controlled flow tube.

Reactive films were prepared by applying 275  $\mu$ L of a solution of  $1 \times 10^{-4}$  M 4-nitrophenol and 3 M citric acid to the inner surface of a quartz tube. Upon irradiation with UV light, the produced HONO was constantly removed from the reactor by a 1 l/min nitrogen flow and quantified using a long path absorption spectrometer (LOPAP).

The citric acid is chemically inert and serves to dilute the nitro phenol in the reactive films and has well-established water content as a function of humidity.

### RESULTS

Photolysis of diluted films of 4-nitrophenol with UV light leads to an instantaneous emission of HONO into the gas phase. This fast response suggests that HONO is a direct product from the photolysis of the nitro phenol (Fig. 2).

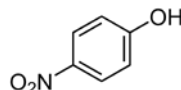


**Fig. 2:** Molecular scheme of 4-nitrophenol.

The observed emissions of HONO from the liquid films revealed a pronounced pH dependence. At a low pH of 3, the release is characterized by a strong initial emissions which slowly decline to reach a steady level. At neutral pH the emissions are lower, but stable over the photolysis time of 1 h. Since under neutral conditions, the majority of nitrite remains unprotonated. It is likely that the dynamics of HONO release is controlled by local pH changes, the buffering capacity, and also the viscosity of the citric acid films.

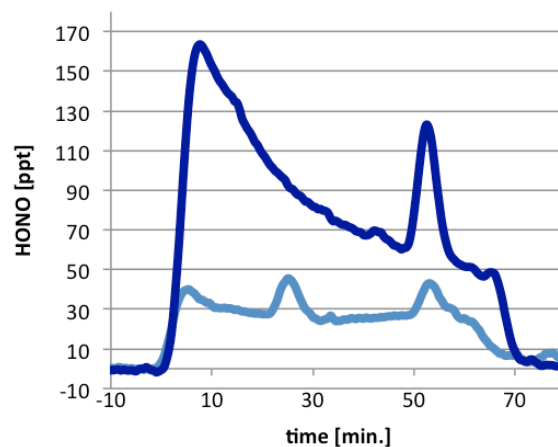


**Fig. 3:** Release of HONO at pH 3 (dark blue) and pH 7 (light blue).

### ACKNOWLEDGEMENT

The PhD grant of EDL is financially supported by Progetto Lagrange - Fondazione CRT.

### REFERENCE

- [1] I. Bejan, et al., Phys. Chem. Chem. Phys., **8**, 2028 (2006).

## UPTAKE OF HO<sub>2</sub> RADICALS TO SECONDARY ORGANIC AEROSOLS

*P.S.J. Matthews (Univ. Leeds), M. Krapf, J. Slovic, J. Dommen (PSI/LAC), L.K. Whalley, T. Ingham (Univ. Leeds), M.T. Baeza-Romero (Univ. Castilla la Mancha), D.E. Heard (Univ. Leeds), M. Ammann (PSI)*

### INTRODUCTION

HO<sub>x</sub> radicals play an important role in the atmosphere by controlling the oxidative capacity of the troposphere, with HO<sub>2</sub> acting as a short-lived reservoir for OH. However, there have been significantly lower measured HO<sub>2</sub> concentrations during several field campaigns than predicted by box models [1,2]. These differences have often been attributed to uptake by aerosols. To our knowledge there are currently no HO<sub>2</sub> uptake studies onto secondary organic aerosols (SOA) published in the literature. Therefore, the aim of this study was to measure the HO<sub>2</sub> uptake coefficient onto two different types of SOA derived from α-pinene (a biogenic alkene) and trimethylbenzene (an aromatic which can result from combustion of fossil fuels).

### EXPERIMENTAL

α-pinene or trimethylbenzene were injected into the main 27 cubic meter smog chamber at PSI. Aerosols were then formed in the PAM (Potential Aerosol Mass) chamber and pumped through the experimental setup which is shown in Fig. 1. Reactive gases were removed by passing the flow from the chamber through a charcoal denuder and also through either two or three cobalt oxide denuders to remove nitrogen oxide species. The chamber flow then either passed through a filter in order to remove all particles or else completely bypassed the filter in order to obtain the maximum aerosol surface area. The aerosol surface area was measured using a Scanning Mobility Particle Sizer (SMPS).

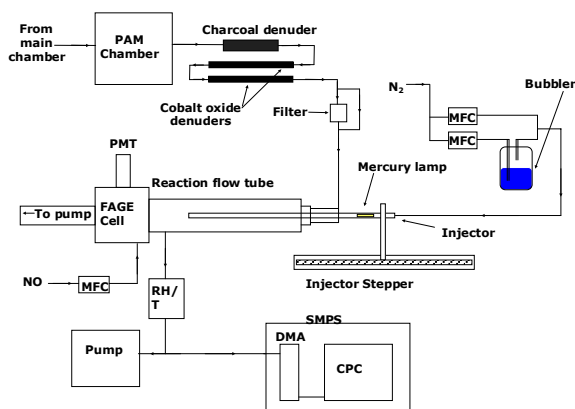


**Fig. 1:** Experimental setup

The HO<sub>2</sub> radicals entered the reaction flow tube out of the end of a moveable injector and were measured using a sensitive Fluorescence Assay by Gas Expansion (FAGE) cell [3].

HO<sub>2</sub> uptake coefficients were measured at room temperature and at pressures in the range of 910 – 940 mbar by moving the injector forwards and backwards

along the flow tube. The HO<sub>2</sub> loss along the flow tube in the presence and absence of aerosols was analyzed assuming first order kinetics:

$$\ln [\text{HO}_2] = \ln [\text{HO}_2]_0 - k_{\text{obs}}t$$

The HO<sub>2</sub> uptake coefficient ( $\gamma_{\text{obs}}$ ) was then obtained by the equation:

$$k_{\text{obs}} = (\gamma_{\text{obs}} w_{\text{HO}_2} S) / 4$$

where  $w_{\text{HO}_2}$  is the molecular thermal speed of HO<sub>2</sub> and  $S$  is the total surface area of the aerosols

### RESULTS

The HO<sub>2</sub> uptake coefficients were measured as  $\gamma < 0.001$  for SOA derived from α-pinene and  $\gamma = 0.004 \pm 0.003$  for SOA derived from trimethylbenzene. The low uptake for α-pinene aerosols may be due to low liquid water content in the aerosols whereas the value for trimethylbenzene was comparable to an uptake coefficient of  $0.003 \pm 0.002$  measured for ammonium sulphate aerosols under the same conditions.

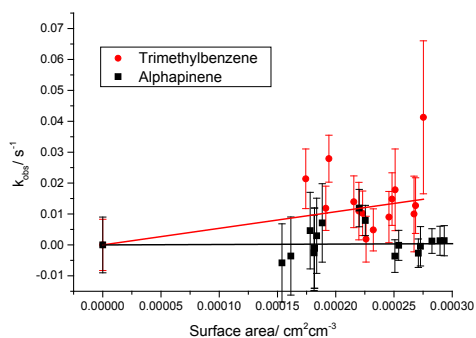


**Fig. 2:** First order loss rate for HO<sub>2</sub> radical loss onto alphapinene and trimethylbenzene SOA.

### ACKNOWLEDGEMENT

This work was supported by the Swiss National Science Foundation (grant no 130175). P.S.J Matthews is grateful to NERC for the award of a studentship. Support of these experiments by M. Birrer, S. Steimer, G. Grzanic and T. Bartels-Rausch is appreciated.

### REFERENCES

- [1] Sommariva et al., *Atmos. Chem. Phys.* **6**, 1135-1153 (2006).
- [2] Kanaya et al., *J. Geophys. Res.-Atmos.* **105**, 24205-24222 (2007).
- [3] Heard et al., *Annual Rev. Phys. Chem.* **57**, 191-216 (2006).

# RADICAL PRODUCTION FROM THE PHOTOSENSITIZATION OF IMIDAZOLES

L. Gonzalez (CU), S. Steimer (PSI), S. Coburn (CU), K. Coue, T. Bartels-Rausch, M. Ammann (PSI), R. Volkamer (CU)

## INTRODUCTION

$\text{HO}_x$  radicals play an important role in the photochemistry of the atmosphere. They largely control the oxidative capacity of the troposphere. This project studies the  $\text{HO}_x$  radical production from the photochemistry of imidazole-2-carboxaldehyde (IC). IC and other imidazoles form as products from the multi-phase chemistry of glyoxal and ammonium sulphate in aqueous aerosols [1,2]. Imidazoles are light absorbing materials and can behave as photosensitizers [1,3]. In aerosols these photosensitizers can autophotocatalyze SOA growth [3]. To our knowledge, ours is the first study of  $\text{HO}_x$  radical production from imidazoles.

## EXPERIMENTAL

A set of experiments were designed and conducted to investigate the radical production from IC photochemistry in a citric acid (CA) matrix. Experiments were performed in a photochemical flow tube reactor at PSI, where IC/CA films were exposed to a stream of NO ( $\sim 1$  ppmv) in  $\text{N}_2/\text{O}_2$  at atmospheric pressure.  $\text{NO}_2$  and HONO production were observed under variable relative humidity (RH) conditions, imidazole concentration and light intensity. Radicals were measured indirectly via sensitive measurements of  $\text{NO}_2$  by University of Colorado Cavity-Enhanced Differential Optical Spectroscopy (CU-CE-DOAS) [4] and HONO by the PSI Long-Path Absorption Photometer (LOPAP). The peroxy radical chemical amplification (PerCA) method (added CO) was employed during selected experiments, and light intensity inside the flow tube was measured by  $\text{NO}_2$  actinometry.

## PRELIMINARY RESULTS

Fig. 1 shows exemplary raw data as measured by the CE-DOAS and LOPAP. The observed formation of  $\text{NO}_2$  and HONO follows the light intensity. In most cases, the produced  $\text{NO}_2$  increased with increasing IC concentration and RH (0-30%, not shown). At about 50% RH the  $\text{NO}_2$  concentration remained flat, i.e.,  $\text{NO}_2$  did no longer increase as RH was increased further. A reaction mechanism that explains our observations is shown in Fig. 2.

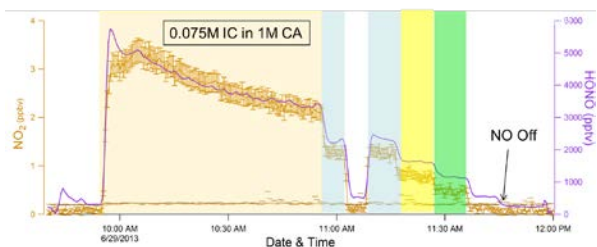


**Fig. 1:** Time series of  $\text{NO}_2$  and HONO without chemical amplification and  $\sim 1$  ppmv NO; pink (7 lamps), blue (4 lamps), yellow (2 lamps), green (1 lamp).

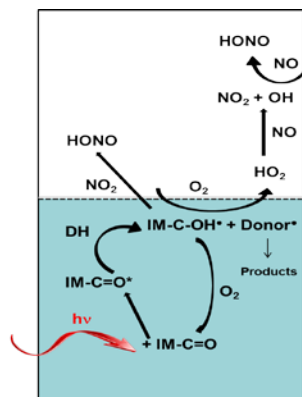


**Fig. 2:** Proposed mechanism, modified and expanded to photosensitization of IC based on refs [5,6]. The reaction in the white square represents the gas-phase, and the blue square represents the aqueous phase. DH is H-donor (e.g. CA, another IC,  $\text{H}_2\text{O}$ ,  $\text{H}_2\text{O}+\text{CA}$  matrix).

The likely fate of the excited IC is to transfer an H atom from a donor (e.g., CA) to  $\text{O}_2$  yielding  $\text{HO}_2$  and recycling the IC.  $\text{HO}_2$  thus produced reacts with the excess NO to form  $\text{NO}_2$  that is measured. HONO may form in the reaction of NO with OH produced in the reaction of  $\text{NO} + \text{HO}_2$  or with OH directly produced in the film (not shown). HONO may also form if H atom transfer occurs to  $\text{NO}_2$ .

In conclusion,  $\text{HO}_2$  and possibly OH radicals are produced from the photochemistry of IC in the CA+ $\text{H}_2\text{O}$  matrix. Notably, OH could form as co-product to  $\text{HO}_2$  if  $\text{H}_2\text{O}$  in the CA/ $\text{H}_2\text{O}$  matrix acts as H-donor DH. A more detailed analysis will have to disentangle the other contributions to radical production. Further experiments are planned to investigate different conditions, and other imidazole species.

## ACKNOWLEDGEMENT

R.V. acknowledges funding by the US National Science Foundation under CAREER award ATM-847793. S. S. and M.A. appreciate the contribution by the EU project PEGASOS and the Swiss National Science Foundation (grant 130175).

## REFERENCES

- [1] Kampf et al., Atmos. Chem. Phys., **12**, 6323-6333, 2012.
- [2] Yu et al., et al., Environ. Sci. Technol., 2011, **45** 6336–6342
- [3] Aregahegn et al., Faraday Discussions, DOI: 10.1039/C3FD00044C, 2013.
- [4] Thalman and Volkamer, Atmos. Meas. Tech., **3**, 1797-1814, 2010.
- [5] Canonica et al., Environ. Sci. Technol., **29**, 1822-1831, 1995.
- [6] George et al., Faraday Discussions., **130**, 195-210, 2005.

# UPTAKE OF OZONE TO SHIKIMIC ACID FILMS AT DIFFERENT HUMIDITIES

*S. Steimer (ETHZ & PSI), A. Huisman, U. Krieger, C. Marcolli, T. Peter (ETHZ), M. Ammann (PSI)*

## INTRODUCTION

Recent findings show that organic particulate matter is capable of forming amorphous solids or semi-solids under atmospheric conditions [1]. Such particles are highly viscous and have low diffusivity within the bulk. This likely slows down chemical reactions in the bulk, thereby increasing the lifetime of these organic compounds. Indications of such behavior were recently found for the reaction of thin protein films with ozone [2] and the formation of organonitrogen compounds [3]. To investigate the influence of the physical state on reactivity we measured the uptake of ozone to shikimic acid in a coated wall flow tube.

## EXPERIMENTAL

A glass tube was coated with a thin film of shikimic acid and conditioned with humidified N<sub>2</sub> at 85% RH (relative humidity). The tube was inserted into the flow system (Fig. 1) while no O<sub>3</sub> was produced. At this point, the injector is in position (a) where the film is not exposed to the injector gas flow when O<sub>3</sub> production is resumed to passivate the system. After equilibrating the film to the humidity of the system, the injector was set to position (b) which exposes the shikimic acid film to O<sub>3</sub>. The injector was moved back to its initial position once during the experiment and again at its end to control for drift in the baseline O<sub>3</sub> concentration. The experiment was performed at six different humidities (0-92%) with an O<sub>3</sub> concentration of 178 ppb and four different O<sub>3</sub> concentrations each (90-1984 ppb) at two different humidities.

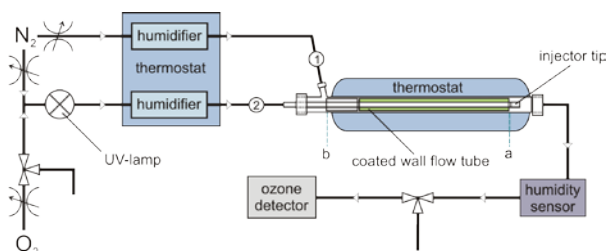


**Fig. 1:** Setup of the flow system. Flow (1) is the N<sub>2</sub> sheath flow. The O<sub>3</sub> containing flow (2) enters the flow tube casing through the injector tip. Position (a): no O<sub>3</sub> flow through the flow tube. Position (b): shikimic acid film exposed to O<sub>3</sub>.

## RESULTS

The uptake coefficient  $\gamma$  is the net flux of O<sub>3</sub> into the shikimic acid film normalized to the gas kinetic collision flux and is obtained from the measured loss of O<sub>3</sub> over the length of the film. Fig. 2 shows the uptake coefficient of O<sub>3</sub> on shikimic acid over exposure time at 24% and 92% RH at four different O<sub>3</sub> concentrations each.

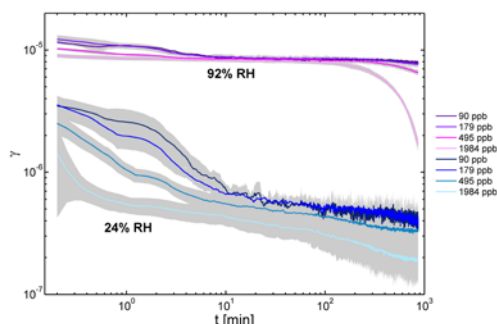


**Fig. 2:** Evolution of the uptake coefficient  $\gamma$  over time for four different O<sub>3</sub> concentrations each at 24% and 92% RH. The standard deviation of repeated measurements is shown in grey.

The uptake proceeds in at least two stages, with an initial plateau followed by a lowered long-term uptake (>16 h). Regardless of concentration, measurements at 92% RH show a higher uptake than at 24% RH. This trend of increasing uptake with increasing humidity is confirmed by further measurements at 0%, 45%, 70%, and 84% RH (not shown). In total, the long-term uptake varies over more than one order of magnitude from  $4 \cdot 10^{-5}$  at 0% RH to  $8 \cdot 10^{-6}$  at 92% RH. Due to water's function as a plasticizer, this can be seen as indication of the relation of physical state and reactivity. Comparing measurements at the same humidity, the initial plateau is clearly dependent on the gas phase O<sub>3</sub> concentration. This points to the initial stage of the reaction being dominated by a Langmuir-Hinshelwood type surface reaction. At high humidity and high O<sub>3</sub> concentration, the long-term uptake decreases significantly. This is due to depletion of the shikimic acid in the film. Further interpretation of the results will be facilitated by using KM-SUB, a multi-layer kinetic model.

## ACKNOWLEDGEMENT

This work is supported by the EU FP7 project PEGASOS.

## REFERENCES

- [1] A. Virtanen et al., *Nature*, **467**, 824 (2010).
- [2] M. Shiraiwa et al., *Proc. Natl. Acad. Sci.*, **108**, 11003 (2011).
- [3] M. Kuwata and S. T. Martin, *Proc. Natl. Acad. Sci.*, **109**, 17354 (2012).

## PROCESSING OF SHIKIMIC ACID PARTICLES OBSERVED VIA MICROSPECTROSCOPY: FINAL RESULTS

S. Steimer (ETHZ & PSI), E. Coz (CIEMAT), G. Gržinić (Univ. Bern & PSI), M. Lampimäki, M. Ammann (PSI)

### INTRODUCTION

Organic constituents of atmospheric aerosols can be solid or semi-solid under atmospheric conditions [1]. Since chemical aging of aerosols changes their physical and chemical properties [2], it is important to understand how this process might be affected by their physical state. In the present work we study the chemical aging of shikimic acid particles under ozone exposure at different humidities. Shikimic acid is a plant metabolite and has been observed in biomass burning particles. It has an endocyclic double bond. The process was monitored *in situ* using scanning transmission X-ray microscopy (STXM) and near edge X-ray absorption fine structure spectroscopy (NEXAFS).

### EXPERIMENTAL

Shikimic acid particles were generated from solution using an ultrasonic nebulizer. The generated particles were dried, selected for size and then impacted on a silicon nitride membrane. The membranes were then placed in an environmental micro reactor [3], which was used to adjust relative humidity during the experiment (12%-82% RH) and facilitate *in situ* exposure to ozone. All STXM and NEXAFS experiments were conducted at the PolLux beamline at the Swiss Light Source (SLS).

### RESULTS

The carbon K-edge spectra for shikimic acid particles show a clear decrease of the shikimic acid double bond peak at 284.4 eV upon oxidation. For the same ozone dose, the decrease is faster at higher humidities (Fig. 1). Since water acts as a plasticizer for shikimic acid, this can be seen as an indication of the relation of physical state and chemical ageing. The oxidation proceeds homogeneously (Fig. 2) but in a size dependent manner, with smaller particles reacting faster. This is apparent from Fig. 2c, where in the smaller particle shikimic acid is depleted more strongly after the same exposure to ozone. Combining this information leaves three different options for the progress of the reaction: a) there is no gradient within the particle bulk. However, due to the size dependence we know that there the reaction occurs at or close to the surface; b) there is a gradient, but it is below the spatial resolution of the measurement (i.e., confined to a very thin layer near the surface of the particles); or c) there is a gradient, but it is below the time resolution of the measurement, meaning that it may have smoothed out again during the time scale of the acquisition of the image stacks.

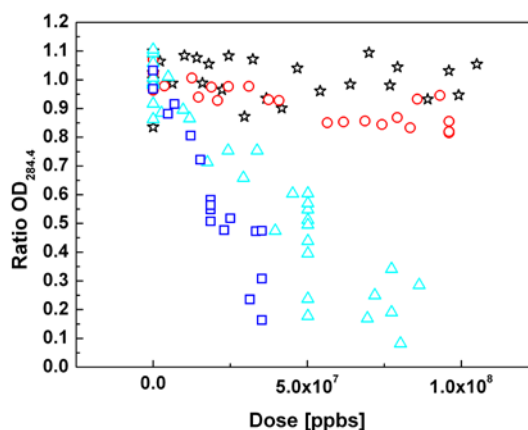


**Fig. 1:** Depletion of shikimic acid as a function of  $O_3$  dose via the decrease in the normalized OD at 284.4 eV at four different relative humidities: 12% RH (black stars), 52% RH (red circles), 71% RH (light blue triangles) and 82% RH (blue squares).

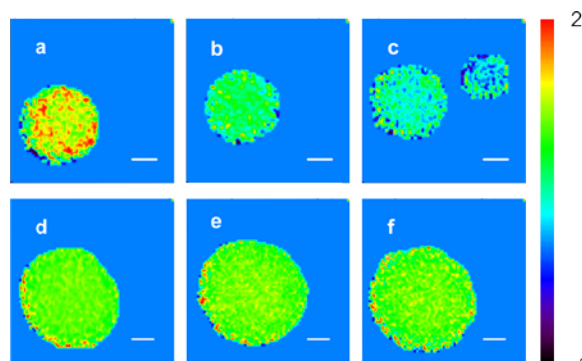


**Fig. 2:** Depletion of shikimic acid via the decrease of OD at the maximum of the  $1s-\pi^*$  transition peak normalized to total carbon. Images a to c show the progress of the reaction for different particles at 71% RH and  $O_3$  doses of 0 ppbs (a),  $5.0 \cdot 10^7$  ppbs (b) and  $7.7 \cdot 10^7$  ppbs (c). Images e to g show the progress of the reaction at 13% RH with  $O_3$  doses of 0 ppbs (d),  $1.4 \cdot 10^7$  ppbs (e) and  $7.9 \cdot 10^7$  ppbs (f).

### ACKNOWLEDGEMENT

We would like to acknowledge B. Watts and J. Raabe for their technical support at the Pollux beamline. This work is supported by the EU FP7 project PEGASOS.

### REFERENCES

- [1] A. Virtanen et al., *Nature*, **467** (2010), p.824-827.
- [2] Y. Rudich et al., *Chem. Rev.*, **103**, 5097 (2003).
- [3] T. Huthwelker et al., *Rev. Sci. Instrum.*, **81**, 113706 (2010).

# FLOW TUBE EXPERIMENTS OF OZONE UPTAKE TO MIXED SODIUM BROMIDE/CITRIC ACID SOLUTIONS

*M.T. Lee, A. Türler (Univ. Bern & PSI), T. Bartels-Rausch, M. Ammann (PSI)*

## INTRODUCTION

The ozone budget in the marine boundary layer has remained a hot topic in the atmospheric chemistry community [1]. The reaction of ozone ( $O_3$ ) with bromide ( $Br^-$ ) at the aqueous solution – air interface is part of the processes contributing to the budgets of bromine and  $O_3$  [2-3]. Recently, the fact that the ocean surface carries a layer consisting of a wealth of organic compounds deriving from marine biota has received a lot of attention, and the impact of these organics on marine halogen chemistry remained unclear [4].

Here we present results of uptake kinetics experiments of  $O_3$  to a mixed solution of sodium bromide (NaBr) and citric acid (CA) with the coated wall flow tube technique.

## EXPERIMENTAL

A commonly used laboratory technique to derive kinetic information of trace gas - aqueous interactions in is the coated wall flow tube (Fig. 1.). It offers the advantage that trace gases are exclusively exposed to the liquid surfaces and thus the results are not disturbed by interactions with the wall material of the sample holder as long as the film thickness is larger than the reactive diffusive length. On the other hand it is limited to liquids viscous enough that the films remain stable over the duration of experiments. Coatings were prepared by applying the precursor solution to the inner wall of the flow tube and equilibrate it to the humidity of the experiment while continuously rotating it to achieve a smooth homogeneous film. For the mixed solutions, we used the hygroscopic properties of NaBr and CA and additivity rules to calculate the water content of the film [5].

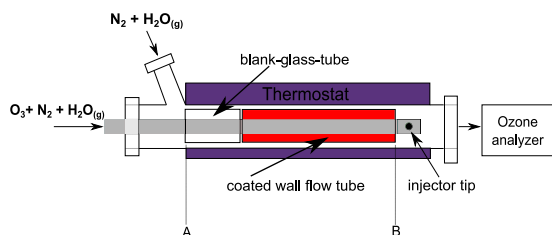


**Fig. 1:** A schematic diagram of the flow tube system used in experiments of  $O_3$  uptake to the coated film.

## RESULTS

The uptake coefficient  $\gamma$ , i.e., the measured loss rate of  $O_{3(g)}$  normalized to the gas kinetic collision rate, is shown in Fig. 2 for three different NaBr to CA mixing ratios and as a function of the  $O_3$  concentration. We also try to reproduce results and compare them with previous year's results.

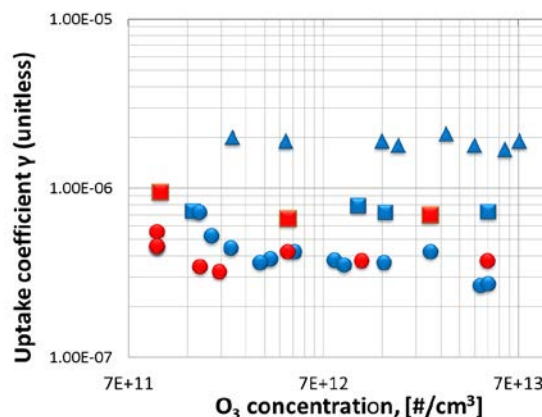


**Fig. 2:** Uptake coefficient  $\gamma$  vs.  $[O_3]_g$  for mixed NaBr/CA films with estimated bromide concentrations of 4.8M (triangles), 0.44M (squares) and 0.11M (circles), respectively, equilibrated at 72% relative humidity and 20°C. Blue symbols: 2012; red symbols: 2013.

The uptake of  $O_3$  to the films with the two higher bromide concentrations is independent of the gas phase concentration and roughly consistent with uptake limited by reaction in the bulk. Also, for the lowest bromide concentration, from the combined datasets of 2012 (blue symbols) and 2013 (red symbols), within uncertainty, there is no evidence of a surface reaction that had been suspected based on the 2012 dataset only and that had been reported for solutions in absence of organics [3].

## STATUS AND OUTLOOK

In order to bridge the gap between the citric acid doped solutions and pure halide solutions, a new flat-bed reactor will be used for lower viscosity solutions and to also allow applying organic surfactants.

## ACKNOWLEDGEMENT

We appreciate support by the Swiss National Science Foundation (grant no. 130175).

## REFERENCES

- [1] Abbatt et al., *Atmos. Chem. Phys.*, 12, 6237-6271, (2012).
- [2] Simpson et al., *Atmos. Chem. Phys.*, 7, 4375-4418, (2007).
- [3] Oldridge and Abbatt, *J. Phys. Chem. A*, 115, 2590-2598, (2011).
- [4] Donaldson and George, *Environmental Science & Technology*, 46, 10385-10389, (2012).
- [5] Zardini et al., *Atmos. Chem. Phys.* 8 (18), 5589-5601, (2008).

# THE AIR-AQUEOUS INTERFACIAL COMPOSITION OF MIXED SODIUM BROMIDE / CITRIC ACID SOLUTIONS

M.T. Lee (Univ. Bern & PSI), S. Kato (PSI), M. A. Brown (ETHZ), J. A. van Bokhoven (PSI/LSK & ETHZ), A. Kleibert (PSI/SLS), M. Lampimäki, A. Türlér, M. Ammann (PSI)

## INTRODUCTION

The aim of this project with the near ambient pressure photoemission endstation (NAPP) was to obtain insight into the surface composition of mixed halogenide / organic acid solutions of relevance to the atmospheric chemistry in marine environments using the liquid microjet setup. The surface composition of the sea water at the ocean surface or in sea spray particles is crucial in the chemistry with gas phase oxidants such as ozone ( $O_3$ ) [1-2]. Earlier photoelectron spectroscopy experiments have provided first indications for the entanglement of iodide ions, cations and surfactant headgroups [3-5], which are important for the release of halogen compounds from the ocean surface or out of sea spray aerosol particles. Our current stage is to look into the effect of a more complex organic compound, citric acid, which represents highly oxidized organic compounds present in the environment, on the concentration of bromide at the interface.

## EXPERIMENTAL

We used ambient pressure XPS on a vacuum liquid microjet (19  $\mu\text{m}$ ). The continuously refreshed free-flowing aqueous filament under vacuum permits photoelectron spectroscopy measurements from volatile aqueous interfaces in absence of beam damage [6]. Measurements were made at the SIM beam line of the Swiss Light Source (SLS) at the Paul Scherrer Institute. Figure 1 depicts the entrance cone with a 500  $\mu\text{m}$  diameter aperture into the electron spectrometer associated with the liquid microjet.

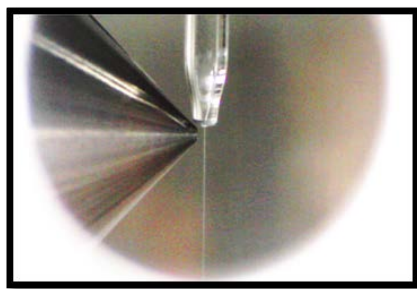


**Fig. 1:** Photograph of the liquid-microjet in action in front of the entrance cone of the electron spectrometer.

## RESULTS

Figure 2 shows three exemplary scans of the region of about 160 eV photoelectron kinetic energy, at 229 eV nominal photon energy set at the beamline. Br3d and Na2s of sodium bromide have a kinetic energy of about 155 eV and 160 eV, respectively, apparent in the traces of all NaBr containing solutions. C1s core levels have binding energies around 290 eV. We therefore

used the presence of second order light available at 458 eV to obtain C1s photoelectrons from citric acid at around 170 eV kinetic energy (1.35 M citric acid solution). Along the same line, we used third order light (687 eV) to observe O1s around 148 eV. Taking the spectra in this way allows obtaining directly an internal reference for the overlap between photon beam and the jet via the O1s or the C1s signals without the need to change the photon energy at the beamline in between.

We are in the process of evaluating the spectra that will be combined with data from previous beamtimes with the liquid jet. We will interpret the results in the context of reactivity studies with the same solutions in our laboratory.

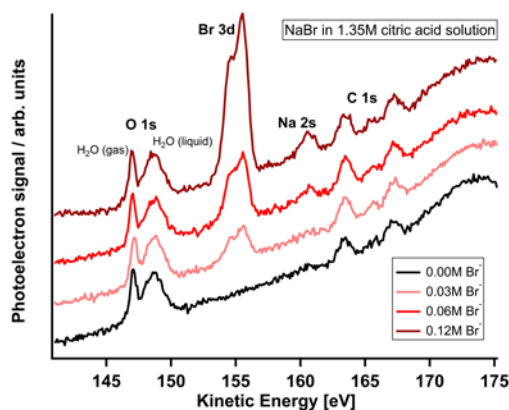


**Fig. 2:** Photoelectron spectra of mixed citric acid / NaBr solutions, taken at primary photon energy of 229 eV set at the beamline. Spectra are offset for display.

## ACKNOWLEDGEMENT

The NAPP endstation has been funded by the Swiss National Science Foundation (SNF R'Equip, grant no 139139), PSI FoKo, SLS QV program, and the Competence Center Energy and Mobility (NADiP project).

## REFERENCES

- [1] Clifford and Donaldson, *J. Phys. Chem. A*, **111**, 9809-9814, (2007).
- [2] Oldridge and Abbatt, *J. Phys. Chem. A*, **115**, 2590-2598, (2011).
- [3] S. Ghosal et al., *Science* **307**, 563 (2005).
- [4] M.A. Brown et al., *Phys. Chem. Chem. Phys.* **10**, 4778 (2008).
- [5] M. Krisch et al., *J. Phys. Chem. C* **111**, 13497 (2007).
- [6] M.A. Brown et al., *Rev. Sci. Instrum.* **84**, 073904 (2013).

# QUANTITATIVE DEPTH PROFILE OF A CERIA NANOCUBE CATALYST UNDER REACTIVE GAS ATMOSPHERES

S. Kato (PSI), C. Proff (PSI/LBK), T. Bartels-Rausch, M. Lampimäki (PSI), T. Huthwelker (PSI/SLS), M. Birrer (PSI), M. T. Lee (PSI/Univ. Bern), C. Paun (PSI/LSK & ETHZ), M. Ammann (PSI), J. A. van Bokhoven (PSI/LSK & ETHZ)

## INTRODUCTION

Ceria-based materials are applied in a wide range of fields such as catalysis, fuel cells, optics, gas sensors, and biology. It is generally accepted that the reactivity of ceria is related to the low redox potential of the  $\text{Ce}^{3+}/\text{Ce}^{4+}$  pair and to the high oxygen storage capacity that allows the oxide to store oxygen under oxidizing conditions ( $\text{Ce}^{4+}$ ) and to release it under reducing conditions, thus creating oxygen vacancies and  $\text{Ce}^{3+}$  defects [1].

A very attractive characteristic of synchrotron X-ray photoelectron spectroscopy (XPS) is its ability to perform depth profiling on a catalytic material via variation of the photoelectron kinetic energy (KE), and thus probing depth, achieved by tuning the energy of the exciting photons. It thus provides *in situ* structural analysis as a function of distance to the catalytically active surface. Through the combined use of soft and hard X-rays elemental composition and oxidation state are accessible over a particularly large range from the surface into the bulk. Here we aimed at obtaining the structure under realistic reaction conditions using near ambient pressure XPS.

## EXPERIMENTAL

The near ambient pressure XPS endstation was installed at the PHOENIX beamline of the Swiss Light Source (energy range 0.8-8 keV). The basis of the XPS endstation is a VG SCIENTA R4000 HiPP-2 analyzer with a differentially pumped electrostatic lens system. It is capable to analyze electron kinetic energies up to 7 keV at pressures (in the analysis chamber) up to currently 20 mbar. A ceria nanocube catalyst (2wt%Pt/CeO<sub>2</sub>) was analyzed in atmospheres of O<sub>2</sub> or H<sub>2</sub> at 1 mbar at 403 K. X-ray photoemission spectra of Ce 3d were taken at photon energies of 2.2 and 6.0 keV in O<sub>2</sub> and 2.2, 3.5, 4.0, 5.0 and 6.0 keV in H<sub>2</sub>. The particle size in the sample was between 30 and 60 nm. The base pressure of the analysis chamber was below 10<sup>-4</sup> mbar and the gas impurity level during the gas dosing was below 0.3% consisting of air.

## RESULTS

Under both reducing and oxidizing conditions, (Fig. 1 for the case of H<sub>2</sub>) the Ce 3d spectrum consists of  $\text{Ce}^{3+}$  and  $\text{Ce}^{4+}$  contributions. The change in the oxidation state was investigated as a function of the probing depth (Fig. 2). In both reducing and oxidizing conditions, the ceria is more reduced on the surface than in the bulk. However, in H<sub>2</sub> the ceria nanocubes are sig-

nificantly more reduced than in O<sub>2</sub>. These measurements demonstrate the great potential of this approach to assess the Ce oxidation state in a catalyst sample under realistic conditions over a large range of probing depths.

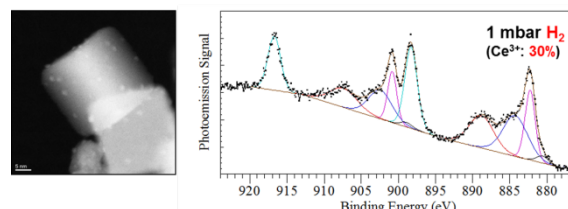


**Fig. 1:** Left: TEM image of ceria nanocubes (2wt%Pt/CeO<sub>2</sub>). The image width is 50 nm. Right: Ce 3d PE spectrum in 1.0 mbar H<sub>2</sub> at 403 K taken at 1.3 keV kinetic energy (2.2 keV photon energy), exhibiting a 30% contribution by Ce<sup>3+</sup>.

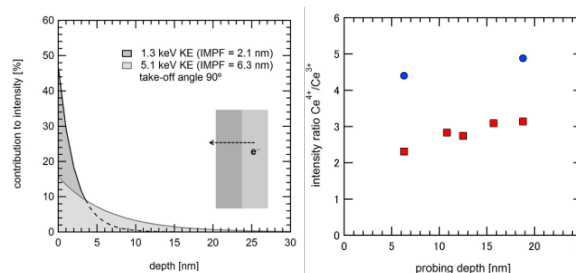


**Fig. 2:** Left: Calculated relative contribution of Ce to the photoemission signal intensity evaluated at 1.3 keV KE and 5.1 keV KE as a function of depth from the solid surface into the bulk, assuming exponential attenuation of electrons in CeO<sub>2</sub>. The corresponding electron inelastic mean free paths (IMPF) are 2.1 nm at 1.3 keV KE and 6.3 nm at 5.1 keV KE [2]. Right: The intensity ratio of Ce<sup>4+</sup> to Ce<sup>3+</sup> of a ceria nanocube catalyst (2wt%Pt/CeO<sub>2</sub>) as a function of the probing depth (defined as IMPF × 3) in O<sub>2</sub> (blue) and H<sub>2</sub> (red).

## ACKNOWLEDGEMENT

The NAPP project is being supported by the Swiss National Science Foundation (SNF R'Equip, grant no 139139), PSI FoKo, SLS QV program, and the Competence Center Energy and Mobility (NADiP project).

## REFERENCES

- [1] A. Trovalrelli, Catalysis by Ceria and Related Materials, Catalytic Science Series, Imperial College Press: London, 2002.
- [2] S. Tanuma et al., Surf. Interface Anal. **21**, 165-176 (1993).

## IN SITU XPS ANALYSIS CHAMBER FOR GAS-SOLID REACTIONS

S. Kato, T. Bartels-Rausch (PSI), C. Proff (PSI/LBK), M. Birrer, M. Lampimäki (PSI), A. Kleibert (PSI/SLS), J. A. van Bokhoven (PSI/LSK & ETHZ), M. Ammann (PSI)

We are investigating the surface chemistry of gas-solid reactions relevant to atmospheric chemistry, e.g., on ice or mineral oxide surfaces, by means of near ambient pressure X-ray photoelectron spectroscopy (XPS) [1,2]. In 2012 and 2013 we have installed our new near ambient pressure photoemission (NAPP) endstation (VG SCIENTA R4000 HiPP-2 analyser) at the Swiss Light Source, first realized with a liquid microjet setup [3].

For *in situ* studies with solid surfaces, we have developed a new analysis chamber (Fig. 1) that can be attached to the NAPP endstation. It hosts a reaction cell with minimized inner dimensions to also allow dosing sticky gases (Fig. 2) and with close access into a differentially pumped molecular beam sampling mass spectrometer (HIDEN HPR-60). The analysis chamber is equipped with a mu-metal liner, which lowers the residual magnetic field down to 0.1  $\mu$ T inside the reaction cell. The reaction cell is operated at pressures from the base pressure of  $10^{-7}$  mbar up to 20 mbar. The reaction cell features a versatile sample mount, prepared for a variety of supports for elevated or low temperatures. Sample positioning with a precision of  $\pm 1$   $\mu$ m along all axes is achieved with linear positioning drives controlled via a LabVIEW program.

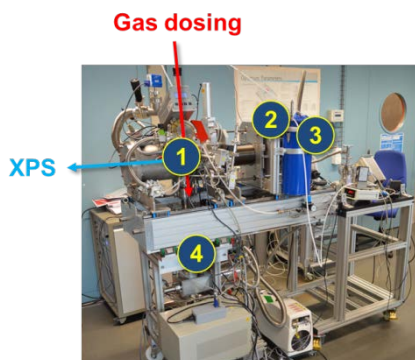


**Fig. 1:** Analysis chamber for gas solid reactions attachable to the NAPP endstation (not shown). 1. Reaction cell. 2. Linear positioning drives. 3. Cryo-N<sub>2</sub> flow cooling unit (inserted into the sample transfer rod). 4. Mass spectrometer.

An exemplary commissioning result is shown in Fig. 3. A TiO<sub>2</sub> powder on Au foil was analysed in an atmosphere of H<sub>2</sub>O at 1 mbar. Adsorbed H<sub>2</sub>O on TiO<sub>2</sub> is evident at 203 eV kinetic energy [2].

For the investigation of ice surfaces, the ice film is prepared on the sample substrate by H<sub>2</sub>O vapor deposition followed by equilibration at the temperature of interest at the water vapor pressure in equilibrium with ice at that temperature. The cryogenic sample mount currently allows adjusting the temperature down to  $173 \pm 1$  K using the N<sub>2</sub> flow cooling unit. This setup

will be used to investigate changes in ice surface composition and alterations of the hydrogen bonding environment during the adsorption of trace gases [1].

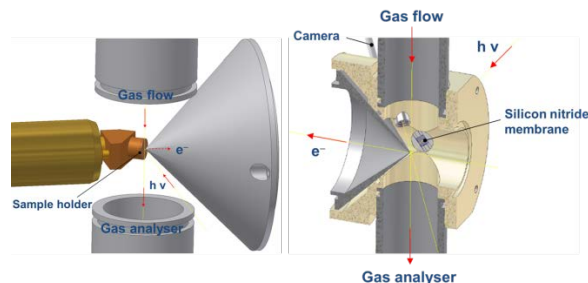


**Fig. 2:** Left: Measurement configuration in the reaction cell. The gas dosing tube has 30 mm inner diameter. The excited photoelectrons are collected through an aperture into the front-cone of the electrostatic lens system of the electron analyzer (distance between the sample and the tip of the front-cone: 0.5 mm). Right: Cross sectional view of the reaction cell assembly (without the sample mount).

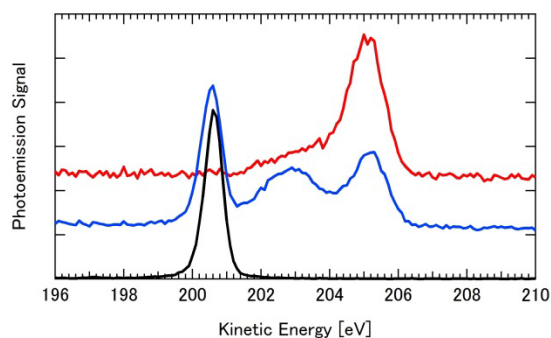


**Fig. 3:** Photoemission spectra of O1s taken at the SIM beamline at 740 eV photon energy and 298 K. Red (—): TiO<sub>2</sub> in vacuum (as is, at the base pressure of  $10^{-7}$  mbar). Blue (—): TiO<sub>2</sub> in H<sub>2</sub>O at 1 mbar. Black (—): H<sub>2</sub>O gas at 1 mbar.

### ACKNOWLEDGEMENT

The NAPP project is being supported by the Swiss National Science Foundation (SNF R'Equip, grant no 139139), PSI FoKo, SLS QV program, and the Competence Center Energy and Mobility (NADiP project).

### REFERENCES

- [1] A. Křepelová et al., J. Phys. Chem. A, **117**, 401-409 (2013).
- [2] M. Lampimäki et al., Chem. Phys. Chem., **14**, 2419-2425 (2013).
- [3] M.A. Brown et al., Rev. Sci. Instrum. **84**, 073904 (2013).

## IMPLEMENTING AUGER ELECTRON YIELD X-RAY ABSORPTION SPECTROSCOPY AT AMBIENT PRESSURE

T. Bartels-Rausch (PSI), X. Wang, J. Krempasky (PSI/GFA), M. Muntwiler, T. Huthwelker (PSI/SLS), S. Kato (PSI), M. A. Brown (ETHZ), J. A. van Bokhoven (PSI/LSK & ETHZ), M. Ammann (PSI)

### INTRODUCTION

X-ray photoelectron spectroscopy (XPS) at near ambient pressure is an emerging technique with the unique ability to deliver information on the molecular interactions on surfaces with relevance to environmental science [1,2]. Auger-electron yield X-ray absorption spectroscopy (AEY-XAS) is a related technique, in which the total yield of Auger electrons is measured as a function of the energy of the exciting photons. In the initial excitation, a core level electron is excited into an unoccupied molecular orbital. Auger electrons are emitted during the relaxation process of the core excited molecule (Fig. 1). Thus in the course of an AEY-XAS measurement the excitations to different unoccupied orbitals are probed. As unoccupied orbitals are further away from the core, they often have a larger spatial extent, and AEY-XAS spectra become sensitive to the molecular environment, e.g. to hydrogen bonds in ice [2].

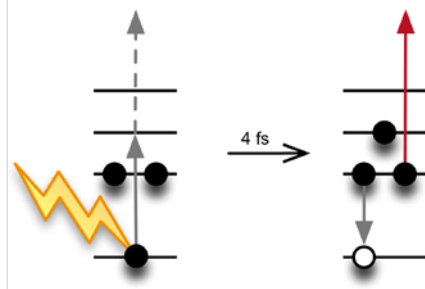


**Fig. 1:** Schematic diagram illustrating the excitation of a core electron to unoccupied orbitals (grey solid line) or above the ionization threshold (grey dashed line). The emission of Auger electrons (red line) during the relaxation is monitored in AEY-XAS.

For the purpose of AEY-XAS measurements under ambient conditions, we have coupled our recently established near ambient pressure XPS endstation (NAPP, [3]), which is based on a VG Scienta electron analyzer, to the beamline control system.

The software implementation of the VG Scienta electron analyzer is made within the popular EPICS *areaDetector* in collaboration with J. O’Hea and F. Yuan, Diamond Light Source Ltd.. The main aspect of the EPICS software is distributed control over Ethernet. Experiment control functionalities such as beam line optics, undulator or VG-Scienta analyzer (optionally including a sample manipulator or an angle resolved setup), are accessible in EPICS. In this context a photoemission experiment is a *Positioner-Trigger-Detector* EPICS programming paradigm. For typical photoemission experiments the *Positioner* is the “set energy” command, *Trigger* is the “set-point OK” from the beamline or sample manipulator, linked

with the *Detector* “Acquire” command - a high-level “wait-for-completion” command streaming spectra with beamline and manipulator data into a HDF file for offline data analysis.

### RESULTS

Fig. 2 shows the first fully automated AEY-XAS of a thin sea salt film on a gold support obtained at the Phoenix beamline. The photon energy was varied between 2818 eV and 2840 eV with a resolution of 1 eV. For each photon energy the sum of the intensity of detected Auger electrons over the full kinetic energy range is plotted. The individual Auger electron spectra have not been corrected for charging of the insulating sample.

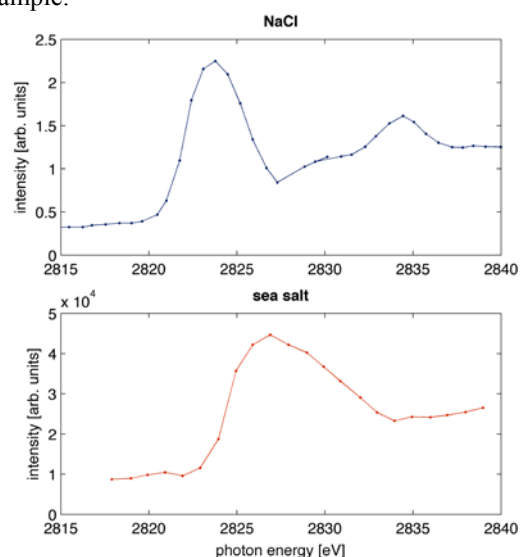


**Fig. 2:** AEY-XAS of chloride in a sea salt sample (bottom). An electron yield XAS of a NaCl sample taken earlier at the Phoenix beam line is plotted for comparison (top).

### ACKNOWLEDGEMENT

The NAPP endstation has been supported by the Swiss National Science Foundation (SNF R’Equip, grant no 139139), PSI FoKo, SLS QV program and the Competence Centre Energy and Mobility (NADiP project). Support by J. O’Hea and F. Yuan, Diamond Light Source Ltd., is appreciated.

### REFERENCES

- [1] M. Lampimäki, et al., *ChemPhysChem*, **14**, 2419-2425 (2013).
- [2] A. Krepelova et al., *J. Phys. Chem. A*, **117**, 401 (2013).
- [3] M. A. Brown et al., *Rev. Sci. Instr.*, **84**, 073904 (2013).

## LATE HOLOCENE TEMPERATURE RECONSTRUCTION FOR SIBERIA

P.-A. Herren (Univ. Bern & PSI), A. Eichler, S. Brütisch (PSI), T. Papina (IWEF), M. Schwikowski (PSI & Univ. Bern)

Current climate change has strong regional patterns. To investigate these spatio-temporal differences, regionally resolved paleoclimate records are required. In particular for remote areas such as Siberia were instrumental data is rare. The Past Global Changes (PAGES) 'PAGES 2k' project aims to produce a global array of regional climate reconstructions for the past 2000 years [1]. Regarding Asia, the reconstruction consists exclusively of tree-rings records and covers the period AD 800-1989 [1]. Additional long-term paleoclimatic records from different archives are necessary for a broader support of the Asian temperature reconstruction.

Here we used the second principle component (PC2) of the geochemical records in the Tsambagarav ice core from the Mongolian Altai as temperature proxy for Siberia ([2], Tab. 1). The PC2 with high loadings of ammonium ( $\text{NH}_4^+$ ) and formate ( $\text{HCOO}^-$ ) reflects biogenic emissions upwind the drilling site. We argue that sources of those biogenic species are emanation from soil and vegetation in the Siberian plains, which are controlled by temperature changes. The calibration was performed with the  $\delta^{18}\text{O}$  based March-November temperature reconstruction from the Belukha ice core located in the Siberian Altai 350 km northwest [3]. The PC2 of the Tsambagarav ice core is significantly correlated with reconstructed temperature from Belukha ( $r = 0.70$ ,  $n = 19$ ,  $p < 0.001$ ).

**Tab. 1:** Loadings of the Tsambagarav PCA performed on the normalized 20-year means of concentrations of nine major ions and the variance explained by each component for the time period 1200 BC to AD 1940.

	PC1	PC2	PC3
$\text{Ca}^{2+}$	<b>0.90</b>	-0.30	-0.10
$\text{Na}^+$	<b>0.89</b>	-0.32	-0.10
$\text{Mg}^{2+}$	<b>0.88</b>	-0.29	0.01
$\text{Cl}^-$	<b>0.88</b>	-0.33	-0.10
$\text{NO}_3^-$	<b>0.81</b>	0.22	0.17
$\text{SO}_4^{2-}$	<b>0.81</b>	0.10	-0.17
$\text{NH}_4^+$	0.75	<b>0.62</b>	-0.06
$\text{HCOO}^-$	0.72	<b>0.52</b>	-0.11
$\text{K}^+$	0.43	-0.03	<b>0.89</b>
Variance explained	64%	12%	10%
	<b>Mineral dust</b>	<b>Biogenic emissions</b>	<b>Biomass burning</b>

The PC2 of the Tsambagarav ice core allows for a temperature reconstruction with 20-year resolution, for the period 1200 BC to AD 1940. From AD 1940 anthropogenic emissions altered the atmospheric concen-

trations in Siberia. Combination with the Belukha ice core record enables to extend the temperature reconstruction to AD 1980.

Fig. 1 shows the reconstructed temperature of the Siberian Taiga belt. For the past 3200 years the temperature anomalies fluctuated between  $-3.0$  and  $5.6^\circ\text{C}$  with rapid transitions from warm to cold periods and vice versa, resulting in high frequency temperature changes. The record allows for a characterization of different well-known climatic periods, such as the Roman Warm Period (RWP), the Dark Ages Cold Period (DACP), the Medieval Warm Period (MWP), the Little Ice Age (LIA) and the present warming.

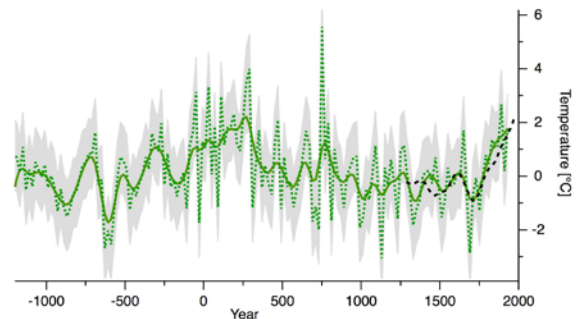


**Fig. 1:** Reconstructed Siberian temperature from Tsambagarav PC2 scores (normalized to the AD 1270 to 1930 period) for the last 3200 years (green dashed line) and smoothed with a 5-point binomial filter (bold green line) and Belukha  $\delta^{18}\text{O}$  based temperature reconstruction (dashed black line).

The temperature reconstruction presented in this study coincides in amplitude and timing with instrumental temperature data. The good agreement confirms Siberia as a fast warming region on the globe [4]. The high sensitivity of the Taiga forests makes its especially vulnerable to temperature and precipitation changes.

### ACKNOWLEDGEMENT

This project was supported by the Swiss National Science Foundation (200021\_119743).

### REFERENCES

- [1] PAGES 2k-Consortium, *Nature Geoscience*, **6**, 5 (2013).
- [2] P.-A. Herren et al., *Quaternary Sci. Rev.* **69**, 59 (2013).
- [3] A. Eichler et al., *Geophys. Res. Lett.*, **36**, 18, (2009).
- [4] J. Hansen, *Proc. Natl. Acad. Sci.*, **103**, 39 (2006).

## RADIATION DRIVEN MELTING AT A MONGOLIAN GLACIER

*P.-A. Herren (Univ. Bern & PSI), A. Eichler, S. Brüttsch (PSI), T. Papina (IWEF), M. Schwikowski (PSI & Univ. Bern)*

In recent decades the geographical region of Siberia experienced enhanced warming [1]. Together with Alaska and Northern Greenland it belongs to the fastest warming regions of the globe. Climate reconstructions are necessary to put these changes in a long-term context. In this study we reconstruct summer melt trends from an ice core collected in the Mongolian Altai. The ice core originates from the Tsambagarav massif. The results are compared with the ice core geochemical records.

Summer surface melt in glaciated regions causes the percolation of meltwater into the ice matrix where it refreezes to distinct layers. The distribution and extent of these melt features can be related to summer warmth (e.g., [2]). We adapted a well-known method to derive annual melt percent (AMP) from the Tsambagarav ice core for the period AD 1815 to 2009 [3].

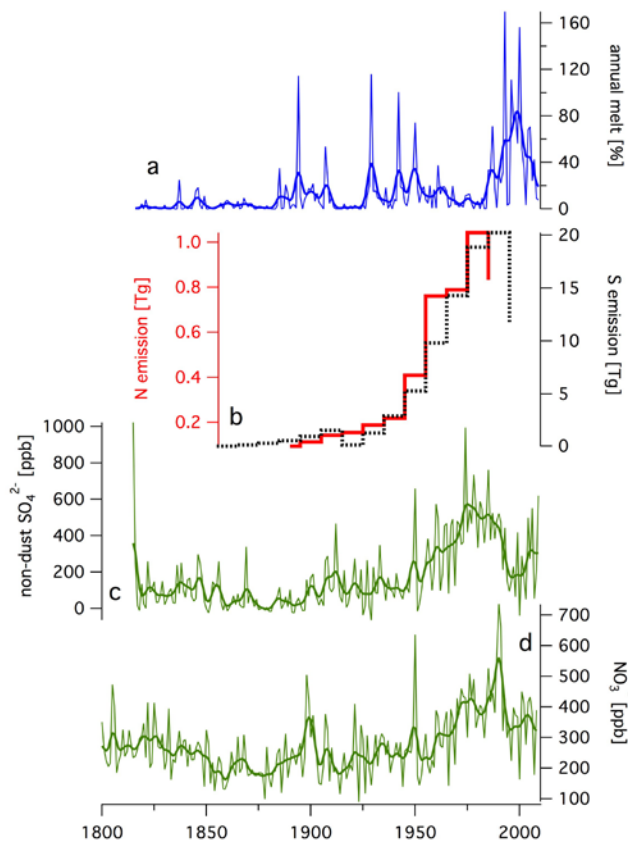


**Fig. 1:** (a) Annual melt percent (AMP) of the Tsambagarav ice core. (b) Historical Eastern European emission estimates of  $\text{NO}_x$  (Tg N) and  $\text{SO}_2$  (TgS). Tsambagarav non-dust  $\text{SO}_4^{2-}$  (c) and  $\text{NO}_3^-$  (d) concentrations. Annual values (thin line) smoothed with a 5-point binomial filter (bold curves).

During the last two centuries the AMP record suggest increased glacier-hostile climate conditions for the whole Altai and indicate severe changes in the mass balance of the glaciers. The higher frequency of intense melt events towards present is in agreement with identified shrinkage of Altai glaciers by former studies (e.g [4]). The long-term trend of the AMP corresponds to observational data that show pronounced warming for the last decades [1].

Periods of low and high AMP in the Tsambagarav reconstruction appear to coincide with the general incident solar radiation pattern at the earth's surface during the 20<sup>th</sup> century [5]. Various studies suggest a widespread decrease in surface solar radiation between the 1950s and 1980s generally referred as 'global dimming' followed by a recovery designated as 'brightening'. Few records from the first half of the 20<sup>th</sup> century suggest an 'early brightening'. The periods of enhanced annual melt (1927-1966 and 1985-ongoing) coincide well with the 'early brightening' and 'brightening' period, whereas the period of reduced melt intensity matches the 'dimming' interval. For the on-going period the melt record peaks at around 2000 and decreases subsequently. This pattern reinforces the hypothesis of 'renewed dimming' in Eastern Asia. This strong relation introduces a potential new proxy to investigate the anthropogenic influence on the earth's energy balance beyond the instrumental period.

The trends of anthropogenic pollutants (non-dust  $\text{SO}_4^{2-}$  and  $\text{NO}_3^-$ ) correspond to the AMP record (Fig 1). The influence of  $\text{SO}_4^{2-}$  on the earth radiative balance corroborates the link between the AMP and the incident solar radiation. This further points to radiation controlled surface melting in the Altai and thus to a potential new proxy to reconstruct earth's energy balance.

### ACKNOWLEDGEMENT

This project was supported by the Swiss National Science Foundation (200021\_119743).

### REFERENCES

- [1] J. Hansen, Proc. Natl. Acad. Sci., **103**, 39 (2006).
- [2] R. Körner, Science, **196**, 4285, (1977).
- [3] K. Henderson et al., J. Geophys. Res., **111**, D3, D03104 (2006).
- [4] F. Pattyn et al., Annals of Glaciology, **37**, (2003).
- [5] M. Wild, J. Geophys. Res., **114**, D10, D00D16, (2005).

## MAJOR ION CONCENTRATIONS IN THE LOMONOSOVFONNA ICE CORE

*I. Wendl (PSI & Univ. Bern), S. Brütsch, A. Eichler (PSI), E. Isaksson (NPI), T. Martma (Univ. Tallinn), M. Schwikowski (PSI & Univ. Bern)*

The 2009 Lomonosovfonna ice core was analyzed for water soluble major ions ( $\text{Na}^+$ ,  $\text{NH}_4^+$ ,  $\text{K}^+$ ,  $\text{Mg}^{2+}$ ,  $\text{Ca}^{2+}$ ,  $\text{MSA}^-$ ,  $\text{Cl}^-$ ,  $\text{NO}_3^-$ ,  $\text{SO}_4^{2-}$ ) with liquid ion chromatography. These ions help to reconstruct climate variability and pollution on historic time scales.

### PRINCIPAL COMPONENT ANALYSIS

In order to identify groups of ionic species that either have a common source or are transported together we performed a principal component analysis (PCA). Anthropogenic influence on the ion concentrations was excluded by only considering preindustrial times (1225-1855 AD).  $\text{NH}_4^+$  was excluded from the PCA because ~12% of the preindustrial concentrations fall below blank values of  $0.15 \pm 0.15 \mu\text{eq/L}$ .

A first group of ions (PC1 in Tab. 1) clearly indicates marine origin because it is dominated by the sea salt species of  $\text{Na}^+$ ,  $\text{Cl}^-$ ,  $\text{K}^+$ , and  $\text{Mg}^{2+}$ . The second group (PC2) suggests a marine biogenic source because  $\text{MSA}^-$  is a marker for marine biota.  $\text{NO}_3^-$  is usually attributed to lightning, biomass burning,  $\text{N}_2\text{O}$  oxidation, and soil exhalation [1]. The high loading in PC2 is therefore unexpected. We suppose that the two ions are related in an indirect way: high atmospheric  $\text{NO}_3^-$  concentrations due to high  $\text{NO}_x$  emissions result in increased  $\text{NO}_3^-$  deposition to the ocean surface water, fertilizing the marine biota which leads to enhanced  $\text{MSA}^-$  production and vice versa. The third (PC3) and fourth (PC4) group are dominated each by only one ion:  $\text{Ca}^{2+}$  and  $\text{SO}_4^{2-}$ , representing a terrestrial mineral dust and a volcanic source, respectively.

**Tab. 1:** Principal component analysis (PCA) of all ionic species with concentrations significantly above the detection limit. Time period: 1225-1855 AD; data:  $\ln(10\text{yr. avg})$ , after VARIMAX rotation. Var. expl. = Variance explained.

Ionic species	PC1	PC2	PC3	PC4
$\text{Na}^+$	0.97	0.11	0.14	0.10
$\text{K}^+$	0.87	0.18	0.04	0.24
$\text{Mg}^{2+}$	0.79	0.37	0.29	0.27
$\text{Cl}^-$	0.96	0.14	0.15	0.10
$\text{MSA}^-$	0.32	0.87	0.20	0.07
$\text{NO}_3^-$	0.07	0.89	0.18	0.25
$\text{SO}_4^{2-}$	0.41	0.38	0.28	0.76
$\text{Ca}^{2+}$	0.19	0.29	0.92	0.17
Var. expl. [%]	47	27	15	11

### MSA<sup>-</sup> AND NO<sub>3</sub><sup>-</sup>

$\text{MSA}^-$  is clearly correlated with the Arctic sea ice extent such that less (more) sea ice results in a smaller (larger) area of sea ice edge available for  $\text{MSA}^-$  production, thus leading to lower (higher)  $\text{MSA}^-$  concentrations (Fig. 1). This correlation is most

prominent in the last century. The  $\text{MSA}^-$  and  $\text{NO}_3^-$  records further correlate well in preindustrial times, supporting the connection indicated by the PCA. From ~1850 onwards the records diverge with a clear trend to higher  $\text{NO}_3^-$  concentrations (Fig. 1). This can be explained by the increasing anthropogenic influence which adds largely to the  $\text{NO}_3^-$  concentrations and is not considered in the PCA.

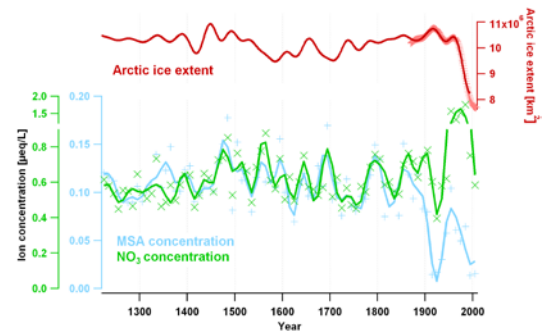


**Fig. 1:** Smoothed  $\text{MSA}^-$  and  $\text{NO}_3^-$  records (markers: 10yr.avg., lines: 40yr. lowpass filter) of the Lomonosovfonna ice core along with the variability of the Arctic sea ice extent [2].

### NH<sub>4</sub><sup>+</sup>

The Lomonosovfonna  $\text{NH}_4^+$  record displays a similar temporal trend as two other Eurasian ice cores with a pronounced increase in recent years compared to low preindustrial concentrations (Fig. 2). This similarity suggests the same Eurasian sources for  $\text{NH}_4^+$  in the three cores being biogenic  $\text{NH}_3$  emissions from Siberian boreal forests and thus confirms Eurasia to be a dominant source region for air pollution in Svalbard.  $\text{NH}_4^+$  concentrations at Lomonosovfonna are about one order of magnitude lower due to the larger distance to the emission sources.

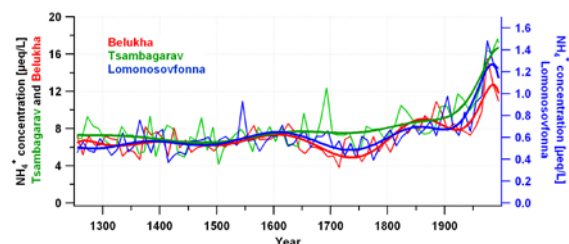


**Fig. 2:**  $\text{NH}_4^+$  record of the Lomonosovfonna compared to those from the Tsambagarav and Belukha ice cores [unpublished]. Data: 10yr.avg., smoothed with a 20 polynomial fit.

### REFERENCES

- [1] Legrand and Mayewski, *Rev. Geophys.*, **35** (3), 219-243 (1997).
- [2] Kinnard et al., *Nature*, **479**, 509-513 (2011).

# BLACK CARBON RECORD FROM THE LOMONOSOVFONNA ICE CORE

*I. Wendl (PSI & Univ. Bern), M. Gysel (PSI/LAC), I. Budde (Univ. Bern), D. Osmont (PSI),  
E. Isaksson (NPI), M. Schwikowski (PSI & Univ. Bern)*

## INTRODUCTION

Light-absorbing impurities in Arctic snow such as black carbon (BC) potentially alter the snow albedo, thus affecting the Arctic radiative balance and enhancing snow melt.

BC is a by-product of incomplete combustion of biomass and fossil fuels. The variability of the BC concentration with time therefore reflects e.g. varying emissions due to anthropogenic activities and/or forest fires, and/or varying strength of air mass transport.

So far, mainly studies on BC in Arctic snow and only one historic BC record from a Greenland ice core exist [1]. The air masses reaching Greenland originate from North America, whereas those reaching Svalbard come mainly from Eurasia. Hence the BC record from Svalbard is expected to differ from that from Greenland. Lomonosovfonna, one of the highest glaciers in Svalbard, was shown to be less affected by melt than other Svalbard sites [2]. Therefore, we expect the BC record from this ice core to be suitable to study BC on historic time-scales and add information to the behavior of BC in the Arctic.

## METHODS

We used a method combining a Single Particle Soot Photometer (SP2, Droplet Measurement Technologies, Boulder, Colorado, USA) with a jet nebulizer (APEX-Q, High Sensitivity Sample Introduction System, Elemental Scientific Inc., USA) to analyze the Lomonosovfonna ice core samples for BC [3]. The ~149 m long ice core was sampled at 3–4 cm resolution to gain a highly-resolved BC record. The samples were kept frozen until analysis, then sonicated for 25 min prior to and stirred during analysis.

## RESULTS & DISCUSSION

The BC record from 2005 to ~1950 reveals that the concentration varies with time (Fig. 1). Seasonal variations are difficult to detect, probably due to some relocation of BC during summer melt events. As such, the expected higher concentration in the end of winter to early spring due to the Arctic Haze phenomenon cannot clearly be distinguished.

The average BC concentration of  $2.6 \pm 3.4 \mu\text{g/L}$  is in good agreement with BC snow studies from Svalbard [4]. The record displays a large peak around 1980 and a less prominent one around 1957 (Fig. 1). These elevated concentrations are probably caused by anthropogenic emissions from Eurasia, because no large forest fires are known to have occurred in Eurasia at those times. In addition, local emissions from Svalbard cannot totally be excluded at this point. After 1982 the record displays reduced concentrations with an average of  $1.9 \pm 2.1 \mu\text{g/L}$  compared to  $3.5 \pm 4.3 \mu\text{g/L}$  prior 1982. This change to lower values resembles the charcoal record in [5] and can probably be related to reduced emissions in Eurasia.

## REFERENCES

- [1] J. R. McConnell et al., *Science*, **317**, 1381 (2007).
- [2] V. A. Pohjola et al., *J. Geophys. Res.*, **107**, D4 (2002), doi:10.1029/2000JD000149.
- [3] I. Wendl et al., submitted to *ES&T*.
- [4] S. Forsström et al., *J. Geophys. Res.*, **114**, D19 (2009), doi:10.1029/2008JD011480.
- [5] S. Hicks and E. Isaksson, *J. Geophys. Res.*, **111**, D02113 (2006), doi:10.1029/2005JD006167.

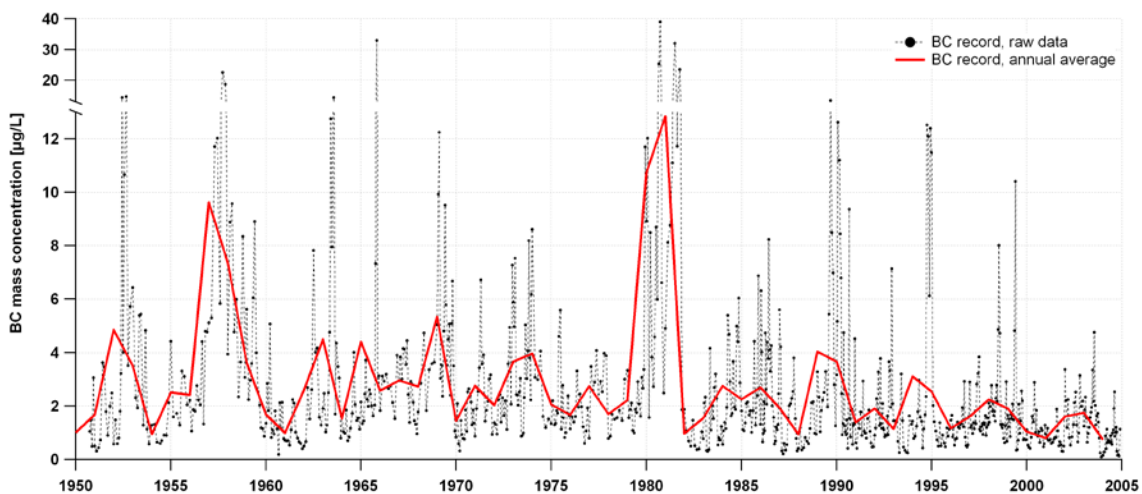


**Fig. 1:** BC mass concentration record.

# RADIOCARBON ( $^{14}\text{C}$ ) OF ORGANIC CARBON AND ELEMENTAL CARBON RECORDED IN AN ALPINE ICE/FIRN CORE OVER 1940-2002

F. Cao (PSI), Y.L. Zhang, S. Szidat (Univ. Bern & PSI), L. Wacker (ETHZ),  
M. Schwikowski (PSI & Univ. Bern)

## INTRODUCTION

Radiocarbon ( $^{14}\text{C}$ ) is a useful tool for studying natural and anthropogenic emissions of carbonaceous particles which comprise organic carbon (OC) and elemental carbon (EC) [1]. Jenk et al. (2006) [2] reconstructed a first long-term record of OC and EC concentrations with corresponding  $^{14}\text{C}$  analysis from Alpine ice core samples from Fiescherhorn glacier (46°33'3.2"N, 08°04'0.4"E; 3900 masl.), covering the period of 1650-1940. However, this  $^{14}\text{C}$ -based source apportionment method has not been applied to the firn section due to difficulties in removing potential contamination. In this study, we analyzed the  $^{14}\text{C}$  content of particulate OC and EC extracted from the upper part of the firn/ice core (1940-2002), in order to determine the natural and anthropogenic contributions in the period of highest anthropogenic emissions.

## METHODS

Detailed procedures on sample preparation, separation of the two fractions and Accelerator Mass Spectrometry (AMS) can be found in [3]. In short, cutting of the ice samples and removal of possibly contaminated outer layers was performed in a cold room ( $-20^\circ\text{C}$ ) using a pre-cleaned stainless-steel band saw. After cutting, all parts were further cleaned by chiseling to remove surface contamination. Afterwards, samples were preserved in pre-cleaned containers which were closed for melting at room temperature. The water-insoluble particles were extracted on quartz filters from melted firn samples, followed by acid treatment to remove carbonate. OC and EC were determined and separated by a recently developed thermal-optical method [4].  $^{14}\text{C}$  measurements were carried out with the MIni Carbon Dating System (MICADAS) with a gas ion source [5].

## RESULTS

In this study, all  $^{14}\text{C}$  measurements are expressed as fractions of modern ( $f_M$ ). The  $f_M$  value for samples from fossil sources is characterized by  $f_M=0$  due to the extinction of  $^{14}\text{C}$  with a half-life of 5730 years. The  $f_M$  values of the contemporary carbon sources are larger than 1 due to the nuclear-bomb  $^{14}\text{C}$  release in the 1950s and 1960s (Fig. 1.) [6]. As a result, to apportion non-fossil contribution,  $f_M$  values have to be converted into fraction of non-fossil ( $f_{\text{NF}}$ ):  $f_{\text{NF}}=f_M/f_{\text{NF,ref}}$ , where  $f_{\text{NF,ref}}$  is a reference value representing  $f_M$  of non-fossil sources for the chronological age of the sample.  $f_{\text{NF,ref}}$  is estimated by long-term time series of  $^{14}\text{CO}_2$  measurements in the atmosphere [6] and a tree-growth model [7].

Fig. 1 shows the record of the bomb-peak corrected  $f_{\text{NF}}$  in both OC and EC fractions covering the period from 1940-2002.  $f_{\text{NF}}$  in OC ( $0.89\pm 0.06$ ) is for all samples larger than the corresponding  $f_{\text{NF}}$  in EC ( $0.42\pm 0.09$ ), generally indicating a larger fossil contribution to EC. The highest fossil contribution to OC and EC is observed in the 1970s, mainly driven by enhanced road traffic emissions. Increasing relative non-fossil contributions after 1970s are attributed to air pollution control measures (i.e. a decrease in coal combustion and the emission factor of vehicle exhaust).

In the future, the corresponding mass concentrations of OC and EC derived from thermal-optical measurement will be included to reconstruct a more comprehensive picture of historical carbonaceous particles emissions.

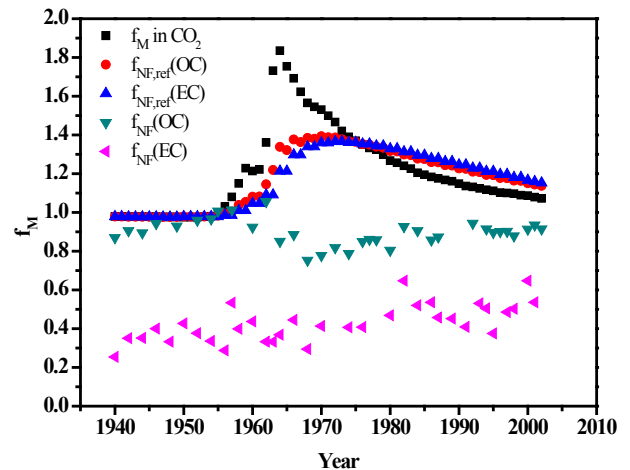


**Fig. 1:** The  $f_M$  of the atmospheric  $\text{CO}_2$ , reference values representing fraction of non-fossil ( $f_{\text{NF,ref}}$ ) of OC and EC, and the corrected record of the  $f_{\text{NF}}$  of OC and EC for the years 1940-2002.

## ACKNOWLEDGMENT

This work was supported by PEGASOS (EU FP7).

## REFERENCES

- [1] S. Szidat et al., *J. Geophys. Res.*, **111**, D07206 (2006).
- [2] T.M. Jenk et al., *Atmos. Chem. Phys.*, **6**, 5381 (2006).
- [3] F. Cao et al., *Radiocarbon*, **55**, 383 (2013).
- [4] Y. L. Zhang et al., *Atmos. Chem. Phys.*, **12**, 10841 (2012).
- [5] L. Wacker et al., *Nucl. Instrum. Methods B.*, **294**, 315 (2013).
- [6] I. Levin et al., *Tellus Series B*, **62**, 26 (2010).
- [7] J. Mohn et al., *Bioresour. Technol.*, **99**, 6471 (2008).

# EVIDENCE OF ENHANCED ANTIMONY POLLUTION SINCE THE EARLY SPANISH CONQUEST IN BOLIVIA ARCHIVED IN AN ILLIMANI ICE CORE

G. Gramlich, L. Tobler, A. Eichler (PSI), T. Kellerhals (KUP), M. Schwikowski (PSI & Univ. Bern)

The Andean Altiplano witnessed a colourful metallogenetic history owing to the mineral rich ores of its polymetallic belt. In a well-dated ice core from Illimani, Bolivia [1] indigenous smelting of silver-enriched lead ores in wind-blown furnaces (Fig. 1) were traced back even to the pre-Incan era of the Tiwanaku-culture (ca. 500 – 900 AD). Because lead is prevalent in the silver ores of the Andean polymetallic belt it was used as indicator for regional silver ore smelting, reflected in a highly resolved lead record of the Illimani ice core. Significant amounts of rock and soil dust deposition on the Illimani glacier, detectable by enhanced lithogenic element concentrations, required dust correction by calculating enrichment factors (EF). This procedure allowed a detailed insight into pre-Columbian anthropogenic lead pollution [2].



**Fig. 1:** A traditional smelting furnace in use for lead production near Porco, Bolivia (photo B. Mills) [3].

Another important anthropogenically-derived element, gaining attention only recently is antimony (Sb) [4]. Sb has a much lower natural abundance than lead (ca. 0.3 ppm upper continental crust concentration compared with 17 ppm of Pb [5]). In the Illimani ice core Sb concentrations are close to the detection limit of 1 pg/g until the mid 16<sup>th</sup> century (Fig. 2a). While the lead record reflects the extent of silver smelting spanning from the Tiwanaku and Inka eras until early colonization [2], the Sb concentrations abruptly increased above background values only beginning in the 1550s. This is even more pronounced after dust correction using enrichment factors (EF) (Fig. 2b). Contrary, Pb emissions increased steadily from the end of 15<sup>th</sup> century on with the onset of the Inka influence in the Altiplano and afterwards with the colonial mining boom. The tremendous intensification of precious metal production by the Spanish conquerors, e.g. in the legendary silver mine Cerro Rico near Potosí beginning 1550 would account for an enrichment of Sb roughly parallel with Pb. A possible reason for the abrupt and distinct appearance of Sb is changes in the smelting technology. Discussed is the parallel operation of the traditional furnaces and high temperature European type bellows furnaces allowing ore roasting or the implementation of Hispanic knowledge leading to a modification of the indigenous smelting methods [6].

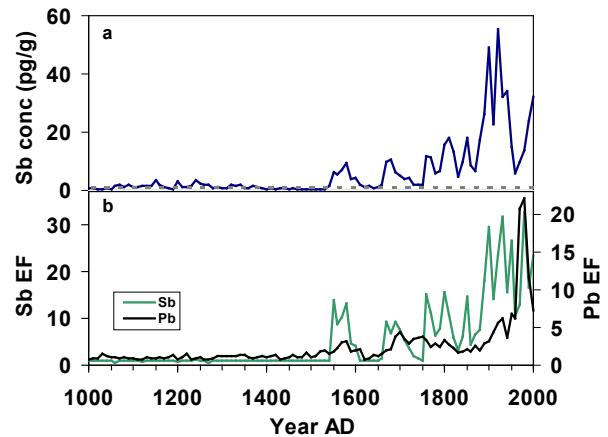


**Fig. 2:** (a) Concentrations of Sb (10 yr averages). The dashed line corresponds to a detection limit of 1 pg/g. (b) Enrichment factors (EF) of Sb (green) and Pb (black) (10 yr medians).

The Sb concentration peak between 1570 and 1580 is followed by a simultaneous decrease of Pb and Sb, parallel with the introduction of the amalgamation process in Potosí at 1572/1573. The drop in Pb and Sb emissions can be attributed to the “cold” silver extraction method that required negligible amounts of fuel and caused, beside extensive volatilization of mercury, probably considerably fewer emissions of Pb and Sb. Accessibility of new mines in the Illimani region may have led to the observed Sb concentration rise in the 17<sup>th</sup> century. The slow decrease after the maximum at 1700 AD is consistent with the beginning of fading silver production in Bolivia [7]. The onset of the industrial revolution at the end of the 19<sup>th</sup> century is reflected by increasing Sb enrichment, typical for non-ferrous metal production and fossil fuel combustion.

## ACKNOWLEDGEMENT

This work was supported by PSI in the frame of the „Förderprogramm für Wiedereinsteigerinnen“.

## REFERENCES

- [1] T. Kellerhals, PhD thesis, Univ. of Bern (2008).
- [2] G. Gramlich et al., *Ann. Rep. Lab. of Radio- & Environ. Chem., Univ. Bern & PSI*, p. 27 (2012).
- [3] T. Rehren, *Archaeology Int.* **13**, 76 (2011).
- [4] M. Krachler et al., *Journal of Environmental Monitoring* **7**, 1169 (2005).
- [5] Wedepohl, H. K. *Geochimica et Cosmochimica Acta* **59**, 1217, (1995).
- [6] M. Van Buren, C. R. Cohen, *Boletín del Museo Chileno de Arte Precolombino* **15**, 29 (2010).
- [7] C. W. Merrill, *Summarized Data of Silver Production*, Bureau of Mines (1930).

## 300 YEARS OF MERCURY EMISSIONS RECORDED IN A BELUKHA ICE CORE

S. Eyrikh (IWEF), A. Eichler, L. Tobler (PSI), T. Papina (IWEF), M. Schwikowski (PSI & Univ. Bern)

Mercury as a global pollutant has been the subject of constant attention of scientists and the public worldwide for many years. In October 2013, the Minamata Convention on Mercury, aiming to protect the human health and the environment from anthropogenic emissions and releases of mercury was signed by 94 countries [1]. However, large uncertainties exist regarding the understanding of the Hg biogeochemical cycle, including quantification of its natural and anthropogenic emissions to the atmosphere, deposition fluxes and re-emission [2]. Environmental archives contain valuable records of Hg concentrations to reconstruct regional atmospheric Hg emission and assess past contributions of natural and anthropogenic sources of atmospheric Hg contamination. Here we present a Hg record from an ice core from Belukha glacier, reflecting the history of atmospheric Hg emission in the Siberian Altai for the period 1700-2001.

Total Hg concentrations in the ice core were determined by atomic fluorescence spectrometry (Mercur, Analytik Jena), details are described in [3]. The obtained detection limit was  $0.02 \text{ ng L}^{-1}$ .

The Hg record (shown as individual values and 5-year averages in Fig. 1) is influenced by natural Hg emission (mainly from volcanoes and dust) and anthropogenic impact from industry, mining, and fossil fuel combustion. One of the highest Hg concentrations is attributed to the Krakatau eruption in 1883. Furthermore, the Hg peak in 1985 is possibly due to a combination of two complementary sources: Hg originating from a local dust storm and the large accident at the Tengiz oil field in June 1985.

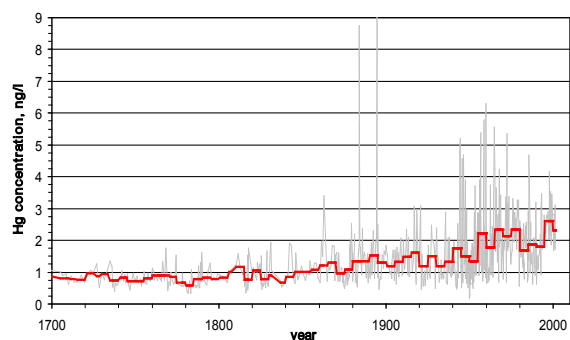


**Fig. 1:** Concentration records of Hg from Belukha ice core during the period 1700-2001: individual values (grey line) and 5-year averages (red line).

Taking into account the history of the industrial development in the Altai region and the world Hg production, we subdivided the record into 3 periods: 1700-1850 (pre-industrial), 1850-1940 (intermediate), and 1940-2001 (industrial). Average Hg concentrations increase from  $0.87 \text{ ng/l}$  (pre-industrial) to  $1.3 \text{ ng/l}$  (intermediate, peak values excluded), and  $1.9 \text{ ng/l}$  (industrial). Hg concentrations during the pre-industrial time are comparable with the values reported from the Col du Dome glacier (Alps) and remote areas (Greenland, Antarctic) [4].

The Hg ice core trend was compared to data on global and USSR Hg primary production [5] (Fig. 2).

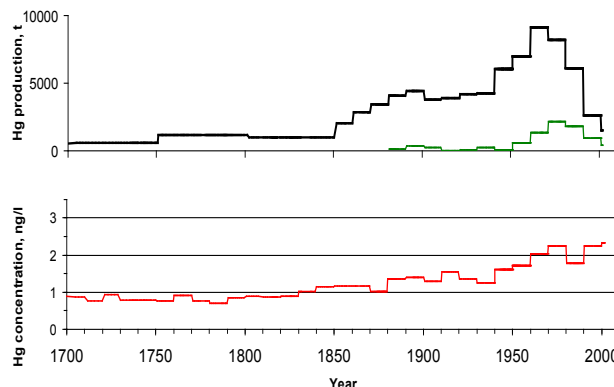


**Fig. 2:** Primary production of Hg (global, black line), (USSR, green line) [5], and 10-year averaged ice core Hg concentrations (red line).

The 10-year trend of the ice-core Hg concentrations is correlated with the history of global and USSR Hg production (Fig. 2). Being constant and low during pre-industrial times, the Hg record in the intermediate time reflects growing emissions from global Hg production and local emissions from mining and metallurgical processing in the Altai region. Increasing Hg concentrations after 1940 can be linked to growing Hg processing, the startup of the Khaidarkan Mercury Plant (KMP) in Kyrgyzstan, the industrial development in Kazakhstan and Siberia, and increasing emissions from coal combustion. Maximum ice core Hg concentrations in the 1970s are consistent with the reported peak in Greenland in the 1970-80s. The decrease in the 1980s is mainly caused by the economic crisis of the USSR, while global mercury mining collapsed in the 1990s and continued to decline in subsequent years. The increasing Hg concentrations observed in the Belukha ice core in the 1990s differ from Greenland and other environmental archives (Upper Fremont ice core, sediments in Canada, etc.) [6]. We assume that it is linked to rising Hg emissions from Asia and an impact from KMP, where Hg production increased during the 1990s.

### REFERENCES

- [1] <http://www.mercuryconvention.org/>
- [2] AMAP/UNEP Technical Background Report for the Global Mercury Assessment 2013. Arctic Monitoring and Assessment Programme, Oslo, Norway/UNEP Chemicals Branch, Geneva, Switzerland. 263 pp (2013).
- [3] S. Eyrikh et al., Annual Report Lab. of Radio- & Environ. Chem., Univ. Bern & PSI, p. 36 (2004).
- [4] D. Durnford and A. Dastoor, J. Geophys. Res., 116, DOI:10.1029/2010JD014809 (2011).
- [5] L.D. Hylander, M. Meili, The Science of the Total Environment 304, 13 (2003).
- [6] M.E. Goodsite et al., Sci. Tot. Environ. 452-453, 196 (2013).

## ALTITUDE EFFECT OF DEUTERIUM EXCESS IN THE ALPINE REGION

*I. Mariani (Univ. Bern & PSI), A. Eichler, T.M. Jenk (PSI), M. Schwikowski (PSI & Univ. Bern)*

### INTRODUCTION

The deuterium excess ( $d$ ), defined by the relationship  $d = \delta D - 8\delta^{18}O$ , is used as a proxy for moisture source conditions during evaporation and to a larger extent for atmospheric circulation [1]. However, secondary evaporation processes may influence this parameter, creating local variations not depending on the atmospheric circulation patterns. The understanding of such processes is particularly important in the Alpine region, where a complex interaction between air masses and topography occurs and altitudinal differences of the isotopic signal were already observed for  $\delta^{18}O$  [2]. The investigation of the altitudinal variation of the deuterium excess was conducted using data from the Fiescherhorn ice core, collected at an altitude of 3900 m a.s.l. [3] as well as from three nearby Global Network of Isotopes in Precipitation (GNIP) stations. The four sites are located in the Northern Alpine region. The GNIP stations of Meiringen (632 m a.s.l.), Guttannen (1055 m a.s.l.), and Grimsel Hospiz (1950 m a.s.l.), located along the Haslital valley, are all less than 20 km distant from the Fiescherhorn glacier (Fig. 1). This way it was possible not only to analyze such records on a spatial resolution not achievable by the models, but also investigate the deuterium excess variability at sites presumably affected by the same precipitation regimes.

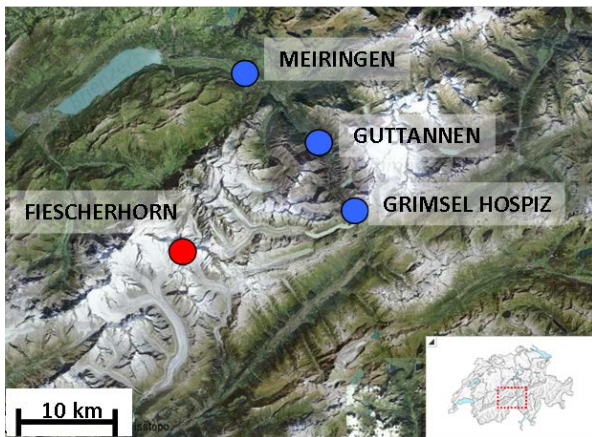


**Fig. 1:** Location of the Fiescherhorn glacier (red) and of the three GNIP stations (blue). The insert gives the location of the sites in Switzerland.

### ANALYSIS OF DEUTERIUM EXCESS RECORD

The common period considered for this analysis cover the years 1993-2001. The deuterium excess record show (i) a general lower variability of the signal at the higher elevation sites Grimsel Hospiz and Fiescherhorn and (ii) an increase of the isotopic signal with altitude (Fig. 2).

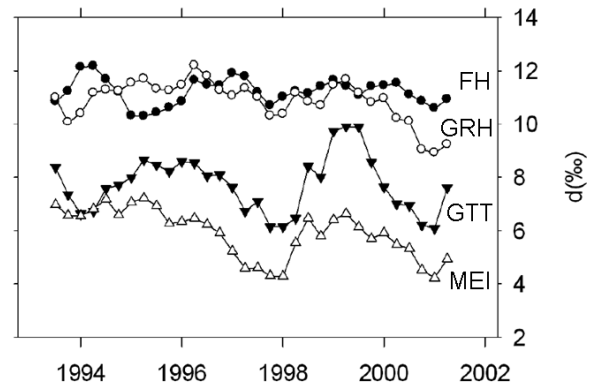


**Fig. 2:** Deuterium excess obtained from the Fiescherhorn (FH) ice core and collected in precipitation from the GNIP stations of Grimsel Hospiz (GRH), Guttannen (GTT) and Meiringen (MEI) for the period 1993-2001. Seasonal values smoothed with a 5 point running mean filter.

The altitudinal increase of the deuterium excess is explained assuming that during a precipitation event the higher altitude sites receive snow whereas for the lower elevation stations precipitation is mostly liquid. When the phase of precipitation is solid the isotopic signal records in-cloud kinetic fractionation related to the vapor deposition onto ice due to the Bergeron-Findeisen process. On the other hand, when precipitation is liquid additional fractionation due to sub-cloud re-evaporation of the raindroplets may occur, with decrease of the deuterium excess in the remaining liquid. The higher the cloud-ground distance, the higher the effect of the sub-cloud processes and therefore the decrease of the deuterium excess in precipitation. This result is consistent with previous findings obtained from analyzing stable isotopes in precipitation in the Austrian Alps [4].

### ACKNOWLEDGEMENT

This work is supported by the NCCR Climate Program of the SNF (Palvarex Project).

### REFERENCES

- [1] L. Merlivat and J. Jouzel, *J. Geophys. Res.*, **84**, 5029 (1979).
- [2] U. Siegenthaler and H. Oeschger, *Nature*, **285**, 314 (1980).
- [3] T.M. Jenk, PhD Thesis, Univ. of Bern (2006).
- [4] K. Froehlich et al., *Isot. Environ. Health S.*, **44**, 61 (2008).

## POLYCHLORINATED BIPHENYLS DEPOSITION HISTORY FROM THE ALPS

P.A. Pavlova (PSI, Empa & Univ. Bern), P. Schmid (Empa), C. Bogdal (ETHZ), M. Schwikowski (PSI & Univ. Bern)

### INTRODUCTION

Polychlorinated biphenyls (PCBs) were used as dielectric and hydraulic fluids and as plasticizers in plastics and coating materials. Considered semi-volatile and hardly degradable in the environment, PCBs belong to the group of Persistent Organic Pollutants (POPs), which were banned worldwide with the Stockholm convention [1]. Today major sources are remaining PCB-containing applications such as joint sealants in buildings, revolatilization from soils, and leaching from landfills. It is hypothesized that in high-mountain areas atmospheric transport, high precipitation rates and decreased air temperatures can lead to additional "cold condensation" enrichment of PCBs. As a consequence of deposition in the past, substances stored in ice can be released by melting at historical levels and, therefore, glaciers can play an important role as secondary source of legacy pollutants [2].

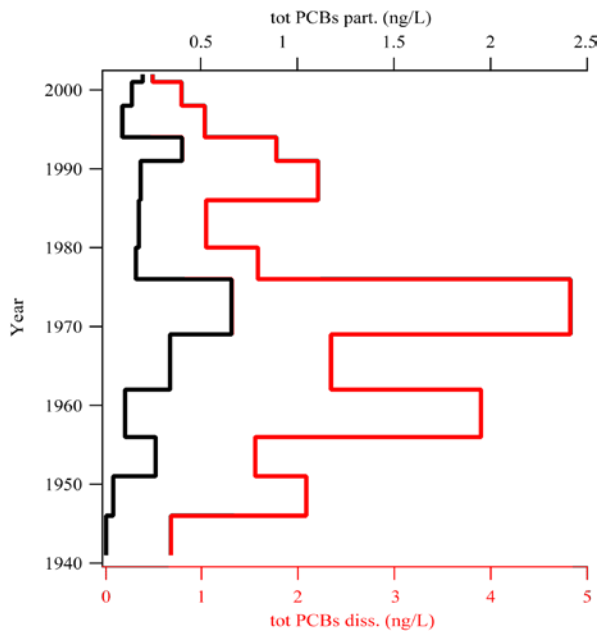


**Fig. 1:** Annual trends of the sum of six PCBs in the dissolved (red, bottom axis) and particle-bound fraction (black, top axis) in the Fiescherhorn ice core.

### STUDY SITE

In order to obtain a quantitative inventory of PCBs input into Alpine glaciers, we analyzed six abundant compounds in an ice core from the Fiescherhorn glacier in the Swiss Alps. Located at around 3900 m, the glacier is characterized by almost no summer melt and percolating water, which ensures the conservation of the deposited atmospheric pollutants in the ice. The age-depth relationship was established with a multiproxy approach using annual layer counting, reference horizons and a density depended ice flow model [3].

### RESULTS

The PCB record obtained from the Fiescherhorn ice core reveals the following temporal concentration trend (Fig. 1). Due to the relatively low particle content in this ice core the dissolved fraction clearly exceeds the particulate one. The calculated annual fluxes of PCBs show a sharp increase around 1970s, followed by a decrease in the 1990s which is in agreement with estimated emissions of the six compounds in Switzerland (Fig. 2) [4]. In contrast to the emission data, the PCB flux does not further decrease after 1993, considered to be the global phase out of the selected compounds. A similar effect has been reported before for the Arctic [5] and might indicate continuous emissions of PCBs from primary sources or even the existence of underestimated emission sources of these legacy pollutants.

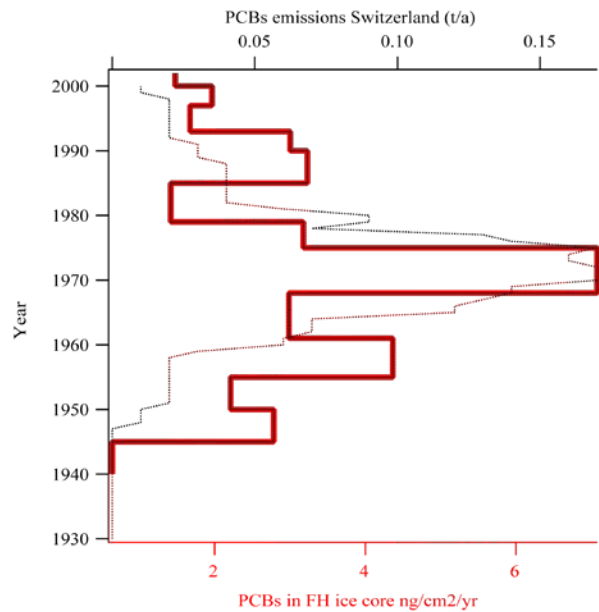


**Fig. 2:** Annual PCB flux (dissolved and particulate) at the Fiescherhorn site (red line, bottom axis), compared to annual PCB emissions in Switzerland (black dashed line, top axis) [4].

### ACKNOWLEDGEMENT

This study was partly supported by the Swiss National Science Foundation (grant number #20020\_149835).

### REFERENCES

- [1] [www.pops.int](http://www.pops.int)
- [2] C. Bogdal et al., *ES&T* **43** (2009).
- [3] T.M. Jenk, PhD Thesis, University of Bern (2006).
- [4] K. Breivik et al., *Sci. Total Environ.* **377** (2007).
- [5] O. Garmash et al., *ES&T* **47** (2013).

## RELEASE OF ENVIRONMENTAL POLLUTANTS BY GLACIER MELTING

P.A. Pavlova (PSI, Empa & Univ. Bern), P. Schmid (Empa), C. Bogdal (ETHZ), M. Jäggi (PSI/ASI),  
F. Anselmetti (Univ. Bern), M. Schwikowski (PSI & Univ. Bern)

### INTRODUCTION

As part of a multidisciplinary project we examine the secondary release of organic pollutants from melting glaciers [1]. Silvretta glacier, the chosen study site, is a temperate glacier in North-Eastern Switzerland with a surface area of around 3 km<sup>2</sup> (Fig. 1). It is situated between 2500 and 3000 m a.s.l. and has retreated more than 300 m since the 1950s, resulting in the formation of two proglacial lakes.

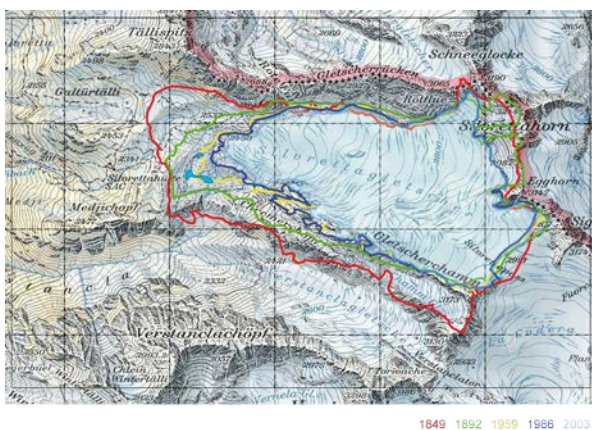


**Fig. 1:** Map of Silvretta glacier and in light blue highlighted the two proglacial lakes. Colored lines show the glacier extent between 1849 (red), 1892 (green), 1959 (yellow), 1983 (dark blue) and 2003 (light blue); adapted from A. Bauder (ETHZ).

### SAMPLING

In summer 2010 and winter 2012, surface sediment cores were collected in the Silvretta lakes and composed to a master core section covering the whole period of interest back to the 1950s.

### ANALYSIS

Sediment dating was based on peaks of <sup>137</sup>Cs which was released from atmospheric nuclear bomb testing (until 1963) and the Chernobyl nuclear power plant accident (1986). The actinides <sup>239,240</sup>Pu and <sup>241</sup>Am were measured to verify both peaks by their characteristic isotope ratios. The age-depth relationship for the composed core was obtained by linear interpolation between the known horizons and was fitted to the formation year of the lower lake (1950), retrieved from aerial images of the glacier retreat (Fig. 1). According to preliminary dating based on radioisotopes <sup>137</sup>Cs, <sup>239,240</sup>Pu, and <sup>241</sup>Am, the average annual accumulation is 4.6 cm/yr in the upper part of the sediment core. For the part of the core below 100 cm depth, the average sedimentation rate was estimated at 2.6 cm/yr. 10-cm-samples were cut, freeze-dried and analyzed for six polychlorinated biphenyls (PCBs), which have been phased-out in the 1990s, but are still ubiquitous organic pollutants [2].

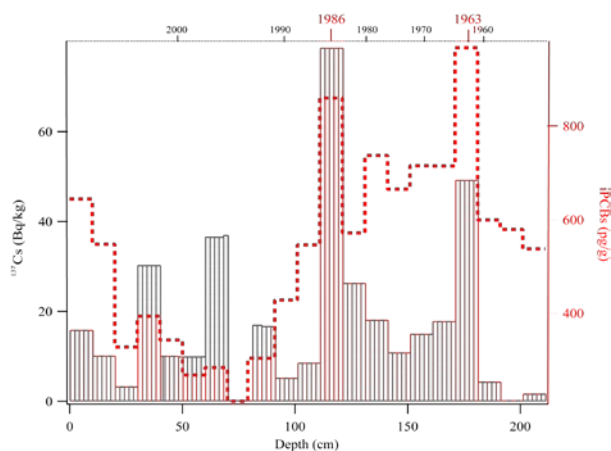


**Fig. 2:** <sup>137</sup>Cs activity concentration (grey bars) and the concentration of the sum of six PCBs in pg/g (red dashed line), plotted versus the depth of the sediment. On the top x-axis, an age scale was added.

### RESULTS

The obtained results are shown in Figure 2. The measured sum of 6 PCBs (iPCBs: PCB28, PCB52, PCB101, PCB138, PCB152, PCB180) is higher in the deeper part of the sediment core, which corresponds to the years 1950-1980, the period of peak production and use of these compounds. After a sharp decrease, the concentrations again increased towards the surface. This confirms the glacier hypothesis, according to which accelerated glacier melting can lead to a release of chemicals previously stored and conserved in the glacier [1, 2].

A similar effect is observed for the <sup>137</sup>Cs profile. The higher activity concentrations of the samples covering 1960-1990 are explained with the atmospheric fallout. Subsequently, a period of low activity with some single peaking events is observed, which may have resulted from the release of <sup>137</sup>Cs from the glacier to the lakes. Still, investigations with other radioisotopes should be performed to further confirm this observation.

### ACKNOWLEDGEMENT

This study was partly supported by the Swiss National Science Foundation (grant number #20020\_149835).

### REFERENCES

- [1] C. Bogdal et al., Environ. Sci. Technol, 43, 8173-8177 (2009).
- [2] P.A. Pavlova et al., Ann. Rep. Lab. of Radio- & Environ. Chem., Uni Bern & PSI, p. 32 (2010).

## TEMPERATE ICE: DATING CHALLENGES FOR THE SILVRETTA ICE CORE

T.M. Jenk (PSI), P.A. Pavlova (PSI, Empa & Univ. Bern), E. Vogel (Univ. Bern), J. Eikenberg (PSI/ASI), M. Schwikowski (PSI & Univ. Bern)

### INTRODUCTION

For the interpretation of climatic proxies recorded in natural archives a good chronology is essential. This is particularly challenging for ice cores from temperate glaciers where post-depositional processes such as dislocation or even removal of deposited species are pronounced due to the presence of percolating liquid water. The commonly used dating approach of annual layer counting (ALC) based on the pronounced seasonal cycles observed in chemical impurities or water stable isotopes is thus hindered. Temperate glaciers have not been explored extensively so far and it is unknown to what extent they can be used as natural archives of the past. However, investigation is worthwhile because both number and spatial coverage of potential records (i.e. sites) is substantially higher than for traditionally investigated archives from cold glaciers. Here we present the challenges to establish a chronology for such an archive collected from Silvretta glacier in April 2011 [1].

### APPROACH AND RESULTS

Not all impurities incorporated in ice are similarly affected by percolating melt water [e.g. 2]. Due to their relatively large size and low solubility, aerosol particles can be considered to be least affected.  $^{210}\text{Pb}$  adsorbed onto the surface of aerosol particles is widely applied for nuclear dating also in ice core research [e.g. 3]. For the Silvretta ice core, 41 samples from the uppermost 20 m weq were analyzed for  $^{210}\text{Pb}$ . Another 45 samples to a depth of 22 m weq were analyzed for  $^3\text{H}$ , which is used to identify the 1963 reference horizon from nuclear bomb test activities. In addition, a more than 80 year long record of mass balance measurements for Silvretta glacier from the Swiss Glacier Monitoring Network [4] was used in a new approach to evaluate potential alteration of the  $^{210}\text{Pb}$  record and its implication on the dating result. By subtracting the cumulative local mass balance (LMB) at year  $x$  from the cumulative LMB at the date of drilling (i.e. surface) each annual measurement of LMB could be associated with a certain ice core depth (no layer thinning considered), see Fig. 1.

The LMB data indicates that the record is not continuous but a significant number of annual layers were removed by melt. The age of the ice at 19.2 m weq results to be 51 years (1960 AD). On the contrary,  $^{210}\text{Pb}$  dating suggests an age of 120 years (1890 AD) at the same depth, see Fig. 2. The  $^{210}\text{Pb}$  profile further displays much larger variations compared to what is observed in records from cold glaciers. Based on the dating relying on the cumulative LMB and considering the missing layers, an expected  $^{210}\text{Pb}$  profile was calculated (Fig. 2). The presence of common features reveals that the observed variations can indeed be

explained by post-depositional removal of snow/precipitation if it is assumed that  $^{210}\text{Pb}$  is not lost but accumulated in the last residual layer. Accordingly, if plotting the  $^{210}\text{Pb}$  profile against an adjusted depth profile (core depth plus cumulative negative LMB; not shown),  $^{210}\text{Pb}$  dating suggests an age of 58 years (1953 AD) at 19.2 m weq. This is coherent with the dating by LMB (within  $1\sigma$ ) and is further supported by  $^3\text{H}$  analysis indicating increased activity (i.e. the year 1963 AD) at that depth. However, more samples need to be analyzed to reach  $^{210}\text{Pb}$  background activity and to detect the entire 1963 AD peak in  $^3\text{H}$ .

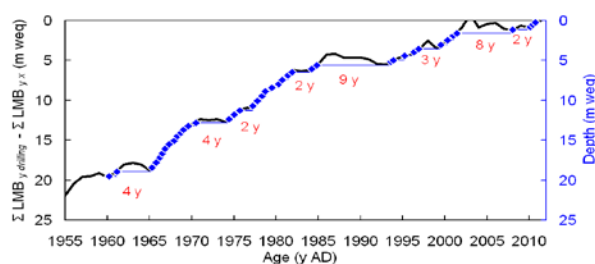


**Fig. 1:** Calculated depth from local MB data (black). True ice core depths sampled for  $^{210}\text{Pb}$  dating (blue). Number of missing/melted annual layers (red).

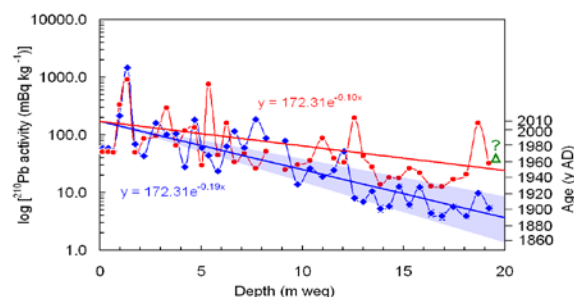


**Fig. 2:** Measured (blue) and calculated (red)  $^{210}\text{Pb}$  profiles (left axis) with resulting age scale and dating uncertainty (for meas. profile only; right axis). Elevated  $^3\text{H}$  activity level (green).

### CONCLUSION AND OUTLOOK

$^{210}\text{Pb}$  dating can be biased if a substantial number of annual layers are missing. However, it might still be applicable if a tracer allowing quantification of this number from calculated enrichment/depletion factors exists [5]. For ice cores from temperate glaciers, insoluble aerosol particles seems most promising due to a presumably constant input over time and evidence that the mobility of  $^{210}\text{Pb}$  (likely attached) is related to its presence.

### REFERENCES

- [1] P.A. Pavlova et al., Ann. Rep. Lab. of Radio- & Environ. Chem., Uni Bern & PSI (2012), p. 38.
- [2] A. Eichler et al., Tellus B, **53**, 2 (2001).
- [3] H.W. Gäggeler et al., J. Glaciol, **29**, 101 (1983).
- [4] A. Bauder, VAW/ETHZ (pers. communication).
- [5] P. Ginot et al., Clim. Past, **2** (2006).

# MEASUREMENT OF WATER STABLE ISOTOPES FROM THE GRENZGLETSCHER ICE CORE WITH A NEW LASER TECHNIQUE

*I. Mariani (Univ. Bern & PSI), S. Brüttsch, A. Eichler (PSI), M. Schwikowski (PSI & Univ. Bern)*

## INTRODUCTION

The Grenzgletscher ice core, extracted in 1994 at an altitude of 4200 m a.s.l. in the Monte Rosa Massif, was extensively analyzed for its chemical components [1]. The investigation of the water stable isotope signal, however, was limited to the  $\delta^{18}\text{O}$  record because  $\delta\text{D}$  was measured in selected samples only (1977-1984 compared to the whole record 1937-1994). Due to the proximity of the site to the Mediterranean Sea the investigation of the deuterium excess record, given by the relationship  $d = \delta\text{D} - 8\delta^{18}\text{O}$ , might provide valuable information about the moisture sources recorded in the glacier. An extension of the deuterium excess record was therefore realized by performing a new sampling of the ice core covering approximately the period 1961-1984.

## MEASUREMENTS OF GRENZGLETSCHER ICE CORE SAMPLES

The 523 samples obtained were melted and transferred into 2 mL vials and kept frozen at  $-20^\circ\text{C}$  until analysis. They were then measured in spring 2011 with an Isotopic Ratio Mass Spectrometer (IRMS) in the Laboratory of Ecosystem Fluxes Group at the Paul Scherrer Institut, using a pyrolysis technique [2]. The  $\delta^{18}\text{O}$  values were obtained with an analytical uncertainty of 0.2‰. However, with this technique it is not possible to simultaneously determine the oxygen and hydrogen isotopic ratios. Moreover, the planned measurement of the  $\delta\text{D}$  with the IRMS was not possible due to technical issues. Meanwhile, in December 2011 a Wavelength Scanned-Cavity Ring Down Spectrometer (WS-CRDS) was installed in our laboratory of the Analytical Chemistry Group. With the WS-CRDS technique, based on the ring-down time measurement of the infrared light absorbed by the water molecules, it is possible to determine both the  $\delta^{18}\text{O}$  and  $\delta\text{D}$  at the same time. After the characterization of the instrument, a Picarro L2130-I spectrometer, the Grenzgletscher samples were analyzed in spring 2012 [3]. The analytical uncertainty associated to the measurement is 0.1‰ for  $\delta^{18}\text{O}$  and 0.5‰ for  $\delta\text{D}$  [3].

The  $\delta^{18}\text{O}$  results obtained with the IRMS and the WS-CRDS techniques are shown in Fig. 1. The good agreement is illustrated by analyzing the discrepancies, which are within the analytical uncertainties of the two instruments. However, deviations of  $\sim 2\text{‰}$  were obtained for some samples in the range of the ice core sections 120-140, with more enriched  $\delta^{18}\text{O}$  measured with the laser spectrometer. Between the measurement with IRMS and WS-CRDS, the samples were stored for almost one year at a temperature of  $-20^\circ\text{C}$ . Partial evaporation and exchange might have occurred due to

(i) not tightly closed vials (ii) the hole in the septum produced by the needle during the first measurement, resulting in an isotopic enrichment in the frozen phase. This outcome shows that even proper storage of the samples at  $-20^\circ\text{C}$  might be not sufficient in order to prevent additional fractionation. The use of new lids after the measurement might partially reduce this effect.

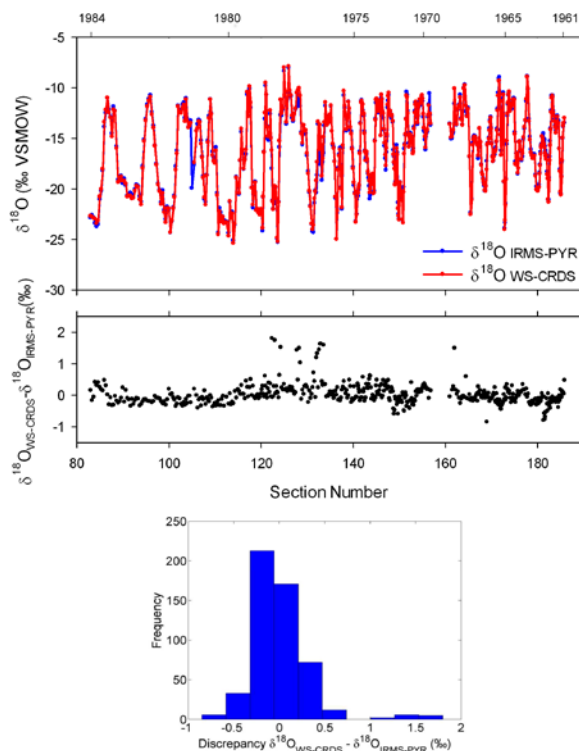


**Fig. 1:** Grenzgletscher  $\delta^{18}\text{O}$  analysed with the IRMS and WS-CRDS. Upper panel: Raw data. Middle panel: Discrepancy plot of  $\delta^{18}\text{O}_{\text{IRMS}} - \delta^{18}\text{O}_{\text{WS-CRDS}}$ . Note that the time axis on top is not linear due to the different number of samples per year. Lower panel: Frequency histogram of the discrepancies.

## ACKNOWLEDGEMENT

This work was supported by the NCCR Climate Program of the SNF (Palvarex Project). We thank Rolf Siegwolf and Matthias Saurer from the Ecosystems Fluxes Group (LAC, PSI) for use of the IRMS.

## REFERENCES

- [1] A. Eichler et al., *Tellus*, 53, 2 (2001).
- [2] A. O'Keefe, and D.A.G. Deacon, *Rev. Sci. Instrum.*, **59**, 2544 (1988).
- [3] I. Mariani, PhD Thesis, University of Bern (2013).

## AIR POLLUTANTS IN SNOW FROM TWO CHILEAN GLACIERS

T.M. Jenk (PSI), A. Rivera (CECS), J. Schindler, M. Schwikowski (PSI & Univ. Bern)

### INTRODUCTION

As a major orographic barrier along the Pacific coast the Andes represent one of the world's most fragile cryosphere regions with a population of ~85 million depending on glacial or snow runoff for drinking water, hydropower and agriculture. Within the framework of a Chilean Swiss joint research program air pollutants in snow from two Chilean sites were investigated. This pilot study presents the first data on carbonaceous particles in snow from Chilean glaciers.

Samples were collected on Olivares Beta glacier (OBG) around 60 km NE of Santiago de Chile and in the area of Glaciar Grey in Patagonia (GGR). All the sampling on OBG was realized in December 2012 in the lower part of the glacier (33°8'48.58"S and 70°11'28.20"W, 4770 m asl.). In a clean snow area, each sample was extracted from the upper 10 cm of a 1 m<sup>2</sup> surface layer. Snow (avalanche remains) and ice (raft) from the GGR area was sampled in November 2012. Ion chromatography and analysis of the water insoluble organic carbon fraction (WIOC) and elemental carbon fraction (EC) of carbonaceous particles by a thermal method (THEODORE) was performed at PSI and University of Bern, respectively. If possible, both fractions were analyzed for radiocarbon (<sup>14</sup>C) by AMS at ETHZ [1]. Additionally, Black Carbon (BC) was analyzed with an optical method (SP2).

### RESULTS AND OUTLOOK

The ice raft from GGR was <sup>14</sup>C dated with an age of 2800 ± 100 yrs calBP. Concentrations of WIOC and EC in the avalanche snow were twice as high as in the ice raft sample, which might reflect a signal from the severe forest fires in the nearby Torres del Paine National Park occurring in December 2011. Generally, the values for both samples are comparable to values found in the Swiss Alps (Fiescherhorn, FH) for WIOC and EC [2], whereas concentrations of major ions are up to ~20 lower than in samples from the industrial period at e.g. Cerro del Plomo [3], OBG or FH. Also, no significant difference in concentrations between the sample from the pre-industrial (ice) and industrial period (snow) was found, see Fig. 1. These findings indicate only insignificant anthropogenic influence at this remote Patagonian site.

At OBG, dust loadings and variations in impurities between samples taken from different patches were higher than expected, indicating significant non-uniformity in deposition (i.e. accumulation) on the snow surface (Fig. 2). Both, WIOC and EC concentrations are ~10 times higher compared with sites such as the European Alps (i.e. FH) or the remote Patagonian area of GGR. Concentration values of major ions on the other hand are typical for the industrial period and comparable with values in surface samples from FH or Plomo (Fig. 1). As expected, WIOC and organic species such as ammonium and formate are highly correlated. For <sup>14</sup>C based source apportionment of WIOC

and EC the turnover time of organic matter for this region was estimated following the approach by [4] using the Southern Hemisphere <sup>14</sup>C calibration data with according zonal bomb curve extension to account for the Suess effect. We found WIOC to be mainly of organic origin (95%), whereas the contribution to EC is around 25% and 75% from the combustion of fossil and non-fossil fuels, respectively (Fig. 2). The high concentrations in WIOC, EC but also in e.g. sulfate indicates significant pollution from the nearby city of Santiago de Chile. The high fractions of biogenic WIOC and EC point to biomass burning as an important pollution source, presumably related to wood heating and cooking. Less can be associated with the combustion of fossil fuels from traffic and industry.

Significant differences between EC and BC results were observed, possibly related to specific sensitivities of the analytical techniques (thermal vs. optical). Different sources and transport paths for the fossil and non-fossil EC, the later likely being attached to dust, might lead to underestimation of this fraction by the optical method, particularly in samples with such high dust content (Fig. 2). This needs further investigation.

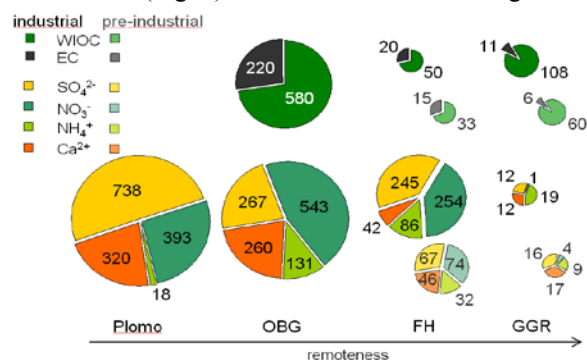


Fig. 1: Concentrations of selected chemical impurities (in ppb) for various sites and time periods, if available.

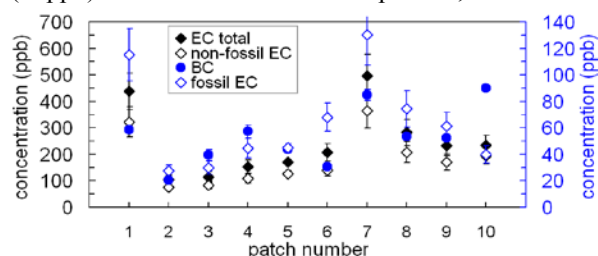


Fig. 2: EC and BC in samples from Olivares Beta glacier. Note the 5 times higher concentrations in total EC (left axis) compared to BC (right axis), while fossil EC and BC are of similar magnitude (right axis).

### ACKNOWLEDGEMENT

This study was funded by the Swiss State Secretariat for Education and Research SER (CJRP-1004).

### REFERENCES

- [1] A. Zapf et al., Radiocarbon **55**, 571 (2013).
- [2] T.M. Jenk et al., ACP **6**, 5381 (2006).
- [3] D. Bolius et al., Ann Glaciol, **43** (2006).
- [4] S. Trumbore, Ann. Earth Planet Sci., **37** (2009).

# AN EXTRACTION SYSTEM FOR RADIOCARBON MICROANALYSES OF DISSOLVED ORGANIC CARBON (DOC)

*J. Schindler (PSI & Univ. Bern), S. Szidat (Univ. Bern), M. Schwikowski (PSI & Univ. Bern)*

## INTRODUCTION

Alpine glaciers offer valuable archives of regional climate history. Precise depth-age relationships are essential for correct interpretation of such archives. For this effort, radiocarbon dating of the organic carbon contained in glacier ice provides a powerful tool. Thus, in complement to the analysis of the particulate fraction (POC) [1], we develop a system to extract the dissolved fraction (DOC) of organic carbon for concentration and radiocarbon analyses. Due to its relatively high concentrations from  $10^1$  to  $10^2$  ppb [2] and a reduced reservoir effect, DOC is a promising candidate for radiocarbon dating. However, its analysis is complicated by its susceptibility to contamination asking for a dedicated, ultraclean extraction system.

## SETUP AND METHOD

The complete system is designed to handle the sample under inert gas or vacuum conditions (Fig. 1). We installed a getter oven for supply of ultraclean helium as inert and carrier gas for the extraction and a turbomolecular pump for the sample processing atmosphere. To minimize contamination or memory effects from the extraction system, an all-glass setup sealed without organic lubricants is used to treat the sample in its liquid state and stainless steel parts with the reduced use of O-rings are used to handle it in its gaseous state. All steel parts were cleaned prior to installation by vacuum baking and assembled in a flow box. To enable operation at constant conditions, control cycles for the cryogenic water trap and the cooling water were installed. To ensure safe operation of the medium pressure mercury lamps used for photo oxidation of DOC, we constructed a housing to shield ultraviolet (UV) radiation from the user, vent unintentionally produced ozone and thereby cool the lamps.

We designed the setup - which is assembled by now - for the following extraction procedure: ice samples are cut and pre-cleaned in the cold room, tempered and further cleaned in a flow box. Up to  $450 \text{ cm}^3$  of ice can be introduced into the melting vessel for final cleaning and melting under helium inert gas. POC is separated by transferring the liquid sample by vacuum filtration through a quartz filter to the quartz photo reactor. The filtrate is acidified with phosphoric acid to degas inorganic carbon (IC). The DOC in the solution is photo oxidized to  $\text{CO}_2$  by irradiation with UV light and degassed with a helium carrier gas stream. A first cryogenic trap collects water vapor from the gas stream before the  $\text{CO}_2$  is frozen out in a second cryogenic trap. Analogous to the THEODORE setup [3], the  $\text{CO}_2$  sample is purified further, its concentration determined manometrically, and it is sampled into glass vials for radiocarbon analysis with the gas inlet system at the MICADAS AMS system [4] at the University of Bern.

## OUTLOOK

After calibration of the manometry unit using standards, next steps include the optimization and quantification of the separation efficiency of POC and IC as well as of the oxidation efficiency of DOC to  $\text{CO}_2$ . Possible loss of volatile DOC species, such as formate and acetate, and trapping efficiencies need to be addressed likewise. Finally, the preservation of the isotopic signal and the method blank need to be determined before validation studies can be started.

## ACKNOWLEDGEMENT

We thank Dave Piguet and Mario Birrer for technical support.

## REFERENCES

- [1] A. Zapf et al., *Radiocarbon*, **55** (2013).
- [2] M. Legrand et al., *Clim. Past*, **9**, 2195 (2013).
- [3] S. Szidat et al., *NIMB*, **223** (2004).
- [4] H.-A. Synal et al., *NIMB*, **259** (2007).

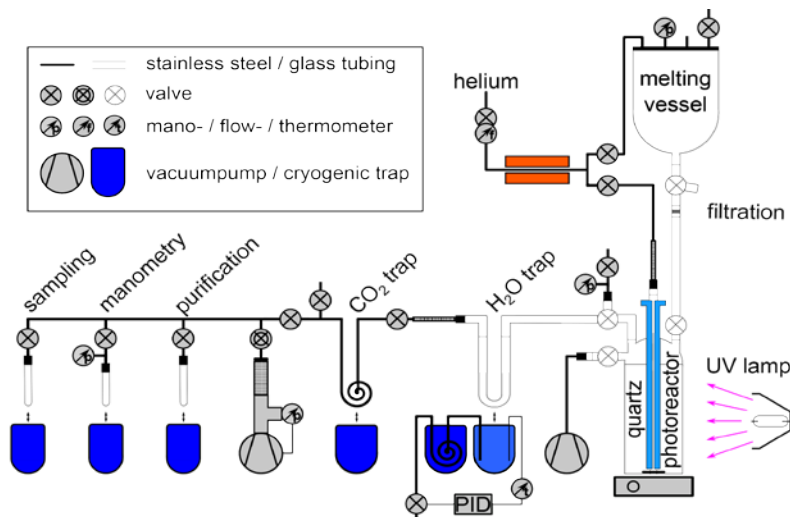


**Fig. 1:** Schematic of the extraction set-up.

# DEVELOPMENT AND FIRST APPLICATION OF A NEW METHOD FOR THE QUANTIFICATION OF GLYOXAL AND METHYLGLYOXAL IN SNOW AND ICE BY STIR BAR SORPTIVE EXTRACTION AND LIQUID DESORPTION-HPLC-ESI-MS

C. Müller-Tautges (Univ. Mainz), A. Eichler (PSI), M. Schwikowski (PSI & Univ. Bern), T. Hoffmann (Univ. Mainz)

In recent years the two smallest  $\alpha$ -dicarbonyls glyoxal (G) and methylglyoxal (MG) have received increasing attention from the scientific community due to their important role in the formation and growth of secondary organic aerosol (SOA), which affects the radiative budget of the earth's atmosphere and human health. G and MG are formed through gas phase oxidation of volatile organic compounds (VOCs) of anthropogenic (i.e. aromatics, alkenes) as well as biogenic (i.e. isoprene) origin [1]. Therefore, the targeted  $\alpha$ -dicarbonyls can be used as tracers of VOC oxidation chemistry and SOA within the analysis of climate archives like ice cores from the Alpine region.

This study presents the development and optimization of a new method for the analysis of G and MG in aqueous samples (snow and ice) and its first application to environmental samples.

The sample preparation comprises extraction, derivatization, and enrichment using stir bar sorptive extraction (SBSE) with liquid desorption (Fig. 1).

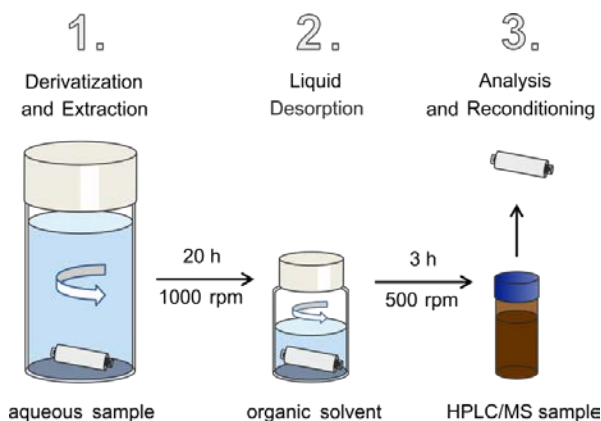


**Fig. 1:** Schematic workflow of the method.

SBSE is an equilibrium technique which uses a polydimethylsiloxan (PDMS) -coated stir bar. The extraction is based on the partitioning of the solutes between the silicon phase and the aqueous sample [2]. In contrast to the commonly used solid phase extraction (SPE), SBSE is less time-consuming and labor-intensive because of the simultaneous derivatization, extraction and enrichment of the analytes. Lower limits of detection can be achieved compared to solid phase micro extraction (SPME), due to a larger volume of the silicon phase.

Measurements were conducted on a reversed phase-high performance liquid chromatography coupled to electrospray ion trap mass spectrometry system (RP-HPLC-ESI-IT-MS). During method development parameters such as extraction time, liquid desorption time, and desorption solvent were optimized and the influences of NaCl addition and sample volume were investigated. To enhance extraction, chromatography and ionization properties, a derivatization step was applied. Best results were obtained by converting the analytes into the corresponding oximes using *O*-benzylhydroxylamin as derivatization reagent. Method calibration and validation parameters are given in Tab. 1.

**Tab. 1:** Calibration data. ILOD, ILOQ instrumental limit of detection/quantification.

	G	MG <sup>a</sup>
slope <sup>a</sup>	0.037	0.025
intercept	-0.018	-0.034
R	0.9988	0.9941
Recovery (%)	78.9 ± 5.6	82.7 ± 7.5
ILOD (ng/mL)	0.242	0.213
ILOQ (ng/mL)	0.807	0.711

<sup>a</sup>determined using the measured signal area quotient (analyte/internal standard)

As proof of principle, two ice core samples from different years (1991 and 1959) from an ice core from the Upper Grenzgletscher in the southern Swiss Alps were analyzed to evaluate the method performance. Resulting concentrations were 0.178 ng/g (3.06 nM) for G and 0.126 ng/g (1.75 nM) for MG in sample 1 and 0.085 ng/g (1.46 nM) for G in sample 2 with MG below detection limit for a sample volume of 15 mL.

The method showed good applicability for the analysis of trace amounts of G and MG in ice; however, a larger dataset is needed in order to obtain detailed information on historic records of the compounds of interest, especially in combination with other marker compounds. Measurements of ice core samples from 1941 to 1993 (date of drilling) are in progress.

## REFERENCES

- [1] T. Fu et al., *J. Geophys. Res.* 113 (D15):D15303 (2008).
- [2] F. David, P. Sandra, *J. Chromatogr. A*, 1152, 54-69 (2007).

## STUDYING $^{10}\text{Be}$ VARIATIONS IN THE FIRST NON-POLAR ICE CORE – TSAMBAGARAV, MONGOLIA

*F. Inceoglu, M. Faurschou Knudsen, C. Karoff, J. Olsen (Aarhus Univ.),  
P.-A. Herren, M. Schwikowski (PSI & Univ. Bern)*

Solar reconstructions covering the last ~500 years are so far only based on  $^{10}\text{Be}$  measurements from polar ice cores. Such reconstructions are potentially misleading as they are sensitive to incomplete mixing of  $^{10}\text{Be}$  in the atmosphere and low deposition rates over the polar regions [1, 2]. These studies provide proxy data for solar activity changes, but we aim at producing a global reconstruction of  $^{10}\text{Be}$  production rates over this period by combining a new high-resolution  $^{10}\text{Be}$  record from a mid-latitude ice-core with existing  $^{10}\text{Be}$  records from Greenland and Antarctica [1, 3, 4, 5]. We apply statistical methods and physical/empirical models in order to reconstruct solar activity back in time and better understand the solar component and climate-related component contained in the high-resolution  $^{10}\text{Be}$  records.

The Tsambagarav ice core, which was collected in 2009 in Mongolia, spans 5-6 millennia [6]. Based on material from this ice core, it is possible to construct a high-resolution  $^{10}\text{Be}$  record over the past approximately 4-600 years. In this project, we have started to measure  $^{10}\text{Be}$  at the highest possible resolution for the last ~300 years.

Appropriate sample preparations are crucial in order to extract the  $^{10}\text{Be}$  signal locked in the ice. After collecting the samples from the ice-core repository of the PSI, 100  $\mu\text{L}$  of  $^9\text{Be}$  carrier was added. The samples were then melted and filtered using filters with a pore size of 0.45  $\mu\text{m}$  in order to trap the  $^{10}\text{Be}$  adhered to the dust particles potentially contained in the ice. Subsequently, filtered ice-core water and  $^9\text{Be}$  carrier were run through BIO-RAD ion-exchange columns to isolate the beryllium. We then extracted the beryllium from the ion-exchange columns by adding 25 ml HCl and then 10 ml  $\text{NH}_3$  to the columns. After extracting  $\text{BeO}$ , the samples were left in an oven at 800 degrees

over night. Following, Nb powder was mixed with the beryllium samples before this combined mixture was pressed into cathodes for AMS measurement. Measurements were carried out at the AMS facility in Uppsala, Sweden.

The preliminary results look promising (Fig. 1). As expected, the known grand solar minima stand out as positive anomalies in the  $^{10}\text{Be}$  concentration, in particular around the Dalton Minimum (~1815 AD), and around ~1716 AD, which corresponds to the termination of the prominent Maunder Minimum (MM). The present  $^{10}\text{Be}$  record from the Tsambagarav ice core only covers the very end of the MM, but further studies are expected to provide new insights into the solar activity level during this well-known solar minimum, which has been associated with climatic changes in the Northern Hemisphere. The present record further shows that large volcanic eruptions, in particular the Mt. Pinatubo eruption in 1991 AD, are associated with abrupt, positive anomalies in the  $^{10}\text{Be}$  concentration. Detailed studies of this relationship will enhance our understanding of how volcanic dust influences the transport and deposition of meteoric  $^{10}\text{Be}$ .

### REFERENCES

- [1] E. Bard et al., *Earth and Planetary Science Lett.* **150**, 453 (1997).
- [2] C.V. Field et al., *J. Geophys. Res.* **111** D15107, doi:10.1029/2005JD006410 (2006).
- [3] M. Vonmoos et al., *J. Geophys. Res.*, **111**, A10105 (2006).
- [4] R. Muscheler et al., *Quaternary Sci. Rev.* **26**, 82 doi:10.1016/j.quascirev.2006.07.012 (2007).
- [5] K. Horiuchi et al., *Quat. Geochronol.*, **3**, 253 (2008).
- [6] P.-A. Herren et al., *Quaternary Sci. Rev.* **69** 59 (2013).

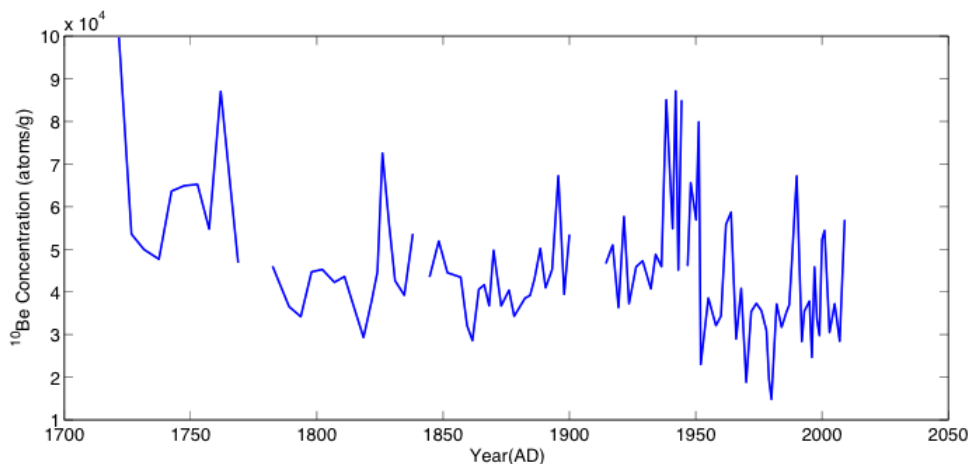


**Fig. 1:** The Tsambagarav  $^{10}\text{Be}$  concentration during the time period 1716-2009.

## RECENT ACCUMULATION RATES ON FINDELENGLETSCHER DERIVED FROM AIRBORNE GPR AND FIRN CORES

L. Sold (Univ. Fribourg), A. Eichler (PSI), M. Hoelzle, M. Huss (Univ. Fribourg), M. Schwikowski (PSI)

The accumulation areas of glaciers contain a record of their past accumulation rates. The water equivalent of annual firn layers can be used to initiate or extend existing time series of local mass balance and, ultimately, to consolidate the knowledge on the response of glaciers to changing climatic conditions. Measurements of the thickness and density of firn layers typically involve drilling in remote areas and core analysis and are thus expensive in terms of time and effort.

Ground-penetrating radar (GPR) provides a non-destructive tool for various applications in glaciology that is sensitive to changes in the material properties such as to density variations at former summer surfaces [1]. Airborne surveys allow measurements to be taken in remote and inaccessible areas. However, to transfer information from the GPR pulse travel time to the depth domain, the dielectric permittivity of the material is required, that can be estimated from the firn density [2]. Furthermore, it must be verified that the detected layers actually represent annual layers.

From 2010 to 2013 airborne 500MHz single-offset GPR measurements were conducted each spring on Findelengletscher, Switzerland, with a penetration depth of  $\sim 10$  m [3]. To complement the GPR data three shallow firn cores were taken in the accumulation area in May 2012. The choice for the sampling sites was based on the availability of GPR data from previous years at these locations. The cores are about 10 m long and were analyzed regarding their density, concentration of major ions and water stable isotope ratio ( $\delta D$ ) with a vertical resolution of  $\sim 6$  cm. The ammonium ( $NH_4^+$ ) concentration is known to show seasonality due to higher source activity and lower stability of the atmosphere in summer [4]. The  $\delta D$  serves as a proxy for air temperature during precipitation formation [5].

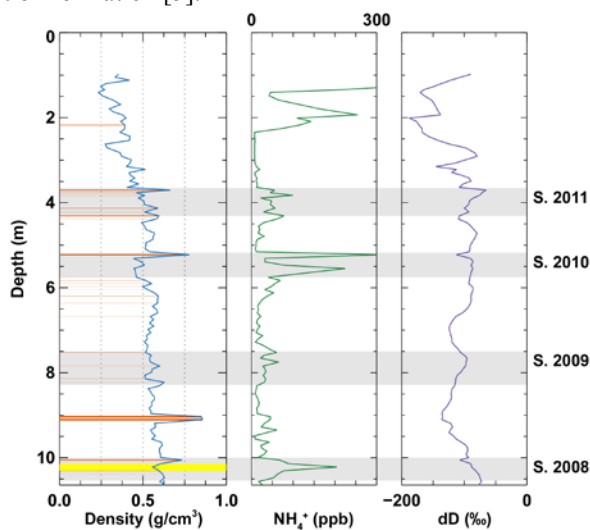


**Fig. 1:** Vertical density profile of core 1, ice layers (orange bars), dust layer (yellow bar),  $NH_4^+$  concentration, and isotope ratio  $\delta D$  with summer layers marked.

For the three firn cores we observed a variable density profile that generally increases with depth (Fig. 1). Peak densities corresponded to ice layers and in many cases to maxima in  $NH_4^+$  concentration. The dust layer that was visible in all three cores can unambiguously be linked to a Sahara dust fall on 28 May, 2008 [6]. Together with the stable isotope ratio  $\delta D$  dating of ice layers as former glacier summer surfaces was established.

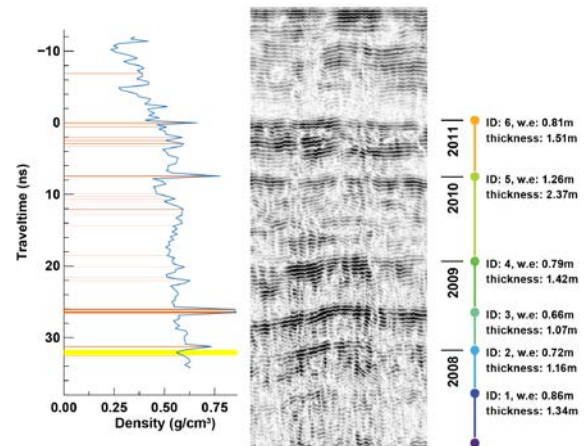


**Fig. 2:** Density profile converted to the traveltime-domain, the corresponding GPR profile and recognized firn layers and summer surfaces for core 1.

From the firn density profiles the GPR wave velocity was estimated using empirical relations [3] allowing a direct comparison between the two methods (Fig. 2). We observed a good agreement of the GPR signal with pronounced changes in the density profile. This underlines the high potential of GPR for the detection of firn layers. However, not all peak-densities and thick ice layers represent a former glacier summer surface but can also be due to melting and refreezing during winter, i.e. between 2008 and 2009. Thus, at Findelengletscher, additional dating information such as from firn cores is necessary. Because GPR data was available for the same location for several consecutive years, the dating of layers could also be derived by tracking the uppermost layers over time. Still, the firn density remained unknown but can be modelled, for instance after [7], to obtain the wave velocity and water equivalent of the layers only based on GPR-measurements.

### REFERENCES

- [1] L.A. Plewes et al. *Prog. Phys. Geogr.* **25**, 203 (2001).
- [2] A.D. Frolov et al. *Hydrol. Process.* **13**, 1755 (1999).
- [3] L. Sold et al. *J. Glaciol.* **59**, 1047 (2013).
- [4] A. Eichler et al. *J. Glaciol.* **46**, 507 (2000).
- [5] W. Dansgaard, *Tellus* **16**, 436 (1964).
- [6] [http://www.meteoschweiz.admin.ch/web/de/wetter/wetterereignisse/foehnsturm\\_27\\_28.html](http://www.meteoschweiz.admin.ch/web/de/wetter/wetterereignisse/foehnsturm_27_28.html)
- [7] N.J. Reeh, *Geophys. Res.* **113**, F03023 (2008).

## TRITIUM FALLOUT FROM FUKUSHIMA ACCIDENT IN SWITZERLAND?

A. Eichler (PSI), J. Eikenberg, M. Rüthi (PSI/ASI), L. Sold, M. Hoelzle (Univ. Fribourg),  
M. Schwikowski (PSI & Univ. Bern)

Atmospheric thermonuclear testing during the 1950s and early 1960s led to a considerable release of anthropogenic tritium, significantly influencing the worldwide precipitation composition for several decades. During March 2011 a series of accidents at the Fukushima Dai-ichi Nuclear Power Plant (FDNPP) released likewise anthropogenic tritium into the atmosphere. Tritium activities of up to 160 TU were observed in precipitation at Tsukuba (170 km SE of Fukushima), comparable to the activities observed in mid-1960's precipitation containing bomb tritium [1]. In this study we aim to investigate, if the tritium activities in precipitation in Switzerland were enhanced following the FDNPP accident.

Three 10 m firn cores were recovered at the Findelen glacier (46° 0' 33" N, 7° 50' 32" E, 3500 m asl.) in May 2012 [2]. The initial purpose of the campaign was to reconstruct past accumulation rates with Ground-Penetrating Radar (GPR) validated with firn core data. Dating of the cores was performed by annual layer counting using the pronounced seasonality of  $\text{NH}_4^+$  concentration and the water stable isotope ratio  $\delta\text{D}$ . Core 1 covers the period summer 2008 - spring 2012 [2], whereas core 2 contains information about the 5-years period summer 2007 - spring 2012 (Fig. 1). Tritium was measured in 27 samples of the core 2 using liquid scintillation spectroscopy.

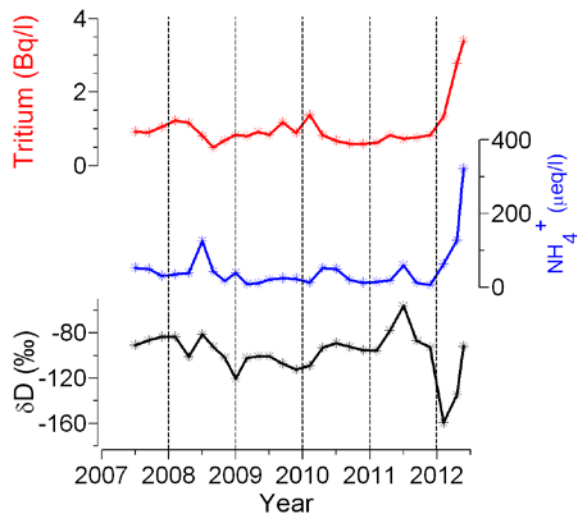


**Fig. 1:** Tritium (red),  $\text{NH}_4^+$  (blue), and  $\delta\text{D}$  (black) records of the Findelen firn core 2.

The tritium record shows enhanced activities in surface layers deposited during winter/spring 2011/12, but is rather smoothed in the period 2007-2011. Two possible reasons for the enrichment will be discussed:

- (1) Tritium fallout from the FDNPP accident
- (2) Smoothing of deeper records by melt water.

(1) To investigate a possible input from the FDNPP accident we compare our record with tritium in Swiss precipitation, measured continuously at ISOT stations until 2010 [3]. Due to the nowadays very low tritium activities, the Federal Office of Public Health (FOPH)

continues measurements only at selected stations as Fribourg and Basel ([3], P. Steinmann, personal comm.). These measurements demonstrate a weak seasonal tritium cycle, revealing generally higher activities in spring due to the enhanced stratosphere - troposphere exchange ("spring leak") (Fig. 2). However, there is no enrichment in precipitation tritium after March 2011.

Contrary to the injection of "bomb-tritium" into the stratosphere, tritium from the FDNPP accident was mainly released into the troposphere. Thus, it was quickly removed from the atmosphere by precipitation close to the site. Accordingly, tritium in precipitation in Japan decreased rapidly with time and reached pre-accident background values within five weeks [1].

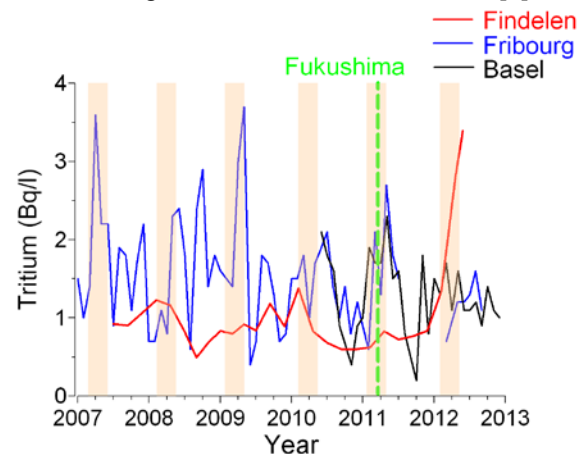


**Fig. 2:** Tritium activity in the Findelen firn core 2 (red) and in precipitation in Binningen (Basel) (black) and Fribourg (blue). Spring precipitation (brown) and the date of the Fukushima accident (green) are marked.

(2) Due to the relatively low altitude of the drilling site, air temperatures partially exceed  $0^\circ\text{C}$  in summer and melting occurs, strongly influencing the chemical and isotopic composition at this temperate glacier. Since the drilling was in spring 2012, surface layers are less affected by melting and the annual cycle with high values in spring/summer and low values in winter is still preserved (see e.g.  $\text{NH}_4^+$  and  $\delta\text{D}$ , Fig. 1). Contrary, enhanced melting during the summer in 2011 and the preceding years led to a smoothing of the seasonal cycle. Thus, we assume that the tritium maximum at the surface layers corresponds to the spring maximum 2012, whereas possible preceding maxima are smoothed out during melt water percolation.

### ACKNOWLEDGEMENT

We thank P. Steinmann from FOPH for providing tritium data of precipitation in Switzerland.

### REFERENCES

- [1] T. Matsumoto et al., *Sci. Tot. Environm.* **445-446**, 365 (2013).
- [2] L. Sold et al., this report, p. 37.
- [3] U. Schotterer et al., *GWA* **12**, 1073 (2010).

## RADIOACTIVE ION BEAMS FROM ACCELERATOR WASTE A TOOL TO INVESTIGATE EXPLOSIVE STARS

R. Dressler (PSI), V. Margerin, A. St.J. Murphy (Univ. Edinburgh), D. Schumann (PSI), C. Seiffert, T. Stora (CERN), T. Stowasser (PSI)

### INTRODUCTION

Massive stars, typically with a mass greater than eight solar masses, end their life as a core collapse supernova explosion, exhibiting extreme temperature and density. In this environment intense nuclear synthesis takes place, and it is therefore thought to be the site of the production of the heavier elements found in the Universe. The details of the physical processes triggering this explosion are still under debate, mainly due to a lack of data originating from the collapse process itself.

The observation of light curves and optical spectra from supernovae remnants provides almost no information about the physical details. Therefore, the isotope  $^{44}\text{Ti}$  is of particular interest both because many supernovae models forecast that the amount of ejected  $^{44}\text{Ti}$  is sensitive to the underlying explosion mechanism, and due to the possibility to observe its decay using space based radio telescopes.

In addition to the  $^{44}\text{Ti}$  production and decay rates, the rates of other reactions must also be well known to interpret a signal. It is expected that the most influential destruction reaction during the explosion phase will be  $^{44}\text{Ti}(\alpha, p)^{47}\text{V}$  [1, 2]. A main ingredient to exploit the obtained signals from space is the determination of the relevant cross-sections at stellar energies.

### EXPERIMENT

We report on experiments performed at REX-ISOLDE (CERN) where the  $^{44}\text{Ti}(\alpha, p)^{47}\text{V}$  reaction was studied in an inverse kinematics approach using a novel technique to generate a radioactive  $^{44}\text{Ti}$  beam.

Samples from the SINQ target irradiation program (STIP) at PSI were used to obtain the needed quantity of  $^{44}\text{Ti}$ . Selected martensitic stainless steel specimens were irradiated from 1998 to 1999. After a subsequent cooling period of more than 10 years it was possible to perform the chemical separation without using dedicated hot cell equipment. Using a series of extraction and precipitation steps, a pure  $\text{TiCl}_4$  fraction with about 50 MBq  $^{44}\text{Ti}$  was obtained. More details of the performed chemical treatments can be found in [3]. The material was transferred into fluoride compounds using HF, evaporated to dryness on a crucible made of Mo-foil and transported to the ISOLDE (CERN) class A hot lab.

A molybdenum crucible was placed into a VADIS FEBIAD ion source to produce a molecular beam of  $\text{TiF}_3^+$  at the General Purpose (mass) Separator Front End of REX-ISOLDE (CERN). The connected LINAC accelerator was utilized to generate a 2.1 MeV/u  $^{44}\text{Ti}^{13+}$  beam with an intensity of  $5 \times 10^5$  to  $2 \times 10^6$  particles per second [4]. This was directed to a He-gas cell equipped with thin entrance and exit Al-windows.

In this manner, the  $^{44}\text{Ti}(\alpha, p)^{47}\text{V}$  reaction could be studied for the first time at a center of mass energy of 4.15 MeV, i.e. within the Gamow window relevant for core collapsed supernovae. A previous investigation (see [5]) used only significantly higher center of mass energies and needs additional models like the NON SMOKER prediction [6, 7] to deduce cross-sections at interesting energies.

During the 4 days beam-time, two experiments were performed, one with the gas-cell filled with He at a pressure of  $\approx 67$  mbar, and one in which it was evacuated. The outgoing light particles were recorded using a  $\Delta E$ -E-telescope. The data analysis comparing the recorded event rates of both experiments taking into account the expectations of different background components from detailed Monte-Carlo simulations revealed no evidence for the observation of the  $^{44}\text{Ti}(\alpha, p)^{47}\text{V}$  reaction. An upper limit of 40  $\mu\text{b}$  at a confidence level of 68% has been established (for more details see [8]). This value is a factor of two lower than the NON SMOKER predictions of 88  $\mu\text{b}$  (see Fig. 1).

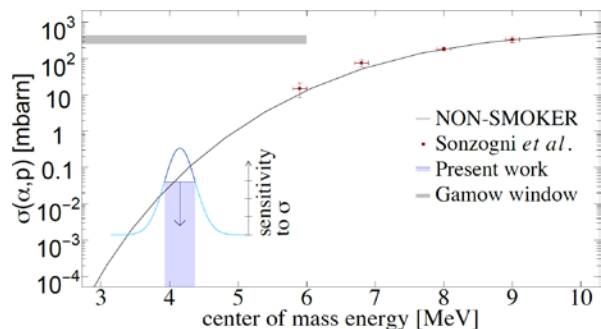


**Fig. 1:** Comparison of the measured cross sections (red points taken from [5]), this experimental limit and the NON-SMOKER prediction (black line) for the  $^{44}\text{Ti}(\alpha, p)^{47}\text{V}$  reaction (from [8]).

### REFERENCES

- [1] G. Magkotsios et al., *Astrophys. J. Suppl. Series*, **191**, 66 (2010).
- [2] L.-S. The et al., *Astrophys. J.*, **504**, 500 (1998).
- [3] R. Dressler et al., *J. Phys. G: Nucl. Part. Phys.*, **39**, 105201 (2012).
- [4] T. Stora, *Nucl. Instr. Meth.*, **B 317**, 402 (2013).
- [5] A.A. Sonzogni et al., *Phys. Rev. Lett.*, **84**, 1651 (2000).
- [6] T. Rauscher and F.-K. Thielemann, in ‘Stellar Evolution, Stellar Explosions and Galactic Chemical Evolution’, ed. A. Mezzacappa (IOP, Bristol), 519 (1998).
- [7] T. Rauscher and F.-K. Thielemann, *At. Data Nucl. Data Tab.*, **75**, 1 (2000) 1 and **79**, 47 (2001).
- [8] V. Margerin et al., submitted to *Phys. Rev. Lett.* (2014).

# DETERMINATION OF THE $^{14}\text{C}$ CONTENT IN ACTIVATED STEEL COMPONENTS FROM A NUCLEAR POWER PLANT

*D. Schumann, T. Stowasser (PSI), I. Günther-Leopold, H.P. Linder (PSI/AHL), E. Wieland (PSI/LES), B. Volmert (NAGRA)*

## INTRODUCTION

Knowledge of the radionuclide inventories is a prerequisite for the quantitative evaluation of the radiological hazard of radionuclides released from a repository for radioactive waste. In the case of nuclear facility hardware, like steel components, the main short- and mid-term dose rate contributors  $^{60}\text{Co}$  and  $^{54}\text{Mn}$  can easily be determined by measuring the intensity of their  $\gamma$  rays. The determination of long-lived isotopes, however, such as  $^{14}\text{C}$  with a half-life of 5730 y requires cost intensive and time consuming chemical separation techniques in the course of the radioanalytical measurements.  $^{14}\text{C}$  is not only of particular interest due to its nuclear properties, but also because of the chemical behavior of the  $^{14}\text{C}$  containing compounds expected to be formed during anoxic steel corrosion. Several studies indicate both the possible formation of volatile organic carbon compounds as well as alcohols, aldehydes and carboxylic acid remaining in solution during steel corrosion [1]. All these species feature a high radiological risk due to their high mobility either in the liquid or in the gas phase. The present study is aimed at determining experimentally the  $^{14}\text{C}$  content in activated steel samples relevant to the Swiss disposal program, originating from the NPP Gösgen (KKG). We applied a wet acid chemistry method for sample digestion. The results obtained by Liquid Scintillation Counting (LSC) are compared with theoretical predictions of the inventory of activation products, using as reference also the values for  $^{54}\text{Mn}$  and  $^{60}\text{Co}$ . The obtained and evaluated values shall serve as basic information in conjunction with future corrosion experiments [2].

## EXPERIMENTAL

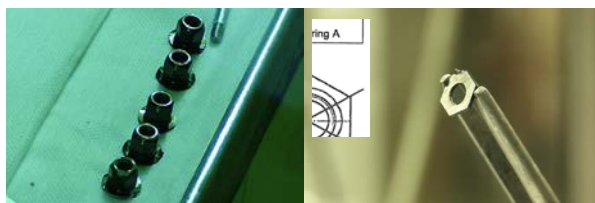


**Fig. 1:** a) Activated steel nuts obtained from KKG, b) Segment prepared from a steel nut. Inset: Cutting scheme of the segment

Five stainless steel guide tube nuts (~5 g each, exposed to neutron flux for 2 years) were retrieved from the storage pool of KKG (Fig. 1a). One of them was cut into slices and following into 6 pieces (Fig. 1b). Digestion in acidic solution was applied for extracting carbon from the metallic sample material. About 100 mg of steel sample were placed into a two-neck reaction vessel and flushed with nitrogen.

The gas flow was led through a reflux condenser, followed by a first gas-sampling unit filled with 50 ml 1 M HCl for catching traces of acid vapor and finally through two gas-sampling units filled with 20 ml 1 M NaOH each, for the absorption of  $\text{CO}_2$ . A mixture of concentrated  $\text{HNO}_3$  and HCl, 5 ml each (aqua regia), was added via an acid reservoir which was tightly connected to the apparatus. The acid solution in the reaction vessel was heated for about 10 min till the steel was dissolved. The remaining carbon was dissolved separately by adding a mixture of  $\text{H}_2\text{SO}_4/\text{HClO}_4/\text{HNO}_3$ . Standard  $\gamma$ -spectrometry and LSC were used for radioanalysis.

For the theoretical predictions, a Monte Carlo n-particle (MCNP) reactor model [3] for the KKG, set up by Nagra for the Swiss NPP decommissioning study 2011 [4] was used as standard model for the present calculations (for details see [5]).

## RESULTS AND DISCUSSION

**Tab. 1:** Mean values of the radionuclide activities at EOB (4.6.2011) for the investigated steel samples; activities are related to the mass of sample material.

Sample	$^{14}\text{C}$ [kBq/g]	$^{54}\text{Mn}$ [MBq/g]	$^{60}\text{Co}$ [MBq/g]
NPP-Screw nut	17.8 ± 1.4	57 ± 1	79.4 ± 0.8
Prediction	4.5	21	34.8

In Tab. 1, the mean values of the radiochemical analysis for  $^{14}\text{C}$ ,  $^{54}\text{Mn}$ , and  $^{60}\text{Co}$  of 3 similar samples are summarized. The experimentally determined activities agree within a factor 2-4 with the theoretical predictions. This difference is acceptable with regard to uncertainties in the underlying assumptions (for details see [5]). Knowledge of the  $^{14}\text{C}$  activities in the studied steel is important in connection with the planned corrosion study focusing on the identification and quantification of  $^{14}\text{C}$  containing organics generated during the anaerobic corrosion of activated steel under simulated near field conditions.

## ACKNOWLEDGEMENT

The project was funded by NAGRA.

## REFERENCES

- [1] E. Wieland et al., PSI report TM-44-10-01, 2010.
- [2] E. Wieland Swiss Nuclear Proposal Nr.2, 2012.
- [3] X-5 Monte Carlo Team, MCNP – A general Monte Carlo n-particle transport code, version 5, LA-UR-03-1987, LANL (2008).
- [4] B. Volmert, M. Pantelias, Jahrestagung Kerntechnik, Berlin, May 14-16 (2013).
- [5] D. Schumann et al., RCA 2014, to be submitted.

## DETERMINATION OF $^{36}\text{Cl}$ IN REACTOR GRAPHITE

T. Stowasser, D. Schumann (PSI), H.-F. Beer, E. Hartmann, H. Kramer (PSI/Rückbau/Entsorgung),  
C. Vockenhuber (ETHZ)

### INTRODUCTION

Two of the three research reactors at PSI, the reactors DIORIT and PROTEUS, contained reactor graphite. Whereas the former research reactor DIORIT has been dismantled completely, the PROTEUS is subject to future decommissioning. The radionuclide inventory of the activated reactor graphite from DIORIT had been reported earlier in [1]. In addition, the  $^{36}\text{Cl}$  activity for both reactor graphite types had to be determined according to the requirements of ENSI [2]. Since the graphite from DIORIT is already conditioned, the  $^{36}\text{Cl}$  content had to be determined afterwards.

### EXPERIMENTAL

16 pulverized graphite samples had been processed. Two different activity measurement methods have been applied depending on the  $^{36}\text{Cl}$  activity range: AMS (Accelerator Mass Spectrometry; ETHZ) for concentration ranges from 0.001 to 5 Bq/g (PROTEUS) and LSC (Liquid Scintillation Counting) for activities above 5 Bq/g (DIORIT). The measurement methods require different digestion methods for the graphite.

DIORIT: 0.05 - 1g graphite and 20 - 50 ml acid ( $\text{H}_2\text{SO}_4$  conc. :  $\text{HNO}_3$  conc. = 2:1) were boiled under reflux until the C was dissolved. The Cl-vapors were transported by a nitrogen stream in two series-connected absorption vessels containing silver nitrate (0.5g  $\text{AgNO}_3$  dissolved in 40ml  $\text{H}_2\text{O}$ ) and 10 mg Cl-carrier. The formed  $\text{AgCl}$  was re-precipitated twice, dissolved in  $\text{NH}_3$  (13%), and mixed with the scintillator Aquasafe 500 plus for measurement.

PROTEUS: 20 mg of graphite, 1 ml of concentrated  $\text{HClO}_4$  and 2 mg  $\text{CrO}_3$  were transferred into a three-neck-flask and heated until dryness. A nitrogen stream transported the Cl-vapors in an absorption vessel containing silver nitrate. The formed  $\text{AgCl}$  was re-precipitated twice and dried at 90°C. The yield of  $\text{AgCl}$  was determined by weighing. Since AMS measures an isotopic ratio of  $^{36}\text{Cl}$ :  $\text{Cl}_{\text{stable}}$ , the number of stable Cl atoms must be calculated from the mass of  $\text{AgCl}$ . Selected DIORIT samples were diluted with inactive  $\text{AgCl}$  and measured via AMS for comparison. The  $^{36}\text{Cl}$  yield cannot be determined exactly, because a certified graphite standard containing a known  $^{36}\text{Cl}$  amount is not available. We used liquid  $^{36}\text{Cl}$  standard and inactive graphite in similar digestion procedures, assuming that  $^{36}\text{Cl}$  released from the activated graphite behaves similar to the liquid standard. However, a correction had to be performed for the  $\text{HClO}_4/\text{CrO}_3$  digestion, due to synproportionation reactions of the chlorine species.

### RESULTS AND DISCUSSION

In Tab.1, the experimental results for both reactor types are summarized. In the last column, the values

for  $^{154}\text{Eu}$ , determined in earlier measurements, are added for comparison.

**Tab. 1:**  $^{36}\text{Cl}$ -activities from DIORIT (no. 1 to 6) and PROTEUS (no. 7 to 16); \* calculated for a graphite content in mortar of 40% \*\* SD = standard deviation <sup>1</sup> one measurement, <sup>2</sup> two measurements, <sup>3</sup> three measurements; n.d.: not determined

No	Origin	Method	$^{36}\text{Cl}$ [Bq/g]±SD**	$^{154}\text{Eu}$ [Bq/g]
1	DIORIT trial 36	LSC	22.5±1.25* <sup>2</sup>	272.5*
2	DIORIT trial 67	LSC	67.5±3.75* <sup>2</sup>	500*
3	DIORIT channel N3	LSC	414±19.40 <sup>3</sup>	586*
4	DIORIT channel N3	LSC	291±23.50 <sup>3</sup>	673
5	DIORIT drum 2425	LSC	35* <sup>1</sup>	437.5*
6	DIORIT drum 4058	LSC	52.5±0.4* <sup>2</sup>	505*
7	PROTEUS 2a	AMS	0.031±0.009 <sup>2</sup>	n.d.
8	PROTEUS MP4	AMS	0.014±0.002 <sup>2</sup>	n.d.
9	PROTEUS MP5	AMS	0.008±0.000 <sup>2</sup>	n.d.
10	PROTEUS MP6	AMS	0.008 <sup>1</sup>	n.d.
11	PROTEUS MP7	AMS	0.014±0.009 <sup>2</sup>	n.d.
12	PROTEUS 1	AMS	0.005±0.000 <sup>2</sup>	<30
13	PROTEUS 2	AMS	0.005±0.002 <sup>2</sup>	<30
14	PROTEUS 3	AMS	0.005±0.002 <sup>2</sup>	<30
15	PROTEUS 4	AMS	0.003±0.000 <sup>2</sup>	<30
16	PROTEUS 5	AMS	0.008±0.007 <sup>2</sup>	<30

The samples from DIORIT are much more activated than those from PROTEUS, the latter being a so called zero power reactor with nominal 1 kW and  $5 \times 10^9$  n/(cm<sup>2</sup>\*s) neutron flux, whereas the DIORIT finally had a power of 30 MW and  $4 \times 10^{13}$  n/(cm<sup>2</sup>\*s) neutron flux. As a result, the values for PROTEUS are far below the Swiss exemption limits (LE), including  $^{36}\text{Cl}$  ranging between 0.003 and 0.031 Bq/g (LE=10 Bq/g  $^{36}\text{Cl}$ ). Therefore, the graphite from the research reactor PROTEUS does not result in radioactive waste. Nevertheless, a small difference can be seen between samples taken from the periphery (Nr. 12 to 16) to those taken from the inner part (Nr. 8 to 11). In contrast, the DIORIT samples [1] showed in all cases values above the exemption limits and had to be conditioned as radioactive waste [3]. The  $^{36}\text{Cl}$  activity is in the same order of magnitude as reported by Hou et al [4] for graphite from the Danish DR2 reactor. There are differences between the samples from DIORIT taken near the beam channel N3 with a higher n-flux and the samples from the periphery with a lower n-flux. The values for  $^{36}\text{Cl}$  correspond in these cases with the values determined for  $^{154}\text{Eu}$ .

The work was part of the IAEA coordinated research project "Treatment of Irradiated Reactor Graphite to Meet Acceptance Criteria for Waste Disposal".

### REFERENCES

- [1] H.-F. Beer, Strahlenschutzpraxis, **4** (2009) 64.
- [2] ENSI-Richtlinie B-05, Anforderung an die Konditionierung radioaktiver Abfälle.
- [3] H.-F. Beer, Strahlenschutzpraxis, **2** (2013) 32.
- [4] X.L. Hou, Anal. Chem. **79** (2007), 3126.

# THERMOCHROMATOGRAPHY STUDY OF ELEMENTAL POLONIUM

*E. A. Maugeri, J. Neuhausen, R. Eichler, D. Piguet, A. Vögele, D. Schumann (PSI), T. Melo Mendonça, T. Stora (CERN/ISOLDE)*

## INTRODUCTION

For a safe use of lead-bismuth eutectic as coolant and spallation target material for accelerator-driven systems, it is necessary to assess the volatility of Po (produced by ( $p, xn$ ) and ( $n, \gamma$ ) reactions with Bi) and its compounds. This report presents a thermochromatography (TC) study of elemental Po, aimed to determine its adsorption enthalpy on fused silica and its sublimation enthalpy. These values will be then used to assess the relative volatility of Po and its compounds.

## EXPERIMENTAL

$^{206}\text{Po}$  was obtained following two different procedures: 1) Implantation of  $^{210}\text{Fr}$  (98% of  $^{210}\text{Fr}$  decays via  $\text{EC}/\beta^+ \rightarrow ^{210}\text{Rn} \xrightarrow{\alpha} ^{206}\text{Po}$ ) obtained by high energy proton irradiation of a uranium target at the CERN-ISOLDE facility, into Mo and Au foils (samples Po01 and Po02 in Tab. 1);

2) 40 MeV proton irradiation of Bi metal. The obtained Po was separated from the Bi matrix by evaporation at 1223 K under He flow and deposition on Au (samples Po03 and Po04).

The experiments were performed using a thermochromatography setup consisting of a fused silica tube in a negative gradient furnace with a temperature profile ranging from 1173 to 298 K (samples Po01 and Po02) and from 1323 to 298 K (samples Po03 and Po04), equipped with a carrier gas in- and outlet and a Ta-getter at the inlet. In the experiments Po03 and Po04, a Ta foil was placed in the temperature gradient, at around 1323 K, to destroy possibly formed oxidic species.

## THERMOCHROMATOGRAPHY WITH INERT AND WITH REDUCING CARRIER GAS

Sample Po01 was studied using  $\text{H}_2$  as carrier gas. The obtained thermochromatogram (TCm), Fig. 1 (A) yellow bars indicates that only one species formed and deposited at 545 K. Considering the chemical potential of the carrier gas and the homologous behavior of Po to previously studied Te only elemental Po or  $\text{H}_2\text{Po}$  can be formed. Using the Monte Carlo simulation method [1] (Fig. 1 (A) red bars) an adsorption enthalpy,  $\Delta H_{\text{ads}}$ , of  $-126 \pm 10 \text{ kJ mol}^{-1}$  was calculated for the deposited species. Using this value in the empirical correlation between  $\Delta H_{\text{ads}}$  and sublimation enthalpy,  $\Delta H_{\text{sub}}$ , [2], a value of  $\Delta H_{\text{sub}}$  of  $171 \pm 40 \text{ kJ mol}^{-1}$  was calculated. A similar result was obtained for the sample Po02 evaporated from Au, grey bars in Fig.1 (A). Sample Po03 was studied using purified He as carrier gas. The obtained TCm, Fig.1 (B) yellow bars reveals a peak centered at 580 K. The  $\Delta H_{\text{ads}}$  and  $\Delta H_{\text{sub}}$  of the

deposited species were calculated to be  $-136 \pm 10 \text{ kJ mol}^{-1}$  and  $186 \pm 40 \text{ kJ mol}^{-1}$ , respectively.

**Tab. 1:** Experimental conditions and results.

Sample number	Po01	Po02	Po03	Po04
Evaporated from	Mo	Au	Au	Au
Carrier gas	$\text{H}_2$	$\text{H}_2$	He	He
$T_{\text{dep}}$ (K)	545	545	580	289
$\Delta H_{\text{ads}}$ ( $\text{kJ mol}^{-1}$ )	$-126 \pm 10$	$-126 \pm 10$	$-136 \pm 10$	-
$\Delta H_{\text{sub}}$ ( $\text{kJ mol}^{-1}$ )	$171 \pm 40$	$171 \pm 40$	$186 \pm 40$	-
Chemical species	Po	Po	Po	$[\text{PoH}_2]$ $[\text{Po}(\text{OH})_x]$

Considering the uncertainty of the method, it was concluded that the same species was obtained using inert (He) and reducing ( $\text{H}_2$ ) carrier gases. The value of  $\Delta H_{\text{sub}}$  calculated in this work is very close to the one reported in [3] for elemental Po,  $188.9 \text{ kJ mol}^{-1}$ . In one experiment, Po04, orange dotted line in Fig. 1(B), a deposition at 289 K was obtained, using He as carrier gas. The formation of this volatile species could be due to the reaction of Po with  $\text{H}^\cdot$  or  $\cdot\text{OH}$  formed by  $\text{H}_2\text{O}$  dissociation on Ta, used to trap the oxides.

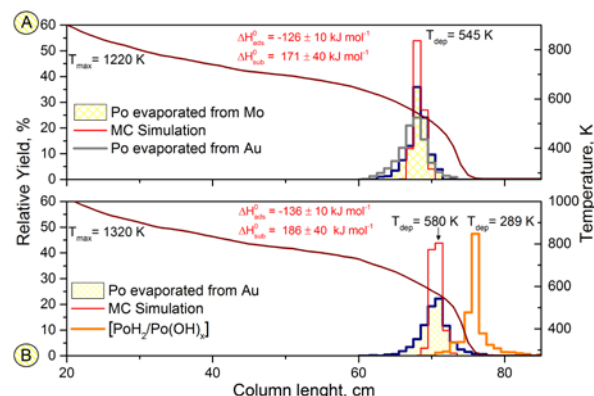


**Fig. 1:** (A) TCm of Po using as carrier gas  $\text{H}_2$ ; (B) TCm of Po and  $[\text{PoH}_2/\text{Po}(\text{OH})_x]$  using as carrier gas He.

## CONCLUSION

One species was obtained in TC experiments using inert and reducing carrier gases, identified as elemental Po. In one experiment a compound more volatile than elemental Po was found. This compound could be Po hydride or an oxyhydroxide.

This work was funded by the EC 7<sup>th</sup> framework (SEARCH) and the LIEBE project.

## REFERENCES

- [1] I. Zvara, Radiochim Acta, **38**, 95 (1985).
- [2] A. Serov et al., Radiochim. Acta, **99**, 95 (2011).
- [3] B. Eichler, PSI-Report No. 02-12, Die Flüchtigkeitseigenschaften des Poloniums, PSI, 2002.

# ADSORPTION OF VOLATILE POLONIUM SPECIES ON GOLD IN VARIOUS GAS ATMOSPHERES

*E. A. Maugeri, J. Neuhausen, R. Eichler, D. Piguet, A. Vögele, D. Schumann (PSI)*

## INTRODUCTION

This report presents the results obtained studying the interaction between Po compounds formed in different atmospheres and gold surfaces by thermochromatography. These results are of crucial importance for the design of filter systems for LBE-based nuclear facilities.

## EXPERIMENTAL & RESULTS

$^{206}\text{Po}$  was obtained by irradiating Bi metal with a 40 MeV proton beam with up to 3  $\mu\text{A}$  of intensity, according to the nuclear reaction:  $^{209}\text{Bi}(p,4n)^{206}\text{Po}$ . After the preparation, Po was separated from the Bi matrix by evaporation at 1223 K under helium flow and deposited at lower temperatures on Au foils. The experiments were performed using a thermochromatography setup (TC) consisting of a fused silica column in a negative gradient furnace with a temperature profile ranging from 1222 to 168 K. The column was lined with a gold foil (thickness 0.02 mm, purity 99.9%) placed along the entire temperature gradient. The thermochromatogram (TCM) of  $^{206}\text{Po}$  obtained using purified  $\text{H}_2$  as carrier gas, Exp. I, is presented in Fig. 1 (A). A single sharp peak centered at 1058 K was obtained. Using the Monte Carlo simulation method [1], the adsorption enthalpy of the deposited species was calculated as  $-254 \pm 7 \text{ kJ mol}^{-1}$ . Considering the instability of  $\text{PoH}_2$  [2], we assign the deposition to elemental Po. In Exp. II performed in moist  $\text{H}_2$ , Fig. 1 (A), a similar deposition was found. This indicates that either no Po hydroxides or hydride are formed or, if formed, they decompose to elemental Po on the gold surface. The TCM of Po obtained using purified He as carrier gas, Exp. III, is presented in Fig. 1 (B). It shows a sharp peak centered at 865 K, indicating that only one species was deposited in the column. Using the Monte Carlo simulation method [1] an adsorption enthalpy of  $-206.5 \pm 7 \text{ kJ mol}^{-1}$  was calculated. Under these conditions, i.e. absence of reactive species in the gas, Po or BiPo may be formed, depending on the chemical form of the evaporating Po. BiPo would probably decompose in pure  $\text{H}_2$ . Hence, it would not occur in Exp. I and III, we assign the deposition at 865 K to BiPo. Exp. IV was performed with moist helium as carrier gas. The deposition pattern, Fig. 1 (B), shows a main deposition centered at 1026 K. Considering the uncertainties in temperature- and position measurement in the polonium deposition pattern ( $\pm 30 \text{ K}$ ), the deposited species is considered to be elemental Po, similar to

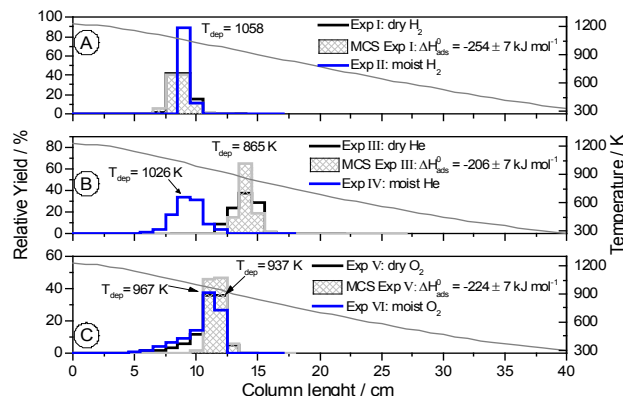


**Fig. 1:** TCM of Po using as carrier gas: (A) dry and moist  $\text{H}_2$ ; (B) dry and moist He. (C); dry and moist  $\text{O}_2$

Exp. I and II. In Exp. V dried oxygen was used as carrier gas. The obtained TCM, Fig. 1 (C), reveals a deposition centered between 967 and 937 K.

The adsorption enthalpy of the deposited species was calculated as  $-224 \pm 7 \text{ kJ mol}^{-1}$ . The most stable valence state of Po in pure  $\text{O}_2$  is +4 [3]. The deposition pattern tails towards high temperature - an indication that the main deposition of  $\text{PoO}_2$  could be the result of a transport process, e.g. following the reaction:



A sample was investigated using moist  $\text{O}_2$  as carrier gas. Fig. (C) shows the obtained TCM, characterized by a broad deposition pattern centered at 967 K. Similarly to the result obtained when using dry oxygen, the main species is probably  $\text{PoO}_2$ , and also in this case it seems to be the result of a transport process.

## CONCLUSIONS

One single Po species was obtained in TC experiments using dry  $\text{H}_2$ , moist  $\text{H}_2$  and moist He carrier gases, identified as elemental Po. A more volatile compound compared to elemental Po, was found using dry He as carrier gas. This species was tentatively assigned to BiPo. One single species was formed using both dry and moist  $\text{O}_2$ . Considering the oxidation potential of the carrier gases, this species was identified as  $\text{PoO}_2$ . Considering that in both cases the obtained patterns tail towards high temperature, we propose that the adsorption chromatography process of this species is superimposed by a transport process.

This work was supported by the project SEARCH, co-funded by the FP7 Euratom.

## REFERENCES

- [1] I. Zvara, *Radiochim. Acta* 38 (1985) 95.
- [2] B. Eichler, J. Neuhausen, PSI-Report Nr. 04-06, PSI, Villigen, Switzerland, 2004.
- [3] A.S. Abakumov, *Uspekhi Khimii* 51 (1982) 1091.

# SOLUTION ENTHALPY AND LOCAL INTERACTION OF Po AND Te WITH SOLID LEAD-BISMUTH EUTECTIC, A COMPUTATIONAL STUDY

K. Rijpstra, A. Van Yperen-De Deyne (CMM, Univ. Gent), J. Neuhausen (PSI),  
V. Van Speybroeck, S. Cottenier (CMM, Univ. Gent)

## INTRODUCTION AND METHODS

Due to its radiotoxicity and scarcity, experiments on Po are never straightforward. Computational modelling is a means of gaining information on Po, with the potential to reduce the number of necessary experiments. In this work [1] the solution enthalpy of Po in solid LBE is evaluated in the quantum physical framework of Density Functional Theory (DFT). Analogous calculations for Te have been performed, showing a strong correlation with the Po behavior (see Fig. 1), suggesting that it should be possible to obtain information on Po out of Te experiments.

All calculations were done scalar-relativistically with the PAW method as implemented in VASP, using the PBE exchange correlation functional. Several calculations were repeated adding spin-orbit coupling as second major relativistic effect. The cut-off energy for the basis set was set at 290 eV. The k-grids were  $\Gamma$ -centered Monkhorst-Pack grids with a density of 125000 k-points/ $\text{\AA}^{-3}$ .

## THE LBE-MODEL

Solid state DFT calculations use a unit cell which is periodically repeated to fill space. This does not allow a direct treatment of disordered solid LBE, but the aim is to study how the local stoichiometry of nearest neighbors influences the solution behavior of Po. Therefore, a ‘disordered supercell’ is constructed: a 2x2x2 hcp supercell with all atom sites randomly filled with a chosen amount of Pb and Bi atoms (see Fig. 2). This structure is allowed to fully relax before being ‘polluted’ with Po or Te.

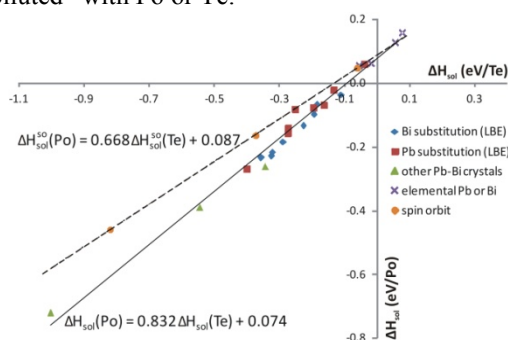


**Fig. 1:** Correlation between the solution enthalpies of Po and Te in the LBE model, elemental Pb and Bi and a few other PbBi-crystals.

## DISSOLVING Po AND Te IN LBE

To find out how much energy it takes to put one Po atom in an LBE matrix we examine the reaction:

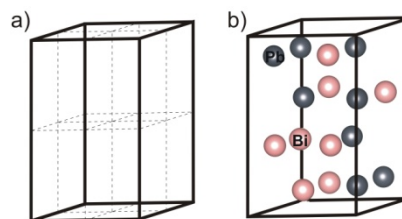
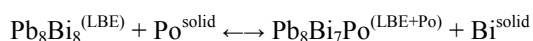


**Fig. 2:** (a) A 2x2x2 supercell of the hexagonal close packed primitive cell. (b) The randomly chosen Pb- and Bi-occupation as model for the disordered Pb/Bi-alloy in this work.

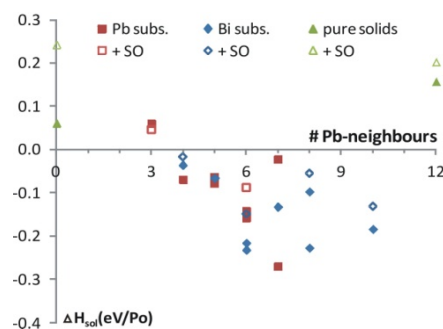
A similar reaction can be written for Po substituting a Pb-atom. This reaction has been studied for all 16 sites in our LBE model. One after the other, every Pb or Bi was replaced by a Po atom, after which the cell was allowed to relax. For each of these cells the solution enthalpy was calculated:

$$\Delta H_{\text{sol}} = [\text{H}(\text{LBE} + \text{Po}) + \mu_{\text{Pb}(\text{Bi})}] - [\text{H}(\text{LBE}) + \mu_{\text{Po}}]$$

wherein  $\mu$  represents the enthalpy of an atom in its elemental solid. The result can be seen in Fig. 3: For most cases a negative solution enthalpy was found, especially when more Pb neighbors are present. However, for the formation of  $\text{PbPo}$ , a known compound (NaCl structure), according to:



an even lower enthalpy of  $-0.60$  eV/Po was calculated,



ed, indicating that the formation of this phase would be favored compared to dissolving Po in LBE.

**Fig. 3:** Solution enthalpy of Po at all positions in the LBE model, and in pure Bi and Pb. On the x-axis the number of Pb-atoms in the first coordination shell of Po. Open symbols are data with spin-orbit coupling added.

Funded by the EC-EURATOM FP7 project SEARCH.

## REFERENCES

- [1] K. Rijpstra et al., J. Nucl. Mat., in press (2013), 10.1016/j.jnucmat.2013.07.004.

# DETERMINATION OF THE DIFFUSION COEFFICIENT OF POLONIUM IN LEAD, BISMUTH AND THEIR EUTECTIC

S. Heinitz (Univ. Bern & PSI), J. Neuhausen, D. Schumann (PSI)

## INTRODUCTION

The behavior of radiotoxic polonium formed in heavy metals used as coolant or spallation target material is of inherent importance for safety and decommissioning of nuclear facilities. Due to its high energetic  $\alpha$ -decay,  $^{210}\text{Po}$  may be released from any solid material containing it by the process of sputtering. Segregation of polonium to the surface [1] even increases its surface concentration and release. To better understand polonium migration phenomena, the bulk diffusion coefficient of polonium has to be systematically measured in relevant materials such as Pb, Bi, and their mixtures. In contrary to Pb and Bi, the diffusion coefficient of polonium in lead-bismuth eutectic (LBE) has never been measured before. In this report we present data for the bulk diffusion coefficient obtained at different temperatures for Pb, Bi and their eutectic.

## EXPERIMENTAL

Polycrystalline cylindrical samples ( $h = 10$  mm,  $r = 3.5$  mm) of Pb, Bi, and LBE were prepared according to the following procedure: a metal rod ( $L = 30$  cm) was cast by pouring liquid inactive Pb, Bi, or LBE into a glass tube sealed on one side under a nitrogen atmosphere. The metal is solidified by slow crystallization from bottom to top. Afterwards, the glass tube is broken and the metal rod is cut in identical cylinders of 10 mm length. Both sides of each cylinder are trimmed with a microtome.

The samples were then annealed in a resistance oven at the temperature at which the diffusion studies are performed later. After the annealing process, polonium was deposited on the top and bottom surfaces of each sample from 100  $\mu\text{l}$  of a 1M  $\text{HNO}_3$  solution containing 1.9 kBq/ml  $^{210}\text{Po}$  by spontaneous deposition.

All samples were then again placed inside the resistance oven at the temperature of their previous annealing. The decrease in surface activity of  $^{210}\text{Po}$  was recorded daily by  $\alpha$ -spectroscopy. Analysis of data was performed using the mathematical relations given in [4].

## RESULTS

Determined values for the diffusion coefficient of Po in Pb, Bi, and LBE at different temperatures are summarized in Figure 1. The measured diffusion coefficient for Pb agrees well with literature values [1, 2] while for Bi, the data deviates from that given in [3].

The dependence of the Po diffusion coefficient on the temperature does not significantly alter between the investigated metals since the slopes of the lines representing least square fits are similar. This indicates that the activation energy for the diffusion process in these materials is comparable. Nevertheless, there is a difference by two orders of magnitude in the measured

diffusion coefficients of Po when comparing the three matrices Pb, Bi, and LBE. In the temperature range between 50 and 100  $^\circ\text{C}$ , the Po mobility in the host materials increases in the sequence  $\text{Bi} < \text{Pb} < \text{LBE}$ . The fact that the diffusion in LBE is the fastest may be explained by the lower melting point of LBE compared to that of Pb and Bi.

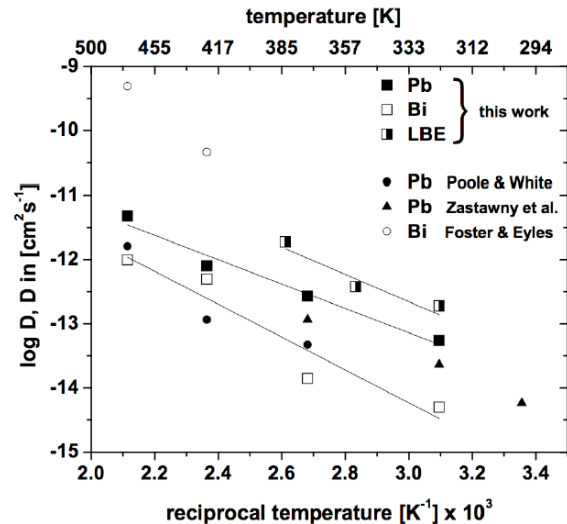


**Fig. 1:** Arrhenius plots for measured Po diffusion coefficients in Pb, Bi, and their eutectic as function of temperature; for comparison, Po thermal diffusion data in polycrystalline Pb reported by [1, 2] and Bi [3] is given.

In order to understand the influence of the grain structure on the dynamics of Po diffusion in Pb and Bi, dedicated experiments using single crystal specimen have to be performed. If polycrystalline materials are to be used, it is important to know the microstructure of the investigated metal. Proper metallographic analysis techniques such as imaging by transmission electron microscopy (TEM), radiography, and depth profiling in combination with chemical analysis of the specimens is mandatory. With the knowledge of the microstructure and the resulting diffusion behavior of Po in the pure metals Pb and Bi, it should be possible to gain further insight into diffusion and segregation processes occurring in LBE.

The project was funded by ESS-CH.

## REFERENCES

- [1] A. Zastawny, J. Bialon, T. Sosinsk, ARI 43 (1992) 1147-1150.
- [2] J.H.J. Poole, J.N.T. White, The scientific proc. of the Royal Dublin Society 27 (1955) 1 - 15.
- [3] K. W. Foster, T. E. Eyles, MLM-569, Mound Laboratory Report (1951).
- [4] F. Auerbach, Handbuch phys.- tech. Mech., Vol. VII, J. A. Barth Verlag, Leipzig (1931).

# $\gamma$ -SPECTROMETRY RESULTS FROM THE ANALYSIS OF THE ABSORBER FOILS IN THE EXPANSION TANK OF THE MEGAPIE TARGET

B. Hammer, A. Türler (Univ. Bern & PSI), D. Schumann, J. Neuhausen (PSI), H.P. Linder, V. Boutellier (PSI/AHL), M. Wohlmuther (PSI/ABK)

## INTRODUCTION

In 2006, the first test-experiment (MEGAPIE) with a liquid heavy metal target in the megawatt power range was successfully performed at PSI, using lead-bismuth-eutectic (LBE) as target material [1]. When LBE is exposed to an intense high energy proton beam, isotopes of practically all chemical elements, ranging from hydrogen up to polonium will be produced by different nuclear reactions. Some of these nuclear reaction products have to be considered as volatile at operation conditions. One of the radiologically most relevant elements is mercury, because it has an isotope with a comparably long half-life ( $^{194}\text{Hg}$ , 520 y), is produced in large quantities and is highly volatile. During operation of the MEGAPIE target, a certain fraction of each volatile element will be transferred to the expansion volume located at the top of the target (Fig. 1), which contains argon as cover gas. Therefore, an absorber was installed in the expansion volume to catch volatile radionuclides like mercury as well as iodine and polonium.

## ABSORBER IN THE EXPANSION VOLUME

Silver has been selected as primary absorber material due to its capability to bind mercury as well as iodine and possibly also polonium. Additionally, a Pd-foil was added to investigate its performance as absorber.

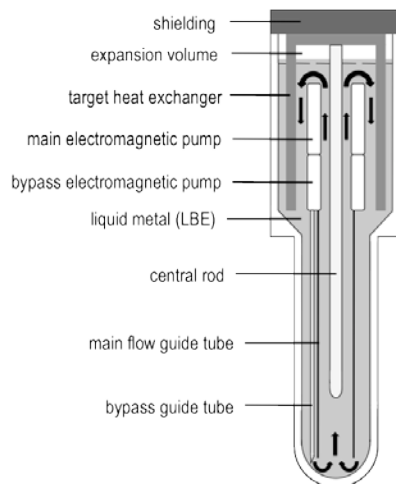


**Fig. 1:** Schematic view of the MEGAPIE target.

The absorber consists of six silver foils and one palladium foil, staggered onto each other. The absorber was mounted in the target expansion volume on the central rod (Fig. 1 & Fig. 2) in a position safely above the free surface of the liquid LBE. After operation, the absorber was retrieved from the irradiated target and analyzed by  $\gamma$ -spectrometry, using only one small piece

(0.2-1g) of each foil that was not contaminated by splashed LBE.

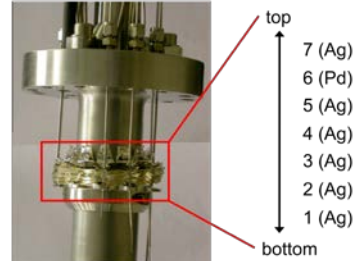


**Fig. 2:** Part of the central rod and the absorber.

## RESULTS

The results from the  $\gamma$ -analyses are shown in Tab. 1. Besides mercury, we also identified  $^{195}\text{Au}$ ,  $^{185}\text{Os}$ , and  $^{106}\text{Ru/Rh}$ . While  $^{195}\text{Au}$  is a daughter of volatile  $^{195}\text{Hg}$ , it may be speculated that the volatilization of Os and Ru results from the formation of volatile tetroxides. The total amount of Hg found on the absorber foils corresponds to approx. 0.1% of the mercury produced in the entire target [2]. Comparing this result with the equilibrium gas phase fraction of Hg in the MEGAPIE expansion tank of  $2 \cdot 10^{-6}$  estimated in [3], a significant affinity of the metal foils for Hg is confirmed. However, a precise assessment of the efficiency of the absorber from the present data is difficult.

**Tab. 1:** Activities of  $^{194}\text{Hg}/\text{Au}$ ,  $^{195}\text{Au}$ ,  $^{185}\text{Os}$  and  $^{106}\text{Ru/Rh}$  found on the Ag & Pd foils (EOB: 21.12.2006).

Absorber	m [g]	$A_{sp}$ [kBq] EOB			
		$^{194}\text{Hg}/\text{Au}$	$^{195}\text{Au}$	$^{185}\text{Os}$	$^{106}\text{Ru/Rh}$
1 (Ag)	9.6299	6.63E+03	4.06E+05	1.97E+08	4.96E+03
2 (Ag)	9.6875	3.25E+04	1.35E+06	8.83E+08	2.41E+04
3 (Ag)	9.3945	2.65E+04	1.44E+06	7.53E+08	2.03E+04
4 (Ag)	9.3988	6.08E+03	3.46E+05	2.01E+08	5.32E+03
5 (Ag)	9.8407	9.52E+03	4.01E+05	3.20E+08	8.23E+03
6 (Pd)	2.3433	5.31E+03	2.76E+05	2.11E+08	5.25E+03
7 (Ag)	9.6419	7.19E+03	3.81E+05	3.17E+08	7.64E+03

The work was funded by the EC projects ANDES and GETMAT in the frame of EURATOM FP7.

## REFERENCES

- [1] W. Wagner et al., J. Nucl. Mater., **377**, 12 (2008).
- [2] B. Hammer et al., J. Nucl. Mat. 2013, <http://dx.doi.org/10.1016/j.jnucmat.2013.09.016>.
- [3] J. Neuhausen et al., J. Nucl. Mater., **415**, 361-366 (2011).

# RADIOCHEMICAL DETERMINATION OF $^{129}\text{I}$ AND $^{208-210}\text{Po}$ IN THE ABSORBER FOILS OF THE MEGAPIE EXPANSION TANK

B. Hammer, A. Türler (Univ. Bern & PSI), D. Schumann, J. Neuhausen (PSI), H.P. Linder, V. Boutellier (PSI/AHL), M. Wohlmuther (PSI/ABK), C. Vockenhuber (ETHZ)

## INTRODUCTION

In Ref. [1] we reported on the  $\gamma$ -analysis of absorber foils (Ag and Pd) installed in the MEGAPIE expansion tank in order to trap radiologically hazardous volatile elements, like for instance  $^{194}\text{Hg}$ . In the present contribution, first results on the radiochemical determination of the nuclides  $^{129}\text{I}$  as well as  $^{208-210}\text{Po}$  – isotopes, which can be measured only after a chemical sample treatment – are shown.

## EXPERIMENTAL

Small pieces (about 20 mg) from the foils from the absorber were used as described in [1]. The first step of the separation procedure for Pd was the dissolution of the foils in  $\text{HNO}_3$  and distillation of chlorine (for the determination of the volatile  $^{36}\text{Cl}$ ) and iodine (including the added stable carriers  $\text{I}_2$  and  $\text{NaCl}$ ) into hydrazine solution, as described in [2,3]. After that, the silver halogenides were precipitated by adding  $\text{HNO}_3$  and  $\text{AgNO}_3$  solution.

The Ag foils were simply dissolved in 7 M  $\text{HNO}_3$  and afterwards iodine carrier (about 12 mg) in hydrazine solution and chlorine carrier (10 mg) were added, leading to a precipitation of  $\text{AgI}$  and  $\text{AgCl}$ . The procedure was performed according to [2,3].

After drying the samples, they were measured using Accelerator Mass Spectrometry (AMS) at ETHZ.

The second step for the Pd foil was the spontaneous deposition of Po onto Ag discs. For this purpose, Po had first to be separated from the solution after distillation, because the spontaneous deposition on silver is not working in the presence of Pd. A precipitation was performed by adding  $\text{HCl}:\text{HNO}_3$  (3:1) and deionized  $\text{H}_2\text{O}$  as described in [4]. The precipitate was dissolved in 10 ml 0.8 M  $\text{HCl}$  while adding ascorbic acid to reduce impurities that will disturb the spontaneous deposition. The deposition was performed for 2 h at  $72^\circ\text{C}$  by stirring the solution containing the silver disc. The spontaneous deposition of Po obtained from the dissolved Ag foils was performed as described in [4].

The Po-activity was determined with an  $\alpha$ -particle spectrometer (CANBERRA) using the GENIE2000 software. Both sides of the Ag discs were measured.

## RESULTS

In the Tabs. 1 and 2, the presently available results for  $^{129}\text{I}$  and  $^{208-210}\text{Po}$  are summarized. The  $^{36}\text{Cl}$  samples, which are already prepared, will soon be measured at ETHZ. We compare the obtained results with predictions of the total amount of these isotopes produced in the MEGAPIE target. Compared to the

FLUKA and MCNPX calculations [5], the evaporated  $^{129}\text{I}$  as well as  $^{208-210}\text{Po}$  amounts represent only a small fraction of the total activities.

**Tab. 1:** Activities of  $^{129}\text{I}$  found on the Ag & Pd foils (EOB: 21.12.2006)

Absorber	m [g]	$^{129}\text{I}$ $A_{\text{sp}}$ [Bq]
1 (Ag)	9.6299	1.81E-09
2 (Ag)	9.6875	3.47E-05
3 (Ag)	9.3945	1.00E-05
4 (Ag)	9.3988	1.49E-05
5 (Ag)	9.8407	8.46E-06
6 (Pd)	2.3433	1.36E-05
7 (Ag)	9.6419	1.19E-05

**Tab. 2:** Activities of  $^{208}\text{Po}$ ,  $^{209}\text{Po}$  and  $^{210}\text{Po}$  found on the Ag & Pd foils (EOB: 21.12.2006)

Ab-sorber	m [g]	$^{208}\text{Po}$ $A_{\text{sp}}$ [Bq]	$^{209}\text{Po}$ $A_{\text{sp}}$ [Bq]	$^{210}\text{Po}$ $A_{\text{sp}}$ [Bq]
1 (Ag)	9.6299	4.07E+02	3.99E+00	5.99E+05
2 (Ag)	9.6875	2.83E+03	7.36E+01	5.31E+06
3 (Ag)	9.3945	3.23E+03	4.14E+01	3.72E+06
4 (Ag)	9.3988	1.34E+03	3.74E+01	1.93E+06
5 (Ag)	9.8407	6.20E+02	1.26E+01	4.56E+05
6 (Pd)	2.3433	9.08E+04	6.51E+02	4.85E+07
7 (Ag)	9.6419	1.42E+02	6.48E+00	3.60E+05

These first, preliminary studies – as well as the results on Hg reported in [1] - demonstrate that Pd and Ag may serve as suitable catchers for volatiles in a possible future facility like MYRRHA [6]. However, for a serious evaluation of the feasibility, dedicated adsorption experiments to quantify the capacity of the selected materials are necessary.

## ACKNOWLEDGEMENT

The work was funded by the EC projects ANDES and GETMAT in the frame of EURATOM FP7.

## REFERENCES

- [1] B. Hammer et al., PSI Annual Report 2013, 46.
- [2] B. Hammer et al., PSI Annual Report 2011, 36.
- [3] D. Schumann et al., Nucl. Instruments Methods Phys. Res. Sect. B Beam Interaction Mater. Atoms, **264**, 83-95 (2007).
- [4] B. Hammer et al., Nucl. Data Sheets, accepted for publication.
- [5] L. Zanini et al., PSI Report Nr. 08-04 (2008).
- [6] <http://myrrha.sckcen.be/>

# ANALYTICS OF $\alpha$ -EMITTERS $^{146}\text{Sm}$ , $^{148}\text{Gd}$ AND $^{150}\text{Gd}$ FROM PROTON IRRADIATED LEAD

T. Lorenz (Univ. Bern & PSI), D. Schumann (PSI), Y. Dai (PSI/LNM), A. Türler (Univ. Bern & PSI)

## INTRODUCTION

The Swiss spallation neutron source (SINQ) at PSI, driven by a 590 MeV proton accelerator, uses solid lead as target material. After two years of operation, the highly activated target system has to be replaced due to degradation of material properties. For an intermediate or final disposal of such a target, information on its radionuclide inventory is required by the Swiss authorities. Currently, the provided information is mainly based on theoretical predictions using advanced codes and models. However, these calculations are very complex, due to the involved nuclear reactions and therefore, experimental data are needed for validation. We reported earlier on the experimental determination of the main  $\gamma$ -emitters and the  $^{208-210}\text{Po}$  content in five samples of SINQ target 4 [1, 2]. In the present work, we deal with the analysis of the  $\alpha$ -emitting lanthanides  $^{148}\text{Gd}$  (74.6 yr),  $^{150}\text{Gd}$  (1.8 Myr) and  $^{146}\text{Sm}$  (68 Myr).

Apart from the analytical aspect, high power spallation targets may serve as potential sources for rare isotopes urgently needed to study fundamental nuclear astrophysical processes. In the frame of the ERAWAST project [3] extraction of some of these isotopes is foreseen to provide the material for dedicated experiments like the precise determination of half-lives and cross sections. These data are required for a better understanding of stellar processes, in which for instance  $^{146}\text{Sm}$  and many others are involved [4].

## EXPERIMENTAL

For the quantitative determination of  $\alpha$ -emitters the preparation of thin samples is required. For this, lead pieces (10 to 60 mg) from the different sample positions were dissolved in 7 M nitric acid as described earlier [1,2]. Aliquots of these sample solutions were spiked with tracers ( $^{139}\text{Ce}$ ,  $^{149}\text{Eu}$  and  $^{153}\text{Gd}$ ) for yield determination and in presence of lutetium carrier  $\text{LnF}_3$  was precipitated. After dissolving in  $\text{H}_3\text{BO}_3$ , the fraction was loaded on an extraction chromatography column (*Ln-Resin*, *Eichrom*). The light lanthanides up to gadolinium were eluted with 0.6 M nitric acid. With a second column the separation of Sm (0.4 M  $\text{HNO}_3$ ) from Gd (0.6 M  $\text{HNO}_3$ ) was performed. Both species were deposited on platinum or glassy carbon, using the Molecular-Plating method at 500 V and 1-5 mA in *i*BuOH. The thin-layer samples were measured with a silicon PIPS detector (Canberra) for 25 to 90 days.

## RESULTS AND DISCUSSION

An  $\alpha$ -spectrum of a  $^{146}\text{Sm}$  sample is shown in Fig. 1. With the applied radiochemical separation procedure a decontamination factor from Gd up to  $10^4$  could be achieved. The total yields were found to be 20 to 45%.

The amounts of produced atoms per gram of lead are shown in Fig. 2.

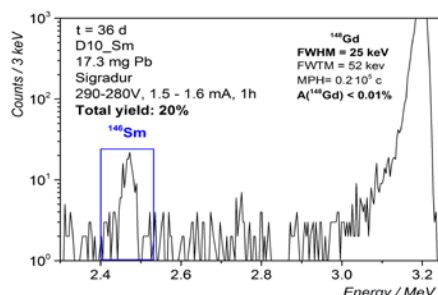


Fig. 1:  $^{146}\text{Sm}$   $\alpha$ -spectrum - 36 days of measurement

The integral production rates of  $^{146}\text{Sm}$  and  $^{148/150}\text{Gd}$  correspond – as expected – to the integral proton charge. The activity concentrations of  $^{148}\text{Gd}$  were found to be between 4 and 40 kBq per gram lead, thus representing a radiological hazard comparable to the radiotoxic isotopes  $^{209}\text{Po}$  (102 yr) of 9 to 66 kBq/g and  $^{210}\text{Pb}/^{210}\text{Po}$  (22.3 yr) of 7 to 50 kBq/g [2]. The contributions of the longer-lived  $^{150}\text{Gd}$  (1 to 10 Bq/g) and  $^{146}\text{Sm}$  (0.05 to 0.5 Bq/g) to the total  $\alpha$ -activity are comparatively small.

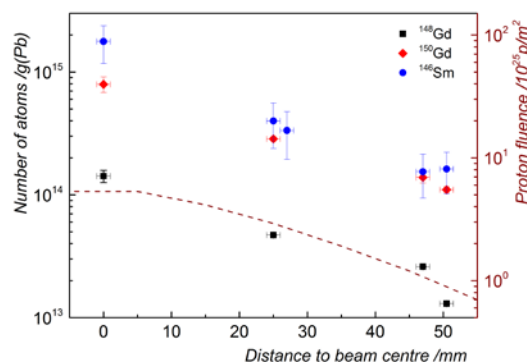


Fig. 2: Integral number of atoms ( $2\sigma$  uncertainty) of  $^{146}\text{Sm}$  and  $^{148/150}\text{Gd}$  per gram of lead, compared to the fluence of the proton beam (dashed line) – Date of measurement: 2013.

For a dedicated experiment with  $^{146}\text{Sm}$  an amount of  $10^{16}$  to  $10^{17}$  atoms (2 to 20  $\mu\text{g}$ ) is required, but its concentration of around  $10^{14}$  atoms/g within these samples seems to be rather low. Several hundreds grams of activated lead would have to be processed in a remote controlled hot cell, due to the high dose rate.

This work is funded by the SNF. Thanks to H. Dorrer for supplying  $^{152}\text{Gd}$ ,  $^{149}\text{Eu}$  and  $^{139}\text{Ce}$ .

## REFERENCES

- [1] T. Lorenz, *Radiochim. Acta* 101 (2013) 661.
- [2] T. Lorenz, *Nucl. Data Sheets* (2013). *Accepted*
- [3] D. Schumann, *J. Phys. G*, 35 (2008) 014046.
- [4] G.J. Wasserburg, *Nucl. Phys. A* 777 (2006) 5.

## <sup>44</sup>Sc PRODUCTION DEVELOPMENT BY CYCLOTRON IRRADIATION OF <sup>44</sup>Ca FOR RADIOPHARMACEUTICAL APPLICATION

M. Bunka, A. Türler (Univ. Bern & PSI), C. Müller, J. Reber, R. Schibli (ETHZ & PSI/CRS), K. Domnanich, N. van der Meulen (PSI)

### INTRODUCTION

The positron emitter <sup>44</sup>Sc ( $t_{1/2} = 3.97$  h,  $E_{\beta^+} = 1475.4$  keV, 94.34%) has attractive properties for positron emission tomography (PET) and could be an alternative to the currently used short-lived <sup>68</sup>Ga ( $t_{1/2} = 68$  min). With a chemistry similar to that of the lanthanides and rare earth elements (<sup>90</sup>Y, <sup>177</sup>Lu), <sup>44</sup>Sc can be used in already established labelling reactions for radiopharmaceutical purposes. The aim of this study was to produce <sup>44</sup>Sc via the <sup>44</sup>Ca(p,n)<sup>44</sup>Sc nuclear reaction at a cyclotron [1-4]. The separation of <sup>44</sup>Sc from irradiated enriched <sup>44</sup>Ca targets was developed and *in vitro* and *in vivo* studies, including PET imaging with <sup>44</sup>Sc-labelled compounds, were performed.

### EXPERIMENTAL

**Irradiation.** <sup>44</sup>Ca-targets were prepared by mixing 10 mg of enriched <sup>44</sup>CaCO<sub>3</sub> with 150 mg graphite powder, pressed and encapsulated in aluminium. The targets were irradiated at PSI with 72 MeV protons, degraded to 11 MeV, at a beam current of 50  $\mu$ A for 1 hour.

**Chemical separation.** 3.0 M HCl was used to dissolve the <sup>44</sup>CaCO<sub>3</sub> and the resultant solution was loaded on to DGA extraction chromatographic resin, where the <sup>44</sup>Sc(III) was sorbed (Fig. 1). As <sup>44</sup>Ca(II) is not retained on the resin under these conditions, it was eluted from the column with further addition of 3.0 M HCl. A small quantity of 0.1 M HCl was utilised to elute <sup>44</sup>Sc(III) from the column.



Fig. 1: <sup>44</sup>Sc production semi-automated system.

A second column consisting of DOWEX 50 cation exchange resin was used to concentrate the <sup>44</sup>Sc-eluate. <sup>44</sup>Sc in 0.1 M HCl solution was sorbed on DOWEX 50 and subsequently eluted with a solution of CH<sub>3</sub>COONH<sub>4</sub>/HCl (0.5 mL, pH 4.5). The <sup>44</sup>Sc-acetate solution was used for labelling of a DOTA-folate con

jugate and DOTATATE for subsequent *in vitro* and *in vivo* experiments.

### RESULTS AND DISCUSSION

Using the abovementioned irradiation conditions, yields of 2.0 to 3.0 GBq per target have been produced. The irradiated <sup>44</sup>CaCO<sub>3</sub> produced a high radio-nuclidic purity of <sup>44</sup>Sc, with less than 1 % of the co-produced, longer-lived <sup>44m</sup>Sc ( $t_{1/2} = 2.4$  d) in the product. The developed separation system showed excellent results. Over 85 % of the initial <sup>44</sup>Sc-activity could be eluted in a volume of 0.5 mL CH<sub>3</sub>COONH<sub>4</sub>/HCl solution for radiolabelling purposes. Radiolabelling of cm09 was achieved with a radiochemical yield of > 96 % at a specific activity of 5.2 MBq/nmol [5]. *In vitro*, <sup>44</sup>Sc-cm09 was stable in human plasma and showed FR-specific binding to KB tumour cells. PET/CT images of mice injected with <sup>44</sup>Sc-cm09 allowed excellent visualization of tumour xenografts (Fig. 2). Comparison of cm09 labelled with <sup>44</sup>Sc and <sup>177</sup>Lu revealed almost identical pharmacokinetics.

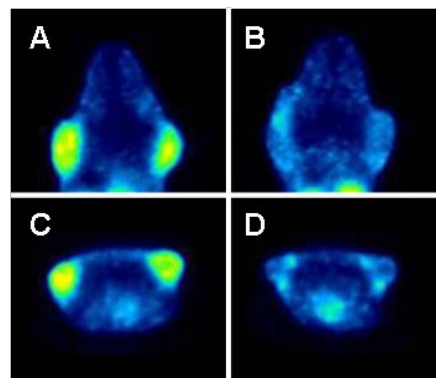


Fig. 2: PET images as coronal (A, B) and transaxial sections (C, D) of KB tumour-bearing mice injected with <sup>44</sup>Sc-cm09 only (A, C) or with <sup>44</sup>Sc-cm09 and preinjected folic acid to block FRs (B, D) [5].

### REFERENCES

- [1] A. Bilewicz et al., 3rd-INCC, Italy, 18-23 September (2011).
- [2] K. Zhernosekov et al., *Radiother. Oncol.* **102**, 141 (2012).
- [3] G. W. Severin et al., *Appl. Radiat. Isot.*, **70**, 1526 (2012).
- [4] E. Koumariou et al., *Appl. Radiat. Isot.*, **70**, 2669 (2012).
- [5] C. Müller et al., *J. Nucl. Med.*, **54**, 1 (2013).

# PRODUCTION AND EVALUATION OF THE THERAPEUTIC RADIONUCLIDE $^{161}\text{Tb}$ - AN ALTERNATIVE TO $^{177}\text{Lu}$ ?

H. Dorrer (Univ. Bern & PSI), C. Müller, S. Haller, J. Reber (PSI/CRS), R. Schibli (ETHZ & PSI/CRS), A. Türler (Univ. Bern & PSI), N. van der Meulen (PSI).

## INTRODUCTION

$^{161}\text{Tb}$  is very similar to the clinically-applied therapeutic radionuclide  $^{177}\text{Lu}$  with respect to  $\beta^-$ -energy, half-life and chemical properties but, in contrast to  $^{177}\text{Lu}$ , it emits a significant number of conversion- and Auger electrons, providing high energy transfer in low range [1, 2]. As a result, a higher therapeutic efficiency can theoretically be expected, but has not been previously confirmed experimentally.

The radionuclide must be produced in high specific activity, radionuclide and chemical purity for the successful radiolabelling of tumour-targeting biomolecules such as peptides, antibodies or vitamins.

## EXPERIMENTAL

$^{161}\text{Tb}$  is produced by the irradiation of highly-enriched  $^{160}\text{Gd}$  (98.2 %) with thermal neutrons at SINQ (PSI) or, alternatively, at the high flux reactor of ILL (Grenoble, France) or FRM II (Munich, Germany).

The isolation of  $^{161}\text{Tb}$  from a  $^{160}\text{Gd}$ -target has been described previously [2].

For assessments of product quality, aliquots of the  $^{161}\text{Tb}$  solution, decayed for several weeks, were analysed by  $\gamma$ -spectrometry to determine the content of longer-lived  $^{160}\text{Tb}$  and by ICP-MS for content of metal ions that can interfere with radiolabeling.

The produced  $^{161}\text{Tb}$  has been applied in a number of preclinical experiments at the Center for Radiopharmaceutical Sciences (CRS). The therapeutic efficiency of  $^{161}\text{Tb}$ -labelled folate conjugates has been compared with that of the  $^{177}\text{Lu}$ -radiolabelled version.

## RESULTS

Up to  $\sim 20$  GBq  $^{161}\text{Tb}$  was produced from the neutron irradiations of  $^{160}\text{Gd}$ , with up to 18.4 GBq  $^{161}\text{Tb}$  obtained after the separation procedure. The preparation contained 12 kBq  $^{160}\text{Tb}$  per GBq  $^{161}\text{Tb}$ , as the only radiochemical impurity, resulting in radionuclidic purity of  $>99.99$  %. The chemical purity was found to be 88 %, with impurities from the stable naturally-occurring metals Zn (5.3 %), Al (2.7 %), Fe (2.4 %) and  $^{159}\text{Tb}$  (1.6 %).

A comparative *in vivo* study of a  $^{161}\text{Tb}$ -labelled and  $^{177}\text{Lu}$ -labelled folate conjugates was performed in mice bearing folate receptor-positive tumour xenografts.

The mice treated with the  $^{161}\text{Tb}$ -labelled folate conjugate showed a reduced relative tumour volume (RTV) and a longer median survival time (group B) than mice

treated with the analogue  $^{177}\text{Lu}$ -labelled biomolecule (group C) and the untreated control mice (group A) (Fig. 1) [3].

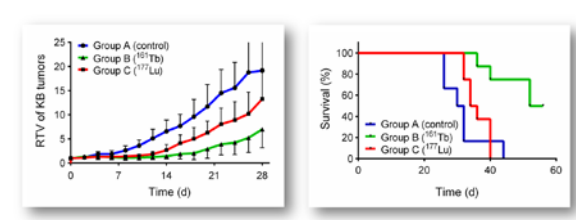


**Fig. 1:** Comparison of the therapeutic efficacy (tumour growth curves (left) and survival curves (right) of  $^{161}\text{Tb}$ -labelled (green) and  $^{177}\text{Lu}$ -labelled tumour-targeting folate conjugate (red) and untreated controls (blue) [3].

## CONCLUSION

$^{161}\text{Tb}$  is produced in useful quantity and excellent quality for preclinical studies at CRS. First experimental evidence of the therapeutic efficiency of  $^{161}\text{Tb}$ , as compared to  $^{177}\text{Lu}$ , has been published. Further studies using other targeting agents will be necessary to draw final conclusions about the clinical applicability of this novel radionuclide.

## ACKNOWLEDGEMENT

This work was supported by the Swiss South African Joint Research Programme (SSAJRP), the Swiss Cancer League and the Swiss National Science Foundation. The authors thank Dr. Ulli Köster, Dr. Mark Harfensteller and Alexander Vögele for the irradiation of  $^{160}\text{Gd}$ , as well as Dr. Ines Guenther-Leopold, Pia Reichel and Heiko-Dirk Potthast for performing ICP-MS-analyses.

## REFERENCES

- [1] S. Lehenberger et al., Nucl. Med. and Biol., **38** (2011), 917-924.
- [2] Müller and Zhernosekov et al., J. Nucl. Med., **53** (2012), 1951-1959.
- [3] C. Müller et al., Eur. J. Nucl. Med. Mol. Imaging, (2013), DOI 10.1007/s00259-013-2563-z.

# CROSS SECTIONS OF PROTON-INDUCED REACTIONS ON $^{152}\text{Gd}$ AND $^{155}\text{Gd}$ WITH EMPHASIS ON THE PRODUCTION OF SELECTED Tb RADIONUCLIDES

G.F. Steyn, C. Vermeulen (iThemba LABS), F. Szelecsényi, Z. Kovács (ATOMKI), A. Hohn (Univ. Medical Centre Rostock), N. van der Meulen (PSI), R. Schibli (PSI/CRS), T.N. van der Walt (CPUT)

## INTRODUCTION

Several members of the radiolanthanides have been studied in recent years for their potential in nuclear medicine. Recently, a preclinical study was reported of new tumor targeting radiopharmaceuticals labelled with a unique quadruplet of Tb radionuclides, namely,  $^{149}\text{Tb}$ ,  $^{152}\text{Tb}$ ,  $^{155}\text{Tb}$ , and  $^{161}\text{Tb}$  [1]. These radionuclides are unique in that they collectively contain properties suitable for all three major modalities of nuclear medicine, namely, PET, SPECT and radionuclide therapy, from the same element.

The majority of the radioterbioms is not yet generally available. Except for the reactor-produced  $^{161}\text{Tb}$ , the large-scale production of the other radioterbioms, with a radionuclidic purity suitable for medical use, has not yet been demonstrated. A particular aspect of the present investigation is to establish whether a commercial 70 MeV cyclotron will be suitable for the large-scale production of  $^{149}\text{Tb}$ ,  $^{152}\text{Tb}$ , and  $^{155}\text{Tb}$ .

## EXPERIMENTAL

The well-known stacked-foil technique was employed to measure the excitation functions of radionuclides produced in  $p + ^{152}\text{Gd}$  and  $p + ^{155}\text{Gd}$ . Only the energy region relevant to the (p,4n) reaction was investigated. Two foil stacks were irradiated using 66 MeV proton beams supplied by the separated-sector cyclotron (SSC) facility of iThemba LABS. The foil stacks were bombarded in an accurately calibrated Faraday chamber mounted at the end of an external beam line [2]. The beam was collimated to a spot of 4 mm in diameter. The average beam current was 50 nA and the irradiation time was 2 h for each stack.

Stacks 1 and 2 contained thin targets prepared from oxides of Gd and Tb using the sedimentation technique as described in [3].

The cross sections of the observed activation products were calculated from their measured  $\gamma$ -ray emissions using decay data from the online compilation of Firestone and Eckström [4], while theoretical excitation functions were calculated using the Geometry Dependent Hybrid (GDH) model as implemented in the code ALICE/ASH [5].

## RESULTS

Excitation functions of  $^{149}\text{Tb}$  and  $^{152}\text{Tb}$  were determined and plotted (Fig. 1 and 2, respectively), indicating that excellent yields can readily be obtained with a commercial 70 MeV cyclotron. Electromagnetic isotope separation, however, may be the only way to achieve  $^{149,152,155}\text{Tb}$  products with a high level of radionuclidic purity and the desired specific activity.

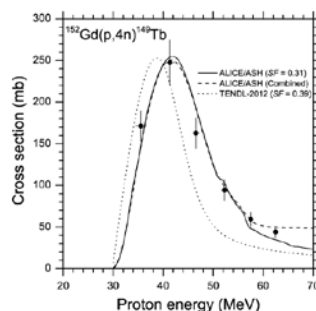


**Fig. 1:** Excitation function for the production of  $^{149}\text{Tb}$  in the irradiation of  $^{152}\text{Gd}$  with protons. Solid circles: this work (Stack 1). The solid curve shows the results from ALICE/ASH calculations [5] and the dotted curve the corresponding values from the TENDL-2012 library [6] for the (p,4n) reaction on  $^{152}\text{Gd}$  only. The dashed curve also shows the ALICE/ASH calculations for the (p,4n) reaction with inclusion of co-produced contributions from the (p,6n) reaction on  $^{154}\text{Gd}$  and the (p,7n) reaction on  $^{155}\text{Gd}$ .

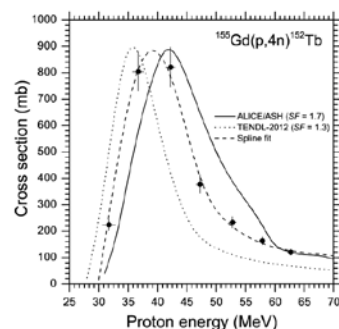


**Fig. 2:** Excitation function for the production of  $^{152}\text{Tb}$  in the irradiation of  $^{155}\text{Gd}$  with protons. Solid circles: this work (Stack 2). See also caption to Fig. 1.

## ACKNOWLEDGEMENT

This work is based on the research supported in part by the National Research Foundation of South Africa (UID 85507). This work is also supported by the Swiss South African Joint Research Programme (JRP12) and the Hungarian Research Foundation (OTKA: K108669).

## REFERENCES

- [1] C. Müller et al., J. Nucl. Med., **53**, 1951-1959 (2012).
- [2] F. Szelecsényi et al., Nucl. Instr. and Meth. in Phys. Res. B, **240**, 625 (2005).
- [3] F. Rösch et al., Radiochim. Acta, **61**, 1 (1993).
- [4] R.B. Firestone, L.P. Eckström, WWW Table of Radioactive Isotopes (2004). Available from: <http://ie.lbl.gov/toi>.
- [5] C.H.M. Broeders et al., Wissenschaftliche Berichte FZKA 7183, Forschungszentrum Karlsruhe (2006).
- [6] A.J. Koning et al., TENDL-2012 version 5 (2013). Available from: <http://www.talys.eu/tendl-2012.html>.

# TOWARDS CONTINUOUS-FLOW AEROSOL SOURCE APPORTIONMENT BY $^{14}\text{C}$ ACCELERATOR MASS SPECTROMETRY HYPHENATION

*K. Agrios, G. Salazar, S. Szidat (Univ. Bern)*

## INTRODUCTION

Analysis of the long-lived radioactive isotope  $^{14}\text{C}$  (radiocarbon) is a unique source apportionment tool. It unambiguously separates fossil from non-fossil sources, as  $^{14}\text{C}$  has completely decayed in fossil fuels, whereas modern materials have the contemporary radiocarbon level [1]. A novel separation method was developed for the direct determination of  $^{14}\text{C}$  in organic carbon (OC) and elemental carbon (EC), two sub-fractions of total carbon (TC) of atmospheric air particulate matter [2]. The installation of the accelerator mass spectrometer (AMS) MICADAS equipped with a gas ion source made  $^{14}\text{C}$  analysis more simple and robust [3]. Additionally, this implementation paved the way for advances in direct measurement in the low sample size range ( $<10\ \mu\text{g}$ ) with high throughput [4].

## TOWARDS ONLINE ANALYSIS

A substantial improvement arises from real-time  $^{14}\text{C}$  measurements of the thermograms provided by the commercial OC/EC analyser (Sunset Inc.). By entrapment of large fractions, our conclusions, although in agreement with generic methods, are sometimes hypothetical and fragmentary. By real-time  $^{14}\text{C}$  measurement, conclusions extracted will no longer be prone to assumptions and laborious trapping process shall be avoided. However, real-time  $^{14}\text{C}$  measurements are currently hindered by the fact that the gas flow outlet of the Sunset OC/EC analyser is about two orders of magnitude higher than what may be tolerated by the gas ion source. Additionally, the nature of the carrier gas (pure oxygen) renders ionization problematic and oxygen should be removed prior to injection.

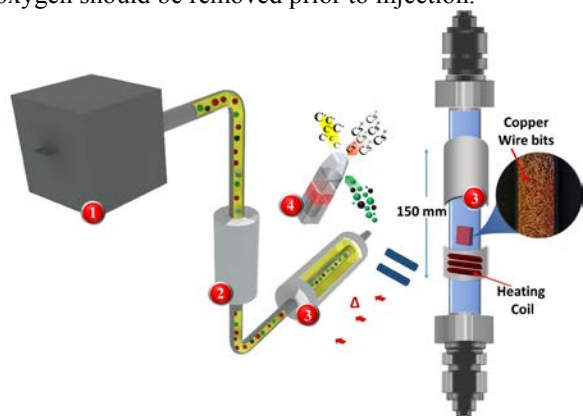


**Fig. 1:** Experimental setup for oxygen removal prior to AMS injection. 1. Sunset OC/EC analyser 2. Water trap 3. Cu reactor. 4. Ion source target. He/CO<sub>2</sub> mixture enters the ion source from a small hole in the side of the target and by collision of Cs<sup>+</sup> ions C<sup>-</sup> are produced. Red=O<sub>2</sub>, blue = H<sub>2</sub>O, green = He, black = CO<sub>2</sub>

Towards this direction, oxygen removal by a reduction reactor interface is examined (Fig. 1). When passing the hot Cu reactor (3), the gas outlet of the Sunset OC/EC analyser is cleaned from oxygen while He and CO<sub>2</sub> diffuse through the metal. In this way, only the tolerated fraction of gases by the ion source is allowed to reach the ionization chamber in an optimized ratio.

## RESULTS

The active life-time of the Cu reactor based on different carrier gas velocities has been found to range between 30 minutes and 1 hour. CO<sub>2</sub> losses in the Cu compartment have been investigated by a comparative study of the NDIR value provided by the Sunset OC/EC analyser and manometric measurement of CO<sub>2</sub> before and after the Cu reactor, respectively (Fig. 2).

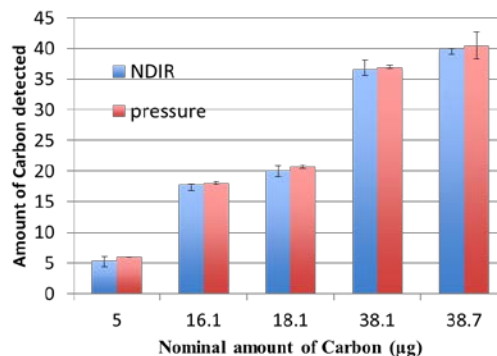


**Fig. 2:** Comparative study of CO<sub>2</sub> losses in the Cu reactor by NDIR and pressure quantification.

## CONCLUSIONS AND OUTLOOK

This study showed that the Cu reactor is a reliable interface for removing oxygen for several Sunset OC/EC measurements. We have achieved to reduce the outlet flow of the Sunset and enrich in CO<sub>2</sub> the inlet flow reaching the gas handling system of the ion source. Real-time mass spectrometry monitoring of CO<sub>2</sub> after the Cu reactor and investigation of peak broadening in relation with further increase in the reduction capacity will provide enough information for finalizing the geometry of the Cu reactor.

## REFERENCES

- [1] S. Szidat, *Chimia*, **63**, 157 (2009).
- [2] Y.L. Zhang et al., *Atmos. Chem. Phys.*, **12**, 10841 (2012).
- [3] H.-A. Synal et al., *Nucl. Instr. and Meth. Phys. Res. B*, **259**, 7 (2007).
- [4] M. Ruff et al., *Radiocarbon*, **52**, 1645 (2010).

# COUPLING OF AN ELEMENTAL ANALYZER WITH AMS OR FAST $^{14}\text{C}$ ANALYSIS OF AEROSOL SAMPLES

G. Salazar (Univ. Bern), Y.L. Zhang (Univ. Bern & PSI), S. Szidat (Univ. Bern)

## INTRODUCTION

For environmental and climate sciences, it is important to apportion the origin of the atmospheric aerosols between wood burning, biogenic emissions and fossil-fuel combustion. This can be achieved by analyzing  $^{14}\text{C}$  in the aerosol by accelerator mass spectrometry (AMS). However, sample preparation is highly effort and time consuming (1 hr/sample of experimental work) [1]. This paper describes the implementation of the method of a previous study [2] for the analysis of aerosol samples. With such a method, sample combustion is carried out with an elemental analyser (EA) and the  $\text{CO}_2$  is injected into an AMS.

## EXPERIMENTAL

The EA is connected to a Gas Injecting System (GIS) that traps the  $\text{CO}_2$  incoming at high flow ( $\sim 80$  mL/min) in a zeolite column; the  $\text{CO}_2$  is released at high temperature ( $450^\circ\text{C}$ ), see Fig. 1. The  $\text{CO}_2$  expands into a 2.7 mL syringe and helium is added to make a pressurized mixture of 5% of  $\text{CO}_2$ . Afterwards, the syringe slowly ( $\sim 40$   $\mu\text{L}/\text{min}$ ) delivers the  $\text{CO}_2$  into the gas ion source of a MICADAS (Mini Carbon Dating System) AMS. The whole system is fully automatic and requires 10 min/sample. 5 samples were punched out ( $\phi = 3$  mm each) from atmospheric quartz filters and wrapped up with a tin foil for flash combustion inside the EA.

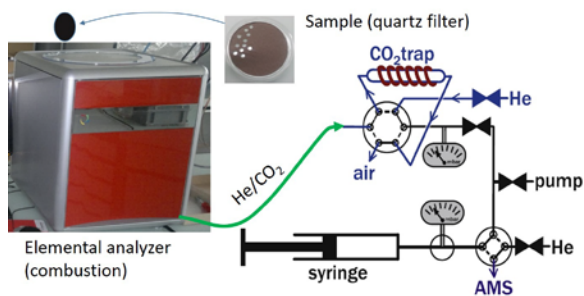


Fig. 1: Illustration of the EA-GIS coupled system.

## RESULTS AND DISCUSSION

The efficiency of the system was characterized by: 1) measuring the effects of the indeterminate contamination and 2) comparing the  $^{14}\text{C}$  results of real samples with a reference method [1]. The effects of small amounts of instrumental or environmental contamination based on a model of a contamination that is constant in carbon mass and  $^{14}\text{C}/^{12}\text{C}$  ratio are shown in Fig. 2. The data agree with the theoretical supposition that the measured  $^{14}\text{C}/^{12}\text{C}$  ratio of a sample will drift from its uncontaminated value depending on the  $^{14}\text{C}/^{12}\text{C}$  ratios and masses of the sample and the con-

taminant, see eq. 2.  $m_c$  is very low, considering the multiple columns and volume of the system. The value of  $R_c$  is lower than the atmosphere value, which indicates that the contaminant is a mix of air and fossil organics.

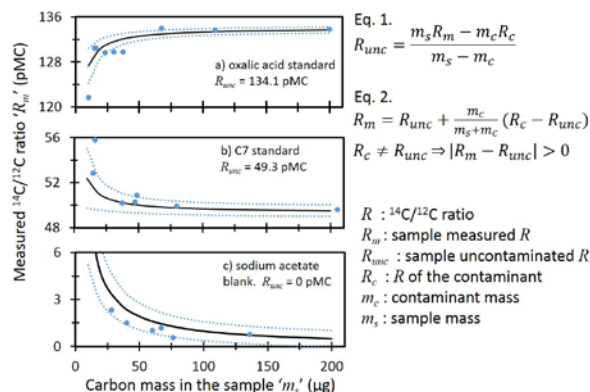


Fig. 2: Constant mass contamination. Fitting factors  $m_c$  and  $R_c$  values were  $1.3 \pm 0.3$   $\mu\text{g}$  and  $76 \pm 19$  pMC.

The measured  $^{14}\text{C}/^{12}\text{C}$  ratios of the aerosol samples, for the EA-GIS method, were corrected to  $R_{unc}$  using eq. 1 and the factors  $m_c$  and  $R_c$  of Fig. 2. The results for both methods show a 1:1 relationship in Fig. 3. This observation indicates that the EA-GIS method can replace the reference method for the investigated range of sample masses and with the proper corrections.

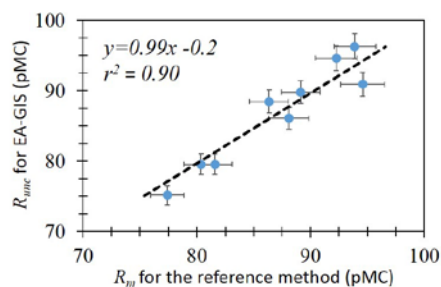


Fig. 3: Comparison of the  $^{14}\text{C}$  results for aerosol samples between the EA-GIS and the reference method.

## CONCLUSIONS

A high-throughput method, faster and more convenient than the reference method, was implemented to measure  $^{14}\text{C}/^{12}\text{C}$  ratios of aerosol samples. The constant contamination model was useful for data corrections.

## REFERENCES

- [1] S. Szidat et al., Nucl. Instr. and Meth. Phys. Res. B, **223-224**, 829 (2004).
- [2] L. Wacker et al., Nucl. Instr. and Meth. Phys. Res. B, **294**, 315 (2013).

# <sup>14</sup>C ANALYSIS AND SAMPLE PREPARATION AT THE NEW BERN LABORATORY FOR THE ANALYSIS OF RADIOCARBON WITH AMS (LARA)

S. Szidat, G. Salazar, E. Vogel, M. Battaglia (Univ. Bern), L. Wacker, H.-A. Synal (ETHZ), A. Türler (Univ. Bern & PSI)

## INTRODUCTION

The accelerator mass spectrometer (AMS) MICADAS (MIni CARbon DAting System) is comparable for <sup>14</sup>C analysis in terms of precision and detection limit with both conventional decay counters and large AMS systems [1]. Moreover, it offers further advantages due to its simplicity and low requirements of sample amounts and process time. The new Bern Laboratory for the Analysis of Radiocarbon with AMS (LARA) is equipped with a MICADAS (Fig. 1), which became operational in March 2013. This work describes the instrumentation of the LARA and first quality assurance measures.

## INSTRUMENTATION AND METHODS

For routine dating, a new sample preparation laboratory was installed and equipped with instruments dedicated for <sup>14</sup>C analysis at the University of Bern. For sample pretreatment of most material such as plant remains, macrofossils, bulk sediment, charcoals, an acid-base-acid (ABA) procedure is performed, whereas cellulose is extracted for wood analysis [2]. For production of solid targets with a typical carbon mass of 1 mg, an automated graphitization equipment (AGE) was installed [3].



**Fig. 1:** The MICADAS at the new Bern Laboratory for the Analysis of Radiocarbon with AMS (LARA). Photo: A. Boutellier.

## RESULTS AND DISCUSSION

The performance of the MICADAS was assessed using IAEA standards C4-C7 after combustion and graphitization as unknowns [2]. Tab. 1 shows the <sup>14</sup>C results of repeated determinations over 4 months. For all of these standard materials, the measured values are not significantly different from the reference values (all within 95% confidence level). The measured <sup>14</sup>C of C6 seems to tend towards lower values than the reference, which will be observed in detail in the future. With fossil sodium acetate, blanks with very low

<sup>14</sup>C amounts could be produced with high reliability making dating possible up to 52 ky BP.

**Tab. 1:** <sup>14</sup>C analysis of IAEA standards from *n* determinations of 5 measurement runs between March and August 2013 with average measurement uncertainty.

Standard	<sup>14</sup> C reference [F14C]	<sup>14</sup> C measured [F14C]
C4 ( <i>n</i> =4)	(0.0020-0.0044)	0.0017±0.0003
C5 ( <i>n</i> =8)	0.2305±0.0002	0.2304±0.0010
C6 ( <i>n</i> =9)	1.5060±0.0011	1.4994±0.0040
C7 ( <i>n</i> =10)	0.4935±0.0012	0.4950±0.0015

The quality of wood dating was evaluated with a series of 10-year segments of mid-European oak samples (Tab. 2). The comparison of the measured and the reference age matched within 95% confidence for all 20 individual determinations as well as for the means of each wood sample.

**Tab. 2:** <sup>14</sup>C analysis (average of 3 determinations) of wood samples, which comprised 10 annual rings and were dated with dendrochronology. The expected <sup>14</sup>C age and its uncertainty were determined from the wood age using the IntCal09 dataset.

Sample code	Expected <sup>14</sup> C age [y BP]	Av. Measured <sup>14</sup> C age [y BP]
BE-1327	376±12	401±16
BE-1311	2076±13	2078±16
BE-1326	2229±14	2234±16
BE-1331	2455±13	2482±17
BE-1332	4003±13	3998±17
BE-1329	4488±13	4478±19
BE-1328	8700±18	8713±20

## ACKNOWLEDGEMENT

Funding of the following institutions is acknowledged: Swiss National Science Foundation (project 206021\_133817), Swiss Federal Office of Public Health, and University of Bern (contributing parties: the University Board of Directors, the Department of Chemistry and Biochemistry, and the Oeschger Centre for Climate Change Research). Wood samples were provided by Ulf Büntgen (WSL), dated with dendrochronology by Willy Tegel (DendroNet) and prepared by Christian Steiner (University of Bern).

## REFERENCES

- [1] H.-A. Synal, *Int. J. Mass Spectrom.*, **349-350**, 192 (2013).
- [2] S. Szidat et al., *Radiocarbon*, in press (2013).
- [3] M. Němec et al., *Radiocarbon*, **52**, 1380 (2010).

# $^{14}\text{C}$ -BASED SOURCE APPORTIONMENT OF ELEMENTAL CARBON AND ORGANIC CARBON AT A BACKGROUND SITE ON HAINAN ISLAND, SOUTH CHINA

Y.L. Zhang (Univ. Bern & PSI), J. Li, G. Zhang (GIG CAS, China), P. Zotter, A.S.H. Prévôt (PSI/LAC), S. Szidat (Univ. Bern)

## INTRODUCTION

Total carbon (TC) is a major fraction of fine particles and is of worldwide concern due to its important impact on climate and human health. TC is often operationally classified into two sub-fractions: elemental carbon (EC) and organic carbon (OC) [1]. Separate radiocarbon ( $^{14}\text{C}$ ) analysis of EC and OC allows a quantitative and unambiguous measurement of their contemporary and fossil contributions, thereby potentially reducing a major uncertainty in the present understanding of organic aerosols emissions [2].

Both fossil-fuel emissions and biomass/biofuel burning in Southeast Asia may have an important impact on regional EC and OC emissions. Here we present a  $^{14}\text{C}$ -based source apportionment study at a regional background site of Jianfeng (JF) on Hainan Island, South China. This is an ideal site to study air pollution outflows from mainland China, as well as the impact of Southeast Asian biomass burning emission.

## METHODS

PM<sub>2.5</sub> samples were collected about once per week from May 2005 to August 2006 using a high-volume sampler ( $\sim 1 \text{ m}^3/\text{min}$ ) for 24 h. All samples were measured for the EC and OC concentrations by the thermal-optical transmittance method (EUSAAR2) [3]. The EC and OC isolation for subsequent  $^{14}\text{C}$  measurements were prepared with an optimized thermo-optical protocol (Swiss\_4S) on the selective samples [4].

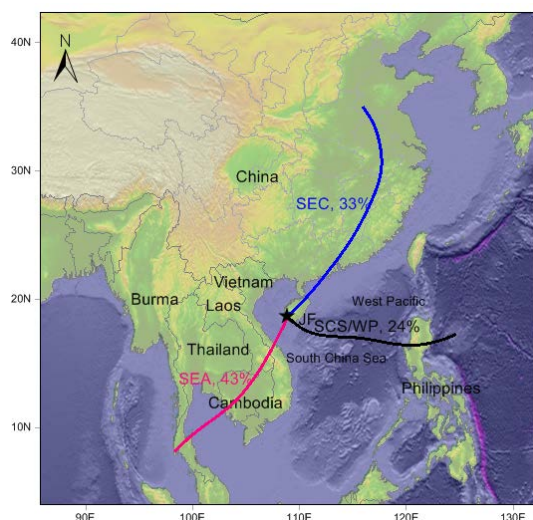


**Fig. 1:** The location of the sampling site (JF) in this study. The backward trajectory types include South China Sea/West Pacific (SCS/WP), Southeast China (SEC) and Southeast Asia (SEA) with occurrence percentage of trajectories ending at JF.

## RESULTS

The average contributions of fossil sources to EC, OC, and WINSOC were  $38 \pm 11\%$ ,  $19 \pm 10\%$ , and  $17 \pm 10\%$ , respectively, indicating generally a dominance of non-fossil emissions at the studied site. The lowest abundance of carbonaceous aerosols was found when air masses travelled through SCS/WP (Fig. 2a) in association with clean marine sources. A higher contribution from fossil sources to EC ( $\sim 51\%$ ) and OC ( $\sim 30\%$ ) was observed with air-mass pathways from Southeast China during autumn (Fig. 2c), due to large fossil-fuel combustion and vehicle emissions in highly urbanized regions of China. In contrast, an increase of the non-fossil contribution by 5-10% was observed when air mass travelled over Southeast Asia or Southeast China during the periods with enhanced open burning (Fig. 2b and 2d, respectively).

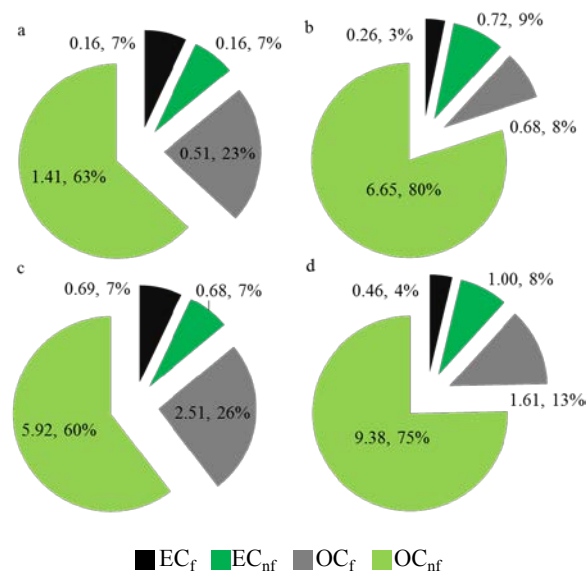


**Fig. 2:** Fossil (f) and non-fossil (nf) fractions (concentrations in  $\mu\text{g}/\text{m}^3$  and % of TC,  $n=2$ ) of OC and EC for samples from different source regions: SCS/WP (a), SEA (b) and SEC. The air mass origin of SEC was further divided into autumn (c) and winter (d).

## REFERENCES

- [1] U. Pöschl, *Angew. Chem. Int. Ed.*, **44**, 7520 (2005).
- [2] S. Szidat et al., *J. Geophys. Res.*, **111**, D07206 (2006).
- [3] F Cavalli et al., *Atmos. Meas. Tech.*, **3**, 79 (2010).
- [4] Y.L. Zhang et al., *Atmos. Chem. Phys.*, **12**, 10841, (2012).

# $^{14}\text{C}$ -BASED SOURCE APPORTIONMENT OF CARBONACEOUS AEROSOLS FROM WINTER SMOG EPISODES IN SWITZERLAND FROM 2008-2012

P. Zotter, V.G. Ciobanu (PSI/LAC), Y.L. Zhang (Univ. Bern & PSI), S. Szidat (Univ. Bern), I. El-Haddad, U. Baltensperger, A.S.H. Prévôt (PSI/LAC)

## INTRODUCTION

Carbonaceous particles (total carbon, TC) are a major fraction of fine aerosols and affect climate and human health. TC is classified into the sub-fractions elemental carbon (EC) and organic carbon (OC). EC originates only from fossil-fuel combustion and biomass burning. OC can be emitted directly as primary organic aerosol from biogenic emissions, wood burning and fossil-fuel combustion or can be formed in-situ in the atmosphere (secondary organic aerosol) [1]. Radiocarbon ( $^{14}\text{C}$ ) analysis is a direct and quantitative tool for distinguishing fossil and non-fossil sources, since  $^{14}\text{C}$  in fossil-fuels is completely depleted, whereas other sources have a modern  $^{14}\text{C}$  level.

## METHODS

This study presents wintertime source apportionment results over a time period of 5 years (2007/2008–2011/2012) using  $^{14}\text{C}$  analysis on aerosol filters collected simultaneously at 16 air quality monitoring stations across Switzerland (Fig. 1). For every year 5 winter smog episode days ( $\text{PM}_{10} > 50 \mu\text{g}/\text{m}^3$ ) were selected, from which filters from all stations were analyzed. This  $^{14}\text{C}$  dataset is worldwide unique concerning the number of analyzed samples ( $n \sim 750$ ) and the duration.



**Fig. 1:** Map of Switzerland with the stations participating in this project. Filters from the red marked stations were only analyzed for 1 or 2 winters.

The filter sampling was conducted using high-volume samplers with  $\text{PM}_{10}$  inlets. Separation of OC and EC was carried out by step-wise combustion [2]. The resulting  $\text{CO}_2$  was cryo-trapped and sealed in glass ampoules for  $^{14}\text{C}$  measurements, performed with the Mini Carbon Dating System MICADAS at ETH Zürich and University of Bern.

## RESULTS AND CONCLUSIONS

$^{14}\text{C}$  results indicate that carbonaceous aerosols are mostly non-fossil, i.e. 84% for OC and 45% for EC (Fig. 2). These high values together with a high correlation with levoglucosan suggest that wood burning is the major source of TC in Switzerland during winter-smog episodes. The highest non-fossil values (100% and 87% for OC and EC, respectively) were registered for alpine valley sites and the lowest at highly traffic-influenced sites (57% for OC and 10% for EC).

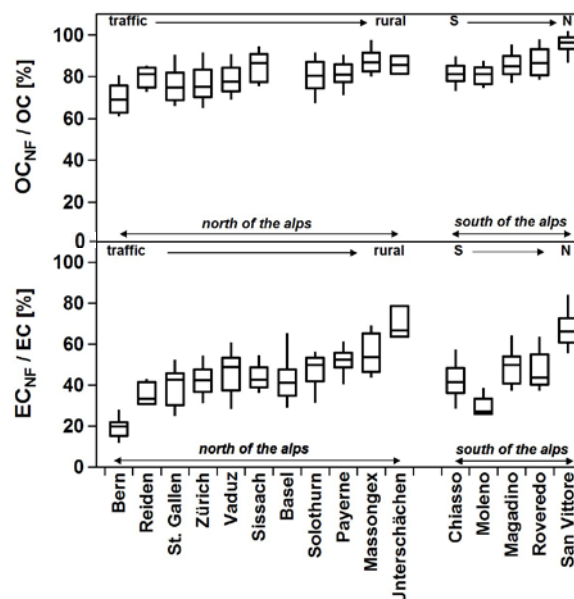


**Fig. 2:** Whisker box plots showing all results for non-fossil EC ( $\text{EC}_{\text{NF}}$ , bottom) and non-fossil OC ( $\text{OC}_{\text{NF}}$ , top). Stations are ordered from left to right from the most traffic-influenced station to the most rural one north of the Alps and from south to north for stations south of the Alps.

The station-to-station variation north of the Alps is low, whereas a spatial trend was found in the south with an increase of the non-fossil values towards the north showing the influence of more fossil air masses advected from the Po Valley.

## ACKNOWLEDGEMENT

This work was supported by the Federal Office for the Environment, the Swiss Cantons BS/BL, GR, SG, SO, TI, UR, VS and the Principality of Liechtenstein.

## REFERENCES

- [1] S. Szidat et al., *J. Geophys. Res.*, **111**, D07206 (2006).
- [2] Y.L. Zhang et al., *Atmos. Chem. Phys.*, **12**, 10841 (2012).

## LIST OF PUBLICATIONS

### HEAVY ELEMENTS

R. Eichler

*First foot prints of chemistry on the shore of the Island of Superheavy Elements*

Journal of Physics: Conference Series **420** (1): 012003, doi: 10.1088/1742-6596/420/1/012003 (2013).

J. V. Kratz, M. Schädel, H. W. Gäggeler

*Reexamining the heavy-ion reactions  $^{238}\text{U}+^{238}\text{U}$  and  $^{238}\text{U}+^{248}\text{Cm}$  and actinide production close to the barrier*

Phys. Rev. C **88** (5): 054615, doi: 10.1103/PhysRevC.88.054615 (2013).

D. Rudolph, U. Forsberg, P. Golubev, L. G. Sarmiento, A. Yakushev, L. L. Andersson, A. Di Nitto, C. E. Düllmann, J. M. Gates, K. E. Gregorich, C. J. Gross, F. P. Hessberger, R. D. Herzberg, J. Khuyagbaatar, J. V. Kratz, K. Rykaczewski, M. Schadel, S. Aberg, D. Ackermann, M. Block, H. Brand, B. G. Carlsson, D. Cox, X. Derkx, K. Eberhardt, J. Even, C. Fahlander, J. Gerl, E. Jäger, B. Kindler, J. Krier, I. Kojouharov, N. Kurz, B. Lommel, A. Mistry, C. Mokry, H. Nitsche, J. P. Omtvedt, P. Papadakis, I. Ragnarsson, J. Runke, H. Schaffner, B. Schausten, P. Thorle-Pospiech, T. Torres, T. Traut, N. Trautmann, A. Türler, A. Ward, D. E. Ward, N. Wiehl

*Spectroscopy of element 115 decay chains*

Phys. Rev. Lett. **111** (11): 112502, doi: 10.1103/PhysRevLett.111.112502 (2013).

A. Serov, R. Eichler, R. Dressler, D. Piguet, A. Türler, A. Vögele, D. Wittwer, H. W. Gäggeler

*Adsorption interaction of carrier-free thallium species with gold and quartz surfaces*

Radiochim. Acta **101** (7): 421-426, doi: 10.1524/ract.2013.2045 (2013).

S. Söllradl, H. Luhrs, Z. Revay, P. Kudejova, L. Canella, A. Türler

*Increasing the dynamic range for the analysis of boron in PGAA*

J. Radioanal. Nucl. Chem. **298** (3): 2069-2073, doi: 10.1007/S10967-013-2739-9 (2013).

A. Türler, V. Pershina

*Advances in the production and chemistry of the heaviest elements*

Chem. Rev. **113** (2): 1237-1312, doi: 10.1021/cr3002438 (2013).

D. Wittwer, R. Dressler, R. Eichler, H. W. Gäggeler, D. Piguet, A. Türler

*Thermal release rate studies of nuclear reaction products from polycrystalline metal matrices*

Nucl. Instrum. Methods Phys. Res., Sect. B **297**: 86-93, doi: 10.1016/j.nimb.2012.11.021 (2013).

D. Wittwer, R. Dressler, R. Eichler, H. W. Gäggeler, A. Türler

*Prediction of the thermal release of transactinide elements ( $112 \leq Z \leq 116$ ) from metals*

Radiochim. Acta **101** (4): 211-220, doi: 10.1524/ract.2013.2027 (2013).

### SURFACE CHEMISTRY

M. Ammann, R. A. Cox, J. N. Crowley, M. E. Jenkin, A. Mellouki, M. J. Rossi, J. Troe, T. J. Wallington

*Evaluated kinetic and photochemical data for atmospheric chemistry: Volume VI – heterogeneous reactions with liquid substrates*

Atmos. Chem. Phys. **13** (16): 8045-8228, doi: 10.5194/acp-13-8045-2013 (2013).

T. Bartels-Rausch

*Chemistry: Ten things we need to know about ice and snow*

Nature **494** (7435): 27-29, doi: 10.1038/494027a (2013).

T. Bartels-Rausch, S. N. Wren, S. Schreiber, F. Riche, M. Schneebeli, M. Ammann

*Diffusion of volatile organics through porous snow: impact of surface adsorption and grain boundaries*

Atmos. Chem. Phys. **13** (14): 6727-6739, doi: 10.5194/acp-13-6727-2013 (2013).

- T. Berkemeier, A. J. Huisman, M. Ammann, M. Shiraiwa, T. Koop, U. Pöschl  
*Kinetic regimes and limiting cases of gas uptake and heterogeneous reactions in atmospheric aerosols and clouds: A general classification scheme*  
 Atmos. Chem. Phys. **13** (14): 6663-6686, doi: 10.5194/acp-13-6663-2013 (2013).
- M. A. Brown, N. Duyckaerts, A. B. Redondo, I. Jordan, F. Nolting, A. Kleibert, M. Ammann, H. J. Wörner, J. A. van Bokhoven, Z. Abbas  
*Effect of surface charge density on the affinity of oxide nanoparticles for the vapor–water interface*  
 Langmuir **29** (16): 5023-5029, doi: 10.1021/la4005054 (2013).
- M. A. Brown, A. B. Redondo, I. Jordan, N. Duyckaerts, M.-T. Lee, M. Ammann, F. Nolting, A. Kleibert, T. Huthwelker, J.-P. Mächler, M. Birrer, J. Honegger, R. Wetter, H. J. Wörner, J. A. van Bokhoven  
*A new endstation at the Swiss Light Source for ultraviolet photoelectron spectroscopy, X-ray photoelectron spectroscopy, and X-ray absorption spectroscopy measurements of liquid solutions*  
 Rev. Sci. Instrum. **84** (7): 073904-8, doi: 10.1063/1.4812786 (2013).
- A. Křepelová, T. Bartels-Rausch, M. A. Brown, H. Bluhm, M. Ammann  
*Adsorption of acetic acid on ice studied by ambient-pressure XPS and partial-electron-yield NEXAFS spectroscopy at 230–240 K*  
 J. Phys. Chem. A **117** (2): 401-409, doi: 10.1021/jp3102332 (2013).
- M. Lampimäki, V. Zelenay, A. Křepelová, Z. Liu, R. Chang, H. Bluhm, M. Ammann  
*Ozone-induced band bending on metal-oxide surfaces studied under environmental conditions*  
 Chem. Phys. Chem., doi: 10.1002/cphc.201300418 (2013).
- A. Liati, P. Dimopoulos Eggenschwiler, D. Schreiber, V. Zelenay, M. Ammann  
*Variations in diesel soot reactivity along the exhaust after-treatment system, based on the morphology and nanostructure of primary soot particles*  
 Combust. Flame **160** (3): 671-681, doi: 10.1016/j.combustflame.2012.10.024 (2013).
- S. Schreiber, M. Kerbrat, T. Huthwelker, M. Birrer, M. Ammann  
*Coupling a Knudsen reactor with the short lived radioactive tracer <sup>13</sup>N for atmospheric chemistry studies*  
 Rev. Sci. Instrum. **84** (3): 035101-035101-13, doi: 10.1063/1.4793405 (2013).

## ANALYTICAL CHEMISTRY

- T. Blunier, T. M. Jenk, Ice core methods | CO<sub>2</sub> studies, in Encyclopedia of Quaternary Science (Second Edition) Elias, S. A. and Mock, C. J. (Editors). Elsevier: Amsterdam. p. 311-318, doi: 10.1016/B978-0-444-53643-3.00310-1 (2013).
- S. Brönnimann, I. Mariani, M. Schwikowski, R. Auchmann, A. Eichler  
*Simulating the temperature and precipitation signal in an Alpine ice core*  
 Clim. Past **9**: 2013-2022, doi: 10.5194/cp-9-2013-2013 (2013).
- F. Cao, Y.-L. Zhang, S. Szidat, A. Zapf, L. Wacker, M. Schwikowski  
*Microgram-level radiocarbon determination of carbonaceous particles in firn and ice samples: Pretreatment and OC/EC separation*  
 Radiocarbon **55**: 383-390, doi: 10.2458/azu\_js\_rc.55.16291 (2013).

- M. R. A. D. Dahl-Jensen, A. Aldahan, N. Azuma, D. Balslev-Clausen, M. Baumgartner, A.-M. Berggren, M. Bigler, T. Binder, T. Blunier, J. C. Bourgeois, E. J. Brook, S. L. Buchardt, C. Buizert, E. Capron, J. Chappellaz, J. Chung, H. B. Clausen, S. M. D. I. Cvijanovic, P. Ditlevsen, O. Eicher, H. Fischer, D. A. Fisher, L. G. Fleet, G. Gfeller, V. Gkinis, S. Gogineni, K. Goto-Azuma, A. Grinsted, H. Gudlaugsdottir, M. Guillevic, S. B. Hansen, M. Hansson, M. Hirabayashi, S. Hong, S. D. Hur, C. S. H. P. Huybrechts, Y. Iizuka, T. Jenk, S. J. Johnsen, T. R. Jones, J. Jouzel, N. B. Karlsson, K. Kawamura, K. Keegan, E. Kettner, S. Kipfstuhl, H. A. Kjær, M. Koutnik, T. Kuramoto, P. Köhler, T. Laepple, A. Landais, P. L. Langen, D. L. L. B. Larsen, M. Leuenberger, C. Leuschen, J. Li, V. Lipenkov, P. Martinerie, O. J. Maselli, V. Masson-Delmotte, J. R. McConnell, H. Miller, O. Mini, A. Miyamoto, M. Montagnat-Rentier, R. Mulvaney, R. Muscheler, A. J. Orsi, J. Paden, F. P. C. Pantou, J.-R. Petit, K. Pol, T. Popp, G. Possnert, F. Prié, M. Prokopiou, A. Quiquet, S. O. Rasmussen, D. Raynaud, J. Ren, C. Reutenauer, C. Ritz, T. Röckmann, J. L. Rosen, M. Rubino, O. Rybak, D. Samyn, C. J. Sapart, A. Schilt, J. S. A. M. Z. Schmidt, S. Schüpbach, I. Seierstad, J. P. Severinghaus, S. Sheldon, S. B. Simonsen, J. Sjolte, A. M. Solgaard, T. Sowers, P. Sperlich, H. C. Steen-Larsen, K. Steffen, J. P. Steffensen, D. Steinhage, T. F. Stocker, C. Stowasser, W. T. S. A. S. Sturevik, A. Sveinbjörnsdottir, A. Svensson, J.-L. Tison, J. Uetake, P. Vallengona, R. S. W. van de Wal, G. van der Wel, B. H. Vaughn, B. Vinther, E. Waddington, A. Wegner, I. Weikusat, J. W. C. White, F. Wilhelms, M. Winstrup, E. W. W. E. Witrant, C. Xiao, J. Zheng  
*Eemian interglacial reconstructed from a Greenland folded ice core*  
Nature **493** (7433): 489-494, doi: 10.1038/nature11789 (2013).
- O. Garmash, M. H. Hermanson, E. Isaksson, M. Schwikowski, D. Divine, C. Teixeira, D. C. G. Muir  
*Deposition history of polychlorinated biphenyls to the Lomonosovfonna glacier, Svalbard: A 209 congener analysis*  
Environ. Sci. Technol. **47** (21): 12064-12072, doi: 10.1021/es402430t (2013).
- P.-A. Herren, A. Eichler, H. Machguth, T. Papina, L. Tobler, A. Zapf, M. Schwikowski  
*The onset of Neoglaciation 6000 years ago in western Mongolia revealed by an ice core from the Tsambagarav mountain range*  
Quat. Sci. Rev. **69**: 59-68, doi: 10.1016/j.quascirev.2013.02.025 (2013).
- T. Kirchgeorg, A. Dreyer, J. Gabrieli, N. Kehrwald, M. Sigl, M. Schwikowski, C. Boutron, A. Gambaro, C. Barbante, R. Ebinghaus  
*Temporal variations of perfluoroalkyl substances and polybrominated diphenyl ethers in alpine snow*  
Environ. Pollut. **178**: 367-374, doi: 10.1016/j.envpol.2013.03.043 (2013).
- T. Papina, T. Blyakharchuk, A. Eichler, N. Malygina, E. Mitrofanova, M. Schwikowski  
*Biological proxies recorded in a Belukha ice core, Russian Altai*  
Clim. Past **9** (5): 2399-2411, doi: 10.5194/cp-9-2399-2013 (2013).
- M. Rubino, D. M. Etheridge, C. M. Trudinger, C. E. Allison, M. O. Battle, R. L. Langenfelds, L. P. Steele, M. Curran, M. Bender, J. W. C. White, T. M. Jenk, T. Blunier, R. J. Francey  
*A revised 1000 year atmospheric  $\delta^{13}\text{C}$ -CO<sub>2</sub> record from Law Dome and South Pole, Antarctica*  
J. Geophys. Res. **118** (15): 8482-8499, doi: 10.1002/jgrd.50668 (2013).
- M. Schwikowski, M. Schläppi, P. Santibañez, A. Rivera, G. Casassa  
*Net accumulation rates derived from ice core stable isotope records of Pío XI glacier, Southern Patagonia Icefield*  
Cryosphere **7** (5): 1635-1644, doi: 10.5194/tc-7-1635-2013 (2013).
- P. Sperlich, C. Buizert, T. M. Jenk, C. J. Sapart, M. Prokopiou, T. Röckmann, T. Blunier  
*An automated GC-C-GC-IRMS setup to measure palaeoatmospheric  $\delta^{13}\text{C}$ -CH<sub>4</sub>,  $\delta^{15}\text{N}$ -N<sub>2</sub>O and  $\delta^{18}\text{O}$ -N<sub>2</sub>O in one ice core sample*  
Atmos. Meas. Tech. **6** (8): 2027-2041, doi: 10.5194/amt-6-2027-2013 (2013).
- A. Zapf, A. Nesje, S. Szidat, L. Wacker, M. Schwikowski  
 *$^{14}\text{C}$  measurements of ice samples from the Juvfonna ice tunnel, Jotunheimen, southern Norway-Validation of a  $^{14}\text{C}$  dating technique for glacier ice*  
Radiocarbon **55** (2-3): 571-578, doi: 10.2458/azu\_js\_rc.55.16314 (2013).

## RADWASTE ANALYTICS

M. Barbagallo, C. Guerrero, A. Tsinganis, D. Tarrío, S. Altstadt, S. Andriamonje, J. Andrzejewski, L. Audouin, V. Becares, F. Becvar, F. Belloni, E. Berthoumieux, J. Billowes, V. Boccone, D. Bosnar, M. Brugger, M. Calviani, F. Calvino, D. Cano-Ott, C. Carrapico, F. Cerutti, E. Chiaveri, M. Chin, N. Colonna, G. Cortes, M. A. Cortes-Giraldo, M. Diakaki, C. Domingo-Pardo, I. Duran, R. Dressler, N. Dzysiuk, C. Eleftheriadis, A. Ferrari, K. Fraval, S. Ganesan, A. R. Garcia, G. Giubrone, K. Goebel, M. B. Gomez-Hornillos, I. F. Goncalves, E. Gonzalez-Romero, E. Griesmayer, F. Gunsing, P. Gurusamy, A. Hernandez-Prieto, D. G. Jenkins, E. Jericha, Y. Kadi, F. Kaeppler, D. Karadimos, N. Kivel, P. Koehler, M. Kokkoris, M. Krticka, J. Kroll, C. Lampoudis, C. Langer, E. Leal-Cidoncha, C. Lederer, H. Leeb, L. S. Leong, R. Losito, A. Manousos, J. Marganiec, T. Martinez, C. Massimi, P. F. Mastinu, M. Mastromarco, M. Meaze, E. Mendoza, A. Mengoni, P. M. Milazzo, F. Mingrone, M. Mirea, W. Mondalaers, T. Papaevangelou, C. Paradela, A. Pavlik, J. Perkowski, A. Plompen, J. Praena, J. M. Quesada, T. Rauscher, R. Reifarth, A. Riego, F. Roman, C. Rubbia, M. Sabate-Gilarte, R. Sarmiento, A. Saxena, P. Schillebeeckx, S. Schmidt, D. Schumann, P. Steinegger, G. Tagliente, J. L. Tain, L. Tassan-Got, S. Valenta, G. Vannini, V. Variale, P. Vaz, A. Ventura, R. Versaci, M. J. Vermeulen, V. Vlachoudis, R. Vlastou, A. Wallner, T. Ware, M. Weigand, C. Weiss, T. Wright, P. Zugec

*High-accuracy determination of the neutron flux at n\_TOF*

European Physical Journal A **49** (12): 1-11, doi: 10.1140/epja/i2013-13156-x (2013).

C.-Y. Chuang, P. H. Santschi, Y.-F. Ho, M. H. Conte, L. Guo, D. Schumann, M. Ayranov, Y.-H. Li

*Role of biopolymers as major carrier phases of Th, Pa, Pb, Po, and Be radionuclides in settling particles from the Atlantic Ocean*

Mar. Chem. **157**: 131-143, doi: 10.1016/j.marchem.2013.10.002 (2013).

B. Gonzalez Prieto, J. Van den Bosch, J. A. Martens, J. Neuhausen, A. Aerts

*Equilibrium evaporation of trace polonium from liquid lead-bismuth eutectic at high temperature*

J. Nucl. Mater., doi: j.jnuclmat.2013.06.037 (2013).

C. Guerrero, A. Tsinganis, E. Berthoumieux, M. Barbagallo, F. Belloni, F. Gunsing, C. Weiß, E. Chiaveri, M. Calviani, V. Vlachoudis, S. Altstadt, S. Andriamonje, J. Andrzejewski, L. Audouin, V. Bécares, F. Bečvář, J. Billowes, V. Boccone, D. Bosnar, M. Brugger, F. Calviño, D. Cano-Ott, C. Carrapico, F. Cerutti, M. Chin, N. Colonna, G. Cortés, M. A. Cortés-Giraldo, M. Diakaki, C. Domingo-Pardo, I. Duran, R. Dressler, N. Dzysiuk, C. Eleftheriadis, A. Ferrari, K. Fraval, S. Ganesan, A. R. García, G. Giubrone, K. Göbel, M. B. Gómez-Hornillos, I. F. Gonçalves, E. González-Romero, E. Griesmayer, P. Gurusamy, A. Hernández-Prieto, P. Gurusamy, D. G. Jenkins, E. Jericha, Y. Kadi, F. Käppler, D. Karadimos, N. Kivel, P. Koehler, M. Kokkoris, M. Krticka, J. Kroll, C. Lampoudis, C. Langer, E. Leal-Cidoncha, C. Lederer, H. Leeb, L. S. Leong, R. Losito, A. Manousos, J. Marganiec, T. Martínez, C. Massimi, P. F. Mastinu, M. Mastromarco, M. Meaze, E. Mendoza, A. Mengoni, P. M. Milazzo, F. Mingrone, M. Mirea, W. Mondalaers, T. Papaevangelou, C. Paradela, A. Pavlik, J. Perkowski, A. Plompen, J. Praena, J. M. Quesada, T. Rauscher, R. Reifarth, A. Riego, F. Roman, C. Rubbia, M. Sabate-Gilarte, R. Sarmiento, A. Saxena, P. Schillebeeckx, S. Schmidt, D. Schumann, P. Steinegger, G. Tagliente, J. L. Tain, D. Tarrío, L. Tassan-Got, S. Valenta, G. Vannini, V. Variale, P. Vaz, A. Ventura, R. Versaci, M. J. Vermeulen, R. Vlastou, A. Wallner, T. Ware, M. Weigand, T. Wright, P. Žugec

*Performance of the neutron time-of-flight facility n\_TOF at CERN*

The European Physical Journal A **49** (2): 1-15, doi: 10.1140/epja/i2013-13027-6 (2013).

B. Hammer, J. Neuhausen, V. Boutellier, H. P. Linder, N. Shcherbina, M. Wohlmuther, A. Türler, D. Schumann

*Analysis of the  $^{207}\text{Bi}$ ,  $^{194}\text{Hg}/\text{Au}$  and  $^{173}\text{Lu}$  distribution in the irradiated MEGAPIE target*

J. Nucl. Mater.: in press, doi: 10.1016/j.jnuclmat.2013.09.016 (2013).

S. Heinitz, D. Schumann, J. Neuhausen, S. Köchli, K. Thomsen, E. Platacis, O. Lielausis, I. Bucenieks, A. Zik, A. Romančuks, K. Kravalis, L. Buligins, A. Türler

*A comparison between the chemical behaviour of lead-gold and lead-bismuth eutectics towards 316L stainless steel*

Radiochim. Acta **101** (10): 637, doi: 10.1524/ract.2013.2063 (2013).

C. Lederer, C. Massimi, S. Altstadt, J. Andrzejewski, L. Audouin, M. Barbagallo, V. Bécaries, F. Bečvář, F. Belloni, E. Berthoumieux, J. Billowes, V. Boccone, D. Bosnar, M. Brugger, M. Calviani, F. Calviño, D. Cano-Ott, C. Carrapiço, F. Cerutti, E. Chiaveri, M. Chin, N. Colonna, G. Cortés, M. A. Cortés-Giraldo, M. Diakaki, C. Domingo-Pardo, I. Duran, R. Dressler, N. Dzysiuk, C. Eleftheriadis, A. Ferrari, K. Fraval, S. Ganesan, A. R. García, G. Giubrone, M. B. Gómez-Hornillos, I. F. Gonçalves, E. González-Romero, E. Griesmayer, C. Guerrero, F. Gunsing, P. Gurusamy, D. G. Jenkins, E. Jericha, Y. Kadi, F. Käppeler, D. Karadimos, N. Kivel, P. Koehler, M. Kokkoris, G. Korschinek, M. Krťička, J. Kroll, C. Langer, H. Leeb, L. S. Leong, R. Losito, A. Manousos, J. Marganec, T. Martínez, P. F. Mastinu, M. Mastromarco, M. Meaze, E. Mendoza, A. Mengoni, P. M. Milazzo, F. Mingrone, M. Mirea, W. Mondelaers, C. Paradela, A. Pavlik, J. Perkowski, M. Pignatari, A. Plompen, J. Praena, J. M. Quesada, T. Rauscher, R. Reifarh, A. Riego, F. Roman, C. Rubbia, R. Sarmento, P. Schillebeeckx, S. Schmidt, D. Schumann, G. Tagliente, J. L. Tain, D. Tarrío, L. Tassan-Got, A. Tsinganis, S. Valenta, G. Vannini, V. Variale, P. Vaz, A. Ventura, R. Versaci, M. J. Vermeulen, V. Vlachoudis, R. Vlastou, A. Wallner, T. Ware, M. Weigand, C. Weiß, T. J. Wright, P. Žugec, T. O. F. Collaboration)  
*Neutron capture cross section of unstable  $^{63}\text{Ni}$ : Implications for stellar nucleosynthesis*  
 Phys. Rev. Lett. **110** (2): 022501, doi: 10.1103/PhysRevLett.110.022501 (2013).

T. Lorenz, Y. Dai, D. Schumann  
*Analysis of long-lived radionuclides produced by proton irradiation in lead targets -  $\gamma$ -measurements*  
 Radiochim. Acta **101** (10): 661, doi: 10.1524/ract.2013.2067 (2013).

E. A. Maugeri, J. Neuhausen, R. Eichler, D. Piguet, T. M. Mendonça, T. Stora, D. Schumann  
*Thermochromatography study of volatile polonium species in various gas atmospheres*  
 J. Nucl. Mater.: in press, doi: 10.1016/j.jnucmat.2013.11.024 (2013).

K. Rijpstra, A. Van Yperen-De Deyne, J. Neuhausen, V. Van Speybroeck, S. Cottenier  
*Solution enthalpy of Po and Te in solid lead–bismuth eutectic*  
 J. Nucl. Mater., doi: 10.1016/j.jnucmat.2013.07.004 (2013).

K. Schmidt, S. Akhmadaliev, M. Anders, D. Bemmerer, K. Boretzky, A. Caciolli, D. Degering, M. Dietz, R. Dressler, Z. Elekes, Z. Fülöp, G. Gyürky, R. Hannaske, A. R. Junghans, M. Marta, M.-L. Menzel, F. Munnik, D. Schumann, R. Schwengner, T. Szűcs, A. Wagner, D. Yakorev, K. Zuber  
*Resonance triplet at  $E_{\alpha}=4.5$  MeV in the  $^{40}\text{Ca}(\alpha, \gamma)^{44}\text{Ti}$  reaction*  
 Phys. Rev. C **88** (2): 025803, doi: 10.1103/PhysRevC.88.025803 (2013).

D. Schumann, M. Ayranov, T. Stowasser, L. Gialanella, A. di Leva, M. Romano, D. Schuermann  
*Radiochemical separation of  $^7\text{Be}$  from the cooling water of the neutron spallation source SINQ at PSI*  
 Radiochim. Acta **101** (8): 509, doi: 10.1524/ract.2013.2078 (2013).

D. Schumann, T. Stowasser, R. Dressler, M. Ayranov  
*Possibilities of preparation of exotic radionuclide samples at PSI for scientific investigations*  
 Radiochim. Acta **101** (8): 501, doi: 10.1524/ract.2013.2058 (2013).

A. Wallner, M. Bichler, K. Buczak, D. Fink, O. Forstner, R. Golser, M. A. C. Hotchkis, A. Klix, A. Krasa, W. Kutschera, C. Lederer, A. Plompen, A. Priller, D. Schumann, V. Semkova, P. Steier  
*High-sensitivity isobar-free AMS measurements and reference materials for  $^{55}\text{Fe}$ ,  $^{68}\text{Ge}$  and  $^{202}\text{gPb}$*   
 Nucl. Instrum. Methods Phys. Res., Sect. B **294**: 374–381, doi: 10.1016/j.nimb.2012.03.029 (2013).

C. Weiß, E. Griesmayer, C. Guerrero, S. Altstadt, J. Andrzejewski, L. Audouin, G. Badurek, M. Barbagallo, V. Bécaries, F. Bečvář, F. Belloni, E. Berthoumieux, J. Billowes, V. Boccone, D. Bosnar, M. Brugger, M. Calviani, F. Calviño, D. Cano-Ott, C. Carrapiço, F. Cerutti, E. Chiaveri, M. Chin, N. Colonna, G. Cortés, M. A. Cortés-Giraldo, M. Diakaki, C. Domingo-Pardo, I. Duran, R. Dressler, N. Dzysiuk, C. Eleftheriadis, A. Ferrari, K. Fraval, S. Ganesan, A. R. García, G. Giubrone, M. B. Gómez-Hornillos, I. F. Gonçalves, E. González-Romero, F. Gunsing, P. Gurusamy, A. Hernández-Prieto, D. G. Jenkins, E. Jericha, Y. Kadi, F. Käppeler, D. Karadimos, N. Kivel, P. Koehler, M. Kokkoris, M. Krťička, J. Kroll, C. Lampoudis, C. Langer, E. Leal-Cidoncha, C. Lederer, H. Leeb, L. S. Leong, R. Losito, A. Mallick, A. Manousos, J. Marganec, T. Martínez, C. Massimi, P. F. Mastinu, M. Mastromarco, M. Meaze, E. Mendoza, A. Mengoni, P. M. Milazzo, F. Mingrone, M. Mirea, W. Mondelaers, C. Paradela, A. Pavlik, J. Perkowski, A. Plompen, J. Praena, J. M. Quesada, T. Rauscher, R. Reifarh, A. Riego, M. S. Robles, F. Roman, C. Rubbia, M. Sabaté-Gilarte, R. Sarmento, A. Saxena, P. Schillebeeckx, S. Schmidt, D. Schumann, G. Tagliente, J. L. Tain, D. Tarrío, L. Tassan-Got, A. Tsinganis, S. Valenta, G. Vannini, V. Variale, P. Vaz, A. Ventura, R. Versaci, M. J. Vermeulen, V. Vlachoudis, R. Vlastou, A. Wallner, T. Ware, M. Weigand, T. Wright, P. Žugec  
*A new CVD diamond mosaic-detector for  $(n, \alpha)$  cross-section measurements at the  $n$ -TOF experiment at CERN*  
 Nucl. Instrum. Methods Phys. Res., Sect. A, doi: 10.1016/j.nima.2013.07.040 (2013).

W. Yang, L. Guo, C.-Y. Chuang, D. Schumann, M. Ayranov, P. H. Santschi  
*Adsorption characteristics of  $^{210}\text{Pb}$ ,  $^{210}\text{Po}$  and  $^7\text{Be}$  onto micro-particle surfaces and the effects of macromolecular organic compounds*  
 Geochim. Cosmochim. Acta **107**: 47-64, doi: 10.1016/j.gca.2012.12.039 (2013).

## RADIONUCLIDE DEVELOPMENT - CHEMISTRY

N. P. v. d. Meulen, T. N. v. d. Walt, G. F. Steyn, H. G. Raubenheimer  
*The production of  $^{82}\text{Sr}$  using larger format  $\text{RbCl}$  targets*  
 Appl. Radiat. Isot. **72**: 96 - 99, doi: 10.1016/j.apradiso.2012.09.017 (2013).

C. Müller, M. Bunka, J. Reber, C. Fischer, K. Zhernosekov, A. Türlér, R. Schibli  
*Promises of cyclotron-produced  $\text{Sc-44}$  as a diagnostic match for trivalent beta(-)-emitters: In vitro and in vivo study of a  $\text{Sc-44-DOTA-folate}$  conjugate*  
 J. Nucl. Med. **54** (12): 2168-2174, doi: 10.2967/Jnumed.113.123810 (2013).

C. Müller, E. Fischer, M. Behe, U. Köster, H. Dorrer, J. Reber, S. Haller, S. Cohrs, A. Blanc, J. Grünberg, M. Bunka, K. Zhernosekov, N. van der Meulen, K. Johnston, A. Türlér, R. Schibli  
*Future prospects for SPECT imaging using the radiolanthanide terbium-155 — production and preclinical evaluation in tumor-bearing mice*  
 Nucl. Med. Biol.: in press, doi: 10.1016/j.nucmedbio.2013.11.002 (2013).

C. Müller, H. Struthers, C. Winiger, K. Zhernosekov, R. Schibli  
*DOTA conjugate with an albumin-binding entity enables the first folic acid-targeted  $^{177}\text{Lu}$ -radionuclide tumor therapy in mice*  
 J. Nucl. Med. **54** (1): 124-131, doi: 10.2967/jnumed.112.107235 (2013).

## ENVIRONMENTAL RADIONUCLIDES UNIVERSITÄT BERN

S. M. Fahrni, L. Wacker, H.-A. Synal, S. Szidat  
*Improving a gas ion source for  $^{14}\text{C}$  AMS*  
 Nucl. Instrum. Methods Phys. Res., Sect. B **294**: 320-327, doi: 10.1016/j.nimb.2012.03.037 (2013).

K. Hippe, F. Kober, L. Wacker, S. M. Fahrni, S. Ivy-Ochs, N. Akçar, C. Schlüchter, R. Wieler  
*An update on in situ cosmogenic  $^{14}\text{C}$  analysis at ETH Zürich*  
 Nucl. Instrum. Methods Phys. Res., Sect. B **294**: 81-86, doi: 10.1016/j.nimb.2012.06.020 (2013).

S. Szidat, G. Bench, V. Bernardoni, G. Calzolari, C. I. Czimeczik, L. Derendorp, U. Dusek, K. Elder, M. Fedi, J. Genberg, Ö. Gustafsson, E. Kirillova, M. Kondo, A. P. McNichol, N. Perron, G. M. d. Santos, K. Stenström, E. Swietlicki, M. Uchida, R. Vecchi, L. Wacker, Y. Zhang, A. S. H. Prévôt  
*Intercomparison of  $^{14}\text{C}$  analysis of carbonaceous aerosols: Exercise 2009*  
 Radiocarbon **55** (2-3): 1496-1509, doi: 10.2458/azu\_js\_rc.55.16314 (2013).

L. Wacker, S. M. Fahrni, I. Hajdas, M. Molnar, H.-A. Synal, S. Szidat, Y. L. Zhang  
*A versatile gas interface for routine radiocarbon analysis with a gas ion source*  
 Nucl. Instrum. Methods Phys. Res., Sect. B **294**: 315-319, doi: 10.1016/j.nimb.2012.02.009 (2013).

Y. L. Zhang, P. Zotter, N. Perron, A. S. H. Prévôt, L. Wacker, S. Szidat  
*Fossil and non-fossil sources of different carbonaceous fractions in fine and coarse particles by radiocarbon measurement*  
 Radiocarbon **55** (2-3): 1510-1520, doi: 10.2458/azu\_js\_rc.55.16278 (2013).

## REPORTS AND TECHNICAL NOTES

D. Schumann, B. Hammer

*ANDES final report*

EC-EURATOM-FP7 Project ANDES Deliverable D4.7, PSI, 30.9.2013

E. A. Maugeri, M. Rizzi, R. Eichler, J. Neuhausen

*Report on results of screening experiments*

EC-EURATOM-FP7 Project SEARCH DELIVERABLE D6.1, PSI, 14.03.2013

D. Schumann, B. Hammer, J. Neuhausen

*Radiochemical analysis of the radionuclide inventory in MEGAPIE*

EC-EURATOM-FP7, Project GETMAT Deliverable D3.3.2, PSI, 15.11.2013

## CONTRIBUTIONS TO CONFERENCES, WORKSHOPS AND SEMINARS

### HEAVY ELEMENTS

N. Chiera

*Formation and stability of sulfides of the superheavy elements Cn and Fl*

GDCh-Wissenschaftsforum Chemie 2013, Darmstadt, Germany, 1-4 September, 2013.

N. Chiera

*Formation and stability of sulfides of the superheavy elements Cn and Fl*

8th Workshop on the Chemistry of the Heaviest Elements, Toyoshima, Japan, 19-21 September, 2013.

N. Chiera

*Formation and stability of sulfides of the superheavy elements Cn and Fl*

5th Asia-Pacific Symposium on Radiochemistry APSORC'13, Kanazawa, Japan, 22-27 September, 2013.

N. Chiera

*Stability of chemical compounds of the superheavy elements Cn and Fl*

Seminar of the Laboratory of Radiochemistry and Environmental Chemistry, Paul Scherrer Institut and University of Berne, Villigen, Switzerland, 6 December, 2013.

R. Dressler, D. Schumann

*PSI - a source of exotic samples and targets*

ATHENA workshop, Darmstadtium Darmstadt, Germany, 18-20 March, 2013.

R. Dressler, D. Schumann

*Capture reactions on cosmogenic isotopes with samples from PSI*

n\_TOF Collaboration / Collaboration Board Universities of Manchester and York, United Kingdom, 7-9 May, 2013.

R. Dressler, D. Schumann, St. Heinitz

*$^{53}\text{Mn}$  n\_TOF and mass separation*

Klausurtagung RadWaste, Oberschan, Switzerland, 24-25 October, 2013.

R. Dressler, D. Schumann, St. Heinitz

*Measurement of the neutron capture cross-sections of  $^{53}\text{Mn}$  at EAR2*

n\_TOF Collaboration / Collaboration Board University of Bologna, Bologna, Italy, 27-29 November, 2013.

R. Eichler

*Superheavy element chemistry in Switzerland*

504 ASRC Seminar, Advanced Science Research Center JAEA, Tokai, Japan, 28 February, 2013.

R. Eichler:

*Superheavy element chemistry – Achievements and prospective*

Symposium on Nuclear Physics: Presence and Future, Boppard, Germany, 29 May - 5 June, 2013.

R. Eichler

*Gas-phase chemistry experiments of elements 112 and 114 performed at the FLNR in Dubna*

8th Workshop on the Chemistry of the Heaviest Elements, Toyoshima, Japan, 19-21 September, 2013.

R. Eichler

*Intermetallic actinide compounds for SHE production targets*

5th Asia-Pacific Symposium on Radiochemistry APSORC'13, Kanazawa, Japan, 22-27 September, 2013.

H.W. Gäggeler, J.V. Kratz, M. Schädel

*The heavy ion reactions  $^{238}\text{U} + ^{238}\text{U}$  and  $^{238}\text{U} + ^{248}\text{Cm}$  revisited*

Flerov Laboratory for Nuclear Reactions, Dubna, Russia, 19 April, 2013.

H.W. Gäggeler

*G.N. Flerov and his connections to Switzerland*

Centennial of G.N. Flerov, Dom Culturey, Dubna, Russia, 24 May, 2013.

H.W. Gäggeler, J.V. Kratz, M. Schädel  
*The heavy ion reactions  $^{238}\text{U} + ^{238}\text{U}$  and  $^{238}\text{U} + ^{248}\text{Cm}$  revisited*  
 Symposium on Nuclear Physics: Presence and Future, Boppard, Germany, 29 May - 5 June, 2013.

H.W. Gäggeler  
*Beyond the actinides*  
 Celebrating the 100th Anniversary of Radioactivity at National Physical Laboratory, London, United Kingdom, 4 June, 2013.

H.W. Gäggeler, N. Gaston, A. Hermann, P. Schwerdtfeger  
*Comparison of single-atom adsorption enthalpies with calculated solid-state properties for copernicium and flerovium*  
 8th Workshop on the Chemistry of the Heaviest Elements, Toyoshima, Japan, 19-21 September, 2013.

P. Steinegger  
*Development of isothermal vacuum Chromatography for superheavy element research*  
 1st Year Graduate Symposium DCB, University of Bern, Switzerland, 9/10 September, 2013.

P. Steinegger  
*Progress in isothermal vacuum chromatography*  
 8th Workshop on the Chemistry of the Heaviest Elements, Toyoshima, Japan, 19-21 September, 2013.

P. Steinegger  
*Diamond Detectors for Isothermal Vacuum Chromatography*  
 5th Asia-Pacific Symposium on Radiochemistry APSORC'13, Kanazawa, Japan, 22-27 September, 2013.

P. Steinegger  
*The Laboratory for Radiochemistry and Environmental Chemistry (LCH) in 3 minutes, Switzerland*  
 5th Asia-Pacific Symposium on Radiochemistry APSORC'13, Kanazawa, Japan, 22-27 September, 2013.

P. Steinegger  
*Isothermal vacuum chromatography using diamond detectors*  
 Seminar of the Laboratory of Radiochemistry and Environmental Chemistry, Paul Scherrer Institut and University of Berne, Villigen, Switzerland, 6 December, 2013.

P. Steinegger  
*Diamond detector design for measuring alpha-decay chains*  
 2nd ADAMAS Workshop, GSI Darmstadt, Wixhausen, Germany, 15-17 December, 2013.

A. Türler  
*Synthese und Charakterisierung superschwerer Elemente*  
 GDCh-Wissenschaftsforum Chemie 2013, Darmstadt, Germany, 1-4 September, 2013.

A. Türler  
*The gas phase chemistry of group 4 and 5 halides revisited*  
 8th Workshop on the Chemistry of the Heaviest Elements, Toyoshima, Japan, 19-21 September, 2013.

A. Türler  
*Advances in the production and chemistry of the heaviest elements*  
 5th Asia-Pacific Symposium on Radiochemistry APSORC'13, Kanazawa, Japan, 22-27 September, 2013.

A. Türler  
 *$^{22}\text{Ne} + ^{244}\text{Pu}$  and Fl chemistry @ PSI/FLNR*  
 TASC Collaboration Meeting, GSI Darmstadt, Wixhausen, Germany, 29 November, 2013.

I. Usoltsev  
*Decomposition studies of molybdenum carbonyl complexes produced by means of hot atom reactions*  
 8th Workshop on the Chemistry of the Heaviest Elements, Toyoshima, Japan, 19-21 September, 2013.

I. Usoltsev  
*New insights into the formation and stability of molybdenum carbonyl compounds*  
 5th Asia-Pacific Symposium on Radiochemistry APSORC'13, Kanazawa, Japan, 22-27 September, 2013.

I. Usoltsev

*Decomposition studies of molybdenum carbonyl complexes produced by means of hot atom reactions*

Seminar of the Laboratory of Radiochemistry and Environmental Chemistry, Paul Scherrer Institut and University of Berne, Bern, Switzerland, 18 October, 2013.

## SURFACE CHEMISTRY

M. Ammann

*Uptake kinetics of ozone to tropospheric particles*

Seminar at Chemistry Department, University of Leeds, Leeds, United Kingdom, 18 March, 2013.

M. Ammann

*Effects of adsorbates on the hydrogen bonding environment at the surface of ice and frozen solutions*

DACA-13 Davos Atmosphere and Cryosphere Assembly 2013, Davos, Switzerland, 8-12 July, 2013.

M. Ammann, T. Bartels-Rausch, A. Krepelova, H. Bluhm

*A molecular level look on acetic acid at the ice surface*

DACA-13 Davos Atmosphere and Cryosphere Assembly 2013, Davos, Switzerland, 8-12 July, 2013.

M. Ammann

*Competition of organics with halogenide ions at the sea salt solution - air interface: implications for the reactivity with ozone*

DACA-13 Davos Atmosphere and Cryosphere Assembly 2013, Davos, Switzerland, 8-12 July, 2013.

M. Ammann

*Observing atmospheric processes in aerosol particles and ice – a ST XM and XPS perspective*

MAX IV User Meeting, Lund, Sweden, 23-24 September, 2013.

T. Bartels-Rausch

*Chemistry in ice and snow: From the atmosphere to the molecular scale*

Atomic and Molecular Physics and Chemistry, Lille, France, 2-5 July, 2013.

T. Bartels-Rausch, S. Wren, S. Schreiber, F. Riche, M. Schneebeli, M. Ammann

*Diffusion through the snow-pack - bridging field and lab studies*

DACA-13 Davos Atmosphere and Cryosphere Assembly 2013, Davos, Switzerland, 8-12 July, 2013.

T. Bartels-Rausch

*Chemistry in ice and snow: From the atmosphere to the molecular scale*

Conference on Physics, Chemistry and Biology of Water, Sofia, Bulgaria, 22-25 October, 2013.

T. Bartels-Rausch

*Snow and ice in the atmosphere: From the global to the molecular scale*

Seminar of the Laboratory of Radiochemistry and Environmental Chemistry, Villigen, Switzerland, 8 November, 2013.

T. Bartels-Rausch, M. Ammann, M. Schneebeli, F. Riche, S. Schreiber, S. N. Wren

*Diffusion of nitrogen oxides and oxygenated volatile organic compounds through snow*

American Geophysical Union Fall Meeting, San Francisco, USA, 9-13 December, 2013.

G. Gržinić, T. Bartels-Rausch, M. Birrer, M. Ammann

*Uptake of <sup>13</sup>N-labeled N<sub>2</sub>O<sub>5</sub> to citric acid aerosol particles*

European Geoscience Union General Assembly, Vienna, Austria, 7-12 April, 2013.

G. Gržinić, T. Bartels-Rausch, A. Türlér, M. Ammann

*Uptake of N<sub>2</sub>O<sub>5</sub> to citric acid aerosol particles*

European Aerosol Conference, Prague, Czech Republic, 1-6 September, 2013.

G. Gržinić

*N<sub>2</sub>O<sub>5</sub> uptake to citric acid aerosol particles: Humidity dependence and other factors*

Seminar of the Laboratory of Radiochemistry and Environmental Chemistry, Bern, Switzerland, 22 November, 2013.

- G. Gržinić, T. Bartels-Rausch, M. Birrer, M. Ammann  
*Humidity dependence of N<sub>2</sub>O<sub>5</sub> uptake to citric acid aerosol particles*  
 American Geoscience Union Fall Meeting, San Francisco, USA, 9-13 December, 2013.
- S. Kato, M. Ammann, M. Lampimäki, M. T. Lee, T. Bartels-Rausch, T. Huthwelker, M. Brown, C. Paun, M. Birrer, J. A. v. Bokhoven  
*Near ambient pressure hard X-ray photoelectron spectroscopy*  
 Gordon Research Conferences "Hydrogen-Metal Systems", Barga, Lucca, Italy, 4-19 July, 2013.
- S. Kato  
*In situ X-ray photoelectron spectroscopy for gas-solid reactions*  
 Seminar of the Laboratory of Radiochemistry and Environmental Chemistry, Villigen, Switzerland, 6 December, 2013.
- M. Lampimäki, S. Schreiber, V. Zelenay, A. Křepelová, M. Birrer, S. Axnanda, B. Mao, R. Chang, H. Bluhm, Z. Liu, M. Ammann  
*Influence of nitrogen oxides and UV-radiation on metal oxide surfaces: XPS investigation*  
 International Meeting on Atomic and Molecular Physics and Chemistry (IMAMPC 2013), Lille, France, 2-5 July, 2013.
- M. T. Lee, A. Türlér, M. Ammann  
*Competition at solution - air interfaces between bromide and citric acid*  
 Thinking Big in a Small World: Creativity in the Molecular Sciences Rigi Kulm, Switzerland, 20-22 January, 2013.
- M. T. Lee, E. Steimle, T. Bartels-Rausch, S. Kato, M. Lampimäki, M. A. Brown, J. A. v. Bokhoven, F. Nolting, A. Kleibert, A. Türlér, M. Ammann  
*Competition at solution-air interfaces between bromide and citric acid via coated wall flow tube experiments and liquid-jet XPS*  
 European Geosciences Union General Assembly 2013, Vienna, Austria, 7-12 April, 2013.
- M. T. Lee  
*Competition at the solution-air interfaces between bromide and citric acid*  
 Seminar of the Laboratory of Radiochemistry and Environmental Chemistry, Villigen, Switzerland, 19 April, 2013.
- M. T. Lee  
*The role of organics in the chemistry at the surface of sea salt solutions*  
 1st year Graduate Student Symposium, University Bern, Switzerland, 9 September, 2013.
- M. T. Lee, M. Lampimäki, S. Kato, M. A. Brown, T. Bartels-Rausch, M. Birrer, M. Ammann, A. Türlér  
*Liquid-jet - XPS study*  
 JUM@P'13: Third Joint Users' Meeting, Paul Scherrer Institut, Villigen, Switzerland, 18-20 September, 2013.
- S. Steimer  
*Understanding uptake kinetics of ozone on shikimic acid - a flux model approach*  
 Seminar of the Laboratory of Radiochemistry and Environmental Chemistry, Villigen, Switzerland, 19 April, 2013.
- S. Steimer, U. Krieger, M. Lampimäki, T. Peter, M. Ammann  
*Shikimic acid ozonolysis - the influence of physical state*  
 Faraday Discussion 165, Tropospheric Aerosol - Formation, Transformation, Fate and Impacts Leeds, UK, 22-24 July, 2013.
- S. Steimer, A. J. Huisman, U. K. Krieger, M. Lampimäki, G. Gržinić, E. Coz, B. Watts, J. Raabe, M. Ammann  
*Ozonolysis of shikimic acid particles caught in the act*  
 European Aerosol Conference, Prague, Czech Republic, 1-6 September, 2013.
- S. Steimer, U. Krieger, M. Lampimäki, T. Peter, M. Ammann  
*Shikimic acid ozonolysis is influenced by its physical state*  
 American Geophysical Union Fall Meeting, San Francisco, USA, 9-13 December, 2013.
- E. S. Thomson, T. Bartels-Rausch, F. Riche, M. Schneebeli, M. Ammann  
*Trace gas - ice interaction measurements with microstructure control*  
 European Geoscience Union General Assembly, Vienna, Austria, 7-12 April, 2013.

T. Ulrich, M. Ammann, T. Bartels-Rausch  
*Long-term uptake of hydrogen peroxide to ice - a laboratory study*  
 European Geoscience Union General Assembly, Vienna, Austria, 7-12 April, 2013.

T. Ulrich, M. Ammann, T. Bartels-Rausch  
*The snow - atmosphere exchange of hydrogen peroxide - the long term fate as seen in the laboratory*  
 DACA-13 Davos Atmosphere and Cryosphere Assembly 2013, Davos, Switzerland, 8-12 July, 2013.

## ANALYTICAL CHEMISTRY

A. Eichler, M. Schwikowski  
*Mit Ionenchromatographie Klima- und Umweltverschmutzung rekonstruieren*  
 Metrohm Anwendertreffen Wasser und Umwelt, Zofingen, Switzerland, 13 March, 2013.

A. Eichler, P.-A. Herren, T. Kellerhals, T. Papina, M. Schwikowski  
*Ammonium concentrations in ice cores - a novel temperature proxies*  
 DACA-13 Davos Atmosphere and Cryosphere Assembly 2013, Davos, Switzerland, 8-12 July, 2013.

S. Eyrikh, T. Papina, M. Schwikowski  
*The definition of historical contribution of natural and anthropogenic mercury impacts into the territory of the Altai region*  
 International Conference on Mercury as a Global Pollutant, 11<sup>th</sup> ICMGP International Conference on Mercury as a Global Pollutant, Edinburgh, Scotland, 28 July - 2 August, 2013.

H.W. Gäggeler, L. Tobler, M. Schwikowski  
*Application of <sup>210</sup>Pb in Glaciology*  
 APSORC'13 - 5th Asia-Pacific Symposium on Radiochemistry, Kanazawa, Japan, 22-27 September, 2013.

H.W. Gäggeler,  
*Impact of Prof. H. Oeschger's ALPENPROJEKT on (paleo)atmospheric research at Jungfrauoch*  
 Int. Foundation Jungfrauoch & Gornergrat, Meeting of the Board, Hotel Royal St. Georges, Interlaken, Switzerland, 25 October, 2013.

P.-A. Herren, A. Eichler, H. Machguth, T. Papina, L. Tobler, A. Zapf, M. Schwikowski  
*Holocene Climate in Western Mongolia from an Altai ice core*  
 PAGES 2nd Young Scientists Meeting, Goa, India, 11-12 February, 2013.

P.-A. Herren, A. Eichler, H. Machguth, T. Papina, L. Tobler, A. Zapf, M. Schwikowski  
*Holocene Climate in Western Mongolia from an Altai ice core*  
 PAGES 4th Open Science Meeting, Goa, India, 13-16 February, 2013.

P.-A. Herren, A. Eichler, H. Machguth, T. Papina, L. Tobler, A. Zapf, M. Schwikowski  
*Holocene climate in Western Mongolia from an Altai ice core*  
 DACA-13 Davos Atmosphere and Cryosphere Assembly 2013, Davos, Switzerland, 8-12 July, 2013.

T.M. Jenk  
*Sources of excess CO<sub>2</sub> in Greenland ice cores*  
 Seminar of the Laboratory of Radiochemistry and Environmental Chemistry, Paul Scherrer Institut and University of Bern, Bern, Switzerland, 3 May, 2013.

T.M. Jenk, M. Rubino, D. Etheridge, M. Bigler, T. Blunier  
*Sources of excess CO<sub>2</sub> in Greenland ice cores*  
 DACA-13 Davos Atmosphere and Cryosphere Assembly 2013, Davos, Switzerland, 8-12 July, 2013.

T.M. Jenk, M. Rubino, D. Etheridge, M. Bigler, T. Blunier  
*Sources of excess CO<sub>2</sub> in Greenland ice cores*  
 Conference on Isotopes of Carbon, Water, and Geotracers in Palaeoclimate, Bern, Switzerland, 26-28 August, 2013.

- I. Mariani, A. Eichler, T. Jenk., M. Schwikowski  
*Water stable isotopes from Alpine ice cores as proxies for temperature and moisture source*  
 DACA-13 Davos Atmosphere and Cryosphere Assembly 2013, Davos, Switzerland, 8-12 July, 2013.
- I. Mariani, A. Eichler, T.M. Jenk, M. Schwikowski  
*Water stable isotopes from Alpine ice cores as proxies for temperature and moisture source*  
 Conference on Isotopes of Carbon, Water, and Geotracers in Palaeoclimate, Bern, Switzerland, 26-28 August, 2013.
- T. Papina, T. Blyacharchyuk, A. Eichler, N. Malygina, E. Mitrofanova, M. Schwikowski  
*Main biological proxies recorded in the Belukha ice core (Russian Altai)*  
 DACA-13 Davos Atmosphere and Cryosphere Assembly 2013, Davos, Switzerland, 8-12 July, 2013.
- P.A. Pavlova, P. Schmid, M. Zennegg, C. Bogdal, C. Steinlin, M. Schwikowski  
*Temporal trends of POPs in precipitation derived from Alpine ice cores*  
 17th International Congress of Comparative Endocrinology (ICCE 2013), Barcelona, Spain, 15-19 July, 2013.
- P. Pavlova, P. Schmid, C. Bogdal, C. Steinlin, M. Schwikowski  
*First PCB record from the Fiescherhorn glacier, Swiss Alps*  
 12<sup>th</sup> International NCCR Climate Summer School "From Climate Reconstructions to Climate Predictions", Grindelwald, Switzerland, 1-6 September, 2013.
- J. Schindler  
*An extraction system for radiocarbon microanalyses of Dissolved Organic Carbon (DOC)*  
 Seminar of the Laboratory of Radiochemistry and Environmental Chemistry, Paul Scherrer Institut and University of Bern, Bern, Switzerland, 3 May, 2013.
- J. Schindler, S. Szidat, M. Schwikowski  
*An extraction system for radiocarbon microanalyses of dissolved organic carbon (DOC)*  
 DACA-13 Davos Atmosphere and Cryosphere Assembly 2013, Davos, Switzerland, 8-12 July, 2013.
- J. Schindler, S. Szidat, M. Schwikowski  
*An extraction system for radiocarbon microanalyses of dissolved organic carbon (DOC)*  
 12<sup>th</sup> International NCCR Climate Summer School "From Climate Reconstructions to Climate Predictions", Grindelwald, Switzerland, 1-6 September, 2013.
- J. Schindler  
*An extraction system for radiocarbon microanalyses of Dissolved Organic Carbon (DOC)*  
 First Year Graduate Student Symposium of the Department of Chemistry and Biochemistry 2013, University of Bern, Bern, Switzerland, 9-10 September, 2013.
- M. Schwikowski  
*Klimageschichte aus alpinen Eisbohrkernen*  
 AMI Seminar, Paul Scherrer Institut, Villigen, Switzerland, 8 February, 2013.
- M. Schwikowski  
*Temperature and precipitation signals in Alpine ice cores over the period 1961-2001*  
 Meteorologisch-Geophysikalisches Kolloquium, Universität Wien, Austria, 23 April, 2013.
- M. Schwikowski  
*Glaciers as frozen archive of past climatic and environmental conditions*  
 Mentoring Lecture Series, Empowering Women to Develop Academic Careers, Universität Wien, Austria, 23 April, 2013.
- M. Schwikowski  
*Radiocarbon dating of glacier ice*  
 Official inauguration of the MICADAS radiocarbon system at the Department of Chemistry and Biochemistry of the University of Bern, Bern, Switzerland, 3 May, 2013.
- M. Schwikowski  
*Glaciers as archives of past climatic and environmental conditions*  
 APECS-IACS Early Career Workshop at the DACA-13 Meeting Davos Switzerland, 7 July, 2013.

M. Schwikowski

*Klimageschichte aus alpinen Eisbohrkernen*

Besuch der Delegation von der WSL am PSI, Paul Scherrer Institut, Villigen, Switzerland, 26 August, 2013.

M. Schwikowski

*Palaeo climate reconstructions from high-alpine ice cores*

International Geochronology Summer School in Switzerland, “Dating Anthropogenic and Natural Changes in a Fragile Alpine Environment”, Bergün, Switzerland, 1-6 September, 2013.

M. Schwikowski, T.M. Jenk, D. Stampfli, F. Stampfli

*A new thermal drilling system for high-altitude or temperate glaciers*

7<sup>th</sup> International Workshop on Ice Drilling Technology, University of Wisconsin, Madison, USA, 9-13 September, 2013.

M. Schwikowski

*High-alpine glaciers as frozen archive of past climatic and environmental conditions*

Colloquium IAC ETHZ, Switzerland, 14 October, 2013.

M. Schwikowski

*Reconstructing air pollution and climate change from high-alpine ice cores*

1<sup>st</sup> Global IC User Meeting, Metrohm International Headquarters, Herisau, Switzerland, 21-23 October, 2013.

M. Schwikowski, A. Eichler, P.-A. Herren, T. Papina

*Temperature and precipitation reconstruction from two Altai ice cores*

International Scientific Conference “Modern Problems of Geography” dedicated to the 80<sup>th</sup> anniversary of the foundation of the Tbilisi State University Vakhushiti Bagrationi Institute of Geography, Tbilisi, Georgia, 7-9 November, 2013.

L. Sold, M. Hoelzle, M. Huss, A. Eichler, M. Schwikowski

*Recent accumulation and firn compaction rates on Findelengletscher derived from airborne GPR and firn cores*

11<sup>th</sup> Swiss Geoscience Meeting, Lausanne, Switzerland, 15-16 November, 2013.

C.C. Steinlin, C. Bogdal, M. Scheringer, P.A. Pavlova, M. Schwikowski, P. Schmid, K. Hungerbühler

*Modeling incorporation and post-depositional processes of PCB in Alpine glaciers*

33rd International Symposium on Halogenated Persistent Organic Pollutants and POPs -DIOXIN 2013, Daegu, Republic of Korea, 25-30 August, 2013.

## RADWASTE ANALYTICS

R. Dressler, D. Schumann:

*PSI - a source of exotic samples and targets*

ATHENA workshop, Darmstadtium, Darmstadt, Germany, 18-20 March, 2013.

G. Giubrone, C. Domingo-Pardo, J.L. Tain, C.Lederer, S. Altstadt, J. Andrzejewsky, L. Audouin, M. Barbagallo, V. Becares, F. Becvar, F. Belloni, E. Berthoumieux, J. Billowes, V. Boccone, D. Bosnar, M. Brugger, M. Calviani, F. Calvi-no, D. Cano-Ott, C. Carrapi\_co, F. Cerutti, E. Chiaveri, M. Chin, N. Colonna, G. Cortes, M.A. Cortes-Giraldo, M. Diakaki, I. Duran, R. Dressler, N. Dzysiuk, C. Eleftheriadis, A. Ferrari, K. Fraval, S. Ganesan, A.R. Garcia, M.B. Gomez-Hornillos, I.F. Goncalves, E. Gonzalez-Romero, E. Griesmayer, C. Guerrero, F. Günsing, P. Gurusamy, D.G. Jenkins, E. Jericha, Y. Kadi, F. Käppeler, D. Karadimos, N. Kivel, Koehler, M. Kokkoris, G. Korschinek, M. Krlicka, J. Kroll, C. Langer, H. Leeb, L.S. Leong, R. Losito, A. Manousos, C. Massimi, J. Marganec, T. Martinez, P.F. Mastinu, M. Mastromarco, M. Meaze, E. Mendoza, A. Mengoni, P. M. Milazzo, F. Mingrone, M. Mirea, W. Mondelaers, C. Paradela, A. Pavlik, J. Perkowski, M. Pignatari, A. Plompen, J. Praena, J.M. Quesada, T. Rauscher, R. Reifhart, A. Riego, F. Roman, C. Rubbia, I. R. Sarmiento, P. Schillebeeckx, S. Schmidt, D. Schumann, G. Tagliente, D. Tarrío, L. Tassan-Got, A. Tsinganis, S. Valenta, G. Vannini, V. Variale, P. Vaz, A. Ventura, R. Versaci, M.J Vermeulen, V. Vlachoudis, R. Vlastou, A. Wallner, T. Ware, M. Weigand, C. Weiss, T. Wright, and P. Zugec  
*Measurement of the  $^{54,57}\text{Fe}(n, \gamma)$  Cross Section in the Resolved Resonance Region at CERN n TOF ND13*, New York, USA, 3-8 March, 2013.

B. Hammer, D. Schumann, J. Neuhausen

*Characterization of LBE samples from MEGAPIE*,

MEGAPIE PCG-PSC Meeting, PSI, Villigen, Switzerland, 18 April, 2013.

B. Hammer, D. Schumann, J. Neuhausen  
*Characterization of LBE samples from MEGAPIE*,  
 Chinese ADS Delegation Meeting, PSI, Villigen, Switzerland, 4 October, 2013.

B. Hammer  
*Distribution of radionuclides in MEGAPIE, a proton-irradiated LBE*  
 Seminar of the Laboratory of Radiochemistry and Environmental Chemistry, Paul Scherrer Institut and University of Berne, Bern, Switzerland, 18 October, 2013.

B. Hammer  
*MEGAPIE analytics*  
 Klausurtagung RadWasteAnalytics, Oberschan, Switzerland, 24-25 October, 2013.

St. Heinitz  
*Migration of Po/Literature Review/On some aspects of  $H_2Po$*   
 Klausurtagung RadWasteAnalytics, Oberschan, Switzerland, 24-25 October, 2013.

C. Lederer, S. Altstadt, J. Andrzejewski, L. Audouin, M. Barbagallo, V. Becares, F. Becvar, F. Belloni, E. Berthoumieux, J. Billowes, V. Boccone, D. Bosnar, M. Brugger, M. Calviani, F. Calvino, D. Cano-Ott, C. Carrapico, F. Cerutti, E. Chiaveri, M. Chin, N. Colonna, G. Cortes, M.A. Cortes-Giraldo, M. Diakaki, C. Domingo-Pardo, I. Duran, R. Dressler, N. Dzysiuk, C. Eleftheriadis, A. Ferrari, K. Fraval, S. Ganesan, A.R. Garcia, G. Giubrone, M.B. Gomez-Hornillos, I.F. Goncalves, E. Gonzalez-Romero, E. Griesmayer, C. Guerrero, F. Gunsing, P. Gurusamy, D.G. Jenkins, E. Jericha, Y. Kadi, F. Käppeler, D. Karadimos, N. Kivel, P. Koehler, M. Kokkoris, G. Korschinek, M. Krticka, J. Kroll, C. Langer, H. Leeb, L.S. Leong, R. Losito, A. Manousos, J. Marganec, T. Martinez, C. Massimi, P.F. Mastinu, M. Mastromarco, M. Meaze, E. Mendoza, A. Mengoni, P.M. Milazzo, F. Mingrone, M. Mirea, W. Mondelaers, C. Paradela, A. Pavlik, J. Perkowski, M. Pignatari, A. Plompen, J. Praena, J.M. Quesada, T. Rauscher, R. Reifarh, A. Riego, F. Roman, C. Rubbia, R. Sarmento, P. Schillebeeckx, S. Schmidt, D. Schumann, G. Tagliente, J.L. Tain, D. Tarrío, L. Tassan-Got, A. Tsinganis, S. Valenta, G. Vannini, V. Variale, P. Vaz, A. Ventura, R. Versaci, M.J. Vermeulen, V. Vlachoudis, R. Vlastou, A. Wallner, T. Ware, M. Weigand, C. Weiss, T.J. Wright, P. Zugec  
*Neutron capture reactions on Fe and Ni isotopes for the astrophysical s-process*  
 ND13, New York, USA, 3-8 March, 2013.

T. Lorenz  
*Analytics of SINQ targets*  
 Klausurtagung RadWasteAnalytics, Oberschan, Switzerland, 24-25 October, 2013.

T. Lorenz  
*Analytics of alpha-emitting radionuclides produced with proton irradiation in lead targets*  
 Seminar of the Laboratory of Radiochemistry and Environmental Chemistry, Paul Scherrer Institut and University of Berne, Villigen, Switzerland, 8 November, 2013.

T. Lorenz  
*Analysis and separation of long-lived radionuclides produced by proton irradiation in lead targets*,  
 Seminar Laboratory of Ion Beam Physics, ETHZ, Switzerland, 20 November, 2013.

C. Massimi, P. Koehler, F. Mingrone, S. Altstadt, J. Andrzejewski, L. Audouin, M. Barbagallo, V. Becares, F. Becvar, F. Belloni, E. Berthoumieux, V. Boccone, D. Bosnar, M. Brugger, M. Calviani, F. Calvino, D. Cano-Ott, C. Carrapico, F. Cerutti, E. Chiaveri, M. Chin, N. Colonna, G. Cortes, M.A. Cortes-Giraldo, M. Diakaki, C. Domingo-Pardo, I. Duran, R. Dressler, C. Eleftheriadis, A. Ferrari, K. Fraval, S. Ganesan, A.R. Garcia, G. Giubrone, I.F. Goncalves, E. Gonzalez-Romero, E. Griesmayer, C. Guerrero, F. Gunsing, A. Hernandez-Prieto, D.G. Jenkins, E. Jericha, Y. Kadi, F. Käppeler, D. Karadimos, N. Kivel, M. Kokkoris, M. Krticka, J. Kroll, C. Lampoudis, C. Langer, E. Leal-Cidoncha, C. Lederer, H. Leeb, L.S. Leong, R. Losito, A. Mallick, A. Manousos, J. Marganec, T. Martinez, P.F. Mastinu, M. Mastromarco, E. Mendoza, A. Mengoni, P.M. Milazzo, M. Mirea, W. Mondelaers, C. Paradela, A. Pavlik, J. Perkowski, A. Plompen, J. Praena, J.M. Quesada, T. Rauscher, R. Reifarh, A. Riego, M.S. Robles, C. Rubbia, M. Sabate-Gilarte, R. Sarmento, A. Saxena, P. Schillebeeckx, S. Schmidt, D. Schumann, G. Tagliente, J.L. Tain, D. Tarrío, L. Tassan-Got, A. Tsinganis, S. Valenta, G. Vannini, V. Variale, P. Vaz, A. Ventura, M.J. Vermeulen, V. Vlachoudis, R. Vlastou, A. Wallner, T. Ware, M. Weigand, C. Weiss, T. Wright, P. Zugec  
*New measurement of the  $^{25}Mg(n, \gamma)$  reaction cross-section*  
 ND13, New York, USA, 3-8 March, 2013.

E.A.Maugeri, J. Neuhausen, R. Eichler, D. Piguet, D. Schumann, T.M. Mendonça, T. Stora  
*Thermochromatography study of volatile Te and Po species in various gas atmospheres.*  
 Seminar of the Laboratory of Radiochemistry and Environmental Chemistry, Paul Scherrer Institut and University of Berne, Villigen, Switzerland, 22 February, 2013.

E.A.Maugeri, J. Neuhausen, R. Eichler, D. Piguet, D- Schumann, T.M. Mendonça, T. Stora  
*Target characterization and analysis: Thermochromatography study of Po species in various gas atmospheres.*  
 LIEBE meeting, Mol, Belgium, 19 September, 2013.

E.A. Maugeri  
*Comparison of radiation effects and thermal quenching*  
 SumGLASS 2013, 2<sup>nd</sup> International Summer School on Nuclear Glass Wasteform, Pont du Gard, France, 23 September, 2013.

E. Maugeri  
*Thermochromatography of Po*  
 Klausurtagung RadWasteAnalytics, Oberschan, Switzerland, 24-25 October, 2013.

J. Neuhausen, M. Rizzi, E. Maugeri, R. Eichler  
*SEARCH WP6 Task6.1: Release, gas phase transport and capture studies of volatiles*  
 SEARCH 3<sup>rd</sup> semi-annual review meeting, CRS4, Pula, Italy, 6-7 May, 2013.

J. Neuhausen, M. Rizzi, E. Maugeri, R. Eichler  
*SEARCH WP6 Task6.1: Release, gas phase transport and capture studies of volatiles*  
 Klausurtagung RadWasteAnalytics, Oberschan, Switzerland, 24-25 October, 2013.

J. Neuhausen  
*Release of volatile radionuclides in ADS and their capture*  
 VKI Lecture Series: Fluid Mechanics and Chemistry for Safety issues in HLM nuclear reactors, Von Karman Institute for Fluid Dynamics, Rhode-St-Genèse, Belgium, 25-27 November, 2013.

J. Neuhausen, M. Rizzi, E. Maugeri, R. Eichler  
*SEARCH WP6 Task6.1: Release, gas phase transport and capture studies of volatiles*  
 SEARCH 4<sup>th</sup> semi-annual review meeting, Rhode-St-Genèse, Belgium, 28-29 November, 2013.

Matthias Rizzi  
*Polonium volatility – Unexpected results from transpiration experiments of liquid metals and possible chemical species involved*  
 Seminar of the Laboratory of Radiochemistry and Environmental Chemistry, Paul Scherrer Institut and University of Berne, Villigen, Switzerland, 22 February, 2013.

D. Schumann, J.-Ch. David  
*Cross sections and excitation functions for the production of long-lived radionuclides in nuclear reactions of lead and bismuth with protons*  
 ND13, New York, USA, 3-8 March, 2013.

D. Schumann  
*The use of accelerator waste for the production of exotic isotopes*  
 University of Yale, USA, 11 March, 2013.

D. Schumann  
*Overview in the MEGAPIE radionuclide inventory*  
 LIEBE meeting, Paris, France, 23-24 April, 2013.

D. Schumann  
*Nuclear Chemistry for Nuclear Physics*  
 University of Edinburgh, United Kingdom, 3 May, 2013.

D. Schumann  
*Radiochemistry for target development*  
 ESS Industry day, PSI, Villigen, Switzerland, 20 June, 2013.

D. Schumann

*Mining of radioisotopes from accelerator waste*

Workshop on fast neutron applications at spallation sources, Abington, United Kingdom, 30 September - 1 October, 2013.

D. Schumann

*Overview on ERAWAST*

Klausurtagung RadWasteAnalytics, Oberschan, Switzerland, 24-25 October, 2013.

T. Stowasser

*Radionuclide separations*

Klausurtagung RadWasteAnalytics, Oberschan, Switzerland, 24-25 October, 2013.

C. Weiss, C. Guerrero, E. Griesmayer, J. Andrzejewski, G. Badurek, E. Chiaveri, R. Dressler, S. Ganesan, E. Jericha, F. Käppeler, P. Koehler, C. Lederer, H. Leeb, J. Marganec, A. Pavlik, J. Perkowski, T. Rauscher, R. Reifarh, D. Schumann, G. Tagliente, V. Vlachoudis, S. Altstadt, L. Audouin, M. Barbagallo, V. B\_e\_cares, F. Be\_cv\_a\_r, F. Belloni, E. Berthoumieux, J. Billowes, V. Boccone, D. Bosnar, M. Brugger, M. Calviani, F. Calvino, D. Cano-Ott, C. Carrapico, F. Cerutti, M. Chin, N. Colonna, G. Cortes, M.A. Cortes-Giraldo, M. Diakaki, C. Domingo-Pardo, I. Duran, 23 N. Dzysiuk, C. Eleftheriadis, A. Ferrari, K. Fraval, A.R. Garcia, G. Giubrone, M.B. Gomez-Hornillos, I.F. Goncalves, E. Gonzalez-Romero, F. Gunsing, P. Gurusamy, A. Hernandez-Prieto, D.G. Jenkins, Y. Kadi, D. Karadimos, N. Kivel, M. Kokkoris, M. Krticka, J. Kroll, C. Lampoudis, C. Langer, E. Leal-Cidoncha, L.S. Leong, R. Losito, A. Mallick, A. Manousos, T. Martinez, C. Massimi, P.F. Mastinu, M. Mastro marco, M. Meaze, E. Mendoza, A. Mengoni, P.M. Milazzo, F. Mingrone, M. Mirea, W. Mondalaers, C. Paradela, A. Plompen, J. Praena, J.M. Quesada, A. Riego, M.S. Robles, F. Roman, C. Rubbia, M. Sabat\_e-Gilarte, R. Sarmiento, A. Saxena, P. Schillebeeckx, S. Schmidt, J.L. Tain, D. Tarrío, L. Tassan-Got, A. Tsinganis, S. Valenta, G. Vannini, V. Variale, P. Vaz, A. Ventura, R. Versaci, M.J. Vermeulen, R. Vlastou, A. Wallner, T. Ware, M. Weigand, T. Wright, P. Zugec

*The (n,  $\alpha$ ) reaction in the s-process branching point  $^{59}\text{Ni}$*

ND13, New York, USA, 3-8 March, 2013.

L. Zanini, U. Köster, J. C. David, Y. Tall, M. Andersson, K. Berg, V. Boutellier, R. Brüttsch S. Cormon, J. Eikenberg, M. Fallo, Y. Foucher, H. Franberg, D. Gavillet, A. Grimberg, F. Gröschel, A. Guertin, T. Kirchner, J. Krbanjevic, S. Leray, I. Leya, E., Manfrin, J. Neuhausen, E. Noah, H. Ravn, D. Schumann, T. Stora, and M. Wohlmuther

*Measurement of volatile production and release rates and post-irradiation analysis of a Pb/Bi filled Ta target irradiated at ISOLDE*

ND13, New York, USA, 3-8 March, 2013.

## RADIONUCLIDE DEVELOPMENT

M. Bunka

*Production of  $^{44}\text{Sc}$  by irradiation of  $^{44}\text{Ca}$  targets at the cyclotron for radiopharmaceutical applications*

Seminar of the Laboratory of Radiochemistry and Environmental Chemistry, Paul Scherrer Institut and University of Berne, Villigen, Switzerland, 19 April, 2013.

M. Bunka

*Zyklotron-Produktion von  $^{44}\text{Sc}$ , dessen Aufreinigung und radiopharmazeutische Anwendung*

Seminar der Abteilung Strahlenschutz und Sicherheit, PSI, Villigen, Switzerland, 23 April, 2013.

H. Dorrer

*Separation of neighboring lanthanides using extraction or cation-exchange chromatography*

Seminar of Nuclear- and Radiochemistry, Institute for Nuclear Chemistry, University of Mainz, Mainz, Germany. 21 April, 2013.

H. Dorrer

*Herstellung der vier Terbiumisotope  $^{149}\text{Tb}$ ,  $^{152}\text{Tb}$ ,  $^{155}\text{Tb}$  und  $^{161}\text{Tb}$  für radio-pharmazeutische Anwendungen*

GDCh-Wissenschaftsforum, Darmstadt, Germany, 1-4 September, 2013.

A. Türler

*Production and preclinical evaluation of diagnostic and therapeutic radionuclides in tumor-bearing mice: recent developments at Paul Scherrer Institute*

5th Asia-Pacific Symposium on Radiochemistry APSORC'13, Kanazawa, Japan, 22-27 September, 2013.

## ENVIRONMENTAL RADIONUCLIDES UNIVERSITÄT BERN

K. Agrios, G. Salazar, S. Szidat

*Radiocarbon measurements of aerosol filters by accelerator mass spectrometry hyphenations*

Conference on Isotopes of Carbon, Water, and Geotracers in Paleoclimate Research, Bern, Switzerland, 26-28 August, 2013.

D. Ceburnis, J. Ovadnevaite, A. Garbaras, S. Szidat, M. Rinaldi, S. Decesari, K.E. Yttri, V. Remeikis, M.C. Facchini, C.D. O'Dowd

*Source apportionment of organic matter by isotope analysis, AMS PMF and HNMR techniques*

Goldschmidt Conference 2013, Florence, Italy, 25-30 August, 2013.

K. Dällenbach, I. El-Haddad, P. Zotter, J. Slowik, F. Canonaco, G. Ciobanu, A. Piazzalunga, P. Fermo, U. Baltensperger, S. Szidat, A.S.H. Prévôt

*Assessing the wintertime contribution of biomass smoke to organic aerosol at 15 sites in Switzerland by analysing filter samples using aerosol mass spectrometry*

European Aerosol Conference 2013, Prague, Czech Republic, 1-6 September, 2013.

U. Dusek, M. Monaco, A. Kappetijn, S. Szidat, H.A.J. Meijer, J. van der Plicht, T. Röckmann

*Fossil and modern sources of aerosol carbon in the Netherlands - A year-long radiocarbon study*

European Geosciences Union (EGU), General Assembly 2013, Vienna, Austria, 7-12 April, 2013.

U. Dusek, M. Monaco, A. Kappetijn, H.A.J. Meijer, S. Szidat, T. Röckmann

*The fossil fraction of carbon in PM<sub>2.5</sub>: Variations on seasonal and diurnal time scales*

European Aerosol Conference 2013, Prague, Czech Republic, 1-6 September, 2013.

G. Salazar, K. Agrios, S. Szidat

*Analysis of aerosol samples using EA-AMS*

11th European Conference on Accelerators in Applied Research and Technology (ECAART), Namur, Belgium, 8-13 September, 2013.

J. Schenzel, E. Wieland, G. Schlotterbeck, I. Günther-Leopold, S. Szidat

*Speciation of C-14 during the anoxic corrosion of activated steel: Set-up of a long-term corrosion experiment*

Workshop "Mechanisms and Modeling of Waste/Cement Interactions", Ghent, Belgium, 6-8 May, 2013.

S. Szidat, G. Salazar, E. Vogel, M. Battaglia, L. Wacker, H.-A. Synal

*First operation of the Bern AMS MICADAS*

DPG Frühjahrstagung, Hannover, Germany, 18-22 March, 2013.

S. Szidat, G. Salazar, E. Vogel, M. Battaglia, L. Wacker, H.-A. Synal

*First operation of the Bern AMS MICADAS*

Symposium "<sup>14</sup>C & Archaeology", Ghent, Belgium, 8-12 April, 2013.

S. Szidat

*<sup>14</sup>C AMS at the University of Bern: facility, research and applications*

Inauguration Symposium "The new <sup>14</sup>C AMS facility at the University of Bern: research and applications", Bern, Switzerland, 3 May, 2013.

S. Szidat

*<sup>14</sup>C in air-borne particulate matter: measurement and application*

Seminar Department of Earth System Science, University of California, Irvine, USA, 5 June, 2013.

S. Szidat, G. Salazar

*<sup>14</sup>C analysis at the new Bern Laboratory for the Analysis of Radiocarbon with AMS*

Conference on Isotopes of Carbon, Water, and Geotracers in Paleoclimate Research, Bern, Switzerland, 26-28 August, 2013.

S. Szidat, P. Zotter, Y.L. Zhang, V.G. Ciobanu, L. Wacker, U. Baltensperger, A.S.H. Prévôt

*Fossil and non-fossil sources of OC and EC in Switzerland for winter-smog episodes*

European Aerosol Conference 2013, Prague, Czech Republic, 1-6 September, 2013.

S. Szidat

*Radiocarbon measurements at the Laboratory of Radiochemistry and Environmental Chemistry, University of Bern*  
Radiochemieseminar, Labor Spiez, Switzerland, 18-19 September, 2013.

Y.L. Zhang, J. Li, G. Zhang, A.S.H. Prévôt, S. Szidat

*Radiocarbon-based source apportionment of elemental carbon and organic carbon at a regional background site on Hainan Island, South China*

European Aerosol Conference 2013, Prague, Czech Republic, 1-6 September, 2013.

Y.L. Zhang, J. Li, G. Zhang, A.S.H. Prévôt, S. Szidat

*Radiocarbon-based source apportionment of EC and OC in fine particulate matter at a regional background site on Hainan Island, South China*

32<sup>nd</sup> Annual Conference of the American Association for Aerosol Research (AAAR), Portland, USA,  
30 September - 4 October, 2013.

P. Zotter, G. Ciobanu, Y. Zhang, I. El-Haddad, S. Szidat, L. Wacker, U. Baltensperger, A.S.H. Prévôt

*<sup>14</sup>C-based source apportionment of carbonaceous aerosols in Switzerland for 2008 - 2012*

European Geosciences Union (EGU), General Assembly 2013, Vienna, Austria, 7-12 April, 2013.

P. Zotter, V.G. Ciobanu, Y.L. Zhang, I. El-Haddad, S. Szidat, L. Wacker, U. Baltensperger, A.S.H. Prévôt

*<sup>14</sup>C-based source apportionment of carbonaceous aerosols in Switzerland for 2008-2012*

32<sup>nd</sup> Annual Conference of the American Association for Aerosol Research (AAAR), Portland, USA,  
30 September - 4 October, 2013.

## **PUBLIC RELATIONS AND OUTREACH ACTIVITIES**

### **Analytical Chemistry**

Gegen alle Hoffnung hoffend, Energiewende – Energiepolitik aus Frauensicht, Evangelische Frauen Schweiz, 66. Delegierten Versammlung, Podiumsgesprächsteilnahme (M. Schwikowski), Aarau  
27 April 2013

Klimageschichte aus alpinen Eisbohrkernen  
Besuchergruppe Kantonsschule Seetal, Paul Scherrer Institut  
26 June 2013.

Klimageschichte aus alpinen Eisbohrkernen  
Besuchergruppe Zunft Höngg, Paul Scherrer Institut,  
26 November 2013

M. Schwikowski, Klimageschichte aus alpinen Eisbohrkernen  
Monatsversammlung SAC Brugg, Windisch, Switzerland  
12 June 2013

### **Heavy Elements**

Neue Züricher Zeitung  
Experimente am Ende des Periodensystems  
11 September 2013

### **Surface Chemistry**

Cold and hard facts  
Nature podcast, <http://www.nature.com/nature/podcast/index-2013-02-07.html>  
07 February 2013

T. Bartels-Rausch, Wie funktioniert die Chemie im Schnee,  
<http://webpaper.nzz.ch/login?referer=/2013/03/06/forschung-und-technik/K4GWO/wie-funktioniert-die-chemie-im-schnee>  
Neue Zürcher Zeitung, Zürich  
06 March 2013

Standardizing Air Chemistry  
<http://cen.acs.org/articles/91/i45/Standardizing-Air-Chemistry.html>  
Chemical & Engineering News  
11 November 2013

### **Environmental Radionuclides Universität Bern**

Swiss Chemistry Olympiad, 2nd round, Bern  
Presentation S. Szidat: The potential of radiocarbon analysis in environmental chemistry  
20 January 2013.

Oeschger News No. 10  
Commissioning of the new  $^{14}\text{C}$ -AMS laboratory is approaching  
[http://www.oeschger.unibe.ch/media/oeschger\\_news/oeschger\\_news\\_10\\_en.html](http://www.oeschger.unibe.ch/media/oeschger_news/oeschger_news_10_en.html)  
01 February 2013

ProClim-Flash No. 56  
A high-tech replacement for the Oeschger Counter  
<http://proclimweb.scnat.ch/portal/ressources/2756.pdf>  
March 2013

Radio SRF 1, Regionaljournal Bern Fribourg Wallis  
Universität Bern will mit neuem Gerät Spitze behaupten  
<http://www.srf.ch/news/regional/bern-freiburg-wallis/universitaet-bern-will-mit-neuem-geraet-spitze-behaupten>  
03 May 2013

Berner Zeitung BZ  
Striptease im Magnetfeld – Hightech für Klimaforschung  
<http://www.bernerzeitung.ch/region/kanton-bern/Striptease-im-Magnetfeld/story/13818180>  
03 May 2013

www.archaeologie-online.de  
Die «Oeschger-Zähler» erhalten einen Hightech-Nachfolger  
<http://www.archaeologie-online.de/magazin/nachrichten/die-oeschger-zaehler-erhalten-einen-hightech-nachfolger-25650/>  
03 May 2013

www.myscience.ch  
Hightech-Nachfolger für Oeschger-Zähler  
[http://www.myscience.ch/de/news/2013/hightech-nachfolger\\_fuer\\_oeschger-zaehler](http://www.myscience.ch/de/news/2013/hightech-nachfolger_fuer_oeschger-zaehler)  
03 May 2013

Der Bund  
1,8 Millionen für Messgerät zur Altersbestimmung  
04 May 2013

Tages-Anzeiger  
Hightechanlage für die Klimaforschung  
04 May 2013

St. Galler Tagblatt  
Neues Hightech-Gerät für Umweltforschung  
04 May 2013

Oeschger News No. 11  
New radiocarbon dating system officially inaugurated  
[http://www.oeschger.unibe.ch/media/oeschger\\_news/oeschger\\_news\\_11\\_en.html](http://www.oeschger.unibe.ch/media/oeschger_news/oeschger_news_11_en.html)  
08 May 2013

## LECTURES AND COURSES

### **Prof. Dr. A. Türler**

Universität Bern, FS2013

*Bachelor*

- Instrumentalanalytik II (with Dr. K. Krämer and Prof. M. Schwikowski) (3 ECTS)
- Allgemeine Chemie (Einführung Radioaktivität) (with Prof. R. Hähner and Prof. J. Hulliger) (4 ECTS)

Universität Bern, HS2013

*Bachelor*

- Physikalische Chemie IV (with Prof. T. Wandlowski) (3,75 ECTS)
- Praktikum Phys. Chemie II (with others) (4 ECTS)
- Biochemische Methoden I (with others) (3 ECTS)

*Master*

- Nuclear and Radiochemistry (with Dr. R. Eichler and Dr. M. Behe) (3 ECTS)
- Lab course: Nuclear and Radiochemistry at Bern, Basel, ETHZ and PSI (with others) (4 ECTS)
- Seminar Radio- und Umweltchemie in collaboration with Paul Scherrer Institut (organized by PD Dr. S. Szidat FS2013 / HS2013)

### **Prof. Dr. M. Schwikowski**

Universität Bern, FS2013

*Bachelor*

- Instrumentalanalytik II (with Prof. A. Türler and Dr. K. Krämer) (3 ECTS)

Universität Bern, HS2013:

*Master*

- Atmospheric and Aerosol Chemistry (3 ECTS)
- Lab course: Nuclear and Radiochemistry at Bern, Basel, ETHZ and PSI (with others) (4 ECTS)

### **Dr. M. Ammann**

ETH Zürich, FS2013

*Bachelor*

- Systempraktikum Atmosphäre und Klima, (with U. Krieger, T. Peter, H. Sodemann) (7 ECTS)

*Master*

- Atmospheric Interface Chemistry (3 ECTS)

ETH Zürich, HS2013

*Bachelor*

- Atmosphärenchemie (with D. Brunner) (3 ECTS)

### **Dr. R. Dressler**

- Nuclear Radiation Measurement Part 1: Basic principles to build up, perform, and understand measurements with semiconductor detectors", Paul Scherrer Institute
- Nuclear Radiation Measurement Part 2: Spectroscopic hardware demonstrations", Paul Scherrer Institute
- Nuclear Radiation Measurement Part 3: Canberra Genie 2000 Software to collect and evaluate measurements", Paul Scherrer Institute

**Dr. T. Bartels-Rausch**

Universität Bern, HS2013

*Master*

- Lab course: Nuclear and Radiochemistry at Bern, Basel, ETHZ and PSI (with others) (4 ECTS)

**Dr. R. Eichler**

Universität Bern, HS2013

*Bachelor*

- Praktikum Phys. Chemie II (with others) (4 ECTS)

*Master*

- Nuclear and Radiochemistry (with Prof. A. Türler and Dr. M. Behe) (3 ECTS)
- Lab course: Nuclear and Radiochemistry at Bern, Basel, ETHZ and PSI (with others) (4 ECTS)

**PD Dr. S. Szidat**

Universität Bern, FS2013

*Bachelor*

- Ergänzungen zur analytischen Chemie für Pharmaziestudierende (2 ECTS)

Universität Bern, HS2013:

*Bachelor*

- Chemie für Studierende der Veterinärmedizin (with C. Leumann) (4.5 ECTS)
- Praktikum Physikalische Chemie II (with others) (4 ECTS)

*Master*

- Environmental Radionuclides and Nuclear Dating (1.5 ECTS)
- Lab course: Nuclear and Radiochemistry at Bern, Basel, ETHZ and PSI (with others) (4 ECTS)

## MEMBERS OF SCIENTIFIC COMMITTEES EXTERNAL ACTIVITIES

### **Dr. Markus Ammann**

- Atmospheric Chemistry and Physics, member of editorial board
- IUPAC Task Group on Atmospheric Chemical Kinetic Data Evaluation, member
- PSI internal research commission (FoKo), member

### **Dr. Thorsten Bartels-Rausch**

- Air-Ice Chemical Interactions (AICI), Member of Steering Committee

### **Dr. Robert Eichler**

- PSI internal research commission (FoKo), member
- Associate Editor of the International Journal of Modern Physics E (IJMPE)  
World Scientific Publishing

### **Dr. Jörg Neuhausen**

- Member of the Expert group on Heavy Liquid Metal Technologies of the OECD/NEA Working Party on Scientific Issues of the Fuel Cycle (WPFC)

### **Dr. Dorothea Schumann**

- Nuklearforum Schweiz, member
- Schweizerische Gesellschaft der Kernfachleute, member
- PSI internal Neutron Source Development Group, member

### **Prof. Dr. Margit Schwikowski**

- Schweizerische Gesellschaft für Schnee, Eis und Permafrost (SEP), vice president
- Council of the International Glaciological Society, elective member
- Oeschger Centre for Climate Change Research (OCCR), member
- ERC starting grant, Panel member
- DACA-13, lead convener of symposium atmospheric-cryospheric chemistry and ice cores

### **PD Dr. Sönke Szidat**

- Bernese Chemical Society (Berner Chemische Gesellschaft, BCG), president
- Oeschger Centre for Climate Change Research (OCCR), member
- Technical Expert, mandated by the Swiss Accreditation Service (SAS)

### **Prof. Dr. Andreas Türler**

- Eidgenössische Kommission für Strahlenschutz und Überwachung der Radioaktivität (KSR), Vizepräsident
- Gesellschaft Deutscher Chemiker (GDCh), Fachgruppe Nuklearchemie, Vorstands-Beirat
- Radiochimica Acta, member of the advisory board
- Oeschger Centre for Climate Change Research (OCCR), Mitglied des Wissenschaftlichen Ausschusses
- Nuklearforum Schweiz, Mitglied des Vorstandes

## DOCTORAL THESIS



**Thomas Ulrich**

*Interactions of peroxyntic acid and hydrogen peroxide with ice and the environmental implications*

Dr. T. Bartels-Rausch / PSI  
Prof. Dr. S. Leutwyler / Uni Bern  
May 2013



**Stephan Heinitz**

*Investigations on physico-chemical aspects of lead-based alloys for nuclear applications*

Dr. D. Schumann / PSI  
Prof. Dr. A. Türler PSI & Uni Bern  
June 2013



**Pierre-Alain Herren**

*Ice core based climate reconstruction from the Mongolian Altai*

Prof. Dr. M. Schwikowski / PSI & Uni Bern

September 2013



**Isabella Mariani**

*Water stable isotopes in Alpine ice cores as proxies for temperature and atmospheric circulation*

Prof. Dr. M. Schwikowski / PSI & Uni Bern

December 2013



**Y. Zhang**

*Radiocarbon ( $^{14}\text{C}$ )-based source apportionment of atmospheric aerosols: method development and applications*

PD Dr. S. Szidat / Uni Bern  
Prof. Dr. A. Türler / PSI & Uni Bern  
December 2013

## **BACHELOR THESIS**

**C. Steiner**

*Optimized  $^{14}\text{C}$  measurements of wood samples*

PD Dr. S. Szidat / Uni Bern  
May 2013

**D. Lechner**

*A novel boron based cation exchanger for nuclear applications*

Prof. Dr. A. Türler / Uni Bern  
May 2013

## AWARDS

### **Y. Zhang**

*received one of the SCNAT/SCS Chemistry Travel Awards by the "Platform Chemistry" of the Swiss Academy of Sciences and the Swiss Chemical Society*

June 2013

### **M. Bunka**

*Zyklotron Produktion von  $^{44}\text{Sc}$  für radiopharmazeutische Zwecke  
Poster Award*

GDCh-Wissenschaftsforum Chemie, Darmstadt, Germany

September 2013

### **J. Schindler**

*An extraction system for radiocarbon microanalyses of Dissolved Organic Carbon (DOC) Best presentation Award*  
First Year Graduate Student Symposium of the Department of Chemistry and Biochemistry 2013, University of Bern,

September 2013

### **P. Steinegger**

*Development of Isothermal Vacuum Chromatography for Superheavy Element Research*

First Year Graduate Student Symposium of the Department of Chemistry and Biochemistry 2013, University of Bern,

September 2013

### **P. Steinegger**

*Diamond Detectors for Isothermal Vacuum Chromatography  
Best PhD presentation award*

5th Asia-Pacific Symposium on Radiochemistry APSORC'13, Kanazawa, Japan

September 2013

## SUMMER STUDENTS

**Michelle Frei**

*Measurement of  $^{210}\text{Po}$  segregation in LBE with an alpha detector*

3 January - 22 February

**Martina Schuppisser**

3-wöchiges Berufspraktikum zur chemischen Analyse von Firnkernen vom Findelengletscher

18 February - 8 March 2013

**Benoit Chappuis**

Kantonsschule Rychenberg, Winterthur

Maturarbeit Gefrieren von Wasser im elektrischen Feld

**Dimitri Osmont**

*Analysis of black carbon in the Lomonosovfonna ice core*

29 April - 9 August 2013

**Kristen Coué**

*Investigating the kinetics of atmospherically relevant photolysis reaction*

1 May - 31 August 2013

**Katharina Domnanich**

*Development of different production routes of diagnostic and therapeutic Sc radionuclides from various target materials.*

1 September - 31 Dezember 2013

## EXCHANGE STUDENTS

**Tais Basaco Bernabeu, Cuba**

Schweizerisches Bundes-Exzellenz-Stipendium

*Practical experience in radionuclide development, labelling procedures and quality control measures*

15 September 2013 - 15 September 2014

## VISITING GUESTS AT PSI 2013

### 4 February

Lucio Calcagnile and Gianluca Quarta, University of Salento, Lecce, Italy  
*Radiocarbon analysis of carbonaceous aerosols*

### 4 February - 19 July

Maria Macchia, University of Salento, Lecce, Italy  
*Fossil and non-fossil sources of OC and EC in Switzerland for winter-smog episodes*

### 18 February - 8 March

Leo Sold, Department of Geosciences - Geography, University of Fribourg, Switzerland  
*Sampling and chemical analysis of three firn cores from Findelengletscher*

### 21-22 February

Tania Mendonça, ISOLDE, Cern, Switzerland  
*Radioactive ion beams at ISOLDE: recent developments*

### 22-25 April

Fadil Inceoglu, Aarhus University, Denmark  
*<sup>10</sup>Be sampling from the Tsambagarav ice core*

### 3 May

Irka Hajdas, Laboratory of Ion Beam Physics, ETH Zürich, Switzerland  
*Absolute dating with <sup>14</sup>C: fascinating archives and samples*

### 3 May

Fortunat Joos, Climate and Environmental Physics, University of Bern, Switzerland  
*<sup>14</sup>C as a tracer of the global carbon cycle*

### 3 May

Thomas Stocker, Climate and Environmental Physics, University of Bern, Switzerland  
*Monitoring of <sup>14</sup>C emissions in Switzerland*

### 3 May

Hans-Arno Synal, Laboratory of Ion Beam Physics, ETH Zürich, Switzerland  
*From the Oeschger Counter to MICADAS*

### 5-28 July

Stella Eyrikh, Institute of Water and Environmental Problems, SB RAS, Barnaul, Russia  
*Chemical analysis of mercury record in the Belukha ice core*

### 15 July

Kumiko Goto-Azuma, National Institute of Polar Research, Japan  
*Discussion on the analysis of black carbon in snow from Greenland*

### 17 July

Tatyana Papina, Institute of Water and Environmental Problems, SB RAS, Barnaul, Russia  
*Discussion about future projects in the Altai region*

### 27 August

Nozomu Tackeuchi, Chiba University, Japan  
*Discussion about potential future collaborations*

**29 August**

Jesper Sjolte, Department of Geology, Lund University, Sweden  
*Modeling of stable isotopes in precipitation: regional and global studies*

**1 September - 30 November**

Ryszard Misiak, Niwodniczanski Institute of Nuclear Physics, Cracow, Poland  
*Development of detection methods for radicals and thermochromatography studies of Po*

**2-6 September, 2-6 December**

Christina Müller-Tantges, Institute of Inorganic and Analytical Chemistry, Johannes Gutenberg University Mainz, Germany  
*Sampling of the Grenzgletscher ice core for analysis of glyoxal, methylglyoxal, and organic acids*

**24-25 October**

Stephaan Cottenier, University of Ghent, Belgium  
*The DFT approach to Po/LBE: why do we do it, and what do we know so far?*  
 Klausurtagung RadWasteAnalytics

**24-25 October**

Kim Rijpstra, University of Ghent, Belgium  
*The interaction between Po and (Bi-contaminated) filters*  
 Klausurtagung RadWasteAnalytics

**24-25 October**

Alexander Aerts/ Borja Gonzales, SCK Mol, Belgium  
*Po and Hg evaporation experiments at SCK-CEN: answers and questions*  
 Klausurtagung RadWasteAnalytics

**18 October**

Stefan Röllin, Labor Spiez, Switzerland  
*Analysis of actinides and other radionuclides in the environment*

**31 October - 5 November**

Rodrigo Zamora, Centro de Estudios Científicos, Valdivia, Chile  
*Ice core drilling training for operation in Antarctica*

**1 November 2013 - 31 January 2014**

Kim Rijpstra, Center for Molecular Modeling, Ghent University, Belgium  
*Theoretical support for Po-volatilization and adsorption studies*

**4-8 November**

Jean-Christophe David, CEA Saclay, France  
*The Liège intranuclear-cascade model (INCL) and its new capabilities for particle-transport codes*

**8 November**

Hans-Werner Jacobi, Université Joseph Fourier Grenoble, LGGE, France  
*Interaction between snow and atmosphere: Interplay of physical and chemical processes*

**11 November**

Myriam Guillevic, Centre for Ice and Climate, University of Copenhagen, Denmark  
*Visit of the ice core laboratories*

**22 November**

Markus Zennegg, EMPA Dübendorf, Environmental and Analytical Chemistry, Switzerland  
*From Seveso to Yushchenko - what have we learned about dioxins?*

**22 November**

Flavio Anselmetti, University of Bern, Institute of Geological Sciences, Switzerland  
*Reading 'mud': Sediments as archives of climate, environment and natural hazards*

**6 December**

Ruth Signorell, ETH Zürich, Laboratory for Physical Chemistry, Switzerland  
*Interaction of light with nano-sized aerosol particles*



## AUTHOR INDEX

- Agrios, K., 52  
 Ammann, M., 9, 10, 11, 12, 13,  
 14, 15, 16, 17, 18, 19, 20  
 Anselmetti, F., 30  
 Asai, M., 4  
 Baeza-Romero, M.T., 12  
 Baltensperger, U., 56  
 Bartels-Rausch, T., 9, 11, 13, 16,  
 18, 19, 20  
 Battaglia, M., 54  
 Beer, H.-F., 41  
 Berkemeier, T., 9, 10  
 Birrer, M., 18, 19  
 Bogdal, C., 29, 30  
 Boutellier, V., 46, 47  
 Brand, H., 4  
 Brown, M.A., 17, 20  
 Brüttsch, S., 21, 22, 23, 32  
 Budde, I., 24  
 Bunka, M., 49  
 Cao, F., 25  
 Chiera, N.M., 7  
 Ciobanu, V.G., 56  
 Coburn, S., 13  
 Cottenier, S., 44  
 Coue, K., 13  
 Coz, E., 15  
 Dai, Y., 48  
 De Laurentiis, E., 11  
 Di Nitto, A., 4  
 Dommen, J., 12  
 Domnanich, K., 49  
 Dorrer, H., 50  
 Dressler, R., 8, 39  
 Düllmann, Ch.E., 4  
 Eichler, A., 21, 22, 23, 26, 27, 28,  
 32, 35, 37, 38  
 Eichler, R., 4, 5, 6, 7, 8, 42, 43  
 Eikenberg, J., 31, 38  
 El Haddad, I., 56  
 Even, J., 4  
 Eyrikh, S., 27  
 Fangli, F., 4  
 Faurschou Knudsen, M., 36  
 Gonzalez, L., 13  
 Gramlich, G., 26  
 Gržinić, G., 9, 10, 15  
 Günther-Leopold, I., 40  
 Gysel, M., 24  
 Haba, H., 4  
 Haller, S., 50  
 Hammer, B., 46, 47  
 Hartmann, E., 41  
 Hartmann, W., 4  
 Heard, D.E., 12  
 Heinitz, S., 45  
 Herren, P.A., 21, 22, 36  
 Hoelzle, M., 37, 38  
 Hoffmann, T., 35  
 Hohn, A., 51  
 Huang, M., 4  
 Huisman, A., 14  
 Huss, M., 37  
 Huthwelker, T., 18, 20  
 Inceoglu, F., 36  
 Ingham, T., 12  
 Isaksson, E., 23, 24  
 Jäger, E., 4  
 Jäggi, M., 30  
 Jenk, T.M., 28, 31, 33  
 Kaji, D., 4  
 Kanaya, J., 4  
 Kaneya, Y., 4  
 Karoff, C., 36  
 Kato, S., 17, 18, 19, 20  
 Kellerhals, T., 26  
 Khuyagbaatar, J., 4  
 Kindler, B., 4  
 Kleibert, A., 17, 19  
 Kovács, Z., 51  
 Kramer, H., 41  
 Krapf, M., 12  
 Kratz, J.V., 4  
 Krempasky, J., 20  
 Krieger, U., 14  
 Krier, J., 4  
 Kudou, Y., 4  
 Kurz, N., 4  
 Lampimäki, M., 15, 17, 18, 19  
 Lee, M.T., 16, 17, 18  
 Li, J., 55  
 Linder, H.P., 40, 46, 47  
 Lommel, B., 4  
 Lorenz, T., 48  
 Marcolli, C., 14  
 Margerin, V., 39  
 Mariani, I., 28, 32  
 Martma, T., 23  
 Matthews, P.S.J., 12  
 Maugeri, E.A., 42, 43  
 Melo Mendonça, T., 42  
 Miyashita, S., 4  
 Morimoto, K., 4  
 Morita, K., 4  
 Müller, C., 49, 50  
 Müller-Tautges, C., 35  
 Muntwiler, M., 20  
 Murakami, M., 4  
 Murphy, A. StJ. 39  
 Nagame, Y., 4  
 Neuhausen, J., 42, 43, 44, 45, 46,  
 47  
 Nitsche, H., 4  
 Olsen, J., 36  
 Ooe, K., 4  
 Osmont, D., 24  
 Papina, T., 21, 22, 27  
 Paun, C., 18  
 Pavlova, P.A., 29, 30, 31  
 Peter, T., 14  
 Piguet, D., 42, 43  
 Prévôt, A.S.H., 55, 56  
 Proff, C., 18, 19  
 Reber, J., 49, 50  
 Rijpstra, K., 44  
 Rivera, A., 33  
 Rüthi, M., 38  
 Schädel, M., 4  
 Salazar, G., 52, 53, 54  
 Sato, T.K., 4  
 Schibli, R., 49, 50, 51  
 Schmid, P., 29, 30  
 Schindler, J., 33, 34

- Schumann, D., 39, 40, 41, 42, 43, 45, 46, 47, 48  
Schwikowski, M., 21, 22, 23, 24, 25, 26, 27, 28, 29, 30, 31, 32, 33, 34, 35, 36, 37, 38  
Seiffert, C., 39  
Shiraiwa, M., 10  
Slovic, J., 12  
Sold, L., 37, 38  
Steiner, J., 4  
Steimer, S., 11, 13, 14, 15  
Steinegger, P., 8  
Steyn, G.F., 51  
Stora, T., 39, 42  
Stowasser, T., 39, 40, 41  
Sumita, T., 4  
Synal, H.A., 54  
Szelecsényi, F., 51  
Szidat, S., 25, 34, 52, 53, 54, 55, 56  
Takeyama, M., 4  
Tanaka, K., 4  
Toyoshima, A., 4  
Tsukada, K., 4  
Tobler, L., 26, 27  
Türler, A., 4, 5, 7, 8, 9, 16, 17, 46, 47, 48, 49, 50, 54  
Usoltsev, I., 3, 4, 5  
Van Bokhoven, J.A., 17, 18, 19, 20  
Van der Meulen, N., 49, 50, 51  
Van Speybroeck, Y., 44  
Van der Walt, T.N., 51  
Van Yperen-De Deyne, A., 44  
Vermeulen, C., 51  
Vione, D., 11  
Vockenhuber, C., 41, 47  
Vogel, E., 31, 54  
Vögele, A., 42, 43  
Volkamer, R., 13  
Volmert, B., 40  
Wacker, L., 25, 54  
Wakabayashi, Y., 4  
Wang, X., 20  
Wang, Y., 4, 5  
Wieland, E., 40  
Wendl, I., 23, 24  
Whalley, L.K., 12  
Wiehl, N., 4  
Wohlmuther, M., 46, 47  
Yakushev, A., 4  
Yamaki, S., 4  
Zhang, G., 55  
Zhang, Y.L., 25, 53, 55, 56  
Zhi, Q., 4  
Zotter, P., 55, 56

## AFFILIATION INDEX

<b>ABK</b>	Accelerator/Concepts and Development ABK Division, Paul Scherrer Institut, 5232 Villigen PSI, Schweiz
<b>AHL</b>	Hot Laboratory Division (AHL) of the Nuclear Energy and Safety Department (NES), Paul Scherrer Institut, 5232 Villigen PSI, Switzerland
<b>ASI</b>	Abteilung Strahlenschutz und Sicherheit (ASI), Paul Scherrer Institut, 5232 Villigen PSI, Switzerland
<b>ATOMKI</b>	Institute of Nuclear Research of the Hungarian Academy of Sciences, Cyclotron Application Department, ATOMKI, P.O. Box 51, H-4001 Debrecen, Hungary
<b>CECS</b>	Centro de Estudios Científicos, Valdivia, Chile
<b>CERN</b>	European Organization for Nuclear Research, CERN CH-1211, Genève 23, Switzerland
<b>CIEMAT</b>	Centro de Investigaciones Energéticas, Medioambientales y Tecnológicas, Avda. Complutense, 40, 28040 Madrid, Spain
<b>CMM</b>	Center for Molecular Modeling CMM, Ghent University, Technologiepark 903, 9052 Zwijnaarde, Belgium
<b>CPUT</b>	Cape Peninsula University of Technology, Faculty of Applied Sciences, P.O. Box 1906, Bellville 7535, South Africa
<b>CRS</b>	Center for Radiopharmaceutical Sciences, Paul Scherrer Institut, 5232 Villigen, Switzerland
<b>CU</b>	University of Colorado, Boulder, CO 80309, USA
<b>Empa</b>	Swiss Federal Laboratories for Materials Science and Technology, Überlandstrasse 129, 8600 Dübendorf, Switzerland
<b>ETHZ</b>	Eidgen. Technische Hochschule Zürich, 8092 Zürich, Switzerland
<b>EU</b>	European Union
<b>FLNR Dubna</b>	Flerov Laboratory of Nuclear Reactions, Joliot Curie 6, 141980 Dubna, Russia
<b>GFA</b>	Large Research Facilities, Paul Scherrer Institut, 5232 Villigen PSI, Switzerland
<b>GIG CAS</b>	Guangzhou Institute of Geochemistry, Chinese Academy of Sciences, 511 Kehua Street, Wushan, Tianhe District, Guangzhou, GD 510640, China
<b>GSI</b>	Helmholtzzentrum für Schwerionenforschung GmbH, 64291 Darmstadt, Germany
<b>HIM</b>	Helmholtz-Institut Mainz, 55099 Mainz, Germany
<b>IMP</b>	Institute of Modern Physics, Chinese Academy of Sciences, Add: 509 Nanchang Rd., Lanzhou, 730000, China
<b>ISOLDE</b>	The on-line isotope mass separator, CERN, 1211 Geneva 23, Switzerland
<b>iThemba LABS</b>	iThemba LABS, P.O. Box 722, Somerset West, 7129, South Africa
<b>IWEP</b>	Institute for Water and Environmental Problems, Siberian Branch of the Russian Academy of Sciences, 105 Papanintsev Str., RU-Barnaul 656099, Russia
<b>JAEA</b>	Japan Atomic Energy Agency, Tokai, Ibaraki 319-1195, Japan
<b>JGU</b>	Johannes Gutenberg-Universität Mainz, 55099 Mainz, Germany
<b>KUP</b>	Climate and Environmental Physics, Physics Institute, University of Bern, Sidlerstrasse 5, 3012 Bern, Switzerland
<b>LAC</b>	Laboratory of Atmospheric Chemistry, Paul Scherrer Institut, 5232 Villigen PSI, Switzerland
<b>LBK</b>	Bioenergy and Catalysis Laboratory, Paul Scherrer Institut, 5232 Villigen PSI, Switzerland
<b>LBNL</b>	Lawrence Berkeley National Laboratory, Berkeley, CA 94720-8169, USA

<b>LES</b>	Laboratory for Waste Management, Paul Scherrer Institut, 5232 Villigen PSI, Switzerland
<b>LNM</b>	Laboratory for Nuclear Materials, Bereich Nuclear Energy and Safety (NES), Paul Scherrer Institut, 5232 Villigen PSI, Switzerland
<b>LSK PSI</b>	Laboratory for Synchrotron Radiation – Catalysis and Sustainable Chemistry, Paul Scherrer Institut, 5232 Villigen PSI, Switzerland
<b>MPIC</b>	Max-Planck-Institut für Chemie (Otto-Hahn-Institut), Joh.-Joachim-Becher-Weg 27, 55128 Mainz, Germany
<b>NAGRA</b>	Nationale Genossenschaft für die Lagerung radioaktiver Abfälle, Hardstrasse 73, Postfach 280, 5430 Wettingen, Switzerland
<b>NPI</b>	Norwegian Polar Institute, N-9296 Tromsø, Norway
<b>PSI</b>	Paul Scherrer Institut, 5232 Villigen PSI, Switzerland
<b>RIKEN</b>	RIKEN, Wako, Saitama 351-0198, Japan
<b>Rückbau/Entsorgung</b>	Fachbereich Logistik (LOG), Paul Scherrer Institut, 5232 Villigen PSI, Switzerland
<b>Saitama U.</b>	Saitama University, Saitama 338-8570, Japan
<b>SLS</b>	Swiss Light Source, Paul Scherrer Institut, 5232 Villigen PSI, Switzerland
<b>SNF</b>	Schweizerischer Nationalfonds SNF, Wildhainweg 3, 3001 Bern, Switzerland
<b>UC Berkeley</b>	University of California, Berkeley, CA 94720-1460, USA
<b>Univ. Aarhus</b>	Aarhus University, Nordre Ringgade 1, DK-8000 Aarhus
<b>Univ. Bern</b>	Departement für Chemie und Biochemie, Universität Bern, Freiestr. 3, 3012 Bern, Switzerland
<b>Univ. Castilla la Mancha</b>	Rectorado de la Universidad de Castilla – La Mancha, Calle Altagracia número 50, 13071 Ciudad Real, Spain
<b>Univ. Edinburgh</b>	The University of Edinburgh, General Enquiries, Old College, South Bridge, Edinburgh EH8 9YL, Scotland
<b>Univ. Fribourg</b>	University of Fribourg, Avenue de l'Europe 20, 1700 Fribourg, Switzerland
<b>Univ. Gent</b>	Universiteit Gent, Sint-Pietersnieuwstraat 25, 9000 Gent, Belgium
<b>Univ. Hiroshima</b>	Hiroshima University, Kagamiyama, Higashi-Hiroshima 739-8526, Japan
<b>Univ. Kyushu</b>	Kyushu University, Higashi-Ku, Fukuoka, 812-8581, Japan
<b>Univ. Leeds</b>	University of Leeds, Leeds LS2 9JT, United Kingdom
<b>Univ. Mainz</b>	Johannes Gutenberg-Universität Mainz, Saarstr. 21, 55122 Mainz, Germany
<b>Univ. Medical Centre Rostock</b>	Universität Rostock, Universitätsplatz 1, 18055 Rostock, Germany
<b>Univ. Niigata</b>	Niigata University, Niigata, Niigata 950-2181, Japan
<b>Univ. Tallinn</b>	Institute of Geology, Tallinn University of Technology, 10143 Tallinn, Estonia
<b>Univ. Torino</b>	Università degli Studi di Torino, Via Verdi, 8, 10124 Torino, Italy





Paul Scherrer Institut :: 5232 Villigen PSI :: Switzerland :: Tel. +41 56 310 21 11 :: Fax +41 56 310 21 99 :: [www.psi.ch](http://www.psi.ch)

